OREGON STATE UNIVERSITY
TRIGA REACTOR
LICENSE NO. R-106
DOCKET NO. 50-243

SAFETY ANALYSIS REPORT

REDACTED VERSION

SECURITY-RELATED INFORMATION REMOVED

Redacted text and figures blacked out
or denoted by brackets

Safety Analysis Report

for the

Oregon State University TRIGA Reactor

OSU
Oregon State
UNIVERSITY

SUMMARY OF CONTENTS

(Detailed contents are given at the beginning of each chapter.)

CHAPTER 1

THE FACILITY

Chapter 1 - Valid Pages
Rev. 0 7/1/2004

i	Rev. 0 7/1/2004
ii	Rev. 0 7/1/2004
1	Rev. 0 7/1/2004
2	Rev. 0 7/1/2004
3	Rev. 0 7/1/2004
4	Rev. 0 7/1/2004
5	Rev. 0 7/1/2004
6	Rev. 0 7/1/2004
7	Rev. 0 7/1/2004

TABLE OF CONTENTS

LIST OF TABLES

THIS PAGE INTENTIONALLY LEFT BLANK

1 THE FACILITY

1.1 Introduction

This safety analysis report supports an application to the U.S. Nuclear Regulatory Commission (NRC) by Oregon State University for the utilization of a TRIGA®-fueled research reactor. The reactor is owned and operated by Oregon State University for the purpose of performing neutron irradiation services for a wide variety of scientific applications. The reactor is known as the Oregon State TRIGA® Reactor (OSTR).

This document addresses only the safety issues associated with the operation of the OSTR. This document reflects experience with the operation and performance of the reactor systems, radiation surveys, and personnel exposure histories related to the operation of the OSTR.

1.2 Summary and Conclusions on Principal Safety Considerations

Analysis of possible accident scenarios is included in Chapter 13. As a TRIGA®-fueled reactor, the primary safety features stem from the use of a fuel with a strong negative temperature confinement which limits the steady-state and peak power achievable, thus preventing fuel damage from credible reactivity accidents. Ejection of the transient rod from the core when the core is operating at the power level scram point will not result in fuel damage. Since experiments are limited to less reactivity worth than the transient rod, experiment failure cannot result in more severe transients. In addition, the licensed operating power level of 1.1 MW results in a decay heat potential in the fuel small enough that loss of reactor water does not result in fuel damage.

For the maximum hypothetical accident where the fuel cladding is removed, the reactor water disappears, and no confinement building exists, the resulting estimated doses to occupational workers and the general public are well within the annual limits given in 10 CFR 20.

1.3 General Description of the Facility

The Oregon State University (OSU) Radiation Center complex is an approximately 47,000-square foot facility located at the northeast corner of 35th Street and Jefferson Way in Corvallis, Oregon. The complex is comprised of three buildings. The TRIGA® reactor is located in a four-story building, which is called the Reactor Building, on the north side of the Radiation Center. The Reactor Building contains primarily the main Reactor Bay, the Reactor Control Room, space for reactor mechanical equipment, two research laboratories, office space for the Reactor Operations Staff, and a small conference room.

The Advanced Thermal Hydraulics Research Laboratory (ATHRL) is a high-bay facility attached to the east side of the Reactor Building; however, [redacted] The ATHRL houses experimental test loops. The Radiation Center Building houses classrooms, offices, a wide variety of radioisotope laboratories, a [redacted] irradiation facility, a large inventory of nuclear instrumentation useful for research applications as well as for radiation protection, and a number of supporting facilities. Access to the Reactor Building from the Radiation Center may be made through two secure locations.

The OSTR is a light-water-cooled, graphite-reflected reactor using [redacted] enriched uranium-zirconium hydride [redacted] fuel elements. These fuel elements are placed in a circular grid with 16 feet of water over the top of the core. The reactor has an authorized maximum steady-state thermal power of 1.1 MW and may be pulsed to a peak power of over 2,000 MW.

The OSTR is owned and operated by Oregon State University under the NRC License Number R-106 (Docket Number 50- 243). It is used for teaching, research, public service, and radionuclide production. Nuclear Engineering students perform a number of tests and experiments using the reactor in order to reinforce their class work on reactor theory. Researchers use the beamports, the rotating rack, the pneumatic transfer system, the cadmium-lined irradiation tube, the in-core irradiation tube, and the thermal column for experiments involving neutron irradiation. Radionuclides are produced for both research and class applications, particularly classes in nuclear reactor chemistry, radiotracer techniques, and other phases of radiochemistry. Public service is provided through a large number of channels, including a forensic neutron activation analysis service for law enforcement agencies and numerous public education programs. Although outside agencies and institutions are regularly accommodated, a significant percentage of the reactor's users come from OSU and other schools within the Oregon University System.

Significant features of the reactor include:

- three standard control rod and drive systems;
- one transient control rod and drive system; and
- numerous irradiation facilities including an In-Core Irradiation Tube, a Cadmium-Lined In-Core Irradiation Tube, a pneumatic transfer system, Sample Holding Dummy Fuel Elements, a Rotating Rack, four Beamports, a Central Thimble, a Thermal Column, and a Thermalizing Column.

1.4 Shared Facilities and Equipment

The OSTR is an integral part the Radiation Center, and thus shares walls, water supplies, sewage, and main electrical supply. The ventilation system, electrical distribution, water distribution, and heating are all separate.

1.5 Comparison with Similar Facilities

The design of the OSTR is similar to those of approximately 50 TRIGA®-type reactors currently operating world-wide. Three facilities that are nearly identical to the OSTR include the U.S. Geological Survey Center - Denver, University of Texas - Austin, and Penn State University. Since most of these reactors have been in operation for more than twenty years, considerable operational information is available and their characteristics are well documented.

1.6 Summary of Operations

The OSTR is a unique and valuable tool for a wide variety of research applications and serves as an excellent source of neutrons and/or gamma rays. The OSTR has a number of irradiation facilities providing a wide range of neutron flux levels and neutron flux qualities, which are sufficient to meet the needs of most researchers. The reactor is normally operated [redacted] week, with the most usual power level being 1 MW. The average energy output per year is approximately 45 MWd. As an indication of operating tempo, operational statistics for reporting year 2003 are given in Table 1-1. Based on the analysis presented in this SAR, there are no limitations on the operating schedule.

Table 1-1 Operating Statistics for Reporting Year 2003

Operation Data	Annual Value
MWh	1,025
MWd	42.7
Number of pulses	10
Hours reactor critical	1,100
Hours reactor at full power	1,023
Number of irradiation requests	215
Number of samples irradiated	2,000

1.7 Compliance With the Nuclear Waste Policy Act of 1982

In accordance with U.S. Department of Energy (DOE) contract DE-AC07-76ER01953 the DOE shall retain title to the fuel and the DOE is obligated to take the spent fuel and/or high level waste for storage or reprocessing.

1.8 Major Facility Modifications and History

The initial construction of the OSU Radiation Center was completed in 1964. The second phase of the facility was completed in 1967 with the addition of the OSTR. Since then, additional space for teaching, computing, and offices was added to accommodate the rapidly-expanding Nuclear Engineering program. More recent additions have been the Advance Plant Experiment (APEX) and the Advanced Thermal Hydraulics Research Laboratory (ATHRL). The current Radiation Center Complex is approximately 47,000 square feet.

A brief chronology of the key dates and events in the history of the OSU Radiation Center and the TRIGA® reactor is given below.

June 1964	Completion of the first phase of the Radiation Center, consisting of 32,397 square feet of office and laboratory space, under the direction of founding Director, C. H. Wang
July 1964	Transfer of the 0.1 W AGN 201 reactor to the Radiation Center. This reactor was initially housed in the Department of Mechanical Engineering and first went critical in January, 1959
September 1965	Initial request for construction permit submitted
August 1966	Issuance of the construction permit (CPRR-93) for the OSTR
October 1966	Completion of the second phase of the Radiation Center, consisting of 9,956 square feet of space for the TRIGA® reactor and associated laboratories and offices.
March 1967	Issuance of the operating license (R-106) for the OSTR
March 1967	Initial criticality of the OSTR. The reactor was licensed to

	operate at a maximum steady-state power level of 250 kW and was fueled with [redacted]
October 1967	Formal dedication of the Radiation Center
August 1969	OSTR licensed to operate at a maximum steady-state power of 1 MW, but could do so only for short periods of time due to lack of cooling capacity
June 1971	OSTR cooling capacity upgraded to allow continuous operation at 1 MW
April 1972	OSTR Site Certificate issued by the Oregon Energy Facility Siting Council
December 1974	AGN-201 reactor permanently shut down
March 1976	Completion of 1,600 square feet of additional space to accommodate the rapidly expanding nuclear engineering program
July 1976	OSTR refueled with [redacted] fuel
July 1977	Completion of a second 1,600 square feet of space to bring the Radiation Center complex to a total of 45,553 square feet
July 1980	AGN-201 reactor decommissioned and space released for unrestricted use
June 1982	Shipment of the original [redacted] OSTR fuel to Westinghouse Hanford Company
December 1988	AGN-201 components transferred to Idaho State University for use in their AGN-201 reactor program
December 1989	OSTR licensed power increased to 1.1 MW
June 1990	Installation of a [redacted]
March 1992	25th anniversary of the OSTR initial criticality
August 1994	APEX inauguration ceremony

January 1999	Installation of the Argon Production Facility in the OSTR
April 1999	Completion of ATHRL facility brings the Radiation Center complex to a total of 47,198 square feet

THIS PAGE INTENTIONALLY LEFT BLANK

CHAPTER 2

SITE CHARACTERISTICS

Chapter 2 - Valid Pages
Rev. 0 7/1/2004

i	Rev. 0 7/1/2004
ii	Rev. 0 7/1/2004
1	Rev. 0 7/1/2004
2	Rev. 0 7/1/2004
3	Rev. 0 7/1/2004
4	Rev. 0 7/1/2004
5	Rev. 0 7/1/2004
6	Rev. 0 7/1/2004
7	Rev. 0 7/1/2004
8	Rev. 0 7/1/2004
9	Rev. 0 7/1/2004
10	Rev. 0 7/1/2004
11	Rev. 0 7/1/2004
12	Rev. 0 7/1/2004
13	Rev. 0 7/1/2004
14	Rev. 0 7/1/2004
15	Rev. 0 7/1/2004
16	Rev. 0 7/1/2004

TABLE OF CONTENTS

LIST OF FIGURES

LIST OF TABLES

2 SITE CHARACTERISTICS

This chapter describes the site characteristics for the vicinity of the OSTR and Radiation Center on the Oregon State University campus and their relation to the safety and operation of the University's TRIGA® reactor.

The conclusion reached in this chapter and throughout this document is that the selected site is well-suited for the OSTR when considering the relatively benign operating characteristics of the reactor, including the Maximum Hypothetical Accident (MHA). This is consistent with the conclusions reached for the other 50 TRIGA® reactors operating throughout the world. Many of them are located on university campuses, in hospitals, and other highly populated areas.

2.1 Geography and Demography

2.1.1 Site Location and Description

Oregon State University's TRIGA® reactor (OSTR) is located in Corvallis, Oregon. Corvallis is located approximately 50 miles from the Oregon Coast and 35 miles from Salem, the state capital.

2.1.1.1 Specification and Location

The OSTR is located on the far west end of the Oregon State University campus and west of downtown Corvallis. The latitude and longitude of the OSTR is [redacted] by [redacted] Corvallis and Oregon State University lie in Benton County in the Willamette Valley. Corvallis lies 5 miles from Philomath, Oregon; 13 miles from Albany, Oregon; 35 miles from Salem, Oregon; and 45 miles from Eugene, Oregon. The reactor is located approximately 400 yards northeast of Oak Creek and 1.5 miles west of the Willamette River. Good Samaritan Hospital is located approximately 3.5 miles to the northeast.

2.1.1.2 Boundary and Zone Area Maps

Figures 2.1 and 2.2 illustrate the location of the OSTR with respect to the State of Oregon and the OSU campus.

2.1.1.3 Population Distribution

The OSTR is located in Corvallis, Oregon. Metropolitan Corvallis has a population of 49,332 (Ref. 2.1), which has increased by 9% over the ten preceding years. The city of Philomath, located 5 miles from the OSTR has a population of 3,838 (2000 census), which

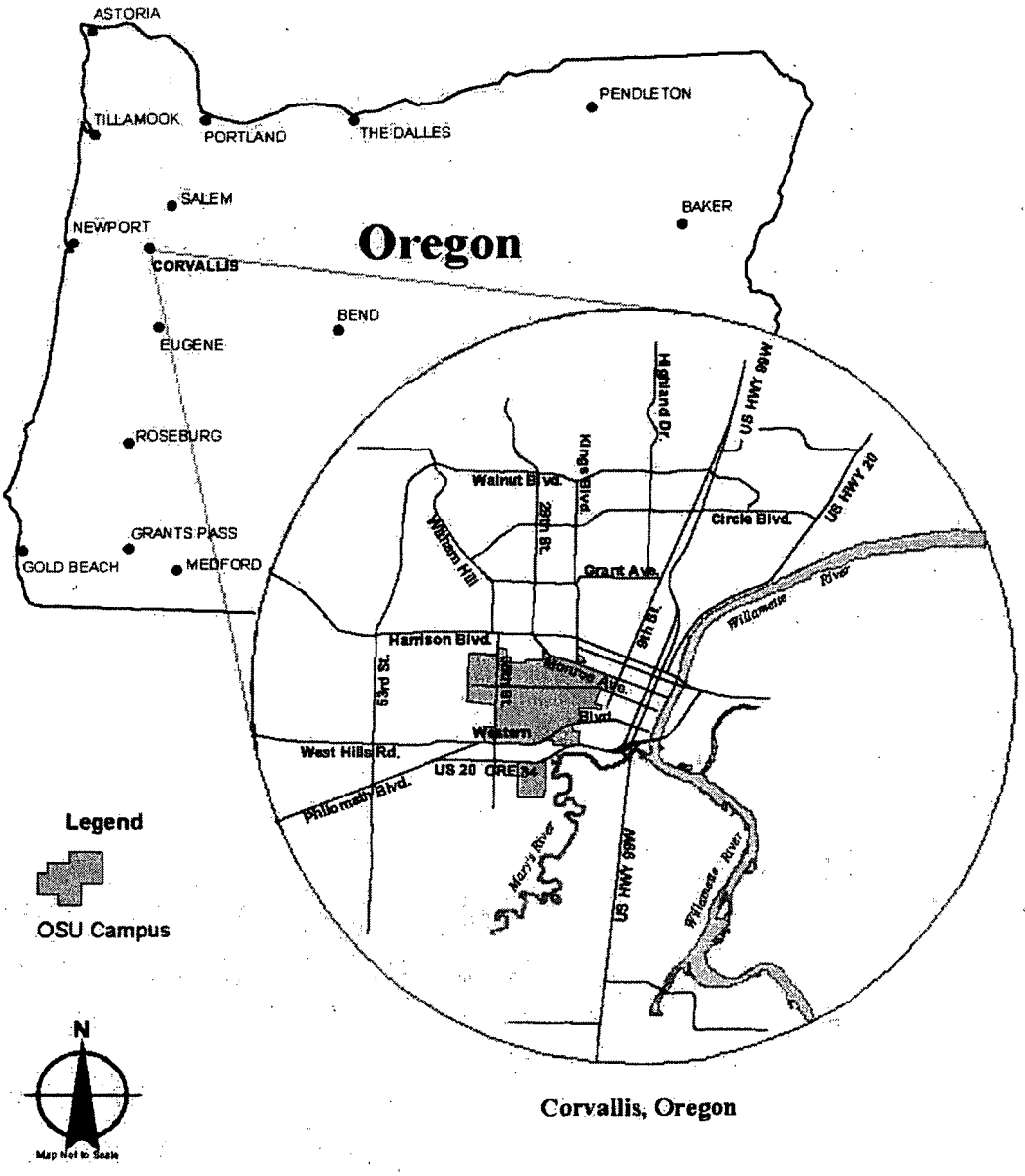

Figure 2.1 Map of Oregon

C01

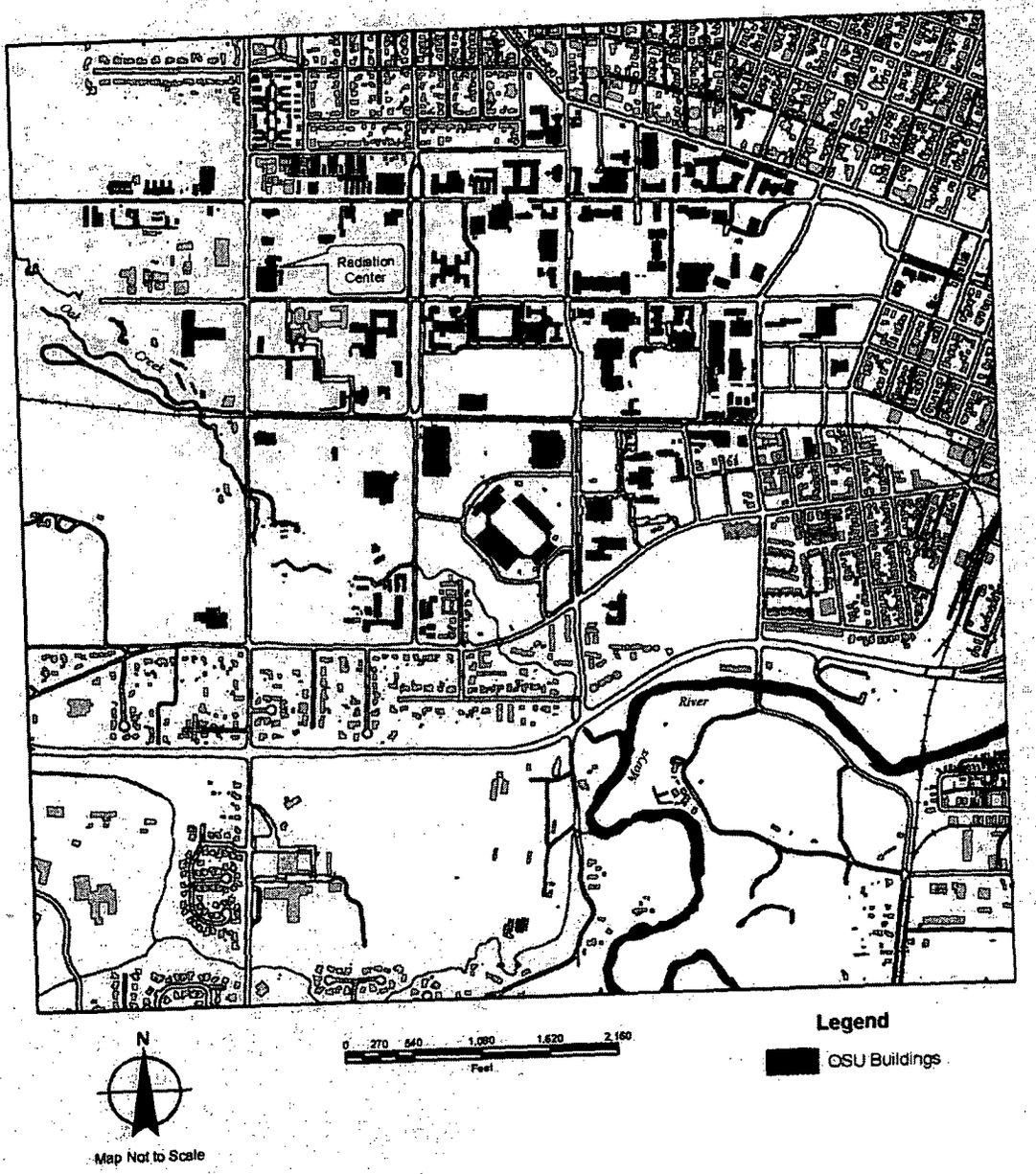

Figure 2.2 Campus Map

C01

has increased 22% over the ten preceding years (Ref. 2.1). The population of Corvallis resides primarily to the north-northeast and south of the OSTR. The total population in all of Benton County is 78,153 (Ref. 2.1). Oregon State University has a population (student and employees) of approximately 23,000 people.

The nearest Oregon State University dormitory, Sackett Hall, is located approximately 1,300 feet to the east of the OSTR. Sackett Hall has 3 floors, and has a capacity of 311 residents including university employees. Reed Hall is directly across from Sackett Hall approximately the same distance from the OSTR. It has a capacity of 54 residents. The typical capacity for all of the residence halls on the Oregon State University campus is 3,500 students (Ref. 2.2). This number of residents only applies during the school year which occurs from late September to early June.

2.2 Nearby Industrial, Transportation, and Military Facilities

2.2.1 Locations and Routes

Figure 2.2 shows the railways near the OSTR. There are no refineries, chemical plants, mining facilities, manufacturing facilities, water transportation routes, fuel storage facilities, military facilities, or rail yards located near the OSTR.

2.2.2 Air Traffic

Six miles south of the OSTR and approximately 5 miles south of downtown Corvallis lies Corvallis Municipal Airport. This small airport has a main runway in the north/south direction (170-350) which is 5,900 feet by 150 feet and is made of asphalt and has a weight limit for double-tandem wheeled aircraft of 75 tons (150,000 lbs). The secondary east/west general aviation runway (90-270) is 3,545 feet by 75 feet. There is no control tower at the airport, but the airport does offer approach lights and ILS instrument approach to its primary runway. The airport averages 106 aircraft operations per day and has 142 aircraft based on it, 115 of which are single engine aircraft (Ref. 2.3). The major airport in Oregon is Portland International Airport (PDX), located approximately 80 miles to the north of the OSTR. The runways at PDX run east/west. Mahlon Sweet Field Airport is located 7 miles northwest of Eugene and located approximately 35 miles from the OSTR. This airport averages 263 aircraft per day, with a maximum weight of 150 tons (300,000 lbs) for a double-tandem wheeled aircraft (Ref. 2.3). This is a controlled airfield with four runways, the primary runway running north/south. There are 173 aircraft based on Mahlon Sweet Field, 131 of which are single engine aircraft.

2.2.3 Analysis of Potential Accidents at Facilities

Local buildings around the OSTR include Oregon State University's Hazardous Waste Facility, the Environmental Protection Agency's Western Ecology Division, Oregon State's Forestry Building, and the O.H. Hinsdale Wave Laboratory.

2.2.3.1 Hazardous Materials Building

The Oregon State University Hazardous Waste Facility is located 100 feet to the north of the OSTR. The facility processes all hazardous waste that is produced in the Oregon State University campus laboratories, including chemistry products, radioactive waste, medical waste, and paint supplies. In 2001, the facility handled approximately 60,000 pounds of waste, 80% of which was in the form of a liquid solvent. This facility stores and packages these wastes for transportation to either a permanent storage location or a destruction facility. [redacted]

An outside contractor provides transportation from the facility on an average of twice per week. Hazardous materials are stored on an 80-day cycle (i.e., wastes are never stored in the facility for more than 80 days) at which point they are transferred to a waste broker. The materials are stored in various containers from 10 to 55 gallons in volume. The maximum inventory of volatile organic fluids with low flash points may reach 150 gallons and they are usually diluted into an aqueous solution. [redacted]

The facility has 3 bays, which are all classified as separate buildings and are connected by sealing fire doors. Each building has an 8-hour burn-through rate to the connected building. All air vents exiting the buildings are monitored and alarmed. Each building has a floor drain with an overflow trench which empties into a 120-gallon, below-grade tank. The mixing station has a blow-out wall that will release at 110 pounds of force. This blow-out wall faces east, away from the OSTR. All of the buildings are also equipped with interior and exterior fire sprinklers.

This facility does not pose a significant threat of accident to the OSTR because of its distance from the reactor, the small quantity of hazardous materials stored, the design, and the building security.

2.2.3.2 EPA Western Ecology Division

The Environmental Protection Agency's Western Ecology Division is located one block west of the OSTR. Included in this facility are a variety of laboratories, plant and animal research facilities, a library, a computer center, and offices. This facility poses no threat to the OSTR.

2.2.3.3 Oregon State's Forestry Building

The forestry building is located one block southeast of the OSTR. It houses the administration office, the forestry dean, accounting offices, and classrooms. There are also offices for the United States Forestry Service. This building also poses no threat to the OSTR.

2.2.3.4 O.H. Hinsdale Wave Research Lab

The O. H. Hinsdale Wave Research Lab is located one blocksouthwest of the OSTR. The building features 3 different wave basins and a control room. This facility poses no threat to the OSTR.

2.3 Meteorology

2.3.1 General and Local Climate

The Willamette Valley is located between the Cascade Mountains and the Coastal Mountain Range. The climate is considered very mild, characterized by cool, wet winters and warm, dry summers. A rain shadow is created over the Willamette Valley by the Coastal Range, which reduces the rainfall totals and coastal winds.

2.3.1.1 Humidity

Relative humidity is highest during early morning hours, and is generally 80-100% throughout the year. During the afternoon, humidity is generally lowest, ranging from 70-80% during January to 30-50% during summer (Ref. 2.4).

2.3.1.2 Wind Stability

Wind rose data is readily available for first order stations (operated by the National Weather Service and fully-instrumented), the closest being Eugene, 45 miles south, and Salem, 35 miles northeast. Annual average data from these two stations taken from 1961 to 1990 are shown in Figures 2.3 and 2.4, respectively (Ref. 2.4).

2.3.1.3 Temperatures

Temperature values for the Corvallis area are shown in Table 2-1. Values are taken from 1971 to 2000. Monthly averages and daily extremes are given for each month. The normal minimum daily temperature extreme is 33.6°F in January and the normal maximum daily temperature extreme is 82.4°F in August. Extreme temperatures have ranged from –7°F to 108°F (Ref. 2.4).

Table 2-1 Monthly Temperatures (Ref. 2.4)

	Monthly Normals			Daily Extremes	
Month	Maximum	Minimum	Mean	Maximum	Minimum
Jan	47	33.6	40.3	64	9
Feb	51	35.4	43.2	68	7
Mar	56.1	37.6	46.9	76	12
Apr	60.7	39.9	50.3	83	27
May	67.1	44	55.6	96	28
Jun	73.4	48.5	61	102	33
Jul	81.2	51.8	66.5	103	38
Aug	82.4	51.5	67	108	37
Sep	77.1	48.2	62.7	103	27
Oct	65.4	41.8	53.6	92	25
Nov	52.9	38	45.5	72	15
Dec	46.4	33.8	40.1	66	-7
Annual	63.4	42	52.7	108	-7

2.3.1.4 Precipitation

Precipitation values, also taken from 1971 to 2000 are shown in Table 2-2. The normal precipitation for the Corvallis area is 43.6 inches per year, with a maximum of 73.21 inches in 1996 and a minimum of 27.15 inches in 1985. The maximum monthly rainfall was 18.28 inches, which fell in November of 1973. Very little precipitation falls as snow.

Table 2-2 Monthly Rainfall in Inches (Ref. 2.4)

	Jan	Feb	Mar	Apr	May	Jun	Jul	Aug	Sep	Oct	Nov	Dec	Annual
Mean	6.5	5.7	4.6	3	2.3	1.5	0.6	0.7	1.5	3	6.9	7.4	43.6
Max	11.59	13.63	8.87	11.42	5.8	4.34	2.55	2.67	3.58	7.21	18.28	17.11	73.21
Min	0.25	1.65	1.04	1.02	0	0.29	0.01	0	0	0.14	1.03	1.47	27.15
S.D.	3.1	3	1.8	1.5	1.3	0.9	0.6	0.8	1.2	1.7	3.8	3.8	10.1

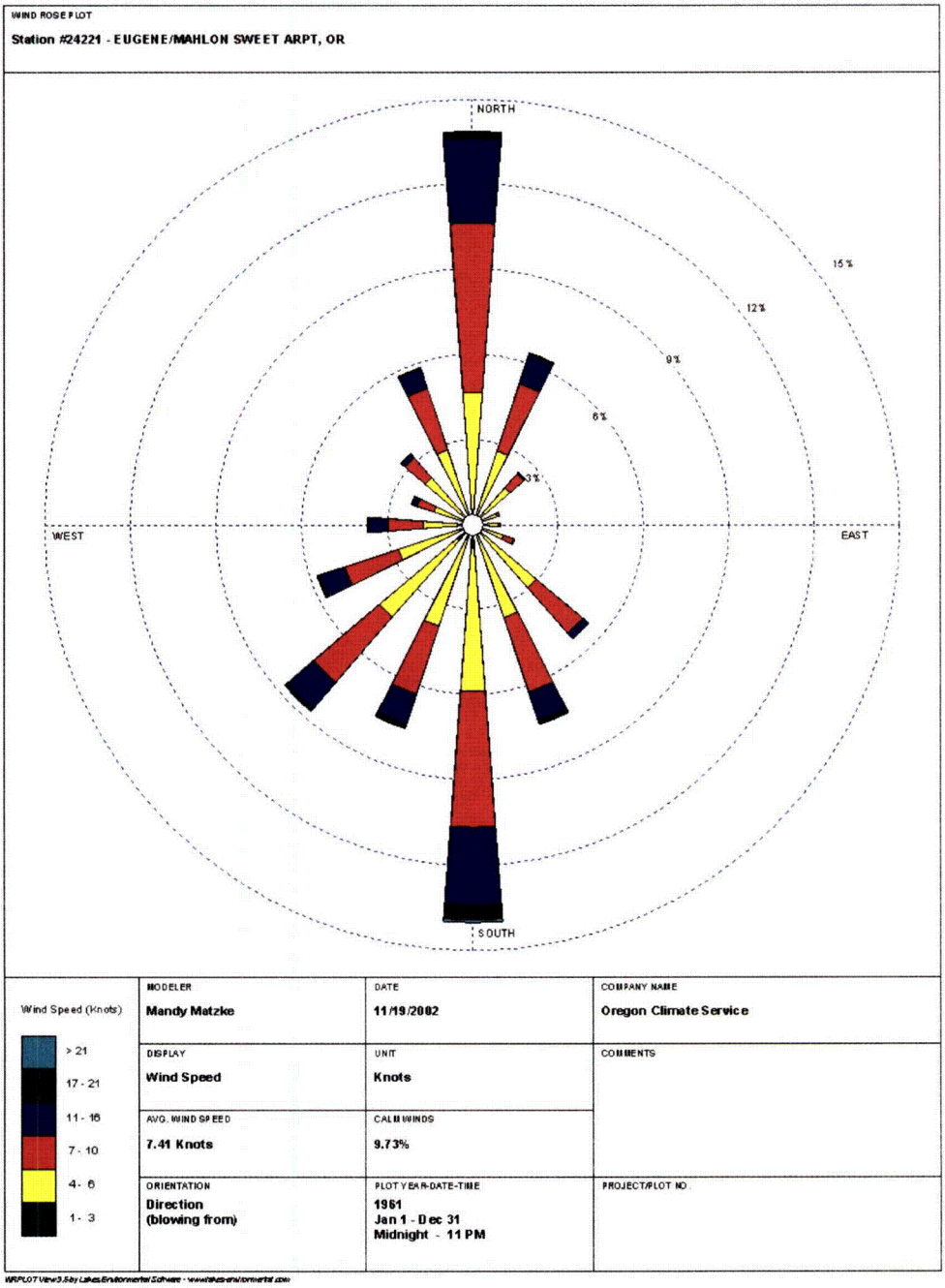

Figure 2.3 Eugene Wind Rose (Annual Average) Ref. 2.4

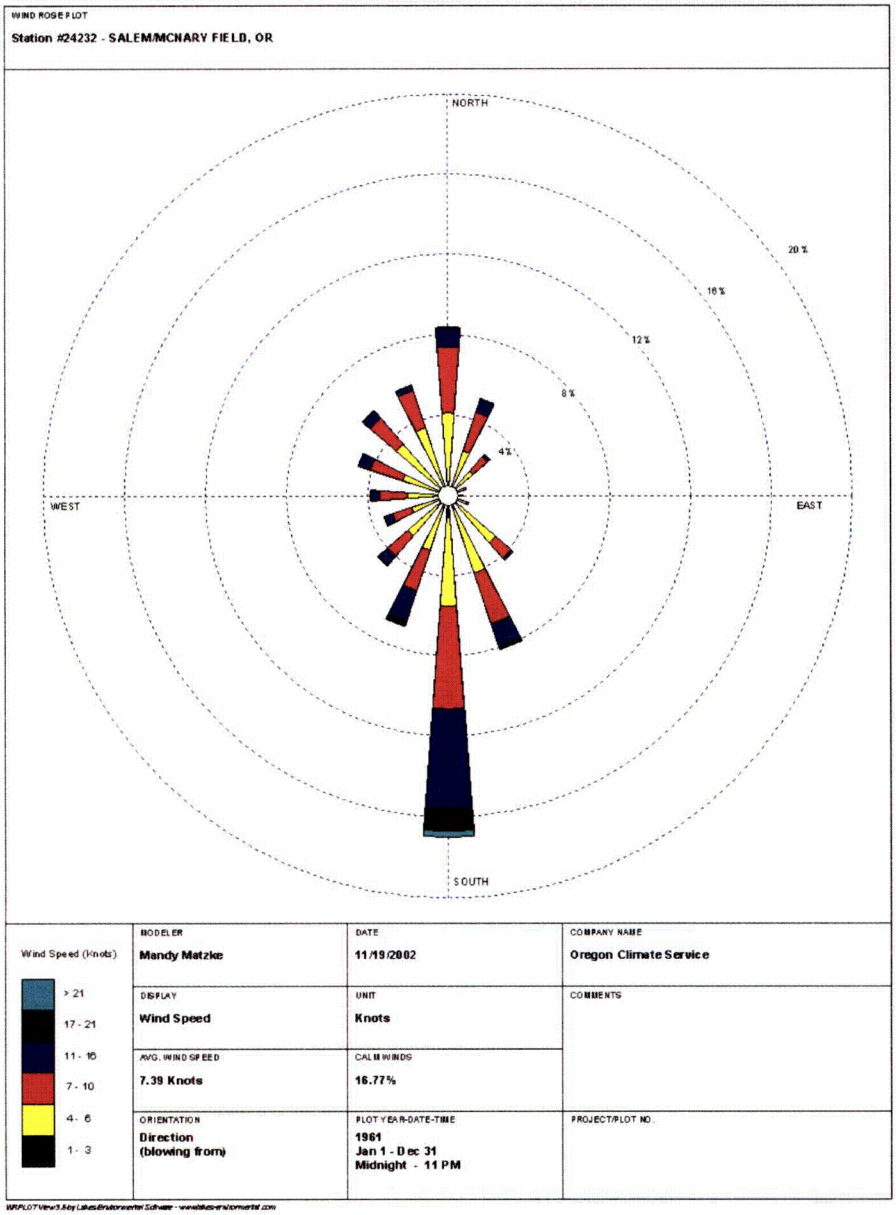

Figure 2.4 Salem Wind Rose (Annual Average) Ref. 2.4

2.3.1.5 Severe Weather Phenomena

Tornadoes in Oregon are quite infrequent due to the mild climate. Between the years 1887 and 1996 there have been only two tornadoes which have measured as an F2 on the Fujita scale. Tornadoes of this magnitude have wind speeds between 113 and 157 mph and have the ability to tear roofs off some buildings, damage trees and mobile homes, and light objects are blown about. These occurred in 1993 at Newberg, OR and in 1968 at an unpopulated forest area in northeast Oregon. In the same 100-year period, only 69 tornadoes were reported in the entire state of Oregon, most of them being of the classification F0, or a gale wind tornado, with wind speeds reaching up to 72 mph. Only 8 of these 69 tornadoes occurred within a 50-mile radius of the OSTR (Ref. 2.6). Because of the low frequency and severity, tornadoes do not represent a significant hazard to the OSTR.

2.4 Hydrology

2.4.1 River Flooding

The only two waterways near the OSTR are Marys River and Oak Creek. The Marys River is located approximately 5,000 feet from the OSTR. Oak Creek is located approximately 1,200 feet from the OSTR. Oak Creek flows into Marys River which subsequently flows into the Willamette River on the east side of Corvallis. The 100-year flood plain for these two waterways is shown in Figure 2.5. The OSTR is not located in either flood plain.

2.4.2 Seismically-Induced Flooding

There are no lakes or dams near the OSTR and, therefore, seismically-induced flooding due to dam failure or seiches is not a risk to the OSTR. Tsunamis are of little concern as well, as the OSTR is located 50 miles from the coastline.

2.5 Geology, Seismology, and Geotechnical Engineering

2.5.1 Regional Geology

Western Oregon geology consists of two primary tectonic plates: the Juan de Fuca Plate, which is located off the Oregon coast and the North American Plate, which lies under all of Oregon. The Juan de Fuca plate is being subducted beneath the North American Plate and the subduction zone, known as the Cascadia Subduction Zone, runs south from Vancouver Island in British Columbia, to Northern California. No great subduction zone event has occurred in Oregon during the 150 years of recorded earthquakes (Ref. 2.7).

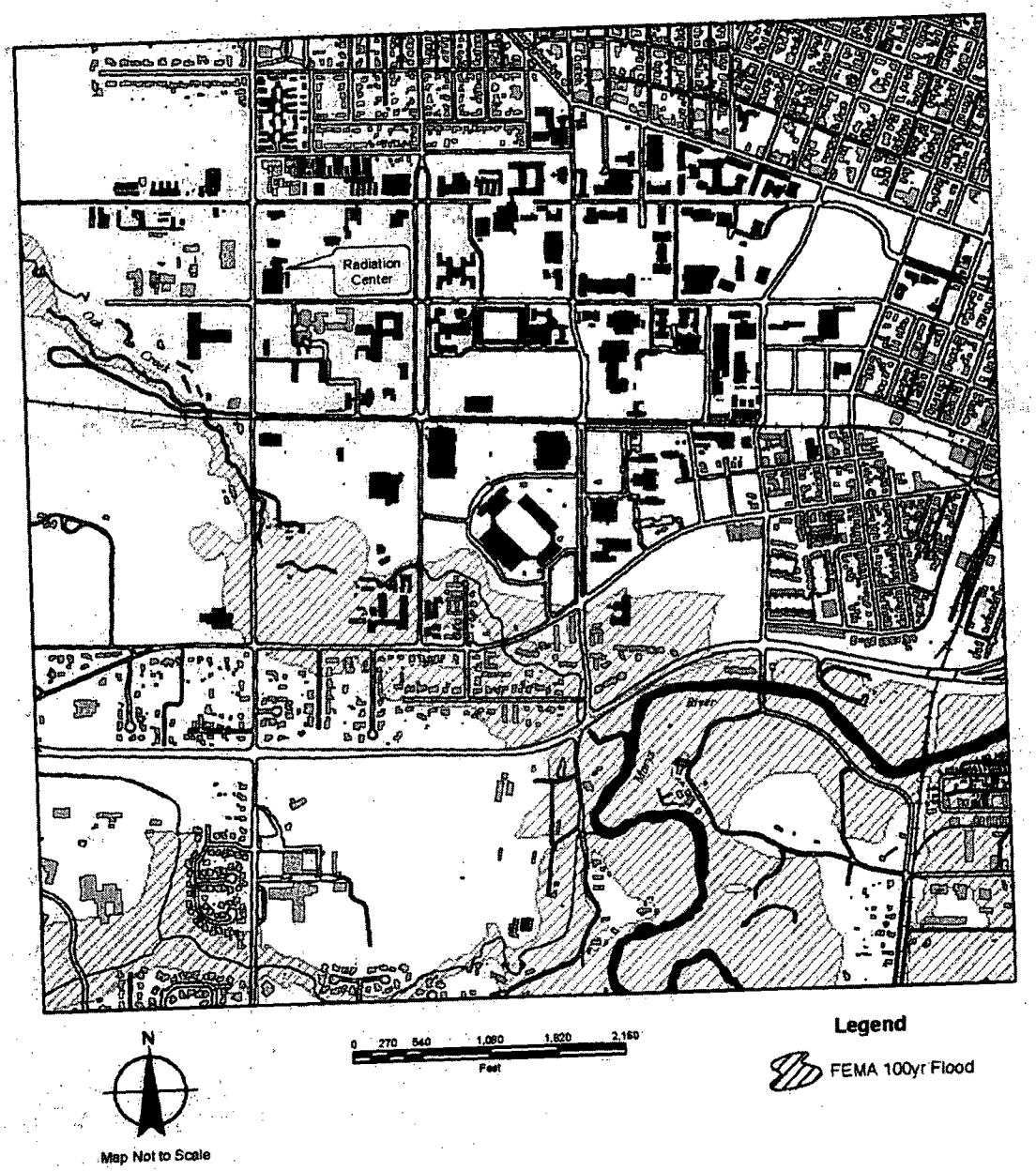

Figure 2.5 OSU Campus 100-year Flood Plain

C05

2.5.2 Site Geology

There are two major fault zones within 5 miles of the OSTR: The Corvallis Fault and the Owl Creek Fault.

2.5.2.1 Corvallis Fault

The Corvallis Fault is located 1.5 miles northwest of the OSTR and is approximately 34 miles long, running northeast. Faulting has been ongoing since the Eocene period with the most recently detectable movement occurring before 28,500 years ago (Ref. 2.8).

2.5.2.2 Owl Creek Fault

The Owl Creek Fault is located 3 miles east of Corvallis and shows Pleistocene period movement, between 10,000 and 30,000 years ago. The fault line is approximately 9 miles long (Ref. 2.8).

2.5.2.3 Faults within 10 miles

There are many other old concealed faults that are located around Corvallis including Bald Hill, Calopooia River, Kings Valley, Lebanon and East Albany faults. None of these show any evidence of movement in the last 1.8 million years (Ref. 2.8).

2.5.3 Seismicity

All recorded earthquakes within 50 miles of the OSTR in the past 150 years have been crustal earthquakes. Only 3 earthquakes of Richter Local Magnitude (M_L) 6 have even been felt in Oregon. Most of the major earthquakes have fallen in the M_L 4 to 5 range. Table 2-3 shows all of the $M_L \geq 3.5$ earthquakes that have occurred within a 50-mile radius of the OSTR (Refs. 2.9 and 2.10).

Table 2-3 Historic Earthquakes Within 50 miles of Corvallis

Year	Month	Day	Hour	Minute	Latitude	Longitude	Depth (km)	Magnitude
1956	May	18	3	41	45	124	Unknown	3.7
1961	August	19	4	56	44.7	122.5	Unknown	4.5
1962	September	5	5	37	44.5	122.9	Unknown	3.5
1963	March	7	23	53	44.9	123.5	47.0	4.6
1993	March	25	13	34	45.0	122.6	20.6	5.6
1993	June	8	00	01	45.0	122.6	20.2	3.7
1995	Feb	8	9	10	45.1	122.7	31.7	3.6

Distant earthquakes that were felt in the city of Corvallis include the following, with the modified Mercalli intensity of the earthquake at the epicenter in parentheses: the 2001 Nisqually Earthquake (II-III); the 1993 Klamath Falls Earthquake (IV); the 1993 Scotts Mills Earthquake (IV); the 1962 Portland Earthquake (I-IV); and the 1873 Crescent City Earthquake (V) (Refs. 2.11, 2.12, 2.13, 2.14). None of these earthquakes, however, caused any damage in the city of Corvallis.

2.5.4 Maximum Earthquake Potential

The Cascade Range is the primary geological structure in the area of Corvallis, running north-south in central Oregon into northern California and Washington. With the exception of Mt. St. Helens, volcanoes in the Cascade Range are all at normal levels of background seismicity. In Oregon, these include Mount Hood, Mount Jefferson, Three Sisters, Newberry, and Crater Lake. The USGS monitors the major volcanoes in the Cascade Range of northern California, Oregon, and Washington. Mt. Hood, considered the most active of the volcanoes in Oregon, last erupted in the 1790s. As of 1999, the largest of the earthquakes at Mt. Hood was a magnitude 4.0 in 1974 (Ref. 2.13).

2.5.5 Vibratory Ground Motion

Devco Engineering performed a peak bedrock accelerations analysis of the site of the OSTR in April of 2003 based on maps available from the USGS website as well as maps prepared for ODOT by Geomatrix in 1995. These estimated bedrock accelerations are given for earthquakes with 10%, 5% and 2% probability of being exceeded in 50 years. These probabilities correspond to approximate return periods of 500, 1,000, and 2,500 years and are shown in Table 2-4. These numbers can also be seen in the USGS map of peak acceleration in Figure 2.6. The values of the maximum accelerations are measured in terms of g, or the acceleration due to gravity. Values are given as a percentage of this acceleration. Acceleration due to gravity is 980 cm/sec/sec so a value of .19 g corresponds to .19 × 980 cm/sec/sec, which is a value of 186 cm/sec/sec.

Table 2-4 Maximum Acceleration for the Corvallis Area as Determined by Geomatrix and USGS

Literature Source	500-year return	1,000-year return	2,500-year return
Geomatrix 1995	.19g	.27g	.37g
USGS 2003	.18g	.26g	.38g

The landslide hazard for the OSTR area and the general Corvallis area is classified as low on a scale of low to very high. The topography of the area contains between a 0 and 5% slope.

2.5.6 Surface Faulting

Subsurface soil conditions near the OSTR include 10 feet of medium stiff, low plasticity, clayey silt. Undrained shear strength compression tests show shear strengths ranging from 1,400 to 1,600 psf. Below 10 feet, the soil turns to very stiff, silty clay. Below 20 feet, the soil becomes sand and gravel until it turns to very stiff clay with silt scattered throughout. The potential for ground rupture at the Radiation Center is considered very low due to the lack of known faulting below the site (Ref. 2.7).

2.5.7 Liquefaction Potential

The OSTR site is underlain with between 20 and 24 feet of medium-stiff to stiff, low plasticity, clayey silt to silty clay. The stiff, cohesive soil profile does not lend itself to liquefaction and is, therefore, not a significant concern to the OSTR (Ref. 2.7).

Figure 2.6 Peak Acceleration (%g) with 10% Probability of Exceedance in 50 Years

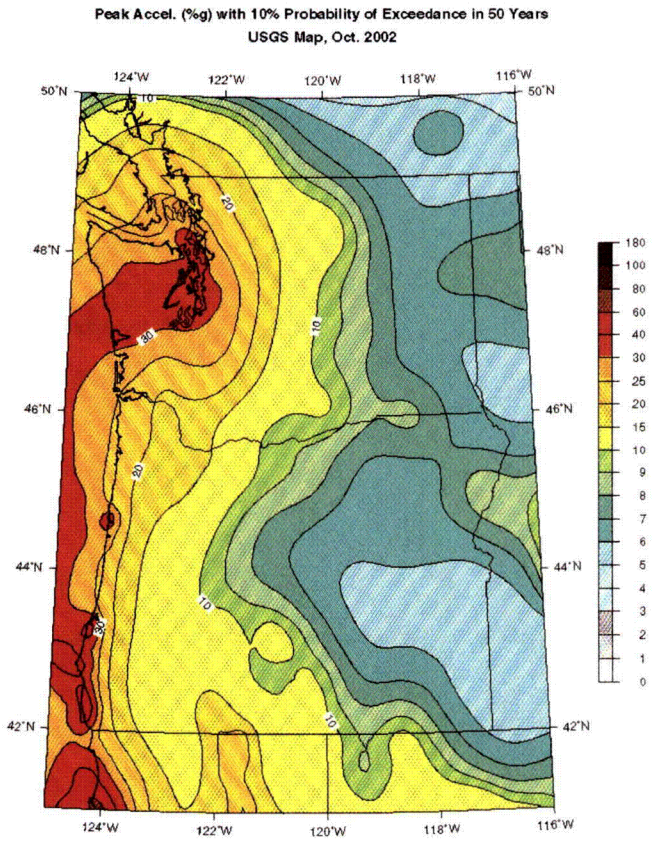

2.6 References

2.1 U.S. Census Bureau, *United States Census 2000.*

2.2 University Housing and Dining Services, 2001, *Utilization of Housing Capacity.*

2.3 AIRNAV.LLC, *Corvallis Municipal Airport,* Morganville, NJ, 2002.

2.4 Oregon Climate Services, www.ocs.orst.edu, July 2003.

2.5 Taylor, Bohman, Foster, *History of Tornadoes in Oregon*, Oregon State University, August 1996.

2.6 National Oceanic and Atmospheric Administration, www.noaa.gov, July 2003.

2.7 Devco Engineering, *OSU Radiation Center Modifications*, April 11, 2003.

2.8 Geomatrix Consultants, 1995, *Final report: Seismic Design Mapping, State of Oregon*: Prepared for Oregon Department of Transportation, Salem Oregon, Personal Services Contract 11688, January, 1995.

2.9 Johnson, Scofield, Madin, 1994, *Earthquake Database for Oregon, 1833 through 1993: Oregon Department of Geology and Mineral Industries.*

2.10 PNSN, 2002, Pacific Northwest Earthquake Catalog Search, 1970 to Present: www.geophys.washington.edu/SEIS/PNSN/CATDAT/catalog.html, University of Washington, Pacific Northwest Seismograph Network.

2.11 Black, G.L., 1996, *Earthquake Intensity Maps for the March 25, 1993, Scotts Mill, Oregon Earthquake: Oregon Geology*, v. 58, no. 2, p. 35-41.

2.12 Madin, Preist, Mabey, Malone, Yelin, Meier, 1993, *1993 Scotts Mills Earthquake-Western Oregon's Wake Up Call: Oregon Geology*, v. 55, no. 3, p. 51-58.

2.13 USGS, 2001, *US Geological Survey*, www.usgs.gov.

2.14 Wong, Bott, 1995, *A Look Back at Oregon's Earthquake History, 1841-1994:* Oregon Geology, v. 57, no. 6, p. 125-139.

THIS PAGE INTENTIONALLY LEFT BLANK

CHAPTER 3

DESIGN OF STRUCTURES, COMPONENTS, EQUIPMENT AND SYSTEMS

Chapter 3 - Valid Pages
Rev. 0 7/1/2004

i	Rev. 0 7/1/2004
ii	Rev. 0 7/1/2004
1	Rev. 0 7/1/2004
2	Rev. 0 7/1/2004
3	Rev. 0 7/1/2004
4	Rev. 0 7/1/2004

TABLE OF CONTENTS

THIS PAGE INTENTIONALLY LEFT BLANK

3 DESIGN OF STRUCTURES, COMPONENTS, EQUIPMENT AND SYSTEMS

3.1 Design Criteria

The OSTR was built in 1966-67. The original reactor installation used fuel and components manufactured by General Atomics (GA), and the specifications to which structures were built were those stated by GA. Specific design criteria were not stated. All building modifications and equipment additions were in conformance with the building codes in existence at the time.

Accident analyses presented in Chapter 13 show that under credible accident conditions, the safety limit on the temperature of the reactor fuel will not be exceeded. Consequently, there would be no fission product release that would exceed 10 CFR 20 allowable radiation levels.

When the OSTR was upgraded to 1 MW in 1976, the principal design criterion was to assure the facility could withstand loss of pool water and any other credible accident with no hazard to the public, without reliance on engineered safety systems. This criterion was met by selecting stainless steel clad TRIGA® fuel with its well-documented characteristics (Ref. 3.1). The design criteria creating this negligible safety risk are the result of the fuel composition and cladding, not of specific features provided in the equipment and building that surrounds the reactor. The accidents described in Chapter 13 conservatively demonstrate that instrumented shutdown actions and building confinement are not necessary to ensure that radiological doses will not exceed allowable limits.

The basic parameter that allows the OSTR to operate safely during either steady-state or transient conditions is the prompt negative temperature coefficient of reactivity ($-\alpha_T$). The fuel-moderator material (U-ZrH) was created such that if all the available excess reactivity were suddenly inserted into the core, the resulting fuel temperature would automatically cause the power excursion to terminate before any core damage resulted (Ref. 3.2). The rise in temperature of the hydride increases the probability that a thermal neutron in the fuel element will gain energy from an excited state of an oscillating hydrogen atom in the lattice. As the neutrons gain energy from the ZrH, their mean-free-path is increased. Since the average chord length in the fuel element is comparable with a mean-free-path, the probability of escape from the fuel element before capture is increased. In the water, where the temperature remains relatively constant, the neutrons are rapidly rethermalized so that the capture and escape probabilities are relatively insensitive to the energy when the neutrons enter the water. The heating of the moderator mixed with the fuel thus causes the spectrum to harden more in the fuel than the water. As a result, there is a temperature-dependent disadvantage factor for the unit cell in the core that decreases the ratio of absorptions in the fuel to total-cell absorptions as the fuel element temperature is increased. This change in disadvantage factor brings about a shift in the core neutron balance, gives a loss of reactivity, and is termed the cell effect (Ref. 3.3).

The $-\alpha_T$ for the [redacted] fuel core is based on the same core spectrum hardening characteristic that occurs in a standard TRIGA® fuel core. However, for a [redacted] fuel element, the uranium loading is ~3.5 times that of a standard TRIGA® element, and this causes the neutron mean-free-path in the [redacted] element to be much shorter. For this reason, the escape probability for neutrons in the fuel is not greatly enhanced as the fuel-moderator material is heated. In the [redacted] fuel, the temperature-hardened spectrum is used to decrease reactivity through its interaction with a low-energy resonance material. Thus erbium, with its double resonance at ~0.5 eV, is used in [redacted] fuel both as a burnable poison and as a material to enhance the $-\alpha_T$. As with the standard fuel, the temperature coefficient is prompt because the fuel is intimately mixed with a large portion of the moderator, and thus fuel and solid moderator temperatures rise simultaneously, producing the temperature-dependent shift (Ref. 3.3).

Routine steady-state power operation is performed with the transient, shim, and regulating rods partially withdrawn. As shown in Chapters 4 and 13, the most rapid possible reactivity insertion rates are adequately compensated for by the negative temperature reactivity coefficient of -1¢ $°C^{-1}$ (7E-4 $\Delta k/k/°C$).

The transient-rod system is specially designed for rapid reactivity insertion. Accidental actuation of the transient rod system may cause a reactivity accident in the sense that it was not planned. However, rapid reactivity additions constitute the normal pulse mode and the maximum reactivity change and the rate of addition are limited by the design of the system (i.e., upper limit switch and bracket).

Natural convection cooling is adequate to dissipate core heat. Many years of operations with TRIGA® reactors have shown that natural convection will provide adequate flow for the removal of heat after several hours of maximum steady-state operation.

3.2 Meteorological Damage

The OSTR reactor core is protected from damage by high winds or tornadoes by virtue of the thick reinforced concrete structure surrounding the reactor tank. The superstructure of the OSTR has been designed for area wind, rain, snow, and ice loads. The OSTR has endured approximately 40 years of local weather conditions with no meteorological damage. Hurricanes, tsunamis, and seiches do not occur in the Corvallis area.

Only a small number of tornadoes, one every few years, have been reported in Oregon. Based on the small probability of occurrences, postulated low intensity, intermittent reactor operation and low fission-product inventory, no criteria for tornadoes have been established for the OSTR structure.

3.3 Water Damage

As discussed in Chapter 2, flooding is not expected at the OSTR site. The OSTR is located comfortably outside the projected 100-year flood plains for nearby rivers and streams. However, even if flooding occurred, reactor safety would not be an issue since the core is located in a water pool.

3.4 Seismic Damage

The Oregon Structural Specialty Code (OSSC 1998) classifies Corvallis, Oregon as Seismic Zone 3. The OSTR was designed and constructed in accordance with Uniform Building Code (UBC 1964) Zone 3 seismic intensity requirements. Meeting these requirements will ensure that the reactor can be returned to operation without structural repairs following any earthquake likely to occur during the plant lifetime.

The likelihood of significant seismic events, discussed in detail in Chapter 2, is low. Furthermore, failure of the reactor tank and loss of the coolant in the event of a very large earthquake have been considered in Chapter 13 and the consequences found acceptable from the standpoint of public safety.

3.5 Systems and Components

3.5.1 Control Rod Drives

The control rod drive assemblies for all control rods are mounted on the reactor bridge structure. The OSTR has three different drive systems.

Two of the shim rods, specifically the shim and safety rods, have electrically-driven rack-and-pinion drives consisting of a two-phase reversible motor, a magnet rod-coupler, a rack-and-pinion gear system, an electromagnet and armature, a dashpot assembly, control rod extension shaft, and a potentiometer used to provide rod position indication. These drives are standard TRIGA® drive mechanisms manufactured by GA. Limit switches are provided to indicate the up and down positions of the magnet and the down position of the rod. The nominal drive speed for these two rods is 18 inches min^{-1}. During a scram, the control rod, rod extension, and magnet armature are detached from the electromagnet and, thus, drop by gravity. The dashpot assembly slows the rate of insertion near the bottom to limit deceleration forces.

The regulating rod is similar to the shim and safety rods except a stepping motor and reduction gear are used in place of the reversible motor. The nominal drive speed for the regulating rod is 24 inches min^{-1}. The stepping motor speed is adjustable with a maximum rod speed of 42 inches min^{-1}. The ability to change the rod drive speed is administratively-

controlled and access to the area is limited to authorized personnel only.

The transient rod drive mechanism is a single-acting pneumatic cylinder manufactured by GA. Compressed air drives a piston (attached to the transient rod though a connecting rod assembly) against the top of a cylinder. The cylinder holding the piston can move up and down by virtue of a motor-driven worm gear engaged with a ball nut assembly. A potentiometer attached to the worm drive provides rod position indication. Limit switches provide indication when the cylinder is fully-up or fully-down.

3.5.2 Ventilation System

Although there are no required engineered safety features for this reactor due to its low operating power and good fission product retention in the fuel, a controlled ventilation system acts to reduce the consequences of fission products released from the fuel or other experimental facilities. Automatic shutdown of the ventilation system confines the free air volume of the reactor building during emergency conditions. Remote monitoring of the conditions within the reactor building can be conducted. The ventilation system is specifically described in Chapter 9.

3.5.3 Confinement

Based on radioactivity release calculations given in Chapter 13, the reactor building is not required to provide a containment function. No special seals for doors or lines which penetrate the walls are provided. All doors are normally closed and locked while operating for security and airflow considerations.

3.6 References

3.1 Safety Analysis Report for the Torrey Pines TRIGA® Mark III Reactor, GA-9064, January 5, 1990.

3.2 The U-ZrH_x Alloy: Its Properties and Use in TRIGA® Fuel, GA-E-117-883, 1980.

3.3 Simnad, M.T., Fabian, C.F. and West, G.B., Fuel Elements for Pulsed TRIGA® Research Reactors; Nuclear Technology 28:31-56; 1976.

CHAPTER 4

OREGON STATE TRIGA® REACTOR

Chapter 4 - Valid Pages
Rev. 0 7/01/2004

i	Rev. 0 7/01/2004	39	Rev. 0 7/01/2004	81	Rev. 0 7/01/2004
ii	Rev. 0 7/01/2004	40	Rev. 0 7/01/2004	82	Rev. 0 7/01/2004
iii	Rev. 0 7/01/2004	41	Rev. 0 7/01/2004	83	Rev. 0 7/01/2004
iv	Rev. 0 7/01/2004	42	Rev. 0 7/01/2004	84	Rev. 0 7/01/2004
1	Rev. 0 7/01/2004	43	Rev. 0 7/01/2004	85	Rev. 0 7/01/2004
2	Rev. 0 7/01/2004	44	Rev. 0 7/01/2004	86	Rev. 0 7/01/2004
3	Rev. 0 7/01/2004	45	Rev. 0 7/01/2004	87	Rev. 0 7/01/2004
4	Rev. 0 7/01/2004	46	Rev. 0 7/01/2004	88	Rev. 0 7/01/2004
5	Rev. 0 7/01/2004	47	Rev. 0 7/01/2004		
6	Rev. 0 7/01/2004	48	Rev. 0 7/01/2004		
7	Rev. 0 7/01/2004	49	Rev. 0 7/01/2004		
8	Rev. 0 7/01/2004	50	Rev. 0 7/01/2004		
9	Rev. 0 7/01/2004	51	Rev. 0 7/01/2004		
10	Rev. 0 7/01/2004	52	Rev. 0 7/01/2004		
11	Rev. 0 7/01/2004	53	Rev. 0 7/01/2004		
12	Rev. 0 7/01/2004	54	Rev. 0 7/01/2004		
13	Rev. 0 7/01/2004	55	Rev. 0 7/01/2004		
14	Rev. 0 7/01/2004	56	Rev. 0 7/01/2004		
15	Rev. 0 7/01/2004	57	Rev. 0 7/01/2004		
16	Rev. 0 7/01/2004	58	Rev. 0 7/01/2004		
17	Rev. 0 7/01/2004	59	Rev. 0 7/01/2004		
18	Rev. 0 7/01/2004	60	Rev. 0 7/01/2004		
19	Rev. 0 7/01/2004	61	Rev. 0 7/01/2004		
20	Rev. 0 7/01/2004	62	Rev. 0 7/01/2004		
21	Rev. 0 7/01/2004	63	Rev. 0 7/01/2004		
22	Rev. 0 7/01/2004	64	Rev. 0 7/01/2004		
23	Rev. 0 7/01/2004	65	Rev. 0 7/01/2004		
24	Rev. 0 7/01/2004	66	Rev. 0 7/01/2004		
25	Rev. 0 7/01/2004	67	Rev. 0 7/01/2004		
26	Rev. 0 7/01/2004	68	Rev. 0 7/01/2004		
27	Rev. 0 7/01/2004	69	Rev. 0 7/01/2004		
28	Rev. 0 7/01/2004	70	Rev. 0 7/01/2004		
29	Rev. 0 7/01/2004	71	Rev. 0 7/01/2004		
30	Rev. 0 7/01/2004	72	Rev. 0 7/01/2004		
31	Rev. 0 7/01/2004	73	Rev. 0 7/01/2004		
32	Rev. 0 7/01/2004	74	Rev. 0 7/01/2004		
33	Rev. 0 7/01/2004	75	Rev. 0 7/01/2004		
34	Rev. 0 7/01/2004	76	Rev. 0 7/01/2004		
35	Rev. 0 7/01/2004	77	Rev. 0 7/01/2004		
36	Rev. 0 7/01/2004	78	Rev. 0 7/01/2004		
37	Rev. 0 7/01/2004	79	Rev. 0 7/01/2004		
38	Rev. 0 7/01/2004	80	Rev. 0 7/01/2004		

TABLE OF CONTENTS

LIST OF FIGURES

LIST OF TABLES

4 TRIGA® REACTOR

4.1 Summary Description

The OSU reactor is a standard design nominal 1-MW (licensed 1.1-MW), natural-convection-cooled TRIGA® pool reactor with the graphite reflector providing accommodation to four beamports (three radial and one tangential), a thermal column, and a pool irradiation facility. The reactor core is located near the bottom of a water-filled aluminum tank [redacted] feet in diameter and about [redacted] feet deep. For personnel shielding, the tank is shielded radially by a minimum of [redacted] of ordinary concrete with a density of 2.3 g/cm^3, 1½ feet of water, 2 inches of lead, and 10.2 inches of graphite. The approximately 16 feet of water above the core provides adequate shielding at the top of the tank. The control rod drives are mounted at the top of the tank on a bridge structure spanning the diameter of the tank. The reactor can be operated in a steady-state mode by either manual or automatic control. The reactor can also be operated in square-wave and pulse mode.

The OSU reactor, although originally taken critical with TRIGA® Standard fuel, is currently fueled with Fuel Life Improvement Program [redacted] TRIGA® fuel rods. Detailed data on TRIGA® fuel rods is given in Table 4-1 below.

Table 4-1 [redacted] and LEU Fuel Parameters

Fuel Element Type	[redacted]	STANDARD
Fuel-moderator material	U-$ZrH_{1.6}$	U-$ZrH_{1.6}$
Uranium content	[redacted] wt%	[redacted] wt%
^{235}U enrichment	[redacted]	[redacted]
^{235}U content (avg) per element	[redacted]	[redacted]
Burnable poison	natural erbium	-
Erbium content	[redacted] wt%	-
Shape	cylindrical	cylindrical
Length of fuel meat	[redacted] inches	[redacted] inches
Diameter of fuel meat	[redacted] inches	[redacted] inches
Cladding material	Type 304 SS	Type 304 SS
Cladding thickness	0.020 inches	0.020 inches

TRIGA® fuel is characterized by inherent safety, high fission product retention, and the demonstrated ability to withstand water quenching with no adverse reaction from temperatures to 2,102°F (1150°C). The inherent safety of this TRIGA® reactor has been demonstrated by the extensive experience acquired from similar TRIGA® systems throughout the world. This safety arises from the strongly negative prompt temperature coefficient that is characteristic of uranium-zirconium hydride fuel-moderator elements used in TRIGA® systems. As the fuel temperature increases, this coefficient immediately compensates for reactivity insertions. This results in a mechanism whereby reactor power excursions are terminated quickly and safely. The analyses that follow establish the safety limits for operation of the OSTR.

4.2 Reactor Core

The OSTR utilizes solid fuel elements, developed by General Atomics (GA), in which the zirconium hydride moderator is homogeneously combined with enriched uranium. The unique feature of these fuel-moderator elements is the prompt temperature coefficient of reactivity, which gives the TRIGA® reactor its built-in safety by automatically limiting the reactor power to a safe level in the event of a power excursion. The reactor core consists of a lattice of cylindrical stainless-steel-clad U-$ZrH_{1.6}$ fuel-moderator elements and aluminum-clad graphite dummy elements. The fuel-moderator elements have 3.5-inch-long graphite end sections that form the top and bottom reflector. Water occupies about one-third of the core volume.

Neutron reflection in the radial direction is provided by 10.2 inches of graphite in an aluminum container. The height of the graphite in the reflector is about 22 inches. Also in this container, at the outer perimeter, is 2 inches of lead which acts as a thermal shield to protect the concrete structure from excessive nuclear heating, and also contributes to reducing the dose outside the concrete shield.

The core components are contained between top and bottom aluminum grid plates. The top grid plate has [redacted] positions for fuel elements and control rods arranged in six concentric rings around a central thimble (used for high flux irradiations).

The power level of the TRIGA® reactor is accurately controlled with four control rods: a regulating rod, a shim rod, a safety rod, and a transient rod.

Four instrumentation channels monitor and indicate the reactor neutron flux and power level on the console. The bulk water temperature and the reactor tank outlet and inlet water temperatures are indicated on the console. The water conductivity, measured at the inlet and outlet of the demineralizer, is displayed on a panel near the console. In addition, primary reactor water is routinely monitored to identify any significant increase in radioactivity.

The reactor core is cooled by natural convection of the demineralized water in the reactor pool. A diffuser nozzle on the reactor tank inlet provides water discharge at a high velocity above the core. This water circulation pattern reduces the dose rate at the pool surface resulting from the ^{16}N formed in the coolant water as it passes through the core.

4.2.1 Reactor Fuel

The active part of each fuel-moderator element, shown in Fig. 4.1, is approximately 1.5 inches in diameter and 15 inches long. TRIGA® fuel is a solid, homogeneous mixture of uranium-zirconium hydride alloy containing from about [redacted] wt% to [redacted] wt% of uranium enriched from [redacted] to [redacted] in ^{235}U. The hydrogen-to-zirconium atom ratio is approximately 1.7 to 1.0. To facilitate hydriding, a 0.19-inch diameter hole is drilled through the center of the active fuel section; a zirconium rod is inserted in this hole after hydriding is complete.

Each element is clad in 0.020 inches of stainless steel, and all closures are made by heliarc welding. Two 3.5-inch sections of graphite are inserted in this can, one above and one below the fuel, to serve as top and bottom reflectors for the core. Stainless steel end fixtures are attached to both ends of the can, making the overall length of the fuel-moderator element approximately [redacted] inches.

The lower end fixture supports the fuel-moderator element on the bottom grid plate. The upper end fixture consists of a knob for attachment of the fuel handling tool and a triangular spacer, which permits cooling water to flow through the upper grid plate. The total weight of a fully loaded fuel element is about [redacted]

An instrumented fuel-moderator element has three thermocouples embedded in the fuel. The sensing tips of the fuel element thermocouples are located halfway between the outer radius and the vertical centerline at the center of the fuel section and 1 inch above and below the horizontal center. The thermocouple leadout wires pass through a seal contained in a stainless steel tube welded to the upper end fixture. This tube projects about 3 inches above the upper end of the element and is extended by two 10-foot lengths of tubing connected by unions to provide a watertight conduit carrying the leadout wires above the water surface in the reactor pool. In other respects, the instrumented fuel-moderator element is identical to the standard element.

The specific characteristics that make TRIGA®-type fuels uniquely suited for use in extremely safe research-type reactors are covered in detail in the following portions of this section. A summary of the characteristics is given below (Ref. 4.1, Ref. 4.2):

Figure 4.1 Typical TRIGA® Fuel Element Assembly

- $ZrH_{1.6}$ is single phase up to 1,200°F (649°C) [delta phase region];
- low hydrogen equilibrium disassociation pressure at normal fuel temperatures;
- high hydrogen retention;
- high heat capacity;
- low thermal expansion coefficient;
- relatively low reactivity in water;
- high fission product retention;
- very large negative prompt temperature coefficient of reactivity;
- high burnup possible by addition of burnable poison; and
- high loading of uranium possible with insignificant change in fuel material properties.

4.2.1.1 TRIGA® Fuel Development

The development and use of U-ZrH fuels for the TRIGA® reactor began at GA in 1957 and continues today. Over 6,000 fuel elements of 7 distinct types have been fabricated for the 60 TRIGA® research reactors in various countries around the world. The earliest of these has now passed 40 years of operation. U-ZrH fuel has exhibited unique safety features including a large negative prompt temperature coefficient of reactivity, high fission product retentivity, chemical stability when quenched from high temperatures in water, and dimensional stability over large swings of temperature. The first TRIGA® reactor to be exported was for the U.S. exhibit at the Second Geneva Conference on the Peaceful Uses of Atomic Energy in 1958.

The standard TRIGA® fuel contains [redacted] uranium [redacted] enriched) as a fine metallic dispersion in a zirconium hydride matrix. The H/Zr ratio is nominally 1.6 (in the face-centered cubic delta phase). The equilibrium hydrogen dissociation pressure is governed by the composition and temperature. For U-$ZrH_{1.6}$, the equilibrium hydrogen pressure is 1 atm at about 1,400°F (760°C). The single-phase, high-hydride composition eliminates the problems of density changes associated with phase changes and with thermal diffusion of the hydrogen. A highly-enriched version of TRIGA® fuel [redacted] with a [redacted] enrichment) contains up to about 3% erbium as a burnable poison in order to increase the core lifetime and also contribute to the large negative prompt temperature coefficient. The calculated core lifetime for [redacted] fuel in a typical TRIGA® reactor is approximately 9 MW-y. Over 25,000 pulses have been performed with the TRIGA® fuel elements at GA, with fuel temperatures reaching peaks of about 2,102°F (1,150°C).

TRIGA® fuel was developed around the concept of inherent safety. A core composition was sought which had a large negative prompt temperature coefficient of reactivity such that if all the available excess reactivity were suddenly inserted into the core, the resulting fuel temperature increase would automatically cause the power excursion to terminate before any core damage resulted. Experiments performed in the late 1950s demonstrated

that zirconium hydride possessed the basic mechanism needed to produce this desired characteristic (Ref. 4.1). Additional advantages were that ZrH has a good heat capacity, allowing construction of a reactor with a relatively small core size and high flux values due to the high-hydrogen content of the fuel rods, and could be used effectively to fabricate rugged fuel rods.

In early 1976, GA undertook the development of fuels containing up to [redacted]wt% uranium ([redacted]g U/cc) in order to allow the use of low-enriched uranium (LEU) (under[redacted] enrichment) to replace the highly-enriched fuels while maintaining long core life. The [redacted]wt% fuel contains a relatively modest [redacted] of uranium. These fuels were fabricated successfully, with the required hydrogen content and erbium loading. The structural features of the hydrated LEU fuel were similar to those of the well-proven [redacted] and [redacted]-wt% fuels, as shown by metallographic, electron microprobe analysis, and x-ray diffraction examination. Detailed evaluations of the new LEU fuel have shown that it performs essentially identically to the older standard TRIGA® fuel in all critical cores (Ref. 4.1).

Additional evaluations included analytical assessments of the prompt temperature coefficient of reactivity and the core lifetime (Table 4-2). Nuclear design and analytical studies have shown that the prompt temperature coefficient for the [redacted]wt% uranium fuel is essentially the same as that for standard fuel over the temperature range of interest [68° to 1,292°F (20° to 700°C)] and greater than that for the [redacted] fuel which it replaces. The prompt temperature coefficient for the more highly-loaded LEU fuel shows a small temperature dependence, whereas the coefficient is relatively constant for standard fuel. The value of the prompt temperature coefficient of reactivity is slightly lower for the [redacted] wt% uranium fuel compared to the highly-enriched fuel it replaces; however, it is still large and significantly higher than the prompt temperature coefficients for any other type of reactor fuel.

Table 4-2 Calculated Beginning of Life Prompt Temperature Coefficient (α_T) and Core Lifetime

TRIGA® Fuel Type	Uranium (wt%)	Erbium (wt%)	Uranium Enrichment (%)	α_T Average (23°-700°C)	Lifetime (MWd)
Standard	[redacted]	0.00	[redacted]	$-1X10^{-4}$	~100
[redacted]	[redacted]	1.58	[redacted]	$-1X10^{-4}$	3,500

Inclusion of erbium burnable poison in the TRIGA® LEU fuel has enabled core lifetimes of up to 3,000 MWd to be predicted for the [redacted]-wt% fuel. It is emphasized that this is the core life from the time of initial refueling to end of useful life.

4.2.1.2 Dissociation Pressures

The hydrogen dissociation pressures of hydrides have been shown to be comparable in the alloys containing up to 75 wt% U (Ref. 4.1). The concentration of hydrogen is generally reported in terms of either weight percent or atoms of H/cm^3 of fuel (N_H). In the delta phase region, the dissociation pressure equilibria of the zirconium-hydrogen binary mixture may be expressed in terms of composition and temperature by the relation:

$$\log P = K_1 + \frac{(K_2 \times 10^3)}{T},$$

where: $K_1 = -3.8415 + 38.6433\ X - 34.2639\ X^2 + 9.2821\ X^3$,
$K_2 = -31.2982 + 23.5741\ X - 6.0280\ X^2$,
P = pressure, atm,
T = temperature, K, and
X = hydrogen-to-zirconium atom ratio.

The higher-hydride compositions (H/Zr>1.5) are single-phase (delta or epsilon) and are not subject to thermal phase separation on thermal cycling. For $ZrH_{1.6}$, the equilibrium hydrogen dissociation pressure is 1 atm at about 1,400°F (760°C). The absence of a second phase in the higher hydrides eliminates the problem of large volume changes associated with a phase transformation at approximately 1,000°F (540°C) in the lower hydride compositions. Similarly, the absence of significant thermal diffusion of hydrogen in the higher hydrides precludes concomitant volume change and cracking. The clad material of stainless steel or nickel alloys provides a satisfactory diffusion barrier to hydrogen at long-term (several years) sustained cladding temperatures below about 570°F (300°C).

4.2.1.3 Hydrogen Migration

Under nonisothermal conditions, hydrogen migrates to lower-temperature regions from higher-temperature regions. The equilibrium dissociation pressure obtained when the redistribution is complete is lower than the dissociation pressure before redistribution. The dimensional changes of rods resulting from hydrogen migration are of minor importance in the delta and epsilon phases.

4.2.1.4 Hydrogen Retention

The rates of hydrogen loss through 250-μm-thick stainless steel cladding are low at cladding temperatures characteristic of TRIGA® fuel elements. A 1% loss of hydrogen per year occurs at about 930°F (500°C) clad temperature (Ref. 4.1).

4.2.1.5 Density

The density of ZrH decreases with an increase in the hydrogen content. The density change is quite high up to the delta phase (H/Zr = 1.5) and then changes little with further increases in hydrogen. The bulk density of massively-hydrided zirconium is reported to be about 2% lower than the results from x-ray defraction analysis (Ref. 4.1).

For TRIGA® fuel with a hydrogen-to-zirconium atom ratio of 1.6, the following relationships for the uranium density, $\rho_{U(A)}$, and weight fraction, ^{w}U, in the U-$ZrH_{1.6}$ alloy apply:

$$\rho_{U(A)} = \frac{^{w}U}{0.177 - 0.125\ ^{w}U}, \text{ and}$$

$$^{w}U = \frac{0.177\ \rho_{U(A)}}{1 + 0.125\ \rho_{U(A)}}.$$

The relationship between the uranium density and the volume fraction of uranium in the alloy is given by:

$$\rho_{U(A)} = 19.07\ V_f^{U(A)},$$

where: $V_f^{U(A)}$ = volume fraction of uranium in the U-$ZrH_{1.6}$ alloy.

4.2.1.6 Thermal Conductivity

Thermal conductivity measurements have been made over a range of temperatures. A problem in carrying out these measurements by conventional methods is the disturbing effect of hydrogen migration under the thermal gradients imposed on the specimens during the experiments. This has been minimized at GA by using a short-pulse heating technique to determine the thermal diffusivity and hence to permit calculation of the thermal conductivity. From measurements by GA of thermal diffusivity coupled with the data on density and specific heat, the thermal conductivity of uranium-zirconium hydride with an H/Zr ratio of 1.6 is 0.042 ±0.002 cal/sec-cm-°C and is insensitive both to the weight fraction of uranium and to the temperature.

4.2.1.7 Volumetric Specific Heat

The volumetric specific heat of zirconium hydride TRIGA® fuel is a function of temperature and composition (Ref. 4.1). The volumetric specific heat of [redacted] wt% U-$ZrH_{1.6}$

is calculated to be

$$C_P = 2.04 + 4.17 \times 10^{-3} T \text{ (W-sec cm}^{-3}\text{) °C (from 0 °C)}$$

and for [redacted] wt% U-$ZrH_{1.6}$ is calculated to be

$$C_P = 2.17 + 4.36 \times 10^{-3} T \text{ (W-sec cm}^{-3}\text{) °C (from 0 °C).}$$

4.2.1.8 Chemical Reactivity

Zirconium hydride has a relatively low reactivity in water, steam, and air at temperatures up to about 1,112°F (600°C). Zirconium hydride has been heated in air for extended periods of time at temperatures up to 1,112°F (600°C) with negligible loss of hydrogen (Ref. 4.1). An oxide film forms which inhibits the loss of hydrogen.

The hydride fuel has excellent corrosion resistance in water. Bare fuel specimens have been subjected to a pressurized water environment at 570°F (299°C) and 1,230 psi during a 400-hour period in an autoclave. The average corrosion rate was 350 mg/cm^2-month weight gain, accompanied by a conversion of the surface layer of the hydride to an adherent oxide film. The maximum extent of corrosion penetration after 400 hours was less than 2 mils.

In the early phases of development of the TRIGA® fuel, water-quench tests were carried out from elevated temperatures. Fuel rods (1-inch dia) were heated to 1,470°F (800°C) and end-quenched to test for thermal shock and corrosion resistance. No deleterious effects were observed. Also, a 6-mm diameter fuel rod was heated electrically to about 1,470°F (800°C) and a rapid stream of water was sprayed on it; no significant reaction was observed. Small and large samples were heated to 1,650°F (900°C) and quenched in water; the only effect observed was a slight surface discoloration. Finely-divided U-ZrH powder was heated to 570°F (300°C) and quenched to 175°F (80°C) in water; no reaction was observed. Later, these tests were extended to temperatures as high as 2,200°F (1,200°C), in which tapered fuel rods were dropped into tapered aluminum cans in water. Although the samples cracked and lost hydrogen, no safety problems arose in these tests.

Low-enriched TRIGA® fuels have been subjected to water-quench safety tests at GA. Quench tests were performed on [redacted]%-enriched TRIGA® fuel samples ([redacted] wt% uranium, [redacted] wt% zirconium, [redacted] wt% erbium, [redacted] wt% hydrogen) to simulate cladding rupture and water ingress into the TRIGA® reactor fuel rods during operation.

These results indicate satisfactory behavior of TRIGA® fuel for temperatures to at least 2,200°F (1,200°C). Under conditions where the clad temperature can approach the fuel temperature for several minutes (which may allow formation of eutectics with the clad), the

results indicate satisfactory behavior to about 1,925°F (1,050°C). This is still about 125° to 210°F (50° to 100°C) higher than the temperature at which internal hydrogen pressure is expected to rupture the clad, should the clad temperature approach that of the fuel. It should be pointed out that thermocouples have performed well in instrumented TRIGA® fuel elements at temperatures up to 1,200°F (650°C) in long-term steady-state operations, and up to 2,100°F (1,150°C) in very short-time pulse tests.

4.2.1.9 Irradiation Effects

Most of the irradiation experience to date has been with the uranium-zirconium hydride fuels used in the Space Nuclear Auxiliary Power (SNAP) Program (containing about 10 wt% uranium) and TRIGA® reactors. The presence of uranium influences the radiation effects because of the damage resulting from fission recoils and fission gases. Some significant conclusions may be drawn from the results of these experiments (Ref. 4.1). The uranium is present as a fine dispersal (about 1 μm-dia) in the U-ZrH fuels, and hence the recoil damage is limited to small regions within the short (~10-μm) range of the fission recoils. The U-ZrH fuel exhibits high growth rate during initial operation, the so-called "offset" growth period, which has been ascribed to the vacancy-condensation type of growth phenomenon over the temperature range where voids are stable.

The swelling of the U-ZrH fuels at high burnups is governed by three basic mechanisms:

- the accommodation of solid fission products resulting from fission of ^{235}U. This growth is approximately 3% $\Delta V/V$ per metal atom % burnup. This mechanism is relatively temperature insensitive;

- the agglomeration of fission gases at elevated temperatures [above 1,300°F (750°C)]. This takes place by diffusion of the xenon and krypton to form gas bubbles; and

- a saturable cavity nucleation phenomenon which results from the nucleation and growth of irradiation-formed vacancies into voids over a certain range of temperatures where the voids are stable. The saturation growth by this mechanism was termed offset swelling. This was deduced from the rapid decrease in fuel-to-cladding ΔT experienced during the early part of the irradiation. The saturation was reached in approximately 1,500 hours.

Burnup tests performed by GA have shown that TRIGA® fuels may successfully be used without significant fuel degradation to burnups in excess of 50% of the contained ^{235}U.

4.2.1.10 Erbium Additions

All available evidence and extensive operating experience indicate that the addition of erbium to the U-ZrH introduces no deleterious effects to the fuel (Ref. 4.1). Erbium has a high boiling point and a relatively low vapor pressure so that it can be melted into the uranium-zirconium uniformly. The erbium is incorporated into the fuel during the melting process. All the analyses that have been made on the alloy show that the erbium is dispersed uniformly, much as is the uranium. Erbium is a metal and forms a metallic solution with the uranium zirconium; thus there is no reason to believe that there will be any segregation of the erbium. Erbium forms a stable hydride (as stable as zirconium hydride) which also indicates that the erbium will remain uniformly dispersed through the alloy. Also, since neutron capture in erbium is an (n-γ) reaction, there are no recoil products.

4.2.1.11 Prompt Temperature Coefficient of Reactivity

The basic parameter which provides the TRIGA® reactor system with a large safety factor in steady-state operation and under transient conditions is the rather constant prompt temperature coefficient of reactivity (α_T). This temperature coefficient, which is a function of the fuel composition and core geometry, allows great freedom in steady-state operation since the effect of accidental reactivity changes occurring from experimental devices in the core is minimized (Ref. 4.1).

The prompt temperature coefficient of reactivity for TRIGA® fuels is based on the neutron spectrum hardening characteristic that occurs in a zirconium hydride fuel. The spectrum hardening is caused by heating of the fuel-moderator elements. The rise in temperature of the hydride increases the probability that a thermal neutron in the fuel element will gain energy from an excited state of an oscillating hydrogen atom in the lattice. As the neutrons gain energy from the ZrH, the thermal neutron spectrum in the fuel element shifts to a higher average energy (the spectrum is hardened), and the mean free path for neutrons in the element is increased appreciably. For a standard TRIGA® element, the average chord length is comparable to a mean free path, and the probability of escape from the element before being captured is significantly increased as the fuel temperature is raised. In the water, the neutrons are rapidly rethermalized so that the capture and escape probabilities are relatively insensitive to the energy with which the neutron enters the water. The heating of the moderator mixed with the fuel in a standard TRIGA® element thus causes the spectrum to harden more in the fuel than in the water. As a result, there is a temperature-dependent disadvantage factor for the unit cell in which the ratio of absorptions in the fuel to total cell absorptions decreases as fuel element temperature is increased. This brings about a shift in the core neutron balance, giving a loss of reactivity.

In the TRIGA® [redacted] and LEU fuel, the temperature-hardened spectrum is used to decrease

the fuel's reactivity through its interactions with a low-energy resonance material. Thus, erbium, with its double resonance at ~0.5eV, is used in the TRIGA® [redacted] and LEU fuels as both a burnable poison and a material to enhance α_T. The ratio of the absorption probability to the neutron leakage probability is increased for TRIGA® [redacted] and LEU fuel relative to the standard TRIGA® fuel because the ^{235}U density in the fuel rod is greater and also because of the use of erbium. When the fuel-moderator material is heated, the neutron spectrum is hardened, and the neutrons have an increasing probability of being captured by the low-energy resonance in erbium. This increased parasitic absorption with temperature causes the fuel's reactivity to decrease as the fuel temperature increases. The neutron spectrum shift pushes more of the thermal neutrons into the ^{167}Er resonance as the fuel temperature increases. As with a standard TRIGA® core, α_T is prompt because the fuel is intimately mixed with a large portion of the moderator; thus, fuel and solid moderator temperatures rise simultaneously, producing the temperature-dependent spectrum shift.

For reasons just discussed, more than 50% of α_T for a standard TRIGA® core comes from the temperature-dependent disadvantage factor, or cell effect, and ~20% each from Doppler broadening of the ^{238}U resonances and temperature-dependent leakage from the core. These effects produce a α_T of $\sim -1.0 \times 10^{-4}$ $\Delta k/k\text{-}°C$, which is essentially constant with temperature. On the other hand, for a TRIGA® [redacted] and LEU core, the effect of cell structure on α_T is smaller. Over the temperature range 75° to 1,300°F (23° to 700°C), about 70% of the coefficient comes from temperature-dependent changes in the parasitic absorption in the ^{167}Er in the core, and more than half of this effect is independent of the cell structure. Most of the remaining component of α_T is due to Doppler broadening of the ^{238}U resonances. Over the temperature range 75° to 1,300°F (23° to 700°C), α_T for [redacted] fuel with [redacted] wt% and [redacted] enrichment in ^{235}U is about -1.5×10^{-4} $\Delta k/k\text{-}°C$ and for TRIGA® LEU fuel with [redacted] wt% and [redacted] enrichment in ^{235}U is about -1.07×10^{-4} $\Delta k/k\text{-}°C$, thus being somewhat greater than the value for standard TRIGA® fuel. The temperature coefficients of fuels containing ^{167}Er as a burnable poison are somewhat temperature dependent.

4.2.1.12 Fission Product Retention

A number of experiments have been performed to determine the extent to which fission products are retained by U-ZrH (TRIGA®) fuel. Experiments on fuel with a uranium density of [redacted] g/cm^3 [redacted] wt% U) were conducted over a period of 11 years and under a variety of conditions (Ref. 4.3). Results prove that only a small fraction of the fission products are released, even in completely unclad U-ZrH fuel. The release fraction varies from 1.5×10^{-5} for an irradiation temperature of 660°F (350°C) to $\sim 10^{-2}$ at 1,475°F (800°C).

The experiments show that there are two mechanisms involved in the release of fission products from U-ZrH fuel, each of which is dominant over a different temperature range.

The first mechanism is that of fission fragment recoil into the gap between the fuel and clad. This effect predominates in fuel at temperatures up to ~750°F (400°C); the recoil release rate is dependent on the fuel surface-to-volume ratio but is independent of fuel temperature. Above ~750°F (400°C), the controlling mechanism for fission product release from U-ZrH fuel is a diffusion-like process, and the amount released is dependent on the fuel temperature, the fuel surface-to-volume ratio, the time of irradiation, and the isotope half-life.

The results of the U-ZrH experiments, and measurements by others of fission product release from Space Nuclear Auxiliary Power (SNAP) Program fuel, have been compared and found to be in good agreement.

The fractional release, ϕ, of fission product gases into the gap between fuel and clad from a full-size standard U-ZrH fuel element is given by:

$$\phi = 1.5 \times 10^{-5} + 3.6 \times 10^{3} e^{-\frac{1.34 \times 10^{4}}{(T+273)}}$$

where T = fuel temperature (0 - 1600 °C). This relationship has also been found to apply to LEU TRIGA® fuels (Ref. 4.2). The first term of this function is a constant for low-temperature release; the second term is the high-temperature portion.

The function given above applies to a fuel element which has been irradiated for a time sufficiently long that all fission product activity is at equilibrium. Actual measured values of fractional releases fall well below that calculated by the function given above. Therefore, for safety considerations, this function gives conservative values for the high-temperature release from U-ZrH fuel.

Studies in the TRIGA® reactor at GA on fission product release from fuel elements with high uranium loadings (up to [redacted] g U/cm^3, [redacted] wt% U) agree well with data from older similar experiments with lower U loadings. As with the lower U loadings, the release was determined to be predominantly recoil-controlled at temperatures ≤750°F (400°C) and controlled by a migration or diffusion-like process above 750°F (400°C). Low-temperature release appears to be independent of uranium loadings, but the high-temperature release seems to decrease with increasing weight-fractions of uranium. The correlation used to calculate the release of fission products from TRIGA® fuel remains applicable for the high uranium loaded (TRIGA® LEU) fuel as well as the [redacted]-wt% U-ZrH fuel for which it was originally derived. This correlation predicts higher fission product releases than measurements would indicate up to 2,010°F (1,100°C). At normal TRIGA® operating temperatures [<1,380°F (750°C)], there is a safety factor of approximately four between predicted and experimentally determined values.

4.2.2 Control Rods

Three motor-driven control rods (1 regulating, 1 shim and 1 safety) and one pneumatic electro-mechanical safety transient rod control the reactor power. The transient rod, located in the C-ring, contains a solid rod of boron-carbide-impregnated graphite as a neutron poison. The transient rod assembly is about [redacted] inches long and is clad in a [redacted]-inch O.D. aluminum tube. The borated graphite poison section is [redacted] inches long. The transient rod has an air-filled follower about [redacted] inches long. The transient rod is guided laterally in the core by a thin-walled aluminum guide tube that passes through the upper and lower grid plates and is screwed into, and supported by, the aluminum safety plate beneath the lower grid.

The fuel-followed safety, shim and regulating rods, located in the D-ring, D-ring, and C-ring, respectively, pass through, and are guided by, 1½-inch-diameter holes in the top and bottom grid plates. The rod exterior cladding is a sealed stainless steel tube approximately [redacted] inches long by [redacted] inches in diameter. A standard control rod is illustrated both withdrawn and inserted in Fig. 4.2. The upper section of the rod is graphite and the next [redacted] inches is the neutron absorber (graphite impregnated with powdered boron carbide). The follower section consists of [redacted] inches of U-$ZrH_{1.6}$ fuel, and the bottom section has [redacted] inches of graphite. An aluminum safety plate attached to the shroud beneath the lower grid plate prevents the possibility of a control rod, accidentally disconnected from its drive, from dropping out of the core.

Vertical travel of the control rods is approximately [redacted] inches. The nominal rod worths of the transient rod, regulating rod, shim rod, and safety rod are about $4.00 (2.60% δk/k), $2.70 (1.76% δk/k), $2.70 (1.76% δk/k), and $2.70 (1.76% δk/k), respectively. That makes the total rod worth about $12.10 (7.87% δk/k). The total excess reactivity in the core does not normally exceed $7.50 (4.88% δk/k). The maximum possible reactivity insertion rate associated with the withdrawal of any rod except the transient rod is approximately $ .214 (0.15% δk/k) per second.

Figure 4.2 Typical Fuel-Follower-Type Control Rod Shown Withdrawn and Inserted

The transient control rod drive is mounted on a steel frame that bolts to the center channel cover plate. Two steel covers keep the mechanism clean. From zero to a maximum of [redacted] inches of rod may be withdrawn from the core; however, [redacted]

A system of limit switches similar to that used with the standard control rod drives is used to indicate the position of the air cylinder and the transient rod. Two of these switches, the DRIVE UP and DRIVE DOWN switches, are actuated by a small bar attached to the bottom of the air cylinder. A third limit switch, the ROD DOWN switch, is actuated when the piston reaches its lower limit of travel. A 10-turn potentiometer driven by the motor shaft controls the position indicator on the console.

4.2.3 Neutron Moderator and Reflector

The reflector is a ring-shaped block of graphite that surrounds the core radially. The graphite is [redacted] inches thick radially, with an inside diameter of [redacted] inches (below the Lazy Susan) and a height of [redacted] inches. The graphite is protected from water penetration by a leak-tight welded aluminum can.

A "well" in the top of the graphite reflector is provided for the rotary specimen rack. This well is also aluminum-lined, the lining being an integral part of the aluminum reflector can. The rotary specimen rack is a self-contained unit and does not penetrate the sealed reflector at any point.

A 2-inch-thick lead thermal shield is located at the periphery of the reflector in the region adjacent to the water. The lead has been flame-sprayed with a molybdenum coating on the inner surface of the aluminum can to assure a good bond for the transfer to the surrounding water of the heat deposited by gamma rays in the lead.

The graphite, lead, and the outer surface of the aluminum can are pierced by an aluminum tube which forms the inner section of the piercing radial beamport. Two additional holes penetrate the graphite and lead; one for a radial beamport and one for the tangential beamport. These holes do not pierce the aluminum can. The tangential beamport terminates outside the reflector can and abuts against the graphite reflector.

4.2.4 Neutron Startup Source

A 3 Curie americium beryllium (^{241}Am-Be) neutron source is used in the OSTR core. The neutron source holder is made of aluminum, is cylindrical in shape, and has a cavity to hold the source. The source holder can be installed in any vacant fuel or graphite element location. A shoulder at the upper end of the holder supports the assembly on the upper grid plate, with the rod itself, which contains the source, extending down into the core region. The neutron source is contained in a cavity in the lower portion of the rod assembly at the [redacted]. This cylindrical cavity is [redacted] in diameter and approximately [redacted] deep. The upper and lower portions are screwed together. A soft aluminum ring provides sealing against water leakage into the cavity. Since the upper end fixture of the source holder is similar to that of the fuel element, the source holder can be installed or removed [redacted]. In addition, the upper end fixture has a small hole through which one end of a stainless steel wire may be inserted to facilitate handling operation from the top of the tank.

4.2.5 Core Support Structure

The reflector assembly rests on an aluminum platform at the bottom of the tank, and provides the support for the two grid plates and the safety plate. Four lugs are provided for lifting the assembly.

The top grid plate is an aluminum plate 5/8 inches thick (3/8 inches thick in the central region) that provides accurate lateral positioning for the core components. The plate is supported by a ring welded to the top inside surface of the reflector container and is anodized to resist wear and corrosion.

[redacted] in diameter, are drilled into the top grid plate in six circular bands around a central hole to locate the [redacted] the control rods and guide tubes, and the pneumatic transfer tube (See Fig. 4.3). A [redacted] diameter center hole accommodates the central thimble. Small holes at various positions in the top grid plate permit insertion of foils into the core to obtain flux data.

A hexagonal section can be removed from the center of the upper grid plate for the insertion of specimens up to 4.4 inches in diameter into the region of highest flux; this requires prior relocation of the six fuel elements from the B ring to the outer portion of the core and removal of the central thimble.

Two generally triangular-shaped sections are cut out of the upper grid plate. Each encompasses two E and one D ring positions. When fuel elements are placed in these locations, their lateral support is provided by a special fixture. When the fuel elements and support are removed, there is room for inserting specimens up to 2.4 inches in diameter.

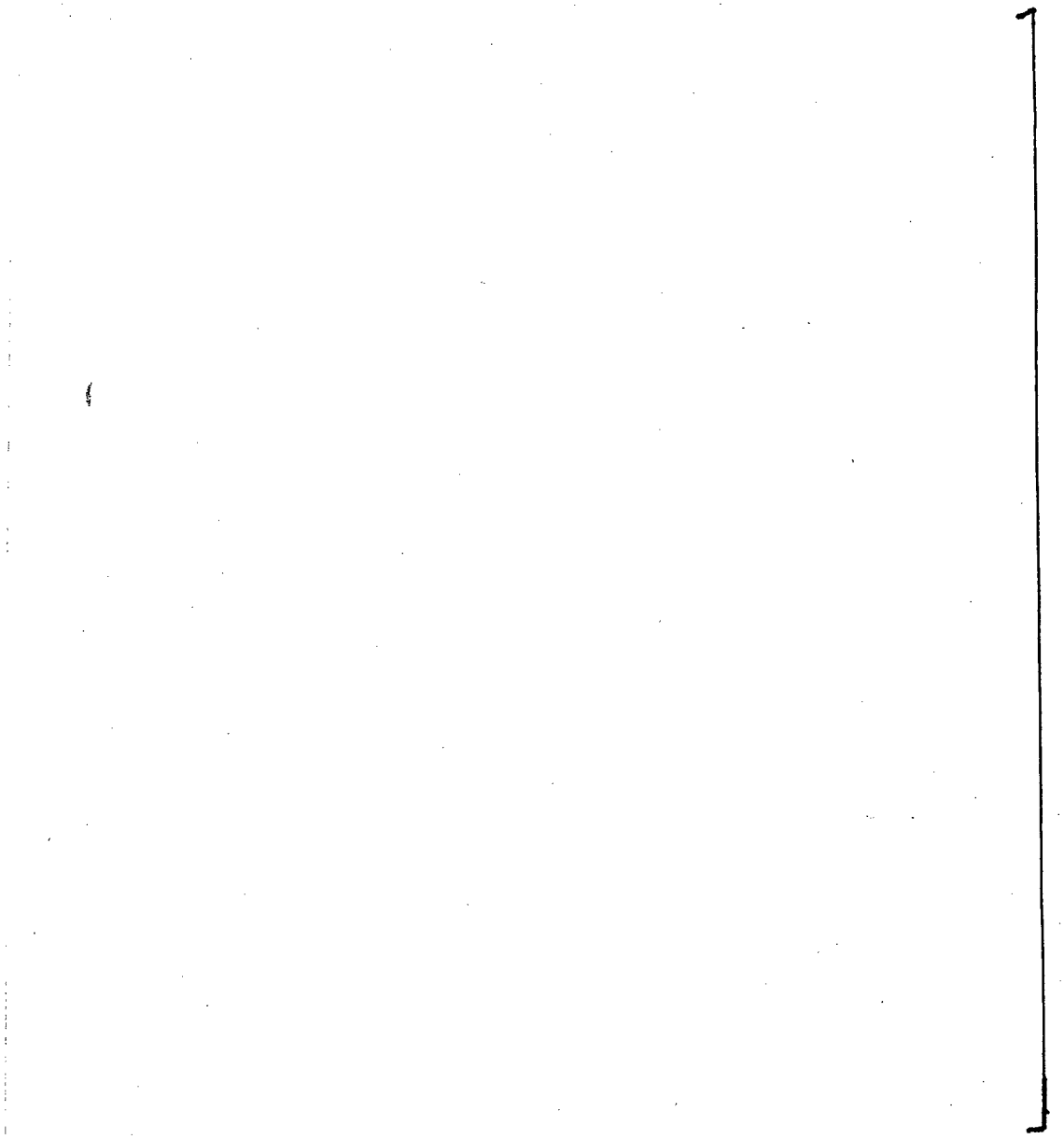

Figure 4.3 Top Grid Plate and Typical Core Configuration

C07

Two ⅜-inch diameter holes between the F and G rings of the grid plate locate and provide support for the source holder at alternate positions.

The differential area between the triangular-shaped spacer blocks at the top of the fuel element and the round holes in the top grid plate permit passage of cooling water through the plate.

The bottom grid plate is an aluminum plate ¾ of an inch thick which supports the entire weight of the core and provides accurate spacing between the fuel-moderator elements. Six pads are welded to a ring which is, in turn, welded to the reflector container support the bottom grid plate.

Holes in the bottom grid plate are aligned with fuel element holes in the top grid plate. They are countersunk to receive the adaptor end of the fuel-moderator elements and the adaptor end of the pneumatic transfer tube.

A central hole [redacted] inches in diameter in the lower grid serves as a clearance hole for the central thimble. Eight additional [redacted]-inch-diameter holes are aligned with upper grid plate holes to provide passage of fuel-follower control rods. Those holes in the bottom grid plate not occupied by control rod followers are plugged with removable fuel element adaptors that rest on the safety plate. These fuel element adaptors are solid aluminum cylinders [redacted] inches in diameter by [redacted] inches long. At the lower end is a fitting that is accommodated by a hole in the safety plate. The upper end of the cylinder is flush with the upper surface of the bottom grid plate when the adaptor is in place. This end of the adaptor has a hole similar to that in the bottom grid plate for accepting the fuel element lower end fitting. With the adaptor in place, a position formerly occupied by a control rod with a fuel follower will now accept a standard fuel element. The adaptor can be removed with a special handling tool.

The safety plate is provided to preclude the possibility of control rods falling out of the core. It is a ½-inch-thick plate of aluminum welded to the extension of the inner reflector liner and placed about [redacted] inches below the bottom grid plate.

4.3 Reactor Tank or Pool

The reactor core is located at the bottom of an aluminum tank, which is in the center of the concrete shield structure described in Section 4.4. The tank has an outside diameter of [redacted], a depth of [redacted], and a minimum thickness of 1/4 inch.

The aluminum tank was manufactured to accommodate the four beamports, the thermal

column, and the thermalizing column in that the tank sections for these facilities are welded to and are an integral part of the aluminum tank.

The inner sections for the facilities have continuous welded joints, and the integrity of the joints was verified by X-ray testing, pressure testing, dye penetrant checking, and soap-bubble leak testing. For corrosion protection from the concrete, the outside of the tank is coated with an adhesive primer followed by several layers of polyethylene tape.

The reactor tank is filled with demineralized water to provide approximately 16 feet of shielding water above the top of the reflector. The tank holds about 5,000 gallons of demineralized water; however, the reactor components displace approximately 400 gallons. Therefore, the net water volume of the tank is about 4,600 gallons. The tank water temperature is generally maintained significantly below 120°F (49°C) because of thermal stress considerations.

The top of the reactor tank is closed by hinged aluminum grating covers. A sheet of Lucite plastic is inserted into the bottom of each grating section to prevent the entry of foreign matter into the tank while still permitting visual observation of the reactor. (The plastic sheets are easily removed for cleaning.) A gap around the perimeter of the plastic and some holes in the plastic permit adequate venting of the small quantities of hydrogen gas which may be released during reactor operations. The reactor tank covers are designed to support only the weight of people who are walking and working over the reactor. Therefore, heavy equipment or isotope casks will not be placed on these tank covers.

Support for the central thimble, rotating rack irradiation facilities, control-rod drive mechanisms, and the tank covers is provided by the center channel assembly. This assembly is placed over the top of the reactor tank and consists of two structural steel channels with steel cover plates. The center channel assembly is designed to support a shielded isotope cask weighing 3½ tons, when placed over the rotating rack access opening.

4.4 Biological Shield

The steel-reinforced concrete shield structure extends about 21 feet above the reactor room floor. In elevation, the shield structure is stepped so that the shielding around the core is much thicker than the shielding above the core.

The bulk-shielding experimental tank, which is [redacted] feet wide by [redacted] feet long and [redacted] feet deep, is located on the west side of the lower part of the reactor structure. (The pool volume holds [redacted] gallons of demineralized water.)

The shield structure provides about [redacted] of concrete in the radial direction from the core.

The concrete shield is pierced radially by the beamports, the thermal column, and the thermalizing column.

Embedded in the concrete are small vent pipes that lead from the thermal column, thermalizing column, and each of the beamports to a manifold which is mounted on the northwest side of the shield structure. An additional vent line from the rotating rack loading tube is also attached to the manifold. An exhaust line connects the manifold to the building ventilation exhaust system. This manifold arrangement permits the purging of ^{41}Ar and other radioactive gases from the thermal column, thermalizing column, and beamports and rotating rack.

The core is shielded radially by (1) ~ of graphite reflector, (2) of lead (inside the reflector can), (3) ~ of water, and (4) of concrete.

4.5 Nuclear Design

The reactor design bases are established by the maximum operational capability for the fuel elements and configuration described in this report. The TRIGA® reactor system has three major areas which are used to define the reactor design bases:

- fuel temperature,
- prompt temperature coefficient, and
- reactor power.

The ultimate safety limit is based on fuel temperature, while the strongly negative temperature coefficient of reactivity contributes to the inherent safety of the TRIGA® reactor. A limit on reactor power is set to ensure operation below the fuel temperature safety limit.

4.5.1 Normal Operating Conditions

Criticality was attained in the GA TRIGA® Mark I reactor with 54 standard (w% enriched) TRIGA® fuel elements ^{235}U) and four water-filled control rod positions. The critical mass for the Advanced TRIGA® Prototype was standard TRIGA® fuel elements ^{235}U) with three fuel followers and one transient rod without a follower. (Fuel followers on control rods are not counted as fuel elements.)

For the GA TRIGA® Mark III reactor, the critical mass was standard TRIGA® fuel elements ^{235}U) using an "A" ring element and four fuel followers. Changes in critical mass occurred with varying control rod configurations and follower materials. Tolerances in the manufacture of the fuel elements (hydrogen and uranium content) also contributed a variance of about ±3% in the critical mass of any given system.

The reflector materials around the core and the absence or presence of graphite reflector elements in empty fuel positions also affected the critical mass rather strongly. Replacing the graphite with a water reflector on the TRIGA® Mark I raised the critical mass about 25%; while placing a row of graphite reflector elements around the water-reflected core cut this difference approximately in half.

4.5.1.1 Critical Mass of the OSTR Using Standard [redacted]% Enriched Fuel

Criticality of the Oregon State TRIGA® was achieved on 8 March, 1967 with [redacted] standard TRIGA® fuel elements and two fuel follower control rods [redacted] ^{235}U). Also in the core was one transient rod with an air (void) follower and [redacted] elements arranged in the "F" ring. The critical configuration resulted in a core excess of [redacted]

4.5.1.2 Critical Mass of the OSTR Using [redacted] Enriched Fuel

Criticality of the upgraded OSTR using [redacted] fuel was attained on 7 August, 1976 with [redacted] TRIGA® fuel elements and three fuel follower control rods [redacted] ^{235}U). The same air follower transient rod was used and the [redacted] elements were placed in the "G" ring. This critical configuration resulted in a core excess of [redacted]

4.5.1.3 Final Core Loading for the Operational 70% Enriched OSTR Core

The operational [redacted] core was finalized on 10 August, 1976 and consisted of [redacted] fuel elements, [redacted] fuel follower control rods, and [redacted] elements in the "G" ring. This core configuration consisted of [redacted] ^{235}U with a core excess of [redacted] The total rod worth was $11.73.

4.5.1.4 Fuel Description

The fuel used in the OSTR core has been both standard TRIGA® and [redacted] fuel elements. The two types of elements are identical in geometry and differ physically only in ^{235}U enrichment, burnable poison content, and the hydrogen to zirconium ratio. It is possible to visually distinguish the element types, however, by the markings on the upper end fixture of the [redacted] fuel. Table 4-1 lists the principal design parameters of [redacted] and Standard TRIGA® elements.

4.5.1.5 Calculated Power Per [redacted] Element

Described in section 4.5.2.2, the power density was calculated using a OSU computer code called DIF. Results of this calculation are listed in Table 4-3. Note that the highest power density occurs in the "B" ring, as expected. The instrumented fuel element, therefore, is

located in the "B"ring. The effect of the graphite elements in the outer ring is to slightly increase the power density in the outer fueled rings and to slightly reduce the power density in the inner fueled rings. This again is expected as part of the reflector flux peaking discussed in earlier sections.

Table 4-4 lists the maximum, minimum, and the average power per element, along with ratios of the maximum-to-minimum power and the maximum-to-average power per element.

Table 4-3
Average Power per Element for [redacted] Fuel at 1 MW

B Ring (kW/element)	C Ring (kW/element)	D Ring (kW/element)	E Ring (kW/element)	F Ring (kW/element)
15.85	14.68	12.63	9.99	9.22

Table 4-4
Calculated Maximum, Minimum and Average Power per Element [redacted]

Maximum Power per Element P_{max} (kW/element)	Minimum Power per Element P_{min} (kW/element)	Average Power per Element P_{avg} (kW/element)	$\frac{P_{max}}{P_{min}}$	$\frac{P_{max}}{P_{ave}}$
15.85	9.22	11.24	1.72	1.41

4.5.1.6 Loss of Coolant Accident[redacted]

If the reactor pool is accidentally drained of water, the fission product decay heat will be removed primarily by natural convection of air. If the decay heat production is sufficiently low or if there is a long enough interval between reactor shutdown and coolant loss, the convective cooling by air will be enough to maintain the fuel at a temperature which will not damage the fuel elements. Texas A&M University analyzed this accident and arrived at the following results (Ref. 4.4):

- demonstration that standard fuel suspended in air can tolerate temperatures as high as 1,650°F (900°C) without damage to the clad [For [redacted] fuel, this value is 1,720°F (938°C)];
- this temperature is not exceeded under the conditions of coolant loss if the maximum thermal power in an element is equal to or less than 21 kW for standard fuel and 24 kW for [redacted] fuel even if the reactor is operated for an infinite time prior to the accident; and
- if reactor operations are limited to 70 MWh per week, power levels up to 24 kW/element for standard fuel and 28 kW/element for [redacted] fuel will not cause element damage in the event of loss of coolant.

Calculations by GA on the Torrey Pines Mark III reactor yielded similar results (Ref. 4.5):

- After prolonged operation at 2,000 kW (about 32 kW per element), an instantaneous loss of water would produce a maximum fuel temperature of about 920°F (490°C), well below the temperature necessary to cause any failure of the cladding.

It can be seen from Table 4-4 that the maximum power level expected in the OSTR is less than 17 kW per element. Also the operation of the OSTR in excess of 70 MWh per week is not foreseen. (Typical averages are [redacted] per week.) Therefore, with the maximum expected power level in the OSTR core of less than 17 kW per element and a conservative prediction of a limiting element power of 24 kW, there is a substantial margin of safety against cladding failure and subsequent release of fission products in the event of a loss of cooling accident.

4.5.2 Reactor Core Physics Parameters

4.5.2.1 Core Description

The OSTR has a circular grid pattern, thus a simple way to identify core loadings is by reference to specific rings (A through G) in the core and the loadings within each ring. Three core loadings which have actually been used are given in Table 4-5. Core #1 was

the initial just-critical core in March, 1967, core #2 was the first operational core in March, 1967, and core #2A was the core configuration in use prior to conversion to [redacted] fuel (Dec. 1974).

Six different possible core configurations were initially examined for the introduction of [redacted] fuel. These cores ranged from various mixed standard [redacted] cores to full [redacted] cores. These six core loadings are given in Table 4-6.

For all six cores the water-filled central thimble is replaced by an aluminum-filled central thimble to avoid flux-peaking problems. The aluminum slug inserted into the central thimble extends over the entire length of the core up to the upper grid plate. An alternate aluminum slug was considered, which is identical in its dimensions to the first one except for a 3/8 inch diameter central hole extending down the entire axis of the slug thus permitting insertion of small samples and/or radiation detectors. The effect of the hole has been analyzed and found negligible (reactivity worth less than $0.10 as compared to solid slug, increase in power density in B ring less than 1%). There are 3 [redacted] fuel-follower control rods in the C and D rings and 1 void-follower control rod (transient rod) in the C ring for all 6 cores. This arrangement matched the earlier Standard OSTR cores, except that [redacted] fuel-followers replaced the standard-fuel-followers as the three control rods. In all 6 cores, an instrumented [redacted] element is located in the B ring, where the highest fuel temperature is expected; this element replaces the instrumented standard element in the B ring of the LEU core.

In all cores, only [redacted] elements are located in the B through D rings. Whenever mixed cores are considered (cores #3 through #6), the [redacted] elements are always located [redacted] Cores #3 and #4, containing only [redacted] would be marginally critical with very low excess reactivity; they are thus not very realistic operational cores, but are included here for completeness. This calculation was also considered realistic since initial receipt of [redacted] fuel only allowed placement of [redacted] fuel out to and including the E-ring.

Table 4-5
Previous OSTR Core Loadings

Table 4-6
Possible OSTR Core Loadings For Mixed Standard [redacted] Cores and Full [redacted] Cores

Cores #5 and #6 are realistic, operational mixed cores. They each contain [redacted] total fuel elements, almost equal to the OSTR LEU loading of [redacted] elements. Standard elements are located outside of the [redacted] region.

Cores #7 and #8 are full [redacted] cores, again containing [redacted] total elements. These cores are representative of the nominal OSTR [redacted] core.

OSU feels that these six cores exhibit the complete spectrum of potential core configurations beyond a typical standard core, ranging from various mixed cores to full-[redacted] cores. Analyses performed on these six cores thus yield values of significant parameters which are representative of future OSTR core loadings.

4.5.2.2 Calculational Methods and Verification

The basic calculations were performed by an OSU computer code called DIF, which is a multigroup, one-dimensional, multiregion diffusion theory code. For these OSTR calculations, 7 energy groups and 11 regions were used. Seven energy groups were chosen so as to correspond to the basic cross section input data (Ref. 4.6) from GA (7-group data). The 11 regions were chosen as follows: 1 region for each core ring (A through G), 3 regions in the graphite reflector, and an outer water reflector region.

Basic input data, such as cross sections, number densities, basic cell data, and axial bucklings, were obtained from GA (Ref. 4.6) since they have been verified by experimental data. Dimensions of each region and volume fractions of the various components in each region were determined for the OSTR core.

The preparation of input data (microscopic cross sections, etc.) for DIF from microscopic cross sections, compositions, etc., was accomplished by another program (DATA PROC) written for this purpose.

To test the accuracy of the input data and to ensure that the results obtained using DIF are meaningful, comparisons were made between certain experimentally-determined parameters and calculated results from corresponding analyses. Three particular cases were used to show the validity of the code. Two of these involved cases for which GA also had performed calculations. Both of these were calculations of the infinite multiplication factor, k_∞, at two different temperatures; one case was for a core of all standard fuel, the other for an all-[redacted] core. The results are given in Table 4-7. As can be seen from the table, the agreement between the OSU calculations and the GA calculations is excellent: less than 0.5% difference in all cases and about 0.1% difference in three of the four cases.

Table 4-7
Comparison of Calculated k_∞ Values: OSU and GA

Type Fuel	Temperature	k_∞		% Difference in k_∞
		OSU	GA	
Standard	23° C	1.3975	1.3905	0.50%
	400° C	1.3526	1.3545	0.14%
[redacted]	23° C	1.3483	1.3495	0.09%
	700° C	1.2578	1.2589	0.09%

The third test was a comparison of measured and calculated values of k_{eff} for two different OSTR cores. The cores chosen were cores #1 and #2 of Table 4-5. The results are given in Table 4-8. The results are again excellent, with less than 0.5% difference in both cases.

Table 4-8
Comparison of Measured Values of k_{eff}
and Calculated Values of k_{eff} Using Program DIF

Core	k_{eff}		% Difference in k_{eff}
	Calculated	Measured	
OSTR #1	0.9980	1.0019	0.39%
OSTR #2	1.0222	1.0272	0.49%

The results of the above three tests have established confidence in the DATA PROC and DIF codes and the basic input data from GA. It is believed that the safety analyses that are performed with these programs will yield realistic and reliable results.

4.5.2.3 Calculational Results

The computer programs yielded, among other results, values of k_{eff}, neutron fluxes, and average thermal power per element in each region. The six cores in Table 4-6 were analyzed, most of them at three different temperatures. These temperatures are given in Table 4-9.

Table 4-9
Temperatures Used in Calculations for Different Element Types

	Actual Temperature		
Designated Temp	Std Fuel	[redacted] Fuel	Graphite, Water, Structural
L	74°F (23°C)	74°F (23°C)	74°F (23°C)
M	482°F (250°C)	752°F (400°C)	74°F (23°C)
H	752°F (400°C)	1,292°F (700°C)	74°F (23°C)

A total of 15 calculations were performed. In all of the calculations, the four control rods were assumed to be completely withdrawn; thus the poison sections were replaced by fuel elements (if the rods had a fuel-follower) or a void (for the void-followed rod). The results of these calculations are given in Tables 4-10 and 4-11. Table 4-10 gives values of k_{eff} and Table 4-11 gives power per element in each fueled region.

Table 4-10
Calculated Values of k_{eff} for Possible OSTR Core Loadings

CORE	k_{eff}		
	Temperature		
	L	M	H
3	0.99105	-	-
4	1.00075	0.97630	-
5	1.06199	1.03561	0.99451
6	1.06835	1.04165	1.00038
7	1.07075	1.04205	0.99754
8	1.07731	1.04845	1.00360

The results presented in Table 4-10 exhibit the expected trends: as temperature increases, k_{eff} decreases. Calculations on cores #3M, #3H, and #4H were not performed since cores #3L and #4M were already subcritical. The effect of adding graphite elements to the outer core ring is to increase k_{eff} (see core #5L vs. #6L, for example).

Table 4-11
Calculated Power per Element
for Each Fueled Region for Possible OSTR Core Loadings

	AVERAGE POWER PER ELEMENT (kW/element) AT TOTAL CORE POWER OF 1000 kW				
	B ring	C ring	D ring	E ring	F ring
3L	24.43	21.66	19.19	11.23	-
4L	24.14	21.53	19.33	11.26	-
4M	24.23	21.64	19.51	11.06	-
5L	16.95	15.63	13.34	11.67	6.87
5M	16.98	15.67	13.40	11.76	6.74
5H	16.82	15.55	13.34	11.80	6.83
6L	16.73	15.48	13.30	11.80	6.89
6M	16.77	15.52	13.36	11.89	6.76
6H	16.61	15.40	13.30	11.93	6.84
7L	15.78	14.62	12.58	9.96	9.30
7M	15.85	14.68	12.63	9.99	9.22
7H	15.93	14.75	12.67	10.01	9.13
8L	15.62	14.52	12.58	10.09	9.27
8M	15.70	14.58	12.62	10.14	9.18
8H	15.74	14.62	12.65	10.13	9.13

As mentioned earlier, cores #3 and #4 are not realistic operational cores. Core #3 is subcritical at room temperature; core #4 is only slightly above critical at room temperature, dropping to subcritical at operating temperatures. As indicated earlier, they are included here for completeness, but are not future core configurations for OSTR.

Cores #5 and #6 are realistic OSTR cores after the initial [redacted] loading, and cores #7 and #8 are realistic final OSTR [redacted] core loadings.

Table 4-11 is of importance, as power density is a very significant parameter to most of the safety analyses. Note that in all of the possible operational cores (#5 through #8), the highest power density occurs in the B ring, as expected. The instrumented fuel element therefore is to be located in the B ring. The effect of the graphite elements in the outer ring is to slightly increase the power density in the outer fueled rings and to slightly reduce the power density in the inner fueled rings (see core #5 vs. core #6, or core #7 vs. core #8). This again is expected, since the thermal flux will increase in the outer fueled rings when

the graphite is added.

Table 4-12 lists maximum, minimum, and average power per element for each core, along with ratios of maximum-to-minimum power and maximum-to-average power per element. The effect of adding graphite is also seen from this table by slight decreases in P_{max}/P_{min} and P_{max}/P_{ave}.

Table 4-12
Calculated Maximum, Minimum, And Average
Power Per Element For Possible OSTR Core Loadings

Core	Maximum Power per Element P_{max} (kW/element)	Minimum Power per Element P_{min} (kW/element)	Average Power per Element P_{ave} (kW/element)	$\frac{P_{max}}{P_{min}}$	$\frac{P_{max}}{P_{ave}}$
5L	16.95	6.87	11.24	2.47	1.51
5M	16.98	6.74	11.24	2.52	1.51
5H	16.82	6.83	11.24	2.46	1.50
6L	16.73	6.89	11.24	2.43	1.49
6M	16.77	6.76	11.24	2.48	1.49
6H	16.61	6.84	11.24	2.43	1.48
7L	15.78	9.30	11.24	1.70	1.40
7M	15.85	9.22	11.24	1.72	1.41
7H	15.93	9.13	11.24	1.74	1.42
8L	15.62	9.27	11.24	1.69	1.39
8M	15.70	9.18	11.24	1.71	1.40
8H	15.74	9.13	11.24	1.72	1.40

The effects of temperature (core #5L vs. #5M vs. #5H, for example) are also rather small; these come about through changes in cross sections with temperature. For the mixed cores, the maximum power per element occurs at temperature "M," whereas for the full-[redacted] cores, the maximum power per element occurs at temperature "H." The changes are again very small percentage changes (about 1%).

Two important results which can be seen from Tables 4-11 and 4-12 are:

- the maximum power per element that occurs for any core (mixed or full-[redacted] and at any temperature, is less than 17 kW per element (considering realistic operational cores only); and
- the full-[redacted] cores have lower maximum power densities than mixed cores.

As more [redacted] fuel is added, the maximum power per element and the ratio of P_{max}/P_{ave} decrease.

These results are consistent with those found by Texas A & M University (Ref. 4.4), and they are the basis for the safety analysis presented in Chapter 13.

Another parameter of interest to safety analysis calculations is the strongly negative α_T. Calculations for two different OSU cores (#5 and #7) are displayed in Fig. 4.4, along with values from GA for a core with standard fuel elements and one with [redacted] fuel elements (Torrey Pines Mark III) (Ref. 4.5). The agreement with the GA values is excellent, considering the slight differences in core structure that exist and the differences in calculational techniques. It is of interest to observe that the OSU mixed core behaves essentially as a full [redacted] core, as far as the temperature coefficient is concerned. The mixed OSU core does not seem to display any of the temperature coefficient characteristics of standard fuel. This is not surprising, since the mixed core is predominantly [redacted] Standard fuel has little effect due to its being in a low importance area.

4.5.3 Operating Limits

4.5.3.1 Reactor Fuel Temperature

The basic safety limit for the TRIGA® reactor system is the fuel temperature; this applies for both the steady-state and pulsed mode of operation.

The TRIGA® fuel which is considered low hydride, that with a H/Zr ratio of less than 1.5, has a lower temperature limit than fuel with a higher H/Zr ratio. The OSTR utilizes fuel with H/Zr ratios between 1.6 and 1.7. (i.e., greater than 1.5). This allows operation at a higher limit. Fig. 4.5 indicates that the higher hydride compositions are single-phase and are not subject to the large volume changes associated with the phase transformations at approximately 1,000°F (530°C) in the lower hydrides. It has been noted in Ref. 4.7 that the higher hydrides lack any significant thermal diffusion of hydrogen. These two facts preclude concomitant volume changes. The important properties of delta phase U-ZrH are given in Table 4-13.

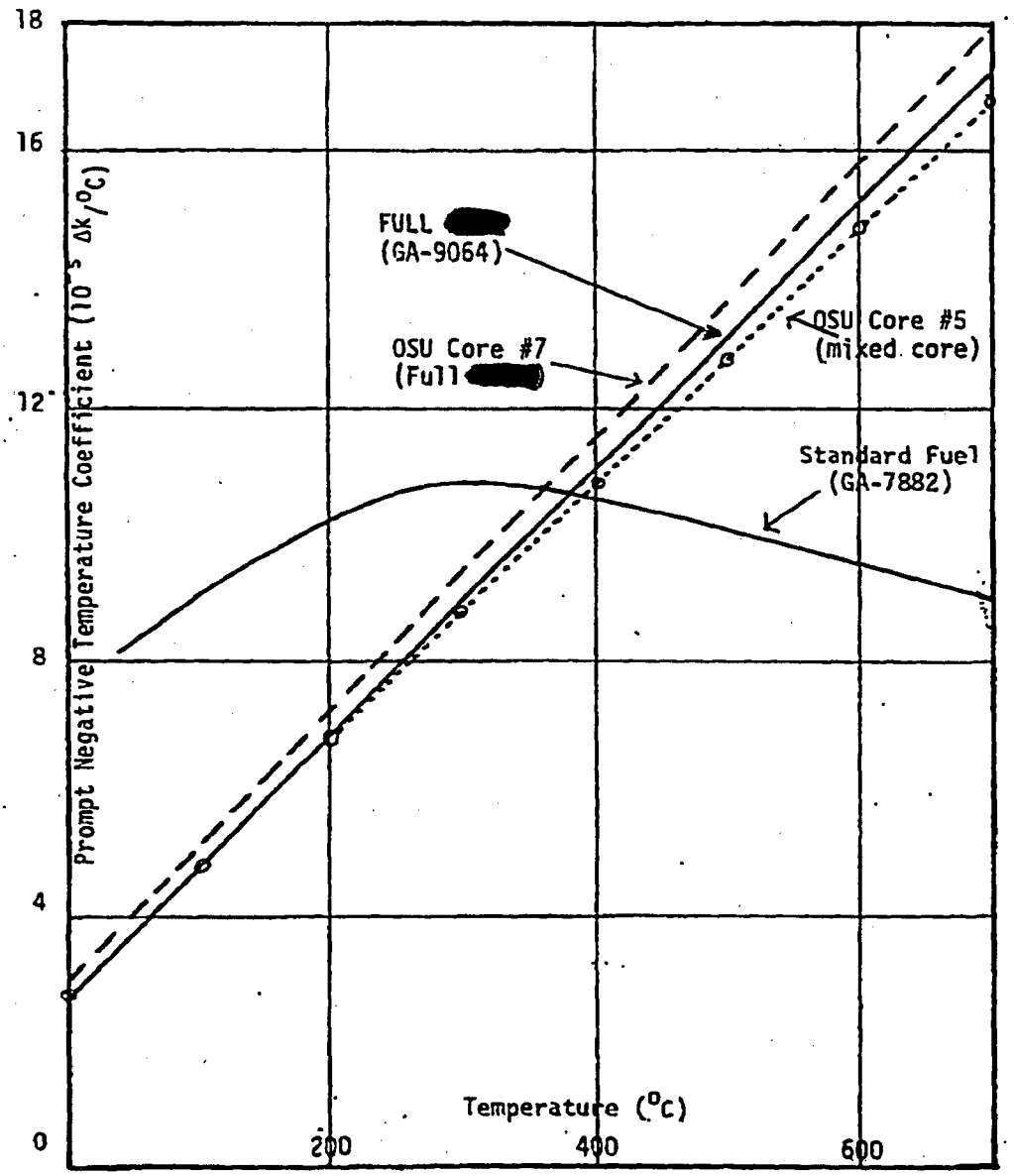

Figure 4.4 Prompt Temperature Coefficient of Reactivity vs. Temperature

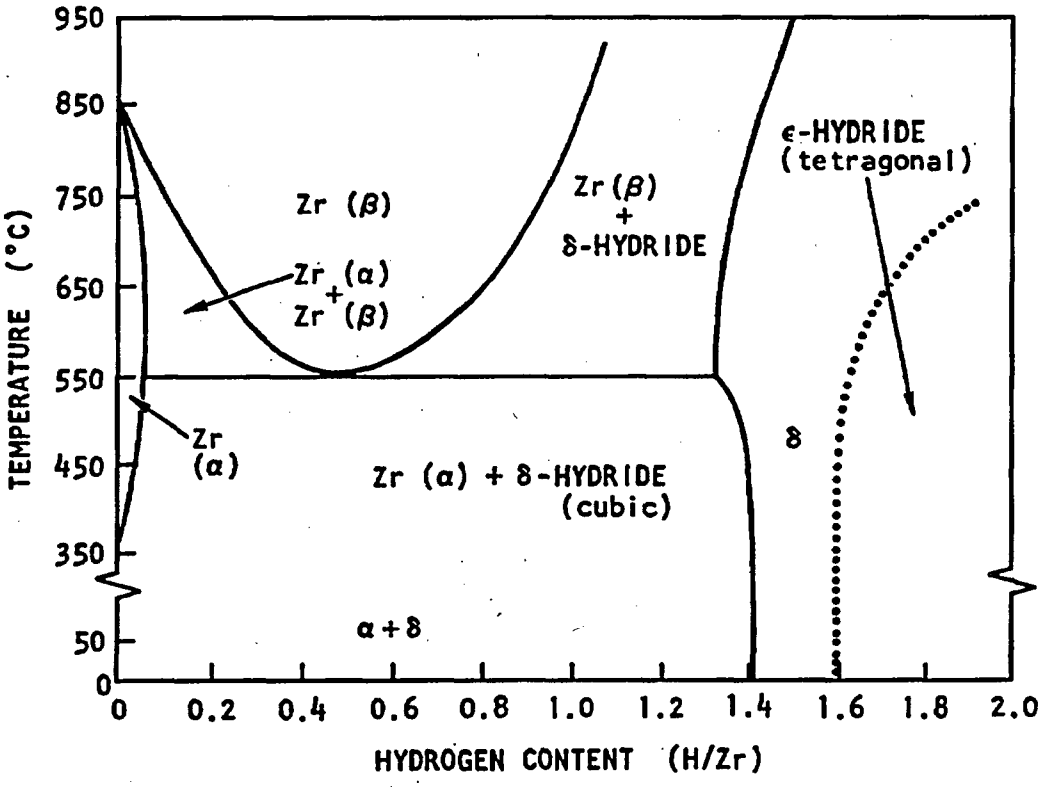

Figure 4.5 Phase Diagram of the Zirconium-Hydrogen System

Table 4-13
Physical Properties of Delta Phase U-ZrH

Thermal conductivity 200°F - 1,200°F (93°C - 650°C)	13 Btu/h - ft^2 - °F
Elastic modulus: 70°F (20°C)	9.1×10^6 psi
1,200°F (650°C)	6.0×10^6 psi
Ultimate tensile strength to 1,200°F (to 650°C)	24,000 psi
Compressive strength 70°F (20°C)	60,000 psi
Compressive yield 70°F (20°C)	35,000 psi
Heat of formation [δH_f^0 570°F (298°C)]	37.72 kcal/g-mole

Among the chemical properties of U-ZrH and ZrH, the reaction rate of the hydride with water is of particular interest. Since the hydriding reaction is exothermic, water will react more readily with zirconium than with zirconium hydride systems. Zirconium is frequently used in contact with water in reactors, and the zirconium-water reaction is not a safety hazard. Experiments carried out at GA show that the zirconium hydride systems have a relatively low chemical reactivity with respect to water and air. These tests (Ref. 4.8) have involved the quenching with water of both powders and solid specimens of U-ZrH after heating to temperatures as high as 1,560°F (850°C), and of solid U-Zr alloy after heating to temperatures as high as 2,190°F (1,200°C). Tests have also been made to determine the extent to which fission products are removed from the surfaces of the fuel elements at room temperature. Results prove that, because of the high resistance to leaching, a large fraction of the fission products are retained in even completely unclad U-ZrH fuel.

At room temperature, the hydride is like a ceramic and shows little ductility. However, at the elevated temperatures of interest for pulsing, the material is found to be more ductile. The effect of very large thermal stresses on hydride fuel bodies has been observed in hot cell observations to cause relatively widely spaced cracks which tend to be either radial or normal to the central axis and do not interfere with radial heat flow. Since the segments tend to be orthogonal, their relative positions appear to be quite stable.

The limiting effect of fuel temperature is the hydrogen gas pressure causing cladding stress. Fig. 4.6 relates equilibrium hydrogen pressure in ZrH with varying hydrogen content as a function of

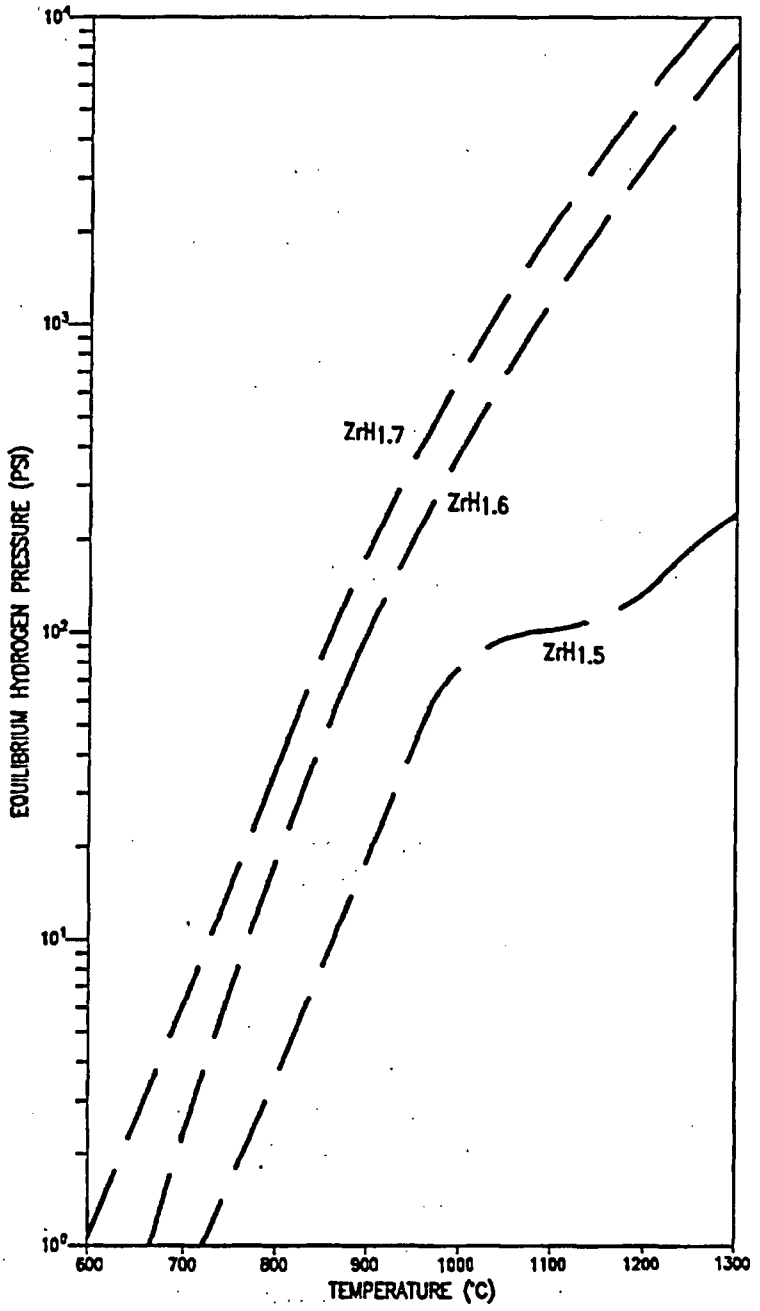

Figure 4.6 Equilibrium Hydrogen Pressure Vs. Temperature from Zirconium-Hydrogen

temperature for three different H/Zr ratios. The main concern regarding hydrogen pressure is to ensure that the cladding ultimate strength is not exceeded by the stress caused by the pressure. The mechanisms in obtaining temperatures and pressures of concern are different in the pulsing and steady-state mode of operation, and each mechanism will be discussed separately.

The OSTR fuel consists of U-ZrH with a H-Zr ratio between 1.6 and 1.7 and with the uranium being [redacted] enriched in ^{235}U to approximately [redacted] The cladding is 0.020- inch thick stainless steel and has an inside diameter of 1.43 inches. The rest of the discussion on fuel temperatures will be concerned with fuel having H/Zr ratios greater than 1.5 [i.e., single-phase and not subject to the large volume changes associated with phase transformation at approximately 985°F (530°C) in the lower hydrides]. Further, it will specifically address fuel with an H/Zr ratio of 1.7 since this is the highest ratio fuel to be used in the OSTR and will produce the highest clad pressure and stress for a given temperature. Fig. 4.7 shows the characteristic of 304 stainless steel with regard to yield and ultimate strengths as a function of temperature.

The stress applied to the cladding from the internal hydrogen gas pressure is given by:

$$S = \frac{Pr}{t}, \qquad (1)$$

where:

S = stress in psi,
P = internal pressure in psi,
r = radius of the stainless steel cylinder, and
t = wall thickness of the stainless steel clad.

Using the parameters given above:

$$S = \frac{P\ (1.43\ in./2)}{0.020\ in.} = 35.75\ P \qquad (2)$$

For safety considerations, it is necessary to relate the strength of the cladding material at its operating temperature to the stress applied to the cladding due to the internal gas pressure associated with the fuel temperature. Fig. 4.8 gives the ultimate cladding strength and the stress applied to the cladding as a result of hydrogen dissociation for fuel having H/Zr ratios of 1.65 and 1.7, both as a function of temperature. This curve shows that the cladding will not fail for fuel with $ZrH_{1.7}$ if both the clad and fuel temperatures are equal and below about 1,700°F (930°C). This is conservative since the cladding temperature will be below the fuel temperature. This establishes the safety limit on fuel temperature for steady-state operations. The actual steady-state peak fuel temperature at 1 MW will be below 932°F (500°C). The remainder of this section deals with the safety limit for transient operation.

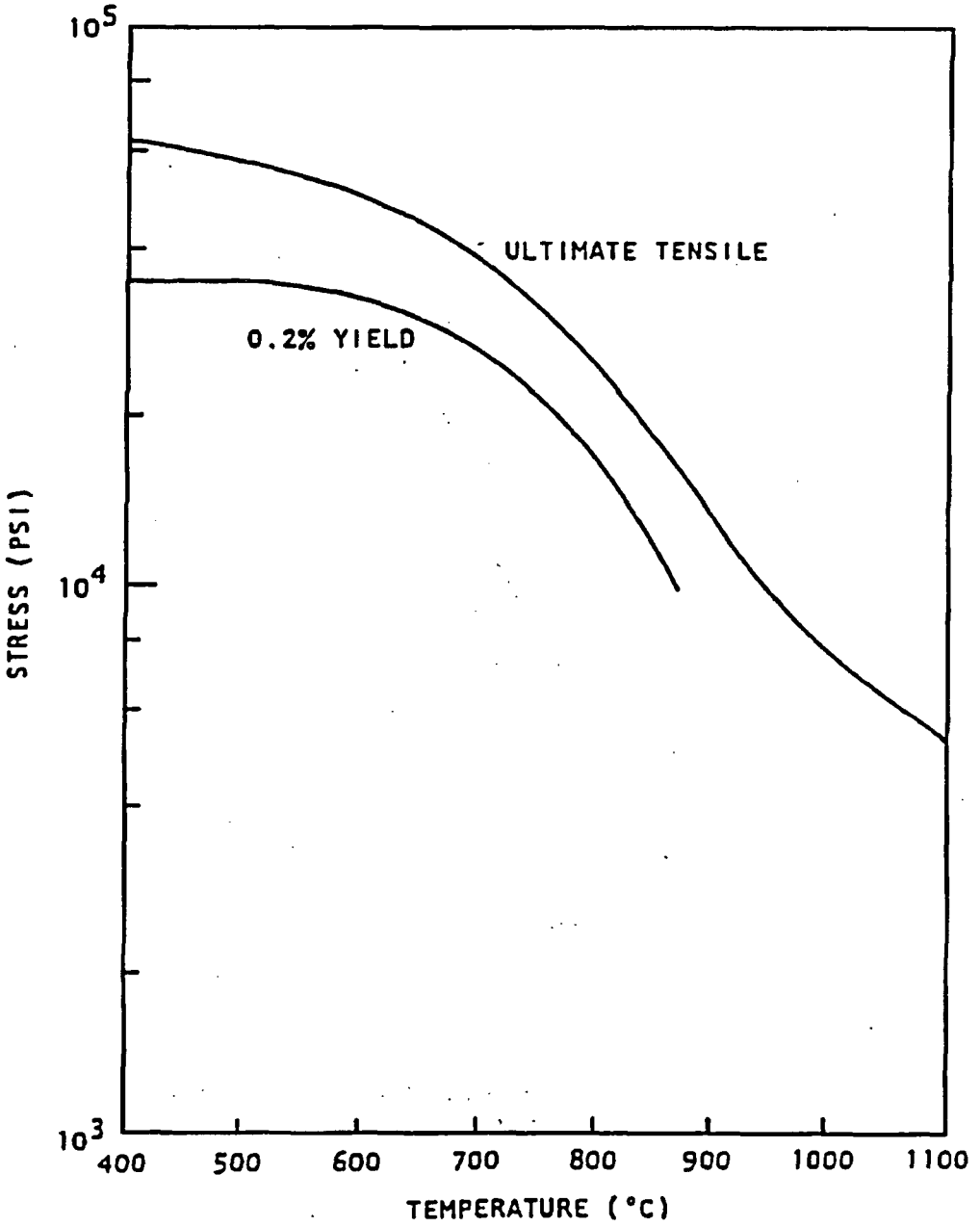

Figure 4.7 Strength of Type 304 Stainless Steel as a Function of Energy

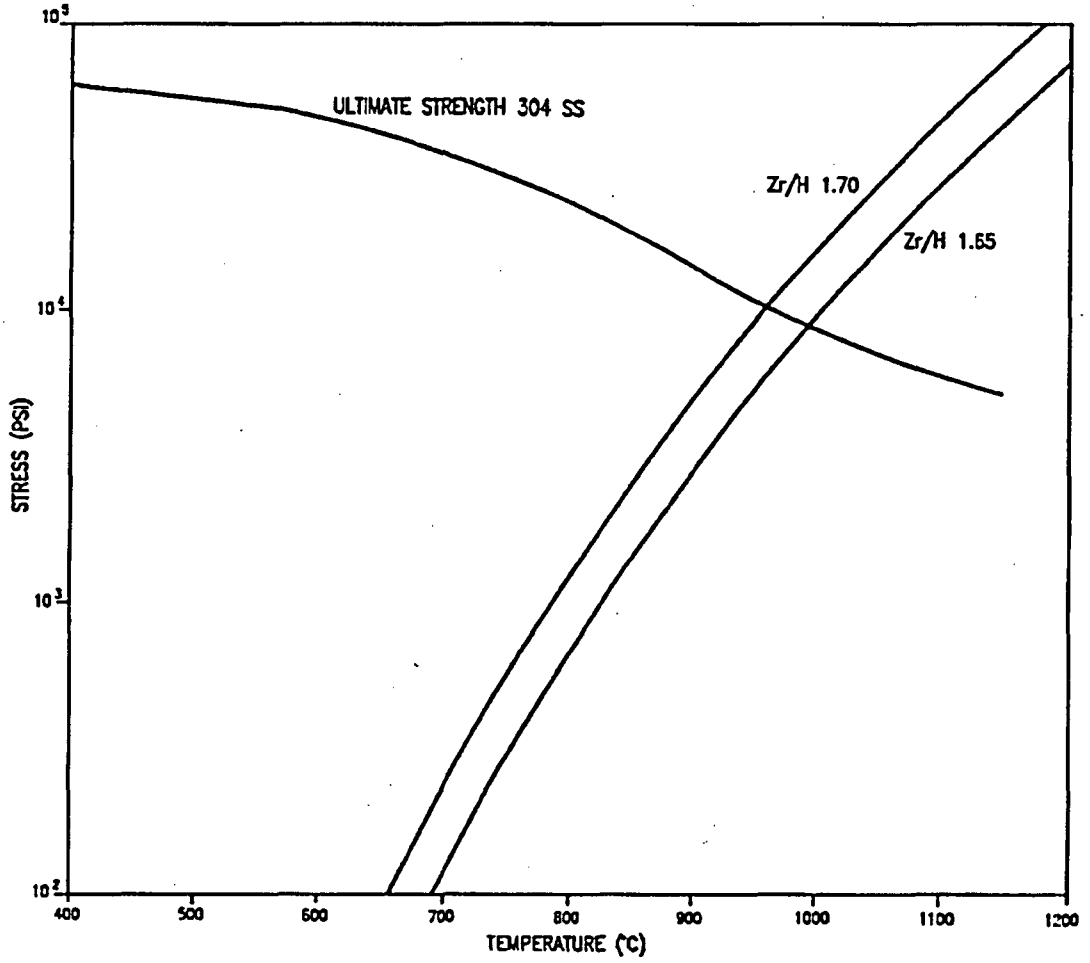

Figure 4.8 Strength and Applied Stress as a Function of Temperature, Equilibrium at Equilibrium Hydrogen Dissociation Pressure

During transient operation, it is necessary to account for the difference in fuel and cladding temperatures to establish a safety limit based on fuel temperature. Additionally, the diffusion of hydrogen reduces peak pressures from those predicted at equilibrium at the peak temperatures. The net result of these two points is that a higher safety limit exists for transient operation. An analysis of the two points is given in the following two subsections.

4.5.3.1.1 Fuel and Clad Temperature

For the steady-state safety limit, it was assumed that the cladding and fuel temperatures were the same. The following discussion shows that the cladding temperature is well below the maximum fuel temperature after a pulse. This allows a higher safety limit on fuel temperature.

The radial temperature distribution in the fuel element immediately following a pulse is very similar to the power distribution shown in Fig. 4.9. This initial steep thermal gradient at the fuel surface results in some heat transfer during the time of the pulse so that the true peak temperature does not quite reach the adiabatic peak temperature. A large temperature gradient is also impressed upon the clad which can result in a high heat flux from the clad into the water. If the heat flux is sufficiently high, film boiling may occur and form an insulating jacket of steam around the fuel elements permitting the clad temperature to approach the fuel temperature.

Thermal transient calculations were made using the RAT computer code. RAT is a 2D transient heat transport code developed to account for fluid flow and temperature dependent material properties. Calculations show that, if film boiling occurs after a pulse, it may take place either at the time of maximum heat flux from the clad, before the bulk temperature of the coolant has changed appreciably, or it may take place at a later time when the bulk temperature of the coolant has approached the saturation temperature, resulting in a reduced threshold for film boiling. Data obtained for transient heating of ribbons in 100°F (38°C) water, showed burnout fluxes of 0.9 to 2.0 MBtu/ft^2-h for e-folding periods from 5 to 90 milliseconds (Ref. 4.9). On the other hand, sufficient bulk heating of the coolant channel between fuel elements can take place in several tenths of a second to lower the departure from nucleate boiling (DNB) point to approximately 0.4 MBtu/ft^2-h. It is shown, on the basis of the following analysis, that the second mode is the most likely; i.e., when film boiling occurs, it takes place under essentially steady-state conditions at local water temperatures near saturation.

A value for the temperature that may be reached by the clad if film boiling occurs was obtained in the following manner. A transient thermal calculation was performed using the radial and axial power distributions in Figs. 4.9 and 4.10, respectively. The thermal resistance at the fuel-clad interface was assumed to be zero. A boiling heat transfer model,

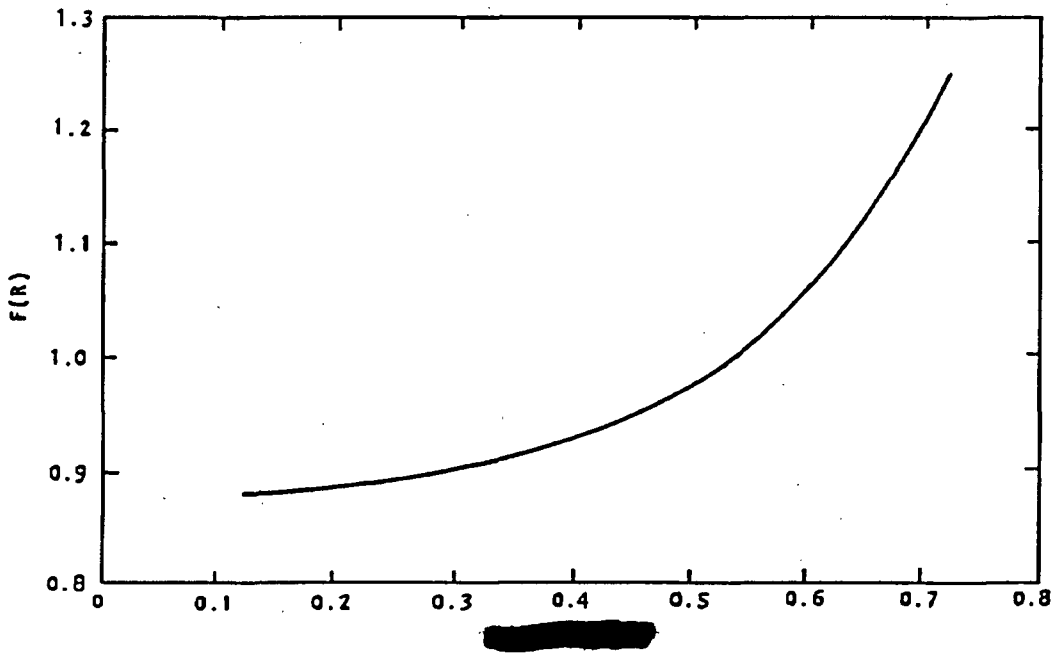

4.9 Radial Power Distribution in the U-ZrH Fuel Element

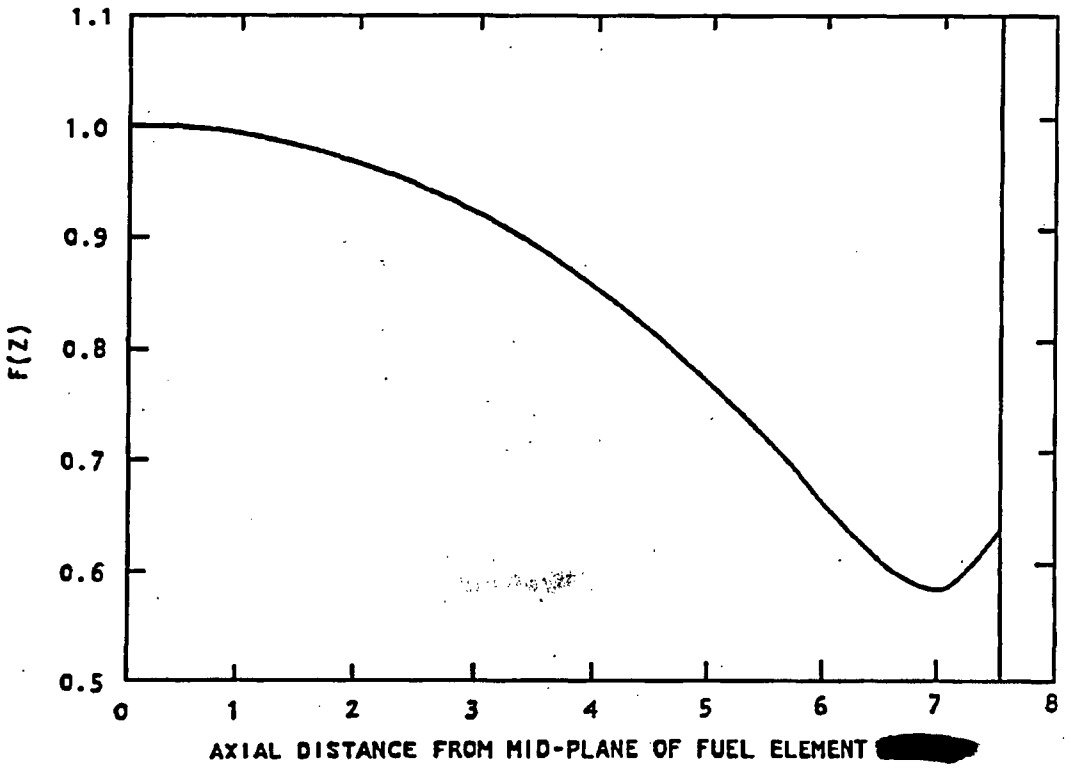

Figure 4.10 Axial Power Distribution in the U-ZrH Fuel Element

as shown in Fig. 4.11, was used in order to obtain an upper limit for the clad temperature rise. The model used the data of McAdams (Ref. 4.10) for the subcooled boiling and the work of Sparrow and Cess (Ref. 4.11) for the film boiling regime. A conservative estimate was obtained for the minimum heat flux in film boiling by using the correlations of Speigler et al. (Ref. 4.12), Zuber (Ref. 4.13), and Rohsenow and Choi (Ref. 4.14) to find the minimum temperature point at which film boiling could occur. This calculation gave an upper limit of 1,400°F (760°C) clad temperature for a peak initial fuel temperature of 1,830°F (1,000°C), as shown in Fig. 4.12. Fuel temperature distributions for this case are shown in Fig. 4.13 and the heat flux into the water from the clad is shown in Fig. 4.14. In this limiting case, DNB occurred only 13 milliseconds after the pulse, conservatively calculated assuming a steady-state DNB correlation. Subsequently, experimental transition and film boiling data were found to have been reported by Ellion (Ref. 4.15) for water conditions similar to those for the TRIGA® system. The Ellion data show the minimum heat flux, used in the limiting calculation described above, was conservative by a factor of 5. An appropriate correction was made which resulted in a more realistic estimate of 880°F (470°C) as the maximum clad temperature expected if film boiling occurs. This result is in agreement with experimental evidence obtained for clad temperatures of 750°F to 930°F (400°C to 500°C) for TRIGA® Mark F fuel elements which have been operated under film boiling conditions (Ref. 4.16). Based on this analysis, the peak cladding temperature will be 880°F (470°C) for a transient fuel temperature of 1,830°F (1,000°C). Further analysis will show that this peak clad temperature is valid for a higher peak fuel temperature.

The preceding analysis assessing the maximum clad temperatures associated with film boiling assumed no thermal resistance at the fuel-clad interface. Measurements of fuel temperatures as a function of steady-state power level provide evidence that after operating at high fuel temperatures, a permanent gap is produced between the fuel body and the clad. This gap exists at all temperatures below the maximum operating temperature (for example, Fig. 16 in Ref. 4.16). The gap thickness varies with fuel temperature and clad temperature: cooling of the fuel or overheating of the clad tends to widen the gap and decrease the heat transfer rate. Additional thermal resistance due to oxide and other films on the fuel and clad surfaces is expected. Experimental and theoretical studies of thermal contact resistance have been reported which provide insight into the mechanisms involved (Refs. 4.17 - 4.19). They do not, however, permit quantitative prediction because the basic data required for input are presently not fully known. Instead, several transient thermal computations were made using the RAT code, varying the effective gap conductance, in order to determine the effective gap coefficient for which departure from nucleate boiling is incipient. These results were then compared with the incipient film boiling conditions of the 1,830°F (1,000°C) peak fuel temperature case.

For convenience, the calculations were made using the same initial temperature distribution as was used for the preceding calculation. The calculations assumed a coolant flow

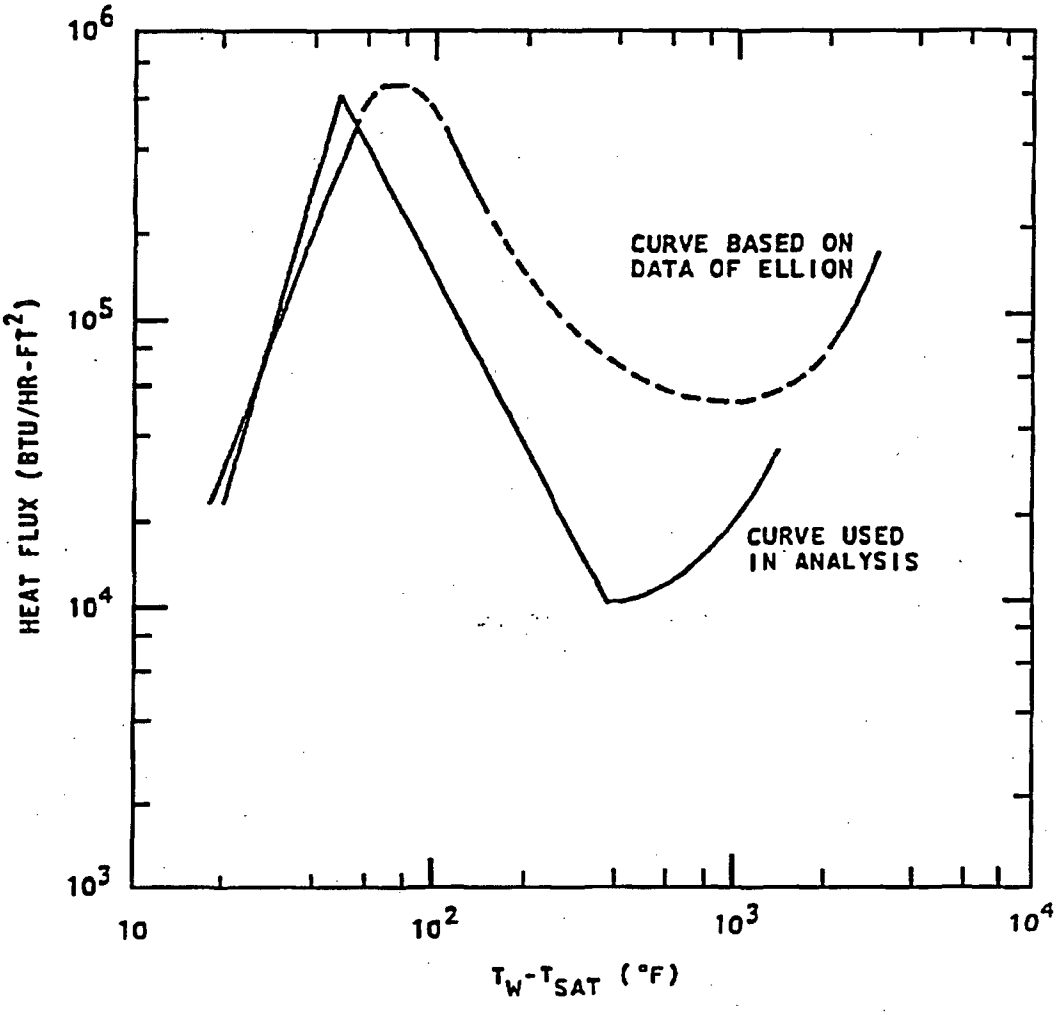

Figure 4.11 Subcooled Boiling Heat Transfer For Water

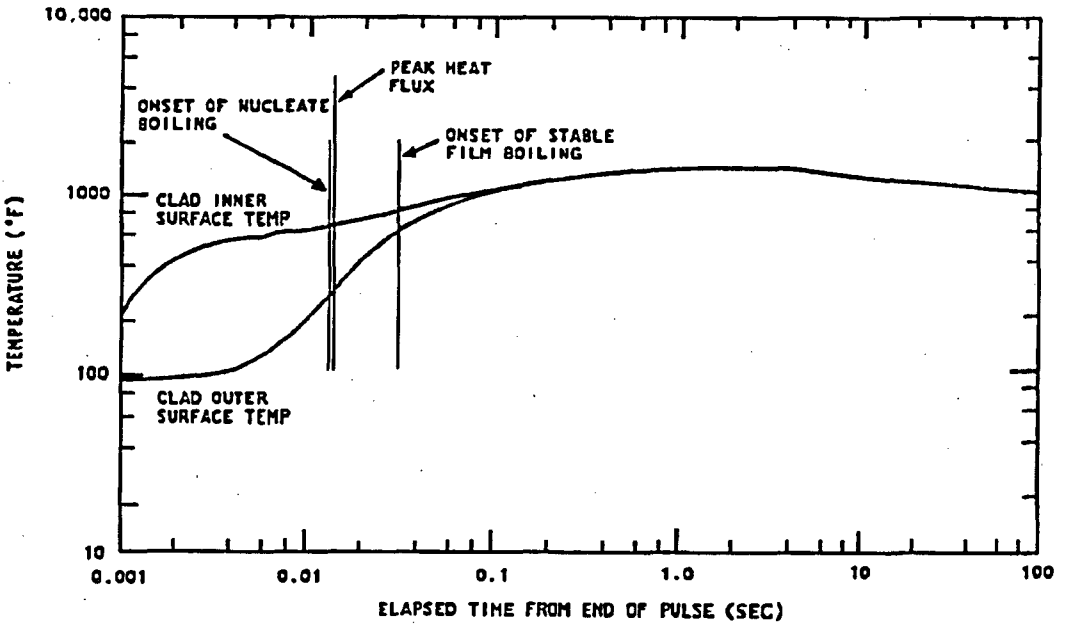

Figure 4.12 Clad Temperature at Midpoint of Well-Bonded Fuel Element

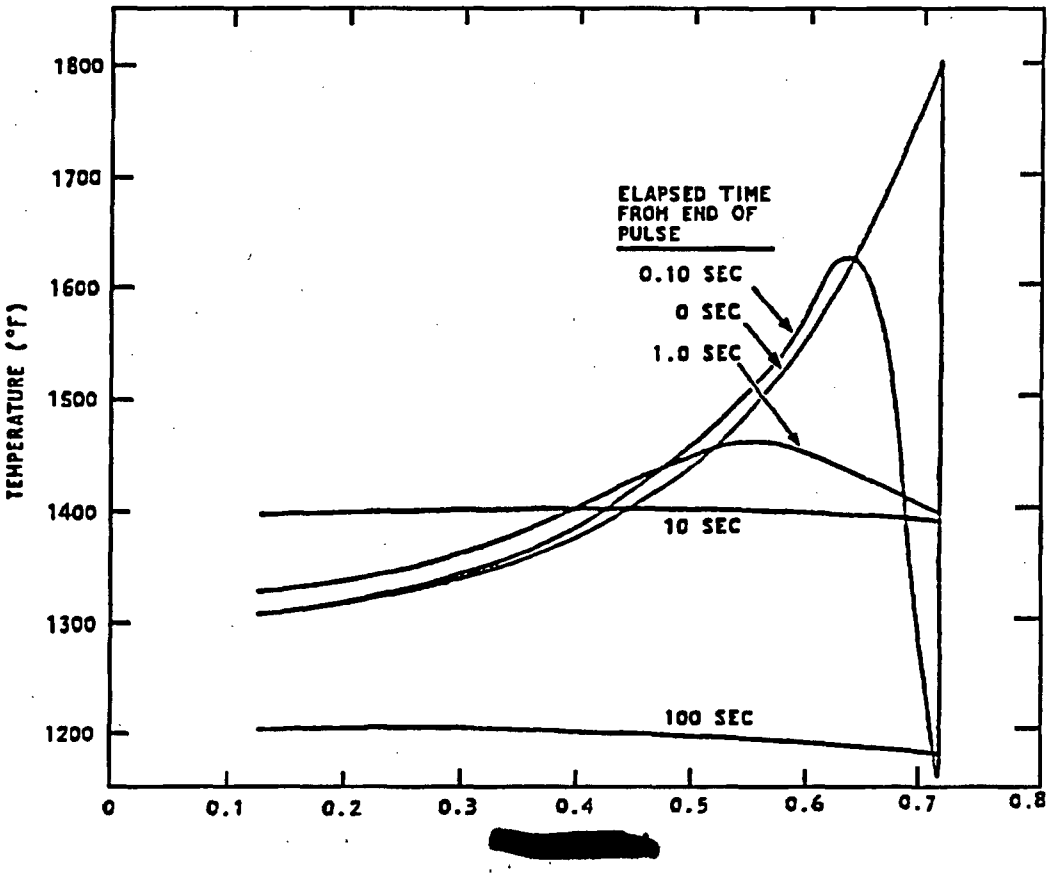

Figure 4.13 Fuel Body Temperatures at Midplane of Well-Bonded Fuel Element After a Pulse

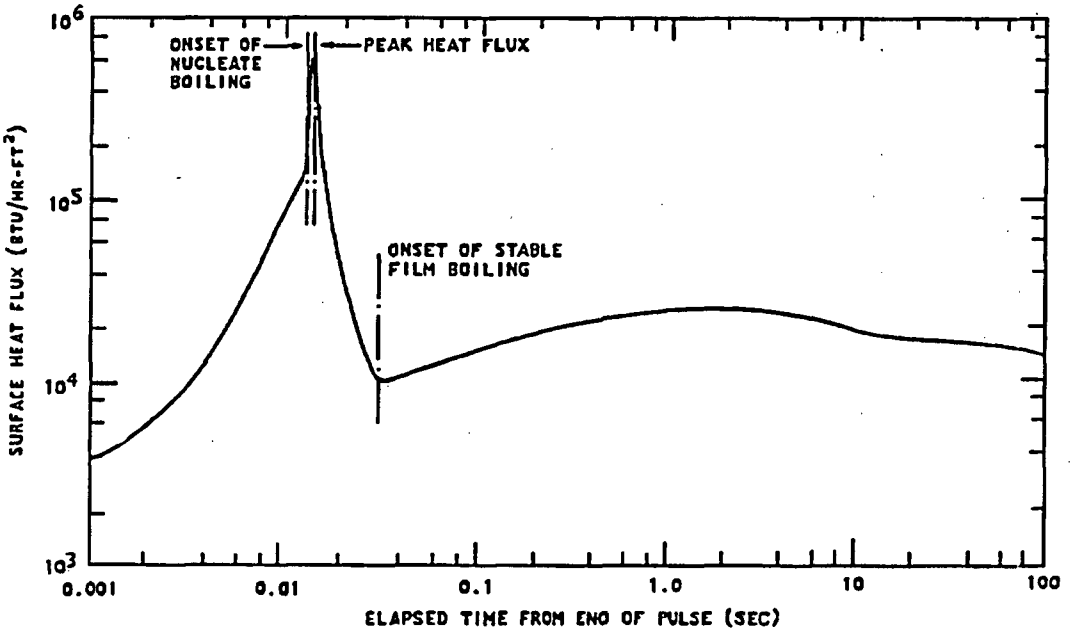

Figure 4.14 Surface Heat Flux at Midplane of Well-Bonded Fuel Element After a Pulse

velocity of 1 foot per second which is within the range of flow velocities computed for natural convection under various steady-state conditions for these reactors. The calculations did not use a complete boiling curve heat transfer model, but instead, included a convection cooled region (no boiling) and a subcooled nucleate boiling region without employing an upper DNB limit. The results were analyzed by inspection using the extended steady-state correlation of Bernath (Ref. 4.20) which has been reported by Spano (Ref. 4.21) to give agreement with SPERT II burnout results within the experimental uncertainties in flow rate.

The transient thermal calculations were performed using effective gap conductances of 500, 375, and 250 Btu/h-ft^2 -°F. The resulting wall temperature distributions were inspected to determine the axial wall position and time after the pulse which gave the closest approach between the local computed surface heat flux and the DNB heat flux according to Bernath. The axial distribution of the computed and critical heat fluxes for each of the three cases at the time of closest approach are shown in Figs. 4.15 through 4.17. If the minimum approach to DNB is corrected to TRIGA® Mark F conditions and cross-plotted, an estimate of the effective gap conductance of 450 Btu/h-ft^2 -°F is obtained for incipient burnout so that the case using 500 is thought to be representative of standard TRIGA® fuel.

The surface heat flux at the midplane of the element is shown in Fig. 4.18 with gap conductance as a parameter. It may be observed that the maximum heat flux is approximately proportional to the heat transfer coefficient of the gap, and the time lag after the pulse for which the peak occurs is also increased by about the same factor. The closest approach to DNB in these calculations did not necessarily occur at these times and places, however, as indicated on the curves of Figs. 4.15 through 4.17. The initial DNB point occurred near the core outlet for a local heat flux of about 340 kBtu/h-ft^2 -°F according to the more conservative Bernath correlations at a local water temperature approaching saturation.

From this analysis, a maximum temperature for the clad during a pulse which gives a peak adiabatic fuel temperature of 1,830°F (1,000°C) is estimated to be 880°F (470°C). This is conservative since it was obtained by assuming no thermal resistance between the fuel and the clad. As was shown above, a value of 500 Btu/h-ft^2 -°F for the gap conduction is more realistic.

As can be seen from Fig. 4.7, the ultimate strength of the cladding at a temperature of 880°F (470°C) is 59,000 psi. If the stress produced by the hydrogen overpressure on the clad is less than 59,000 psi, the cladding will not be ruptured. Referring to Fig. 4.8, and considering U-$ZrH_{1.7}$ fuel with a peak temperature of 1,830°F (1,000°C), one finds the stress on the clad to be 24,000 psi. Analysis in the next section which considers diffusion will show that the actual hydrogen pressure produced in a pulse is less than the equilibrium

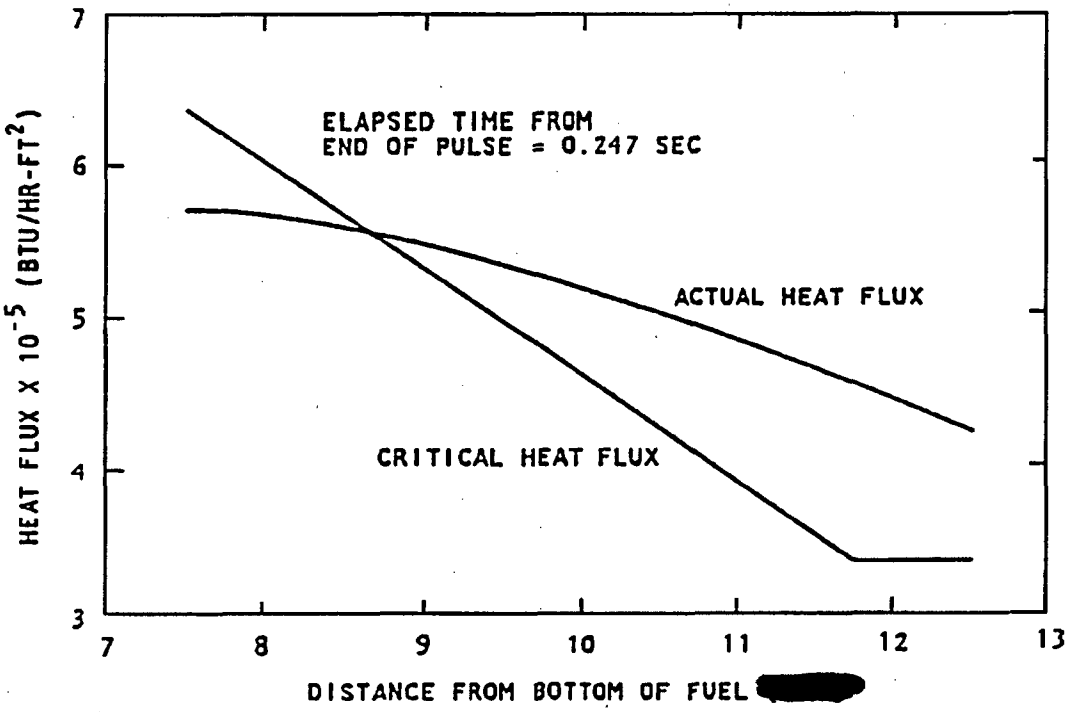

Figure 4.15 Surface Heat Flux for Standard Nongapped (h_{gap}=500) Fuel Element After a Pulse

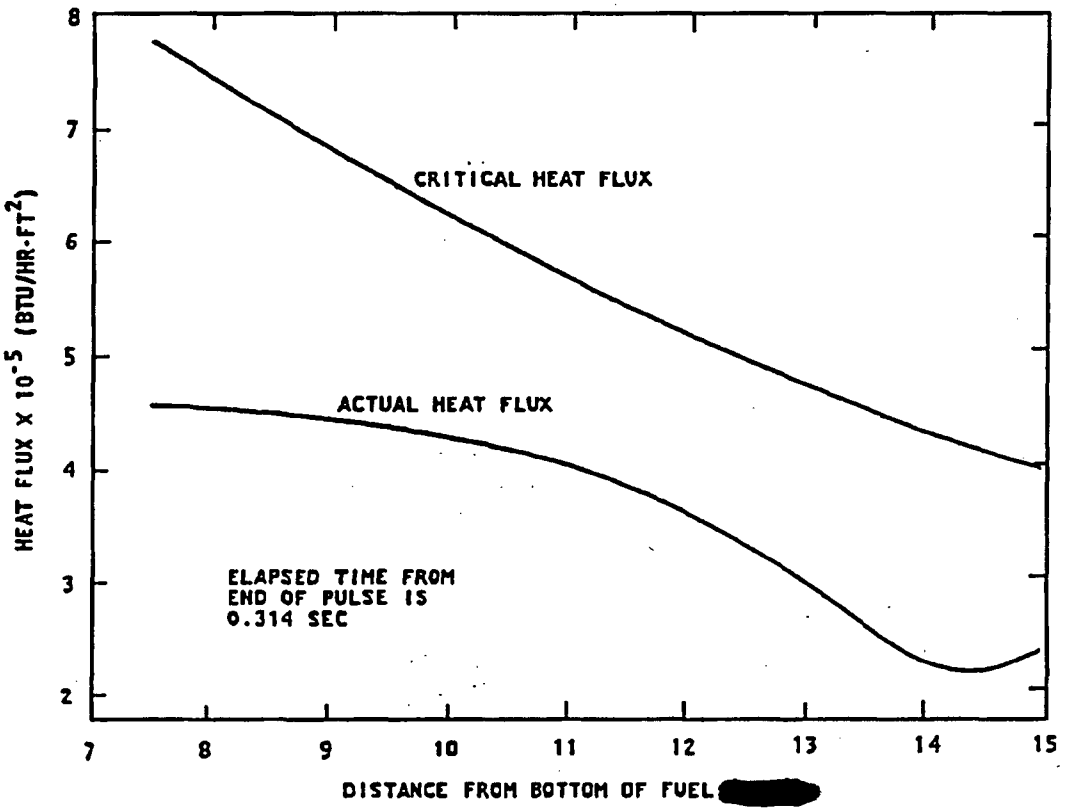

Figure 4.16 Surface Heat Flux for Standard Nongapped (h_{gap}=375) Fuel Element After a Pulse

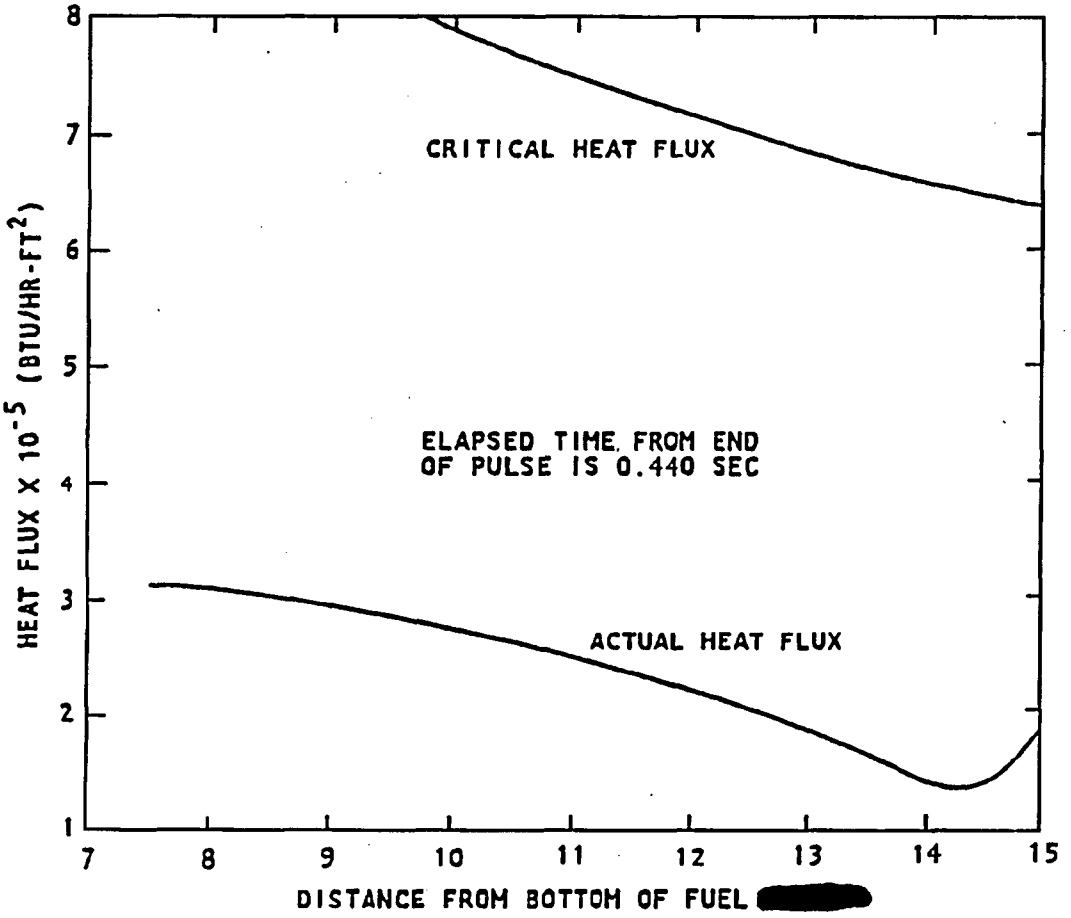

Figure 4.17 Surface Heat Flux for Standard Nongapped (h_{gap}=250) Fuel Element After a Pulse

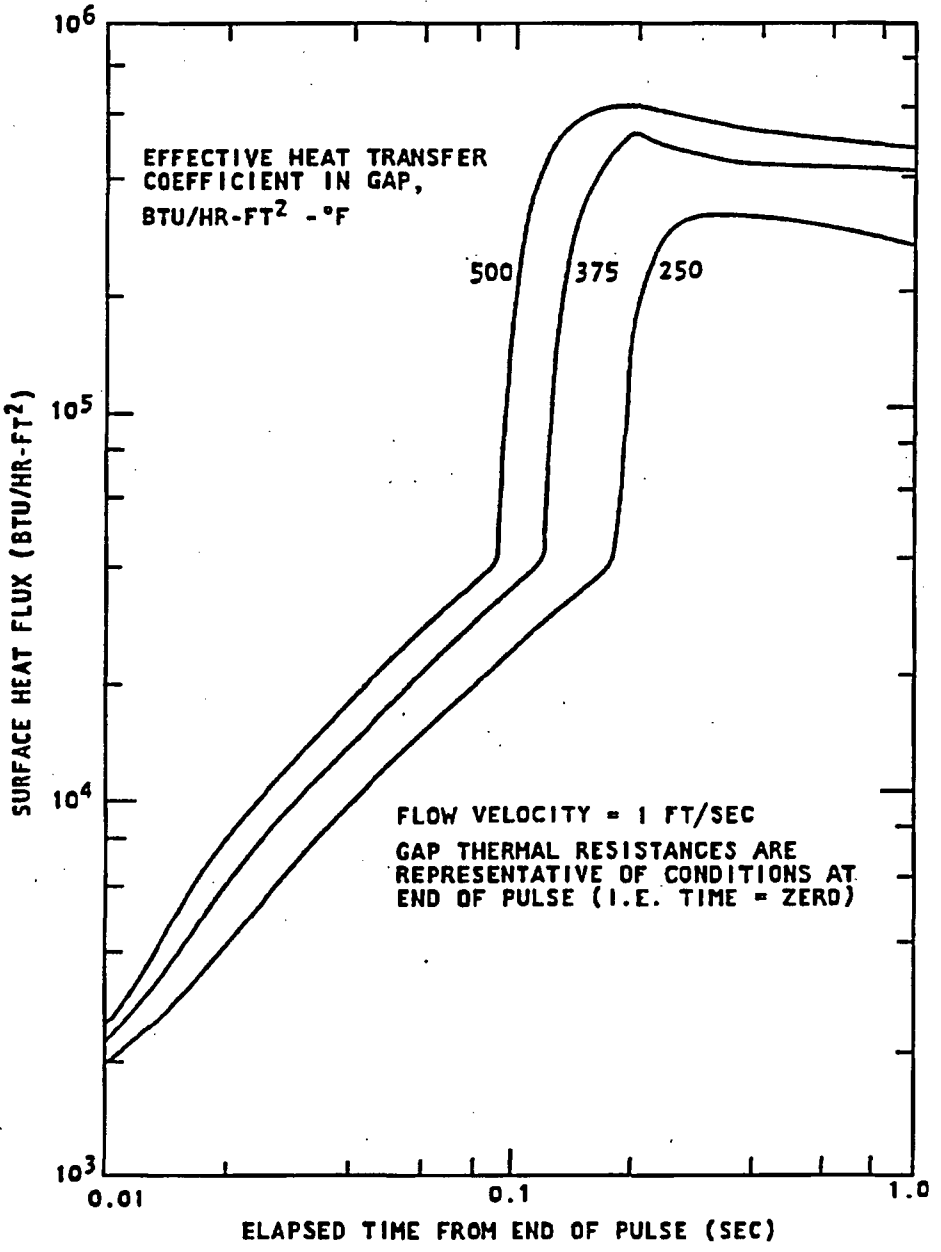

Figure 4.18 Surface Heat Flux at Midpoint Vs. Time For Standard Nongapped Fuel Elements After a Pulse

pressure for the peak temperature. This allows a safe limit on fuel temperature to be 2,012°F (1,100°C). TRIGA® fuel with a hydrogen to zirconium ratio of at least 1.6 has been pulsed to temperatures approaching 2,100°F (1,150°C) without damage to the clad (Ref. 4.22).

4.5.3.1.2 Finite Diffusion Rate

To assess the effect of the finite diffusion rate and the rehydriding at the cooler surfaces, the following analysis is presented.

As hydrogen is released from the hot fuel regions, it migrates to the cooler regions and the equilibrium pressure that is obtained is characteristic of some temperature lower than the maximum. To evaluate this reduced pressure, diffusion theory is used to calculate the rate at which hydrogen is evolved and reabsorbed at the fuel surface.

Ordinary diffusion theory provides an expression describing the time dependent loss of gas from a cylinder:

$$\frac{\bar{c} - c_f}{c_i - c_f} = \sum_{n=1}^{\infty} \frac{4}{Z_n^2} \exp - \frac{Z_n^2 Dt}{r_0^2}, \qquad (3)$$

Where:

$\bar{c}, c_i, c_f$	=	the average, the initial, and the final gas concentration in the cylinder, respectively;
Z_n	=	the roots of the Bessel function of the first kind where $J_0(x) = 0$;
D	=	the diffusion coefficient for the gas in the cylinder;
r_0	=	the radius of the cylinder; and
t	=	time.

Setting the term on the right-hand side of Equation 3 equal to κ, one can rewrite Equation 3 as:

$$\bar{c}/c_i = c_f/c_i + \left(1 - c_f/c_i\right) \kappa \qquad (4)$$

and the derivative in time is given by

$$\frac{d\left(\bar{c}/c_i\right)}{dt} = \left(1 - c_f/c_i\right)\frac{d\kappa}{dt}. \qquad (5)$$

This represents the fractional release rate of hydrogen from the cylinder, f(t). The derivative of the series in the right-hand side of Equation 3 was approximated by

$$\frac{d\kappa}{dt} = -\left(7.339e^{-8.34\varepsilon} + 29.88e^{-249\varepsilon}\right)\frac{d\varepsilon}{dt}, \qquad (6)$$

where $\varepsilon = Dt/r_0^2$.

The diffusion coefficient for hydrogen in zirconium hydride in which the H/Zr ratio is between 1.56 and 1.86 is given by

$$D = 0.25\, e^{-17800/[R(T+273)]}, \qquad (7)$$

where:

R = the gas constant; and
T = the zirconium hydride temperature in °C.

Equation 3 describes the escape of gas from a cylinder through diffusion until some final concentration is achieved. Actually, in the closed system considered here, not only does the hydrogen diffuse into the fuel-clad gap, but also diffuses back into the fuel in the regions of lower fuel temperature. The gas diffuses through the clad at a rate dependent on the clad temperature. Although this tends to reduce the hydrogen pressure, it is not considered in this analysis. When the diffusion rates are equal, an equilibrium condition will exist. To account for this, Equation 5 was modified by replacing the concentration ratios by the ratio of the hydrogen pressure in the gap to the equilibrium hydrogen pressure, P_h/P_e. Thus,

$$f(t) = \frac{d(c/c_i)}{dt} = \left(1 - \frac{P_h(t)}{P_e}\right)\frac{d\kappa}{dt} \qquad (8)$$

where:

$P_h(t)$ = the hydrogen pressure, a function of time; and
P_e = the equilibrium hydrogen pressure over the zirconium hydride which is a

function of the fuel temperature and H/Zr ratios.

The rate of change of the internal hydrogen pressure, in psi, inside the fuel element cladding is

$$\frac{dP_h}{dt} = \frac{14.7\, f(t)\, N_h}{6.02 \times 10^{23}} \frac{22.4}{V_g} \frac{T + 273}{273} \qquad (9)$$

where:

N_h = the number of molecules of H_2 in the fuel;
T = the gas temperature (°C);
$f(t)$ = the fractional loss rate from Equation 8; and
V_g = the free volume inside the fuel clad (liters).

For a fuel volume of 400 cm^3, the moles of H_2 available from fuel with $ZrH_{1.65}$ and $ZrH_{1.7}$ is 19.9 and 20.6 moles, respectively. The free volume is assumed to consist of a cylindrical volume, at the top of the element, 1/8 inch high with a diameter of 1.43 inches for a total of 3.3 cm^3. The temperature of the hydrogen in the gap was assumed to be the temperature of the clad. The effect of changing these two assumptions was tested by calculations in which the gap volume was decreased by 90% and the temperature of the hydrogen in the gap was set equal to the maximum fuel temperature. Neither of these changes resulted in maximum pressures different from those based on the original assumptions although the initial rate of pressure increase was greater. For these conditions

$$P_h = A \times 10^3 (T + 273) \int f(t)dt \qquad (10)$$

where A = 7.29 for $ZrH_{1.65}$ and 7.53 for $ZrH_{1.7}$.

The fuel temperature used in Equation 7 to evaluate the diffusion coefficient is expressed as:

$$T(z) = T_0;\ t < 0,$$

$$T(z) = T_0 + (T_m - T_0) \cos [2.45\ (z - 0.5)];\ t \geq 0, \qquad (11)$$

where:

T_m = the peak fuel temperature (°C),
T_0 = the clad temperature (°C),
z = the axial distance expressed as a fraction of the fuel length, and
t = the time after step increase in power.

It was assumed that the fuel temperature was invariant with radius. The hydrogen pressure over the zirconium hydride surface when equilibrium prevails is strongly temperature dependent as shown in Fig. 4.6, and for ZrH, can be expressed by:

$$P_e = 2.07 \times 10^9 e^{-1.974 \times 10^4/(T+273)} . \quad (12)$$

The coefficients have been derived from data developed by Johnson (Ref. 4.23). The rate at which hydrogen is released or reabsorbed takes the form:

$$g(t,z) = \frac{[P_e(z) - P_h(t)]}{P_e(z)} f(t,z) , \quad (13)$$

where:

f(t, z) = the derivative given in Equation 8 with respect to time evaluated at the axial position z,

$P_h(t)$ = the hydrogen pressure in the gap at time t, and

$P_e(z)$ = the equilibrium hydrogen pressure at the ZrH temperature at position z.

The internal hydrogen pressure is then

$$P_h(t) = A \times 10^3 (T_0 + 273) \int_0^t \int_0^l g(t,z) dz .$$

This equation was approximated by:

$$P_h(t_i) = A \times 10^3 (T_0 + 273) \times \sum_{i=1}^{n} \sum_{j=1}^{m} \left[1 - \frac{P_h(t_{i-1})}{P_e(z_j)} \right] l \times f(t_i, z_j) \& \delta, \quad (14)$$

where the inner summation is over the fuel element's length increments and the outer summation is over time.

For the cases where the maximum fuel temperature is 2,100°F (1,150°C) for $ZrH_{1.65}$ and 2,020°F (1;100°C) for $ZrH_{1.7}$, the equilibrium hydrogen pressure in ZrH is 2,000 psi, which leads to an internal stress of 72,000 psi. Using Equation 14, it is found that the internal pressure for both $ZrH_{1.65}$ and $ZrH_{1.7}$ increases to a peak at about 0.3 sec, at which time the

pressure is about one-fifth of the equilibrium value or about 400 psi (a stress of 14,700 psi). After this time, the pressure slowly decreases as the hydrogen continues to be redistributed along the length of the element from the hot regions to the cooler regions.

Calculations have also been made for step increases in power to peak $ZrH_{1.65}$ fuel temperatures greater than 2,100°F (1,150°C). Over a 390°F (200°C) range, the time to the peak pressure and the fraction of the equilibrium pressure value achieved were approximately the same as for the 2,100°F (1,150°C) case. Similar results were found for fuel with $ZrH_{1.7}$. Thus, if the clad remains below about 930°F (500°C), the internal pressure that would produce the yield stress in the clad (35,000 psi) is about 1,000 psi and the corresponding equilibrium hydrogen pressure is 5,000 psi. This corresponds to a maximum fuel temperature of about 2,280°F (1,250°C) in $ZrH_{1.65}$ and 2,160°F (1,180°C) in $ZrH_{1.7}$. Similarly, an internal pressure of 1,600 psi would produce a stress equal to the ultimate clad strength (over 59,000 psi). This corresponds to an equilibrium hydrogen pressure of 5 × 1,600 or 8,000 psi and a fuel temperature of about 2,370°F (1,300°C) in $ZrH_{1.65}$ and 2,260°F (1,240°C) in $ZrH_{1.7}$.

Measurements of hydrogen pressure in TRIGA® fuel elements during steady-state operation have not been made. However, measurements have been made during transient operations and compared with the results of an analysis similar to that described here (Ref. 4.1 and 4.3). These measurements indicated that, in a pulse in which the maximum temperature in the fuel was greater than 1,830°F (1,000°C), the maximum pressure ($ZrH_{1.65}$) was only about 6% of the equilibrium value evaluated at the peak temperature. Calculations of the pressure resulting from such a pulse using the methods described above gave calculated pressure values about three times greater than the measured values.

An instantaneous increase in fuel temperature will produce the most severe pressure conditions. When a peak fuel temperature is reached by increasing the power over a finite period of time, the resulting pressure will be no greater than that for the step change in power analyzed above. As the temperature rise times becomes long compared with the diffusion time of hydrogen, the pressure will become increasingly less than for the case of a step change in power. The reason for this is that the pressure in the clad element results from the hot fuel dehydriding faster than the cooler fuel rehydrides (takes up the excess hydrogen to reach an equilibrium with the hydrogen overpressure in the can). The slower the rise to peak temperature, the lower the pressure because of the additional time available for rehydriding.

4.5.3.1.3 Summary

The foregoing analysis gives a strong indication that the cladding will not be ruptured if fuel temperatures are never greater than in the range of 2,190°F to 2,280°F (1,200°C to 1,250°C), providing that the cladding temperature is less than about 930°F (500°C).

However, for fuel with a $ZrH_{1.7}$, a conservative safety limit of 2,012°F (1,100°C) has been chosen for this condition. As a result, at this safety limit temperature the pressure is about a factor of 4 lower than would be necessary for cladding failure. This factor of 4 is more than adequate to account for uncertainties in cladding strength and manufacturing tolerances. As a safety limit, the peak adiabatic fuel temperature to be allowed during transient conditions is considered to be 2,012°F (1,100°C) for U-ZrH fuel with ratios up to 1.70.

Under any condition in which the cladding temperature increases above 930°F (500°C), the temperature safety limit must be decreased as the cladding material loses strength at elevated temperatures. To establish this limit, it is assumed that the fuel and the cladding are at the same temperature. There are no conceivable circumstances that could give rise to a situation in which the cladding temperatures was higher than the fuel temperature.

In Fig. 4.8, the stress imposed on the clad by the equilibrium hydrogen pressure as a function of the fuel temperature is plotted. Also shown is the ultimate strength of 304 stainless steel at the same temperatures. The use of these data for establishing the safety limit for conditions in which the cladding temperature is greater than 930°F (500°C) is justified as:

- the method used to measure ultimate strength requires the imposition of the stress over a longer time than would be imposed for accident conditions, and
- the stress is not applied biaxially in the ultimate strength measurements as it is in the fuel clad.

The point at which the two curves in Fig. 4.8 intersect (for $ZrH_{1.7}$) is the safety limit, that is, 1,710°F (930°C) for conditions in which the cladding temperature is above 930°F (500°C). At that temperature, the equilibrium hydrogen pressure would impose a stress on the cladding equal to the ultimate strength of the clad.

The same argument about the redistribution of the hydrogen within the fuel presented earlier is valid for this case. In addition, at elevated temperatures the cladding becomes quite permeable to hydrogen. Thus, not only will hydrogen redistribute itself within the fuel to reduce the pressure, but some hydrogen will escape from the system entirely.

The use of the ultimate strength of the cladding material in the establishment of the safety limit under these conditions is justified because of the transient nature of accidents. Although the high cladding temperatures imply sharply reduced heat transfer rates to the surroundings (and consequently longer cooling times), only slight reductions in the fuel temperature are necessary to reduce the stress sharply. For a fuel with $ZrH_{1.7}$, a 70°F (40°C) decrease in temperature from 1,700°F to 1,630°F (930°C to 890°C) will reduce the stress by a factor of 2.

4.5.3.2 Prompt Temperature Coefficient

The basic parameter which allows the TRIGA® reactor system to operate safely with large step insertions of reactivity is the strongly negative α_T associated with the TRIGA® fuel and core design. This temperature coefficient allows a greater freedom in steady-state operation as the effect of accidental reactivity changes occurring from the experimental devices in the core is greatly reduced.

GA, the designer of the reactor, has developed techniques to calculate α_T accurately and, therefore, predict the transient behavior of the reactor. This temperature coefficient arises primarily from a change in the fuel utilization factor resulting from the heating of the uranium-zirconium hydride fuel-moderator elements. The coefficient is prompt because the fuel is intimately mixed with a large portion of the moderator, thus, fuel and solid moderator temperatures rise simultaneously. A quantitative calculation of α_T requires a knowledge of the energy dependent distributions of thermal neutron flux in the reactor.

The basic physical processes which occur when the fuel-moderator elements are heated can be described as follows: the rise in temperature of the hydride increases the probability that a thermal neutron in the fuel element will gain energy from an excited state of an oscillating hydrogen atom in the lattice. As the neutrons gain energy from the ZrH, their mean free path is increased appreciably. This is shown qualitatively in Fig. 4.19. Since the average chord length in the fuel element is comparable with a mean free path, the probability of escape from the fuel element before capture is increased. In the water, the neutrons are rapidly rethermalized so that the capture and escape probabilities are relatively insensitive to the energy with which the neutron enters the water. The heating of the moderator mixed with the fuel, thus, causes the spectrum to harden more in the fuel than in the water. As a result, there is a temperature dependent fuel utilization factor for the unit cell in the core, which decreases the ratio of absorptions in the fuel to total cell absorptions as the fuel element temperature is increased. This yields a loss of reactivity.

The temperature coefficient then depends on spatial variations of the thermal neutron spectrum over distances of the order of a mean free path with large changes of the mean free path occurring because of the energy change in a single collision. A quantitative description of these processes requires a knowledge of the differential slow neutron energy transfer cross section in water and zirconium hydride, the energy dependence of the transport cross section of hydrogen as bound in water and zirconium hydride, the energy dependence of the capture and fission cross sections of all relevant materials, and a multigroup transport theory reactor description which allows for the coupling of groups by speeding up as well as by slowing down.

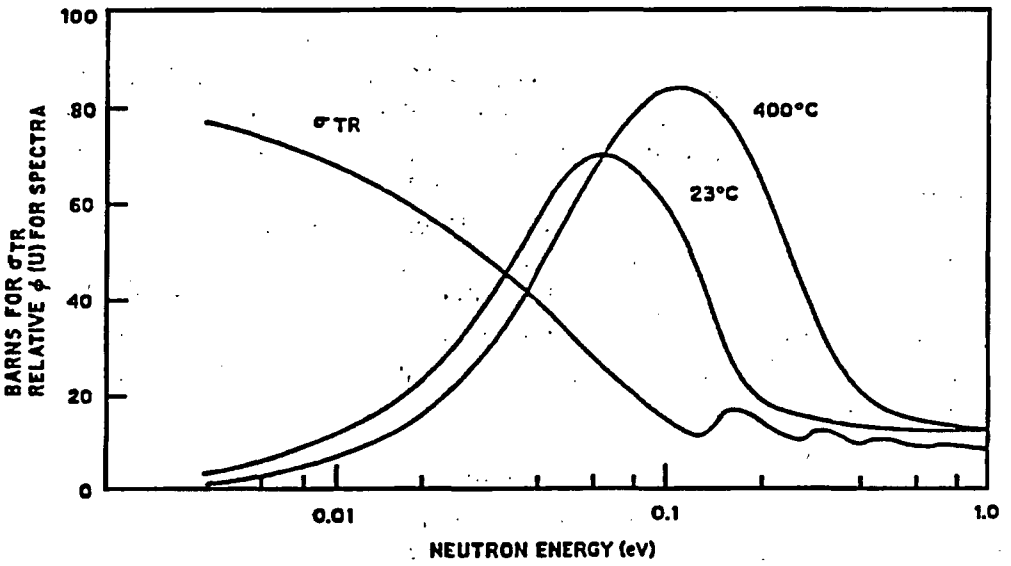

Figure 4.19 Transport Cross Section for Hydrogen in ArH and Average Neutron Spectra in Fuel Element

4.5.3.2.1 Codes used for Calculations

Calculational work on α_T made use of a group of codes developed by GA: GCC-3 (Ref. 4.24; GAZE-2 (Ref. 4.25); and GAMBLE-5 (Ref. 4.26), as well as DTF-IV (Ref. 4.27), an S_n multigroup transport code written at Los Alamos. Neutron cross sections for energies above thermal (>1 eV) were generated by the GGC-3 code. In this code, fine group cross sections (~100 groups), stored on tape for all commonly used isotopes, are averaged over a space independent flux derived by solution of the B_1 equations for each discrete reactor region composition. This code and its related cross-section library predict the age of each of the common moderating materials to within a few percent of the experimentally determined values and use the resonance integral work of Adler, Hinman, and Nordheim (Ref. 4.28) to generate cross sections for resonance materials which are properly averaged over the entire region.

Thermal cross sections were obtained in essentially the same manner using the GGC-3 code. However, scattering kernels were used to describe properly the interactions of the neutrons with the chemically bound moderator atoms (ZrH). The bound hydrogen kernels used for hydrogen in the water were generated by the THERMIDOR code (Ref. 4.29) using the thermalization work of Nelkin (Ref. 4.30). Early thermalization work by McReynolds et. at. (Ref. 4.31) on zirconium hydride has been greatly extended at GA (Ref. 4.32) and work by Parks resulted in the SUMMIT code (Ref. 4.33) which was used to generate the kernels for hydrogen as bound in ZrH. These scattering models have been used to predict adequately the water and hydride (temperature dependent) spectra as measured at the GA linear accelerator as shown in Figs. 4.20, 4.21, and Ref. 4.34.

4.5.3.2.2 ZrH Model

Qualitatively, the scattering of slow neutrons by zirconium hydride can be described by a model in which the hydrogen atom motion is treated as an isotropic harmonic oscillator with energy transfer quantized in multiples of ~0.14 eV. More precisely, the SUMMIT model uses a frequency spectrum with two branches, one for the optical modes for energy transfer with the bound proton, and the other for the acoustical modes for energy transfer with the lattice as a whole. The optical modes are represented as a broad frequency band centered at 0.14 eV, and whose width is adjusted to fit the cross section data of Woods et. al. (Ref. 4.35). The low frequency acoustical modes are assumed to have a Debye spectrum with a cutoff of 0.02 eV and a weight determined by an effective mass of 360.

This structure then allows a neutron to slow down by the transition in energy units of ~0.14 eV as long as its energy is above 0.14 eV. Below 0.14 eV, the neutron can still lose energy by the inefficient process of exciting acoustic Debye type modes in which the hydrogen atoms move in phase with the zirconium atoms, which, in turn, move in phase

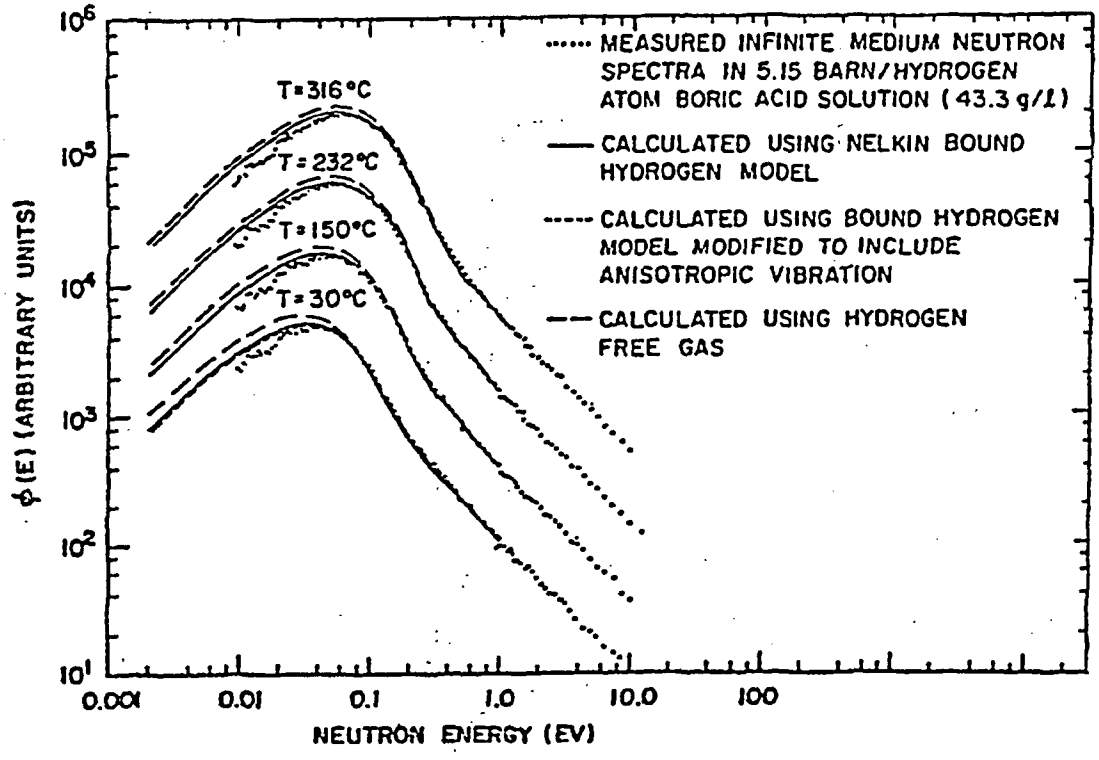

Figure 4.20 A Comparison fo Neutron Spectra Between Experiments and Several Hydrogen Models

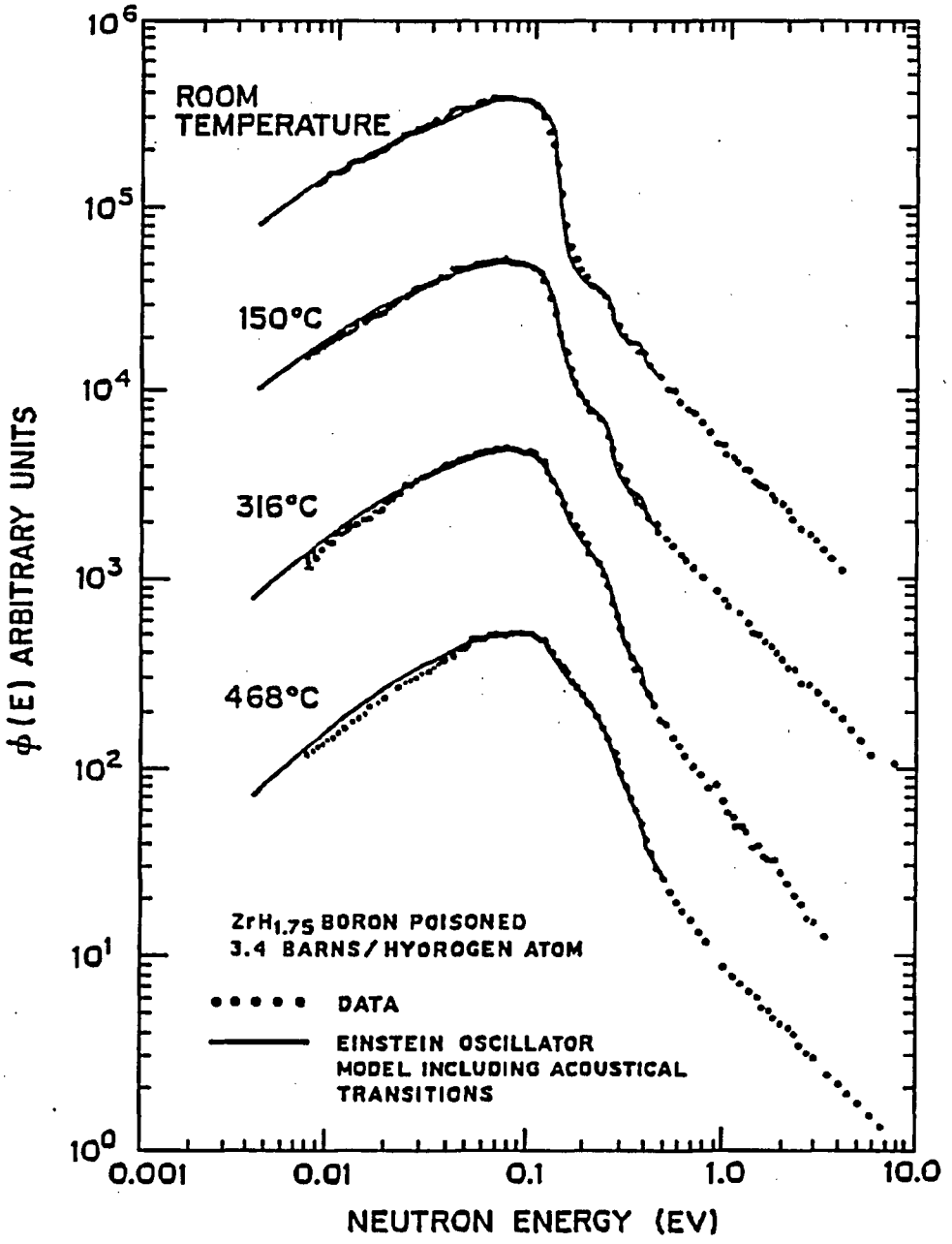

Figure 4.21 Effect of Temperature Variation on ZrH Neutron Spectra

with one another. These modes, therefore, correspond to the motion of a group of atoms whose mass is much greater than that of hydrogen, and indeed, even greater than the mass of zirconium. Because of the large effective mass, these modes are very inefficient for thermalizing neutrons, but for neutron energies below 0.14 eV, they provide the only mechanism for neutrons slowing down within the ZrH. (In a TRIGA® core, the water also provides for neutron thermalization below 0.14 eV.) In addition, in the ZrH, it is possible for a neutron to gain one or more energy units of ~ 0.14 eV in one or several scatterings from excited Einstein oscillators. Since the number of excited oscillators present in a ZrH lattice increases with temperature, this process of neutron speeding up is strongly temperature dependent and plays an important role in the behavior of ZrH-moderated reactors.

4.5.3.2.3 Calculations

Calculations of α_T were done in the following steps:

- multigroup cross sections were generated by the GGC-3 code for a homogenized unit cell. Separate cross-section sets were generated for each fuel element temperature by use of the temperature dependent hydride kernels and Doppler broadening of the ^{238}U resonance integral to reflect the proper temperature. Water at room temperature was used for all prompt coefficient calculations;

- a value for k_∞ was computed for each fuel element temperature by transport cell calculations, using the P_1 scattering treatment. Comparisons have shown S_4 and S_8 results to be nearly identical. Group dependent disadvantage factors were calculated for each cell region (fuel, clad, and water) where the disadvantage factor is defined as the ratio: ϕ_g^r / ϕ_g^c (region/cell);

- the thermal group disadvantage factors were used as input for a second GGC-3 calculation where cross sections for a homogenized core were generated which gave the same neutron balance as the thermal group portion of the discrete cell calculation; and

- the cross sections for an equivalent homogenized core were used in a full reactor calculation to determine the contribution to α_T due to the increased leakage of thermal neutrons into the reflector with increasing hydride temperature. This calculation still requires several thermal groups, but transport effects are no longer of major concern. Thus, reactivity calculations as a function of fuel element temperature have been done on the entire reactor with the use of diffusion theory codes.

Results from the above calculations indicate that more than 50% of α_T for a standard TRIGA® core comes from the temperature-dependent disadvantage factor or "cell effect" and approximately 20% each from Doppler broadening of the ^{238}U resonances and

temperature dependent leakage from the core. These effects make α_T approximately -0.01% δk/k-°C, which is rather constant with temperature. The temperature coefficient is shown in Fig. 4.22 for a typical high-hydride TRIGA® core.

4.5.3.3 Steady-State Reactor Power

The following evaluation has been made for a TRIGA® system operating with cooling from natural convection flow around the fuel elements. This analysis investigates the limits to which such a system may be operated.

The analysis was conducted by considering the hydraulic characteristics of the flow channel from which the heat rejection rate is a maximum. The geometrical data from this channel is given in Table 4-14. All symbols in Equations 16 through 45 are defined in the list of nomenclature in Section 4.5.3.10.

Table 4-14
Hydraulic Flow Parameters

Flow area (ft^2/elem)	0.00580
Wetted perimeter (ft/elem)	0.3861
Hydraulic diameter (ft)	0.0601
Fuel element diameter (ft)	[redacted]
Fuel surface area (ft^2)	[redacted]

The heat generation rate in the fuel element is distributed axially in a cosine distribution shaped at the end such that the peak-to-average ratio is 1.25. The number of fuel elements in the core is assumed to be [redacted] elements for 1 MW operation, but the departure from nucleate boiling (DNB) ratio is conservatively evaluated on the basis of [redacted] elements.

The driving force is supplied by the buoyancy of the heated water in the core. Countering this force are the contraction and expansion losses at the entrance and exits to the channel, the acceleration and potential energy and friction losses in the cooling channel itself.

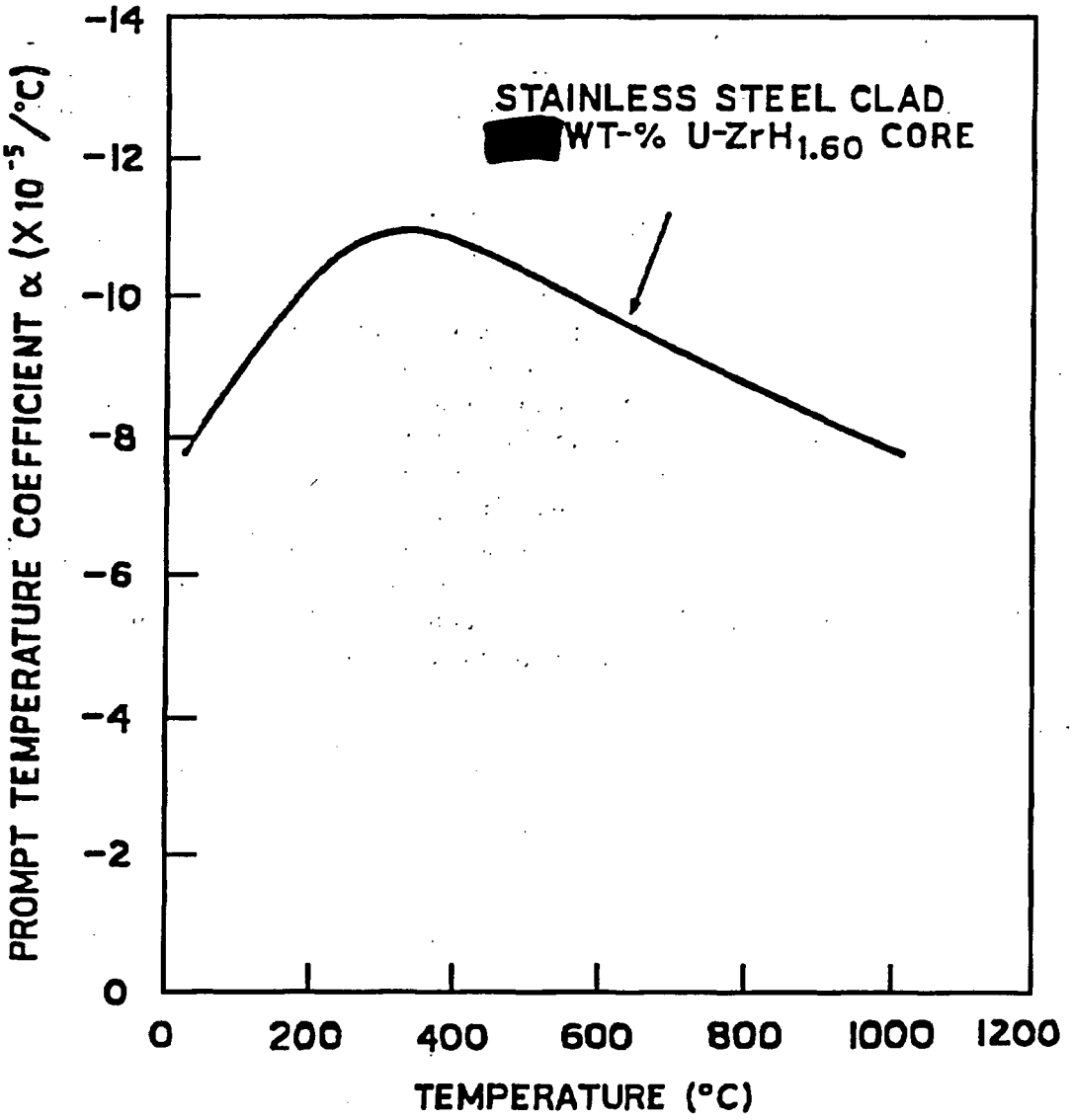

Figure 4.22 Prompt Temperature Coefficient of Reactivity Vs. Average Fuel Temperature for TRIGA® Standard Fuel

Fig. 4.23 illustrates schematically the natural convection system established by the fuel elements bounding one flow channel in the core. The system shown is general and does not represent any specific configuration. Steady-state flow is governed by the equation

$$\delta p_i + \delta p_e + \delta p_l + p_u + \sum_{j=1}^{n} wp_j = z_t / v_0 \ , \qquad (16)$$

where the left-hand members represent the pressure drops through the flow channel due to entrance, exit, friction, acceleration, and gravity losses and the right-hand member represents the driving pressure due to the static head in the pool. The pressure drops through the flow channel are dependent on the flow rate while the available static driving pressure is fixed for a known core height and pool temperature. The analysis, therefore, becomes an iterative one in which the left-hand side of Equation 16 is evaluated on the basis of an assumed flow rate and compared with the known right-hand side until equality is achieved. The method has been programmed for digital computer solution. The methods of evaluating each of the δp terms in Equation 16 for known power distribution and flow geometry and assumed flow rates are discussed below.

4.5.3.3.1 Entrance Loss δp_i

The entrance loss, δp_i, may be evaluated in the usual way as a fraction of the velocity head in the lower grid plate hole:

$$\delta p_i = \frac{k_{i_1} + k_{i_2}\ v_0}{2g\ A_i^2} (NW)^2 \ , \qquad (17)$$

where:

N = the number of channels which receive their flow from a single hole in the lower grid plate,

k_{i1} = the loss factor for the entrance to the hole in the lower grid plate. For even slight rounding of the entrance, k_{i1} will be no greater than 0.30, and

k_{i2} = the loss factor covering transfer of the flow from the hole in the lower grid plate to the coolant channels. In most cases this can be satisfactorily approximated as a sudden expansion using $k_{i2} = 1.0$.

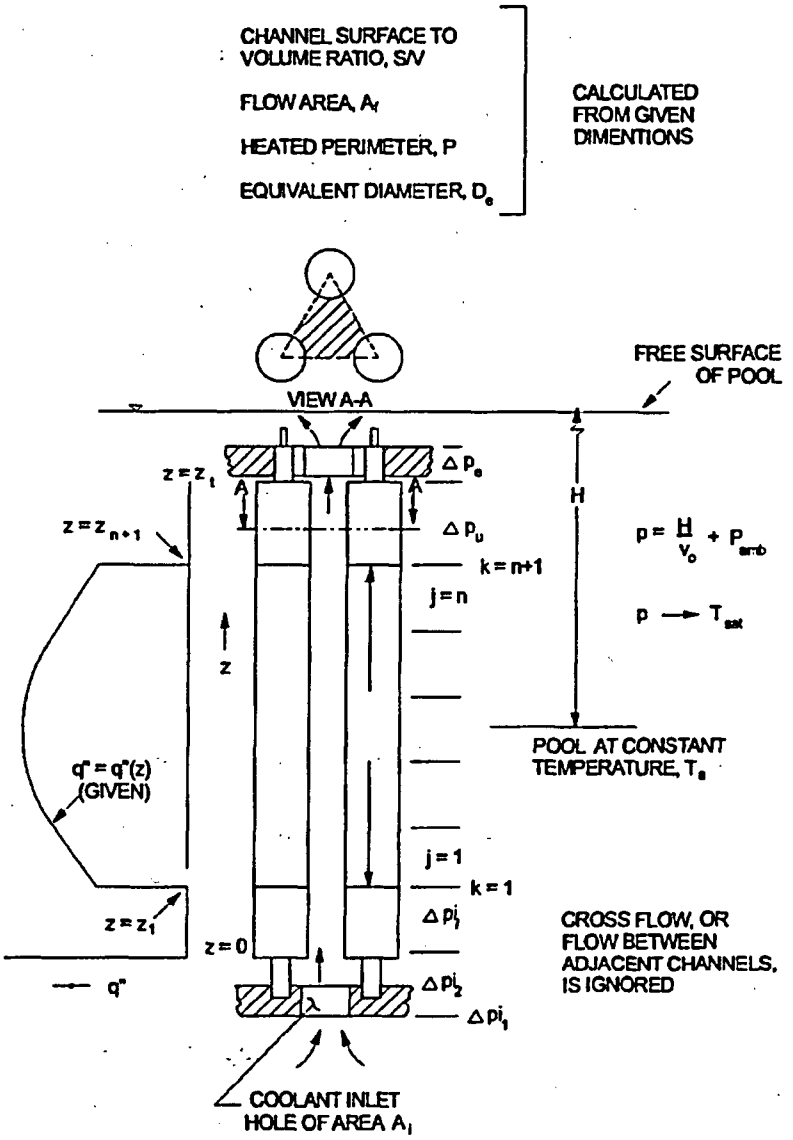

Figure 4.23 General Fuel Element Configuration for Single Coolant Channel in TRIGA® Fuel

4.5.3.3.2 Exit Loss δp_e

The exit loss is expressed in terms of a coefficient K_e which is the fraction of the velocity head in the flow channel which is not recovered:

$$\delta p_e = \frac{K_e\, v_{n+1}}{2gA_f^2}\, W^2 \,. \tag{18}$$

The term v_{n+1} is the specific volume at the highest axial station along the heated length of the core. It is evaluated from the temperature T_{n+1} which is obtained from an overall heat balance:

$$T_{n+1} = \frac{q_t}{WC} + T_0 \,, \tag{19}$$

where:

$$q_t = P\int_{z_1}^{z_{n+1}} q''(z)\,dz \,.$$

4.5.3.3.3 Loss Through Portion of Channel Adjacent to Lower Reflector δp_l

The flow is isothermal at the bulk pool temperature so that

$$\delta p_l = \frac{f_m v_0 \delta z_l}{2gD_e A_f^2}\, W^2 + \frac{\delta z_l}{v_0} \,. \tag{20}$$

The term f_m is evaluated from the Moody chart (assuming smooth surface) on the basis of a Reynolds number which is

$$R_e = \frac{D_e v_0}{A_f \nu_0} W \,. \tag{21}$$

4.5.3.3.4 Loss Through Portion of Channel Adjacent to Upper Reflector, δp_u

The flow is isothermal at T_{n+1} where T_{n+1} is determined by Equation 19. Thus,

$$\delta p_u = \frac{f_m v_n \delta z_u}{2g D_e A_f^2} W^2 + \frac{\delta z_u}{vn} . \quad (22)$$

The term f_m is again evaluated from the Moody chart, assuming smooth surface, on the basis of a Reynolds number which is

$$R_e = \frac{D_e v_n}{A_f \nu_n} W . \quad (23)$$

4.5.3.3.5 Loss Through Each Increment of the Channel Adjacent to the Fueled Portion of the Elements, δp_i

It is initially assumed that the entire heated portion of the channel is in subcooled boiling. This implies that the wall temperatures calculated from subcooled boiling correlations are lower than those calculated for convection alone and that the liquid is below its saturation temperature at all locations. The pressure drop through an increment is given by

$$\delta p_{n-(n+1)} = \frac{v_{m_{k+1}} - v_{m_k}}{g A_f^2} W^2 + \frac{f_{b_j} v_{m_j} \delta z}{2g A_f^2 D} W^2 + \frac{\delta z}{v_{m_j}} . \quad (24)$$

(acceleration) (friction) (gravity)

4.5.3.3.6 Acceleration Term

The term v_m denotes the mean specific volume and is larger than the liquid specific volume, because of the vapor voidage:

$$v_m = \frac{v}{(1-\alpha)} . \quad (25)$$

Where α is the void fraction or the fraction of a channel cross section which is occupied by vapor. The term α may be calculated from the vapor volume (cubic inches vapor/square inches heating surface) and the flow channel geometry. Denoting the vapor volume as ξ,

$$\alpha = \xi\left(\frac{S}{V}\right) . \quad (26)$$

where S/V is the surface to volume ratio of the coolant channel. The parameter ξ is dependent on the surface heat flux, the subcooling of the liquid and the velocity of the liquid. It can be evaluated only by experiment. Data given by Jordan and Leppert (Ref. 4.36) were used to estimate ξ; these data are plotted in Figs. 4.24 and 4.25. Most of this represents a flow velocity of 4 ft/sec and appears to be the only available data applicable under the thermal conditions encountered in TRIGA®-type reactors. Extrapolations from these data are made for flow velocities different from 4 ft/sec. The extrapolations were based on a small amount of data given for flow velocities other than 4 ft/sec. The liquid temperature at a station, T_k, may be calculated from:

$$T_k = \frac{P\int_{z_1}^{z_k} q''(z)dz}{WC} + T_0 \ . \qquad (27)$$

Therefore, one finds ξ (Fig. 4.25) from $T_{sat} - T_k$ and q_k'', where T_{sat} and q_k'' are known.

Since $\alpha_k = \xi_k$ (S/V) and v_k is a function of T_k, v_m may be evaluated from Equation 25.

4.5.3.3.7 Friction Term

The term v_{mj} denotes a linear average of the mean specific volumes at the upper and lower boundaries of an increment. The approximate mean value is assumed to apply over the entire increment so that:

$$v_{m_j} = \frac{v_{m_k} + v_{m_{k+1}}}{2} \ , \qquad (28)$$

A friction factor, f_{bj}, is applied locally to calculate the friction pressure drop over the

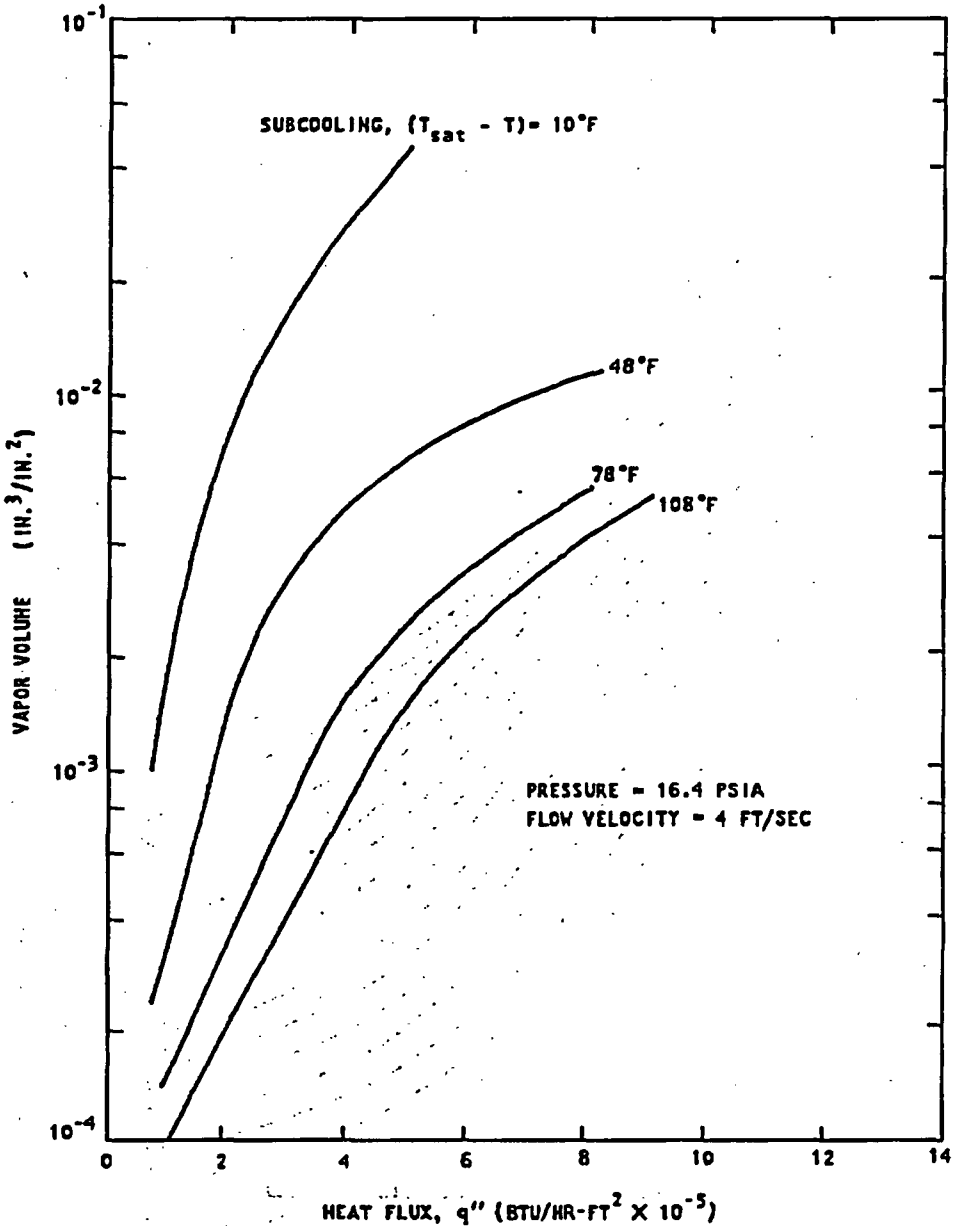

Figure 4.24 Experimentally Determined Vapor Volumes for Subcooled Boiling in a Narrow Vertical Annulus

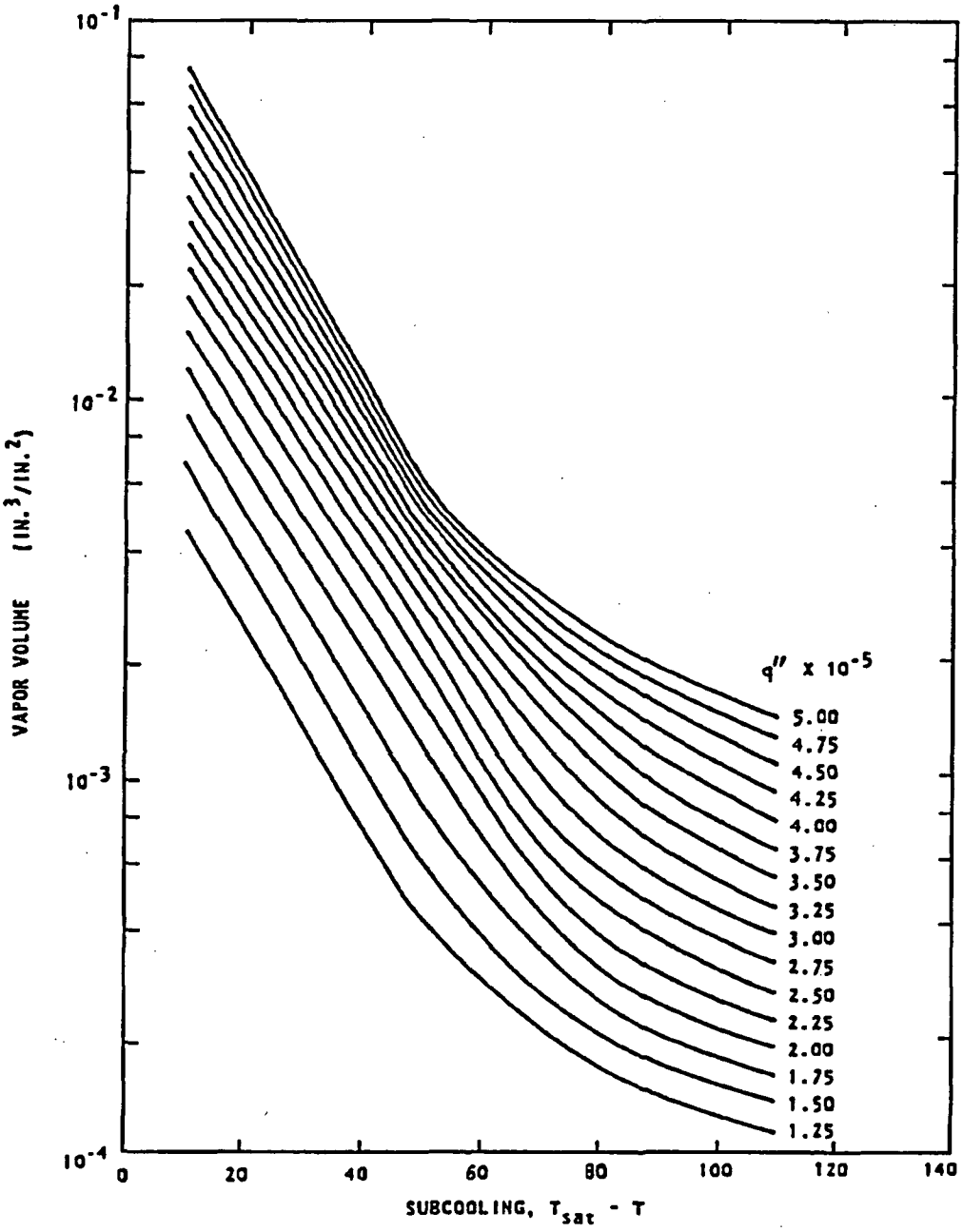

Figure 4.25 Cross Plot of Figure 4.23 Used in Calculations

increment in subcooled boiling. Jordan and Leppert developed the correlation

$$f_b = 8S_t = \frac{8h_b}{\rho CV} = \frac{8\,q''}{\rho\, CV(T_W - T)} \tag{29}$$

and provide experimental verification near atmospheric pressure in the range $0.0015 < S_t < 0.0050$. This is simply an extension of Reynold's analogy to the case of subcooled boiling. The equation of continuity is used to write Equation 29 as:

$$f_b = \frac{8\,q''\,A_f}{WC\,(T_W - T)}, \tag{30}$$

which may be evaluated if T_W is known. For subcooled boiling, the heat transfer is usually defined by an experimentally determined correlation of q″ vs. $(T_W - T_{sat})$, which has been obtained over a given range of flow velocity and pressure. McAdams (Ref. 4.37) gives such a correlation for pressures between 2 and 6 atmospheres and flow velocities between 1 and 12 ft/sec. This correlation will be used to determine T_W for use in Equation 30.

Approximate mean values are assumed to apply over the entire increment so that:

$$f_{b_j} = 1/2\frac{8\,A_f}{WC}\left[\frac{q''_k}{T_{wk} - T} + \frac{q''_{k+1}}{T_{wk+1} - T_{k+1}}\right] \tag{31}$$

and

$$T_W - T_{sat.j} = \frac{\Phi(q''_k) + \Phi(q''_{k+1})}{2},$$

where $\Phi(q'')$ is the correlation of McAdams previously cited.

4.5.3.3.8 Gravity Term

The gravity term is evaluated using v_j calculated from Equation 28.

As implied in Section 4.5.3.3.5, each increment must be checked to determine whether heat is being transferred by subcooled boiling or by convection. The term T_W is evaluated at the lower boundary of the increment on the basis of both the correlation from McAdams for subcooled boiling and a standard correlation for convection (Dittus-Boelter). If the T_W

calculated from convection correlations is less than that obtained for subcooled boiling, boiling is assumed not to be present in the increment. Equation 24 still applies, but since there is no boiling, and hence no vapor void, v_m becomes v and f_b becomes f_m.

In the foregoing analysis, an assumption was made that all of the vapor formed on the surface of the fuel element detaches and adds to the fluid buoyance. This is not a conservative assumption. The position where vapor bubbles first leave the heated surface is obtained from two considerations; first, the balance of the forces exerted on the vapor bubble while it is in contact with the wall (buoyancy, surface tension, and friction), and second, the temperature distribution in the single phase liquid away from the walls.

Determination of the buoyancy forces resulting from the formation and subsequent detachment of vapor bubbles is complicated by the difficulty in predicting the point at which the vapor detaches, and the fraction of that vapor which subsequently condenses. The problem was simplified by making use of an analysis performed by Levy (Ref. 4.38) to determine the position at which the vapor detaches from the wall, assuming that at that point all of the vapor detaches and, finally, that there is no recombination of the vapor with subcooled fluid.

According to Levy, the position at which the vapor leaves the surface is obtained from considering the balance of forces exerted on the vapor bubble while it is in contact with the wall, and the temperature distribution in the single phase liquid away from the wall.

The forces acting on the bubble in the vertical direction consist of a buoyant force, F_B, a frictional force, F_F, exerted by the liquid on the bubble, and a vertical component of the surface tension force, F_S.

The buoyant force, F_B, is given by:

$$F_B = \frac{C_B\, r_B^3 (\rho_L - \rho_v) g}{g_c}, \qquad (32)$$

where r_B is the bubble radius, C_B is a proportionality constant, ρ_L and ρ_v are the liquid and vapor density, g is the acceleration due to gravity and g_c is the conversion ratio from lb-force to lb-mass. The frictional force, F_F, is related to the liquid frictional pressure drop per unit length, $(-dp/dz)_F$. The pressure differential across the bubble is proportional to the pressure differential times the bubble radius and acts across an area proportional to the square of the bubble radius. Relating the pressure differential to the wall shear stress, τ_w, by:

$$-(dp/dz)_F = 4\,\tau_w / D_H, \qquad (33)$$

the following result for F_F is then obtained:

$$F_F = C_F \frac{\tau_w}{D_H} r_B^3 , \tag{34}$$

where C_F is a constant of proportionality and D_H is the hydraulic diameter (four times the cross-sectional area divided by the wetted perimeter). The surface tension force, F_S, is given by:

$$F_S = C_S r_B \sigma , \tag{35}$$

where C_S is a proportionality constant and σ is the surface tension. Assuming upward flow, the balance of these forces results in the following solutions for the bubble radius:

$$r_B = \left[\frac{C_S \sigma}{C_B \frac{g}{g_c}(\rho_L - \rho_v) + C_F \frac{\tau_w}{D_H}} \right] 1/2 . \tag{36}$$

Assuming that the distance from the wall to the tip of the bubble is proportional to the bubble radius, a non-dimensional distance corresponding to this real distance can be given by:

$$Y_B = C \frac{(\sigma g_c D_H - \rho_L)^{1/2}}{\mu_L} \left[1 + C' \frac{g}{g_c} \frac{(\rho_L - \rho_v)}{\tau_w} \right]^{-1/2} , \tag{37}$$

where C and C' are appropriate constants. For those cases where the fluid forces are considerably greater than the buoyant forces, this expression reduces to:

$$Y_B = C(\sigma g_c D_H - \rho_L)^{1/2} 1/\mu_L . \tag{38}$$

For the bubble to detach, the fluid temperature at the tip of the bubble must exceed the saturation temperature by an amount such that the pressure differential acting across the interface at the tip of the bubble balances the surface tension forces at the same position. By using the Clausius-Clapeyron solution of this pressure differential, one finds that the fluid temperature-saturation temperature difference can be assumed to be zero.

The temperature at the tip of the bubble can be specified from existing solutions for the fluid temperature distribution. Thus, if the flow is assumed to be turbulent, and using the solution proposed by Martinelli, we have:

$$T_w - T_B = \theta P_r Y_B \quad ; \quad 0 \le Y_B \le 5 \tag{39}$$

$$= 50 \{P_r + \ln [1 + P_r (Y_B/5 - 1)]\} \quad ; \quad 5 \le Y_B \le 30$$

$$= 50 \{P_r + \ln [1 + 5 P_r] + 0.5 \ln [Y_B/30)]\} \quad ; \quad Y_B > 30.$$

The parameter θ is a non-dimensional term defined through the heat flux and liquid specific heat, that is,

$$\theta = \frac{q/A}{\rho_L C_{pL} \left(\tau_w g_c / \rho_L\right)^{1/2}} . \tag{40}$$

Levy obtained values for the constants C and C′ by correlation with available experimental data. Using the accepted heat-transfer relation from Dittus-Boelter, one obtains:

$$hD_H/k_L = 0.023 \ (WD_H/\mu_L)^{0.8} (Pr)^{0.4} . \tag{41}$$

Calculating the friction factor from:

$$f = 0.0055 \{1 + [20{,}000 (\epsilon/D_H) + 10^6/(WD_H/\mu_L)]^{1/3}\} , \tag{42}$$

we are able to find the wall shear stress from:

$$\tau_w = (f/8) (W^2/\rho_L g_c) . \tag{43}$$

The correlation with experimental results yielded values for the constants of:

$$c = 0015 \text{ and} \tag{44}$$

$$C' = 0$$

Finally, from the definition of the heat transfer coefficient, one obtains:

$$T_W - T = q''/h \tag{45}$$

and setting the bubble tip temperature, T_B, equal to the saturation temperature, T_{sat}, we can express the relationship between the saturation temperature, the wall temperature, and the

fluid temperature at which the bubble would detach from the wall by:

$$(T_w - T_{sat}) / (T_w - T) = 0.023 \, (WD_H / \mu_L)^{-0.2} \, (Pr)^{-0.6} \, (f/8)^{-0.5} \Omega \qquad (46)$$

where:

$$\Omega = Pr \, Y_B \; ; \qquad 0 < Y_B < 5$$

$$= 5 \, \{Pr + \ln [1 + Pr \, (0.2 \, Y_B - 1)]\} \; ; \; 5 < Y_B < 30$$

$$= 5 \, \{Pr + \ln [1 + 5Pr) + 0.5 \ln (Y_B/30)\} \; ; \; Y_B > 30.$$

4.5.3.3.9 Results of Calculations

The solution of the force balance equation with void detachment was accomplished by iterating on the void detachment point to find where the right and left sides of Equation 46 were equal. The point at which the void was assumed to separate from the surface was taken as the point at which equality was obtained.

The peak heat flux, that is, the heat flux at which there is a departure from nucleate boiling and the transition to film boiling begins, was determined by two correlations. The first, given by McAdams (Ref. 4.39) indicates that the peak heat flux is a function of the fluid velocity and the fluid only. The second correlation is due to Bernath (Ref. 4.40). It encompasses a wider range of variables over which the correlation was made and takes into account the effect of differential flow geometries. It generally gives a lower value for the peak heat flux and is the value used for determining the minimum DNB ratio, that is, the minimum ratio of the local allowable heat flux to the actual heat flux. In general, the McAdams correlation gives a DNB ratio 50% to 80% higher than the Bernath correlation.

Fig. 4.26 shows the results of this analysis. This figures shows the maximum channel heat flux for which the DNB ratio is 1, with bulk pool water temperature as a parameter. It is assumed that all the vapor above the detachment point separates from the heated surface. From this figure, it can be seen that with the design cooling water temperature at the core inlet (120°F) the maximum heat flux is 325 kBTU/h-ft^2. For a [redacted]element core with an overall peak-to-average power density ratio of 2.0, this heat flux corresponds to a maximum reactor power of 1,675 and 1,900 kW, respectively.

4.5.3.3.10 Nomenclature

A	cross-sectional area, ft^2
A_f	channel free flow area, ft^2
C	coolant specific heat, Btu/lb-°F
d	diameter, inches
D_e	channel equivalent diameter, ft
D_H	hydraulic diameter, ft
f_b	friction factor with subcooled boiling, dimensionless
f_m	friction factor without boiling, dimensionless
F	forces acting on vapor bubble
g	constant, 4.18×10^8 ft/h^2
h_b	heat transfer coefficient with subcooled boiling, Btu/h-ft^2-°F
H	distance from midplane of heated channel to free surface of pool, ft
K	pressure loss factor at channel inlet or exit, dimensionless
n	number of equal axial increments into which heated length of core is subdivided
N	Number of channels which receive their flow from a single opening in the lower grid plate
p	absolute pressure, lb/ft^2
P	heated perimeter of channel, ft
Pr	Prandtl number
δp	pressure loss, lb/ft^2
q	heat load, Btu/h
q_t	total heat load to channel, Btu/h
q"	heat flux, Btu/h-ft^2
q_p"	peat or "burnout" heat flux, Btu/h-ft^2
r_B	bubble radius
R_e	Reynolds number, dimensionless
S/V	channel surface to volume ratio, in-.1
T	coolant temperature, °F
T_{sat}	coolant saturation temperature, °F
v	specific volume, ft^3/lb
V	flow velocity, ft/h
W	mass flow rate, lb/h
Y	non-dimensional radius
z	axial coordinate in channel, ft
z_t	total length of channel, ft
δz	length of a calculation increment in the channel, ft
μ	dynamic viscosity, ft-lb/h
α	void fraction or fraction of a channel cross section which is occupied by vapor, dimensionless

σ	surface tension, lb/ft
ξ	vapor volume, or volume of vapor produced per unit area of heated surface, cubic inch/square inch
ν	kinematic viscosity, ft^2/h
τ	shear stress, lb/ft^2
ρ	density, lb/ft^3
ϵ/D_e	relative roughness

Subscripts

e	conditions at channel exit
i	conditions at channel entrance or inlet
l	conditions in portion of channel adjacent to lower reflector
m	conditions averaged over the liquid and vapor phases
o	bulk pool conditions
u	conditions in portions of channel adjacent to upper reflector
j	axial increment index
k	axial station index
w	conditions at cladding outer surface
v	vapor
L	liquid

4.6 Thermal-Hydraulic Design

Very extensive thermal-hydraulic design studies and extensive actual performance tests have been done by GA over the years on reactor cores utilizing TRIGA®-type fuel. This well known volume of analysis and testing (See Refs. 4.4, 4.5, 4.41, and 4.42) will not be repeated here in this SAR and only the relevant results as they apply to the OSTR will be presented.

The calculated and measured heat transfer characteristics of three TRIGA® reactors, including the OSTR, are given in Table 4-15. The SNRS reactor (1 MW) was essentially equivalent to the OSTR with the exception that it operated throughout its lifetime with only LEU fuel. All calculations and tests were done under conditions of natural convection circulation of water through the various cores. Design-basis conditions evaluated for TRIGA® reactors using stainless steel clad U-$ZrH_{1.7}$ fuel elements provide a generous safety margin for the OSTR. These general evaluations are supported by extensive experience in operation of TRIGA® cores at equivalent fuel temperatures and power levels. No adverse results are reported from operation of TRIGA® cores at fuel temperatures and power levels greater than this design. Table 4-16 lists the pertinent heat transfer and hydraulic parameters for the typical TRIGA® operating at 1 MW.

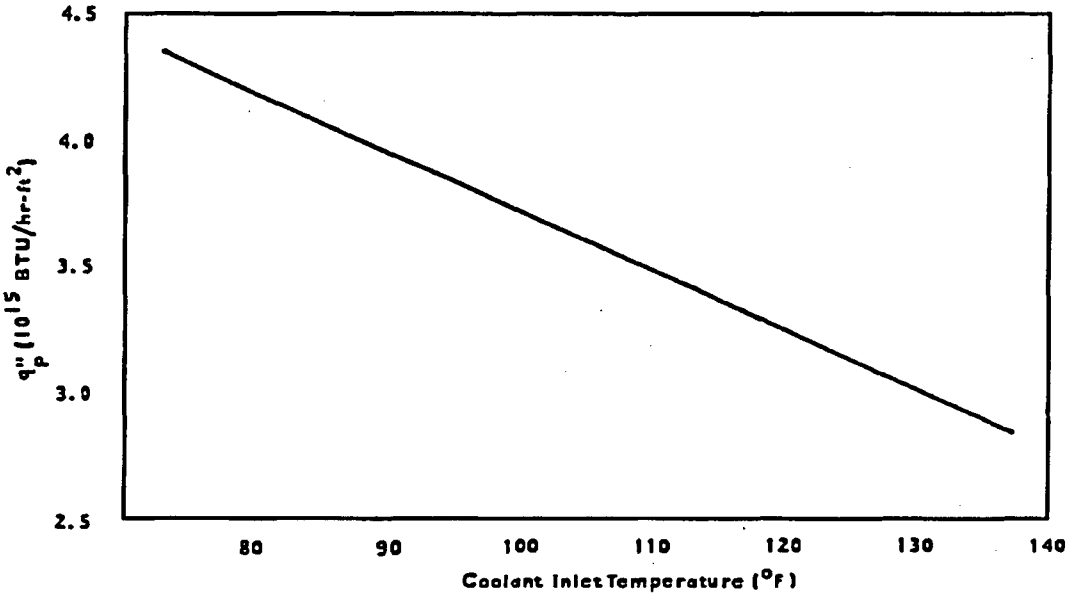

Figure 4.26 Plot for Which DNB Ratio is 1.0 of Maximum Heat Flux Vs. Coolant Temperature

Table 4-15
Comparison of Heat Removal from a Standard TRIGA® Reactors

	Standard TRIGA®	SNRS TRIGA®	OSTR
Reactor Power (MW)	1.5	1.0	1.0**
No. of Elements	[redacted]	[redacted]	[redacted]
Fuel Element Diameter (inches)	[redacted]	[redacted]	[redacted]
Hydraulic Diameter (ft)	0.0601	0.0601	0.0601
Max. Heat Flux (Btu/h/ft^2)	284,500	157,100	166,500
Fuel Surface Area (ft^2/rod)	[redacted]	[redacted]	[redacted]
Heat Transfer Surface (ft^2)	35.71	43.44	41.03
Saturation Temp. (°F)	239	-	-
Inlet Temp. (°F)	60	120	-
Exit Subcooling (°F)	0	-	-
Mass Flow Rate (#/h in^2)	1160*	-	-
Min. DNB Ratio	1.15*	2.0	-

* Extrapolated
** Licensed 1.1 MW

Table 4-16
1 MW TRIGA® Heat Transfer And Hydraulic Parameters

Number of fuel elements	[redacted]
Diameter	[redacted] inches
Length (heated)	[redacted] inches
Flow area	0.522 ft^2
Wetted perimeter	[redacted]
Hydraulic diameter	0.0601 ft
Heat transfer surface	[redacted]
Inlet coolant temperature	120°F (48.9°C)
Exit coolant temperature (average)	174°F (78.9°C)
Coolant mass flow	63,700 lb/h
Average flow velocity	0.55 ft/sec
Average fuel temperature	500°F (260°C)
Maximum wall temperature	280°F (138°C)
Maximum fuel temperature	842°F (450°C)
Average heat flux	78,600 Btu/h-ft^2
Maximum heat flux	157,100 Btu/h-ft^2
Minimum DNB ratio	2.0

4.7 References

4.1 "The U-ZrH_x Alloy: Its Properties and Use in TRIGA® Fuel," GA Report 414, February 1980, Mt. Simnad.

4.2 "Fission Product Releases from TRIGA®-LEU Reactor Fuels," GA-A16287, November 1980, Baldwin, Foushee, and Greenwood.

4.3 "Summary of TRIGA® Fuel Fission Product Release Experiments," Gulf-EES-A10801, September 1971.

4.4 "Amendment II to the Safety Analysis Report - Texas A&M University Nuclear Science Center," November 1, 1972.

4.5 "Final Safety Analysis Report - Stationary Neutron Radiography System," McClellan Air Force Base, Sacramento, CA, Prepared by Argonne National Laboratory-West, January 1992.

4.6 "Amendment No. 6 to the SAR for the OSU TRIGA Reactor Conversion from HEU to LEU Fuel," OSU-RC-9303, March 1993.

4.7 Merten, U., et. al., "Thermal Migration of Hydrogen in Uranium-Zirconium Alloys," General Dynamics, General Atomic Division Report GA-3618, 1962.

4.8 G. A. Report, "Low Enriched TRIGA Fuel-Water Quench Safety Test," GA-15413, June 1979.

4.9 Johnson, H. A., et. al., "Temperature Variation, Heat Transfer, and Void Volume Development in the Transient Atmosphere Boiling of Water," SAN-1001, University of California, Berkeley, 1961.

4.10 McAdams, W. H., Heat Transmission, 3rd Ed, McGraw-Hill Book Co., New York, 1954.

4.11 Sparrow, E. M. and R. D. Cess, "The Effect of Subcooled Liquid on Film Boiling," Heat Transfer, 84, 149-156 (1962).

4.12 Speigler, P., et. al., "Onset of Stable Film Boiling and the Foam Limit," Int. J. Heat and Mass Transfer, 6, 987-989 (1963).

4.13 Zuber, W., "Hydrodynamic Aspects of Boiling Heat Transfer," AEC Report AECV-4439, TIS, ORNL, 1959.

4.14 Rohsenow, W., and H. Choi, Heat, Mass and Momentum Transfer, Prentice-Hall, 1961, pp. 231-232.

4.15 Ellion, M. E., "A Study of the Mechanism of Boiling Heat Transfer," Jet Propulsion Laboratory Memo, No. 20-88, 1954.

4.16 Coffer, C. O., et. al., "Characteristics of Large Reactivity Insertions in a High Performance TRIGA® U-ZrH Core," General Dynamics, General Atomic Division Report GA-6216, 1965.

4.17 Fenech, H., and W. Rohsenow, "Thermal Conductance of Metallic Surfaces in Contact," USAEC NYO-2130, 1959.

4.18 Graff, W. J., "Thermal Conductance Across Metal Joints," Machine Design, Sept. 15, 1960, pp. 166-172.

4.19 Fenech, H., and J. J. Henry, "An Analysis of a Thermal Contact Resistance," Trans. Am. Nucl. Soc. 5, 476 (1962).

4.20 Bernath, L., "A Theory of Local Boiling Burnout and Its Application to Existing Data," Heat Transfer - Chemical Engineering Progress Symposium Series, Storrs.

4.21 Spano, A. H., "Quarterly Technical Report, SPERT Project," April, May, and June 1964, 150-170.

4.22 Dee, J. B., et. al., "Annular Core Pulse Reactor," General Dynamics, General Atomics Division Report GACD-6977, Supplement 2, 1966.

4.23 Johnson, H. E., "Hydrogen Disassociation Pressures of Modified SNAP Fuel," Report NAA-SR-9295, Atomics International, 1964.

4.24 Adir, J., et. al., "Users and Programmers Manual for the GGC-3 Multigroup Cross Section Code," General Dynamics, General Atomics Division Report GA-7157, 1967.

4.25 Lenihan, S. R., "GAZE-2: A One-Dimensional, Multigroup, Neutron Diffusion Theory Code for the IBM-7090," General Dynamics, General Atomic Division Report GA-3152, 1962.

2.26 Dorsey, J. P., and R. Froehlich, "GAMBLE-5 - A Program for the Solution of the Multigroup-Neutron-Diffusion Equations in Two Dimensions, with Arbitrary Group Scattering, for the UNIVAC-1108 Computer," Gulf General Atomic Report GA-8188, 1967.

4.27 Lathrop, D. K., "DTF-IV, A GORTRAN-IV Program for Solving the Multigroup Transport Equation with Anisotropic Scatterings," USAEC Report LA-3373, Los Alamos Scientific Laboratory, New Mexico, 1965.

4.28 Adler, F. T., G. W. Hinman, and L. W. Nordheim, "The Quantitative Evaluation of Resonance Integrals," in Proc. 2nd Intern. Conf. Peaceful Uses At. Energy (A/CONF. 15/P/1983), Geneva, International Atomic Energy Agency, 1958.

4.29 Brown, H. D., Jr., Gulf General Atomic Inc., "THERMIDOR - A FORTRAN-II Code for Calculating the Nelkin Scattering Kernel for Bound Hydrogen (A Modification of Robespierre)," unpublished date.

4.30 Nelkin, M. S., "Scattering of Slow Neutrons by Water," Phys. Rev. 119, 741-746 (1960).

4.31 McReynolds, A. W., et. al., "Neutron Thermalization by Chemically-Bound Hydrogen and Carbon," in Proc. 2nd Intern. Conf. Peaceful Uses At. Energy (A/CONF. 15/P/1640), Geneva, International Atomic Energy Agency, 1958.

4.32 Whittemore, W. L., "Neutron Interactions in Zirconium Hydride," USAEC Report GA-4490 (Rev.), General Dynamics, General Atomic Division, 1964.

4.33 Bell, J., "SUMMIT: An IBM-7090 Program for the Computation of Crystalline Scattering Kernels," USAEC Report, General Dynamics, General Atomic Division Report GA-2492, 1962.

4.34 Beyster, J. R., et. al., "Neutron Thermalization in Zirconium Hydride," USAEC Report, General Dynamics, General Atomic Division Report GA-4581, 1963.

4.35 Woods, A. D. B., et. al., "Energy Distribution of Neutrons Scattered from Graphite, Light and Heavy Water, Ice, Zirconium Hydride, Lithium Hydride, Sodium Hydride, and Ammonium Chloride, by the Beryllium Detector Method," in Proc. Symp. Inelastic Scattering of Neutrons in Solids and Liquids, Vienna, Austria, Oct. 11-14, International Atomic Energy Agency, 1960.

4.36 Jordon, D. P., and G. Leppert, "Pressure Drop and Vapor Volume with Subcooled Nucleate Boiling," Int. J. Heat Mass Trans. 5, 751-761 (1962).

4.37 McAdams, op. cit., pp. 390-392.

4.38 Levy, S., "Forced Convection Subcooled Boiling-Prediction of Vapor Volumetric Fraction," Int. J. Heat Mass Trans. 10, 861-965 (1967).

4.39 McAdams, op. cit., p. 392.

4.40 Bernath, op. cit., pp. 95-116.

4.41 "Safety Analysis Report for the Torrey Pines TRIGA® Mark IV Reactor," GA-9064, Gulf General Atomic, January 5, 1970.

4.42 "Annular Core Pulse Reactor," General Dynamics, General Atomic Division Report GACD 6977, Supplement 2, September 30, 1966.

CHAPTER 5

REACTOR COOLANT SYSTEMS

Chapter 5 - Valid Pages
Rev. 0 7/1/2004

i	Rev. 0 7/1/2004
ii	Rev. 0 7/1/2004
1	Rev. 0 7/1/2004
2	Rev. 0 7/1/2004
3	Rev. 0 7/1/2004
4	Rev. 0 7/1/2004
5	Rev. 0 7/1/2004
6	Rev. 0 7/1/2004

TABLE OF CONTENTS

LIST OF FIGURES

THIS PAGE INTENTIONALLY LEFT BLANK

5 REACTOR COOLANT SYSTEMS

5.1 Summary Description

Water is used in the OSTR to cool the reactor, to provide a shield for the reactor while still maintaining visibility, and to moderate (thermalize) the fast neutrons to enable the fission reactions to take place. The reactor core is located at the bottom of a shielded [redacted] diameter, [redacted] foot deep aluminum open-top tank. Water level over the core is normally maintained at [redacted] to provide radiation shielding over the core. The reactor core is cooled by natural circulation water flow through the core area combined with a forced-flow of water into and out of the reactor tank. A remote secondary heat exchanger transfers core heat from the reactor tank primary flow to a fan-assisted, roof-mounted, water-to-air heat exchanger to assist in maintaining low coolant temperatures during extended 1-MW full-power operations.

5.2 Primary Coolant System

The primary coolant system, shown in Figure 5.1, consists principally of a pump and heat exchanger connected by suitable four-inch diameter aluminum piping to the reactor tank. The stainless steel case and impeller primary pump deliver approximately 490 gpm of water through the secondary heat exchanger. The pump is directly-coupled to a 20-hp motor.

Approximately 50 gpm of the primary coolant return-flows through a diffuser nozzle pointing down onto the top of the core. This has the effect of delaying ^{16}N as it rises to the surface of the reactor tank.

Temperature probes in the primary water system assist the operator in monitoring water temperatures at various locations to assess system operation and ensure that the maximum tank water temperature is not exceeded. In the event of coolant system leakage, an underground holding tank collects and stores the fluid for eventual discharge. In-tank level alarms provide operator notification of decreasing tank level. Minimum water level in the tank is maintained by siphon break holes in the in-tank system piping at 22 inches below normal tank level.

5.3 Secondary Coolant System

The secondary coolant system, shown in Figure 5.2, consists principally of a pump, heat exchanger, cooling tower, connecting piping and associated instrumentation. The flow rate in this water system is set at approximately 700 gpm.

Figure 5.1 Primary Coolant System Schematic

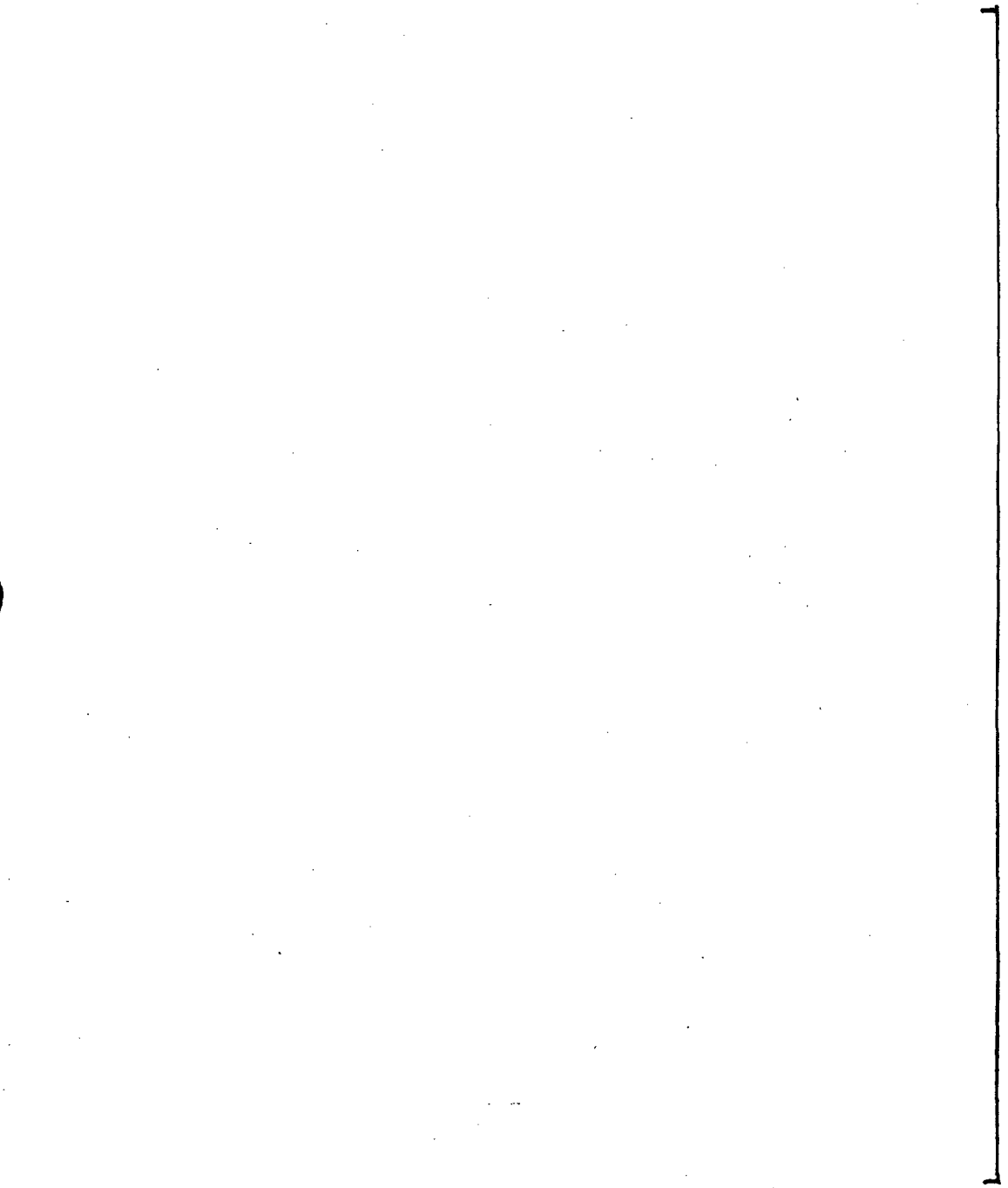

Figure 5.1 Primary Coolant System Schematic

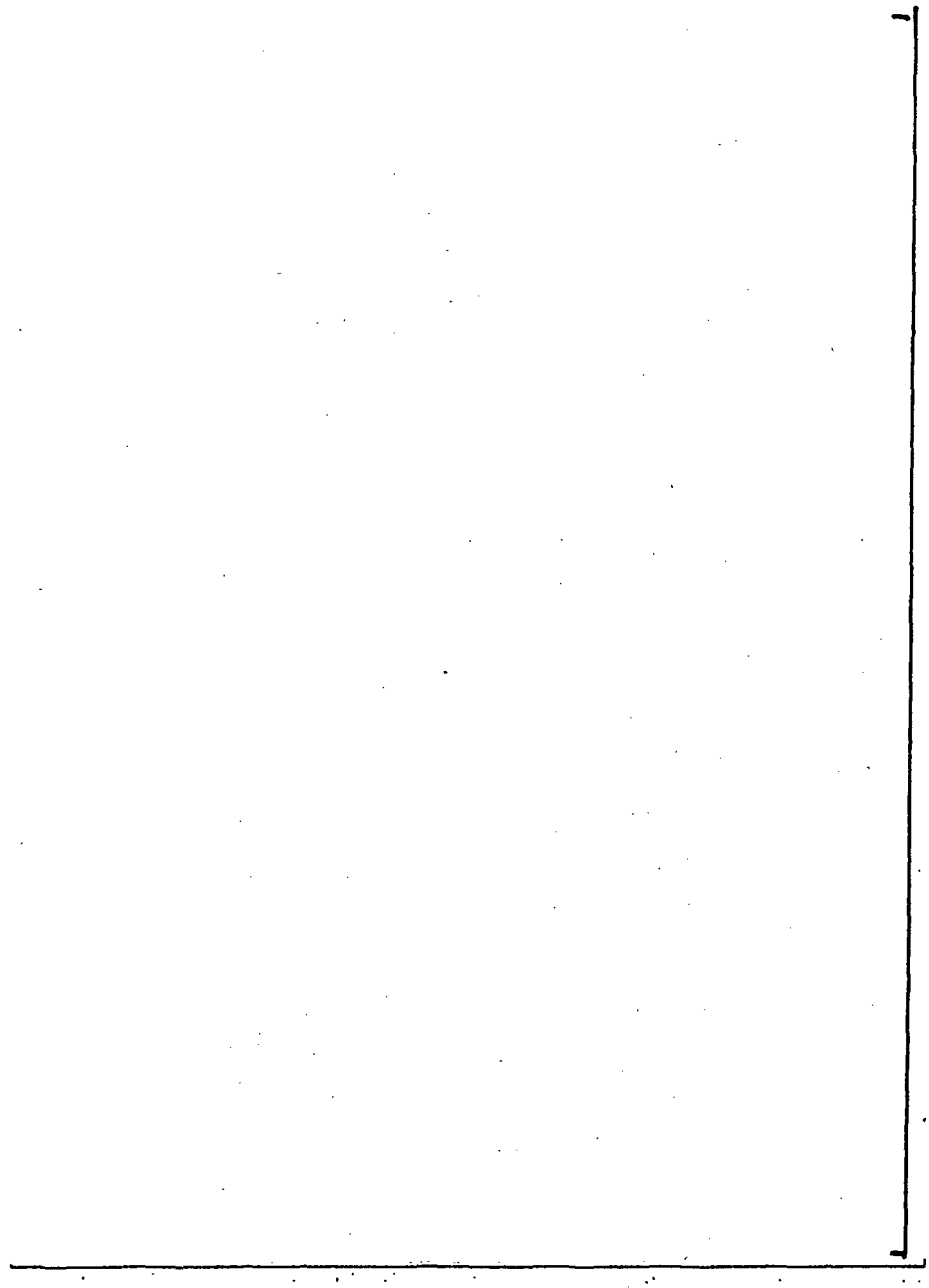

Figure 5.2 Secondary Coolant System Schematic

A tube-and-shell type heat exchanger is used for the removal of heat from the reactor primary coolant loop. The carbon steel shell contains 72 U-shaped stainless steel tubes that are welded into a removable stainless steel tube bundle. All parts of the heat exchanger that are in contact with the demineralized primary water are made of Type 304 stainless steel. The water in the secondary coolant system flows into the carbon steel shell side of the heat exchanger. The heat exchanger has an operating capacity of approximately 1 MW of thermal energy.

The secondary system cooling tower is located on the reactor building roof and holds approximately 400 gallons of water. The tower basin has a "V"-shaped trough that is designed for self-cleaning. A set of coarse screens is mounted in the basin to catch coarse debris. Forced air for cooling the inlet water spray is provided by two, 3-phase motors, each turning a set of three squirrel cage fans. Secondary system pressure exceeds primary system pressure to ensure that a heat exchanger leakage results in the containment of potentially contaminated primary fluid.

Make-up water to the cooling tower comes from the city water system and is automatically added as needed by a float valve. An overflow is provided to prevent accidental overfilling of the cooling tower basin which would flood into the squirrel cage fans.

To prevent damage from freezing, the cooling tower is fitted with two automatic heaters that will turn on at a preset water temperature. Secondary chemistry is maintained by an automatic water conditioning system. One portion of the system helps control corrosion, which is important from the standpoint of equipment longevity and maintaining good heat transfer capabilities in the heat exchanger, while another chemical addition loop helps control water-born biological growth and maintain the water conductivity.

As shown in Figure 5.3, the chemical addition and blow-down regime is based on cooling tower makeup flow. A flow pulse meter valve located on the cooling tower makeup line sends a signal to a dual pulse timer. After a given amount of flow, the timer will start a chemical addition pump for a preset time period. Later, the timer will blow down the secondary coolant for a given period of time. The timer only operates when the secondary pump is in operation.

5.4 Primary Coolant Cleanup System

The primary water purification system, also shown in Figure 5.1, consists principally of a pump; a monitoring chamber that contains probes for measuring temperatures, radioactivity, and conductivity; two fiber cartridge filters; a mixed-bed demineralizer; and a flow meter. A small portion of the inlet primary flow is diverted to the purification system components and is returned directly to the reactor tank. The purification system is constructed of 1-inch aluminum and 1-inch PVC plastic piping. A siphon break hole

provides protection against water loss due to pipe leakage. The purification system pump is a 0.75-hp pump driven by a directly-coupled induction motor. The demineralizer vessel contains 3 cubic feet of resin with an equal and homogenous mixture of anion and cation resin. It is mounted behind a concrete shield wall. Local area radiation monitoring is provided to evaluate collected debris. Maximum water flow through the demineralizer is maintained at 10 gpm. Replaceable fiber cartridges of 25-micron ratings are used in the purification system to remove insoluble particulate matter from the reactor water system. Four pressure gauges are positioned in the demineralizer lines to measure the pressure drop (ΔP) across the filters as an aid in determining the extent of filter clogging. An aluminum cylinder in the purification system acts as a water monitoring vessel and contains: (1) a temperature probe for measuring demineralizer inlet water temperature, (2) a conductivity probe for measuring demineralizer inlet water purity, and (3) a Geiger tube for detecting any radioactivity in the water. An additional conductivity probe is located in the demineralizer outlet line to monitor resin bed efficiency.

A surface skimmer is provided to assist in maintaining the cleanliness of the reactor tank water surface. The surface skimmer collects foreign particles on the surface of the reactor tank water. The floating foreign particles are collected in a floating basket as the skimmer draws in water from the surface. The skimmer is connected to the primary coolant system suction line by a small diameter aluminum pipe and throttle valve.

5.5 Primary Coolant Makeup Water System

The makeup water system provides distilled water from a common facility reverse osmosis distilling unit for the reactor and bulk shield makeup tanks. This very pure water source is used to prolong resin life and further reduce primary water activity. Makeup water to compensate for reactor tank evaporation and sampling is added by pumping water from the makeup tank through the demineralizer and its discharge system directly to the reactor tank.

5.6 ^{16}N Control System

A portion of the reactor tank inlet water is diverted through a diffuser located above the core to create a lateral dispersion of ^{16}N rising from the core. This dispersion significantly increases ^{16}N hold-up time.

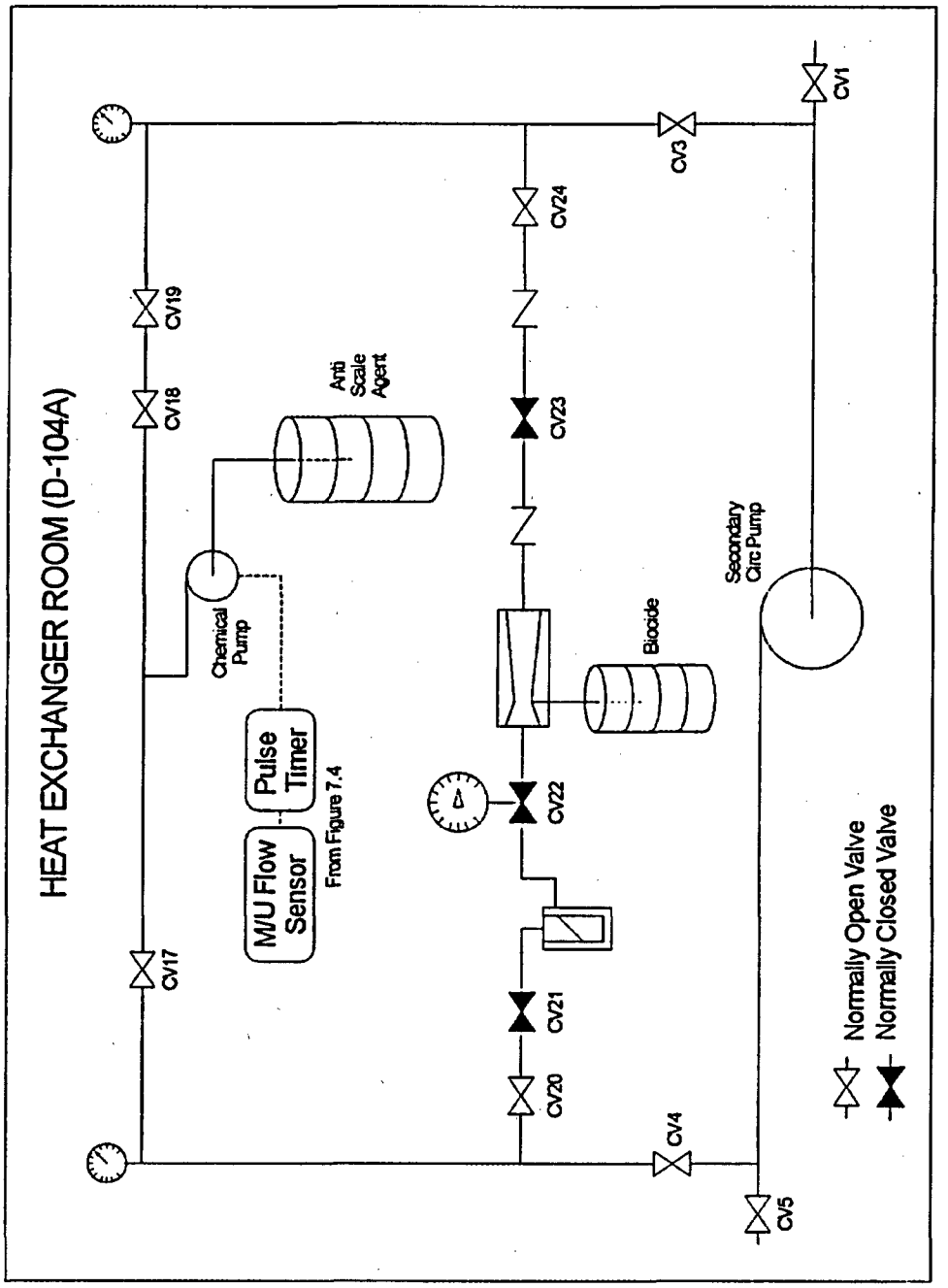

Figure 5.3 Secondary Coolant Chemical Treatment System

CHAPTER 6

ENGINEERED SAFETY FEATURES

(The OSTR does not have any credited Engineered Safety Features)

THIS PAGE INTENTIONALLY LEFT BLANK

CHAPTER 7

INSTRUMENTATION AND CONTROL SYSTEMS

Chapter 7 - Valid Pages
Rev. 0 7/01/2004

i	Rev. 0 7/01/2004
ii	Rev. 0 7/01/2004
1	Rev. 0 7/01/2004
2	Rev. 0 7/01/2004
3	Rev. 0 7/01/2004
4	Rev. 0 7/01/2004
5	Rev. 0 7/01/2004
6	Rev. 0 7/01/2004
7	Rev. 0 7/01/2004
8	Rev. 0 7/01/2004
9	Rev. 0 7/01/2004
10	Rev. 0 7/01/2004
11	Rev. 0 7/01/2004
12	Rev. 0 7/01/2004
13	Rev. 0 7/01/2004
14	Rev. 0 7/01/2004

TABLE OF CONTENTS

LIST OF FIGURES

THIS PAGE INTENTIONALLY LEFT BLANK

7 INSTRUMENTATION AND CONTROL SYSTEMS

7.1 Summary Description

The reactor is operated from a console located in the control room. Additional instrumentation is housed in cabinets on either side of the console. An annunciator panel is mounted above the console.

The operating mode of the reactor is determined by a five-position mode switch on the console. In Automatic and Steady-State modes, the reactor can operate at power levels up to 1 MW. In Square Wave mode, a step insertion of reactivity rapidly raises reactor power to a steady-state level up to 1 MW. In Pulse High and Pulse Low modes, a large-step insertion of reactivity results in a short duration reactor power pulse.

The reactor instrumentation is all solid-state analog circuitry with the exception of the console digital data recorders which have no control functions.

7.2 Design of Instrumentation and Control Systems

Three independent power measuring channels provide for a continuous indication of power from the source level to peak power resulting from the maximum allowed pulse reactivity insertion. Trips are provided for over power, high rate, and loss of operability of the channels. Fuel temperature is measured for display as well as use by the reactor protection system. Parameters not used by the reactor protection system are also monitored and displayed.

7.2.1 Design Criteria

The instrumentation and control system is designed to provide the following:

- complete information on the status of the reactor and reactor-related systems;
- a means for manually withdrawing or inserting control rods;
- automatic control of reactor power level;
- automatic scrams in response to over power, excessive rate of change of power, and high fuel temperature;
- automatic scrams in response to a loss of operability of the power measuring channels; and
- monitoring of radiation and airborne radioactivity levels.

7.2.2 Design-Basis Requirements

The primary design basis for the OSTR is the safety limit on fuel temperature. To prevent exceeding the safety limit, automatic scrams are provided for high fuel temperature and high power conditions. Interlocks limit the magnitude of transient reactivity insertions.

7.2.3 System Description

7.2.3.1 Reactor Power Measurements

Reactor power is measured by three separate detectors; a fission chamber and two uncompensated ion chambers. The signal from the fission chamber is used by the wide range log channel, the period channel, and the wide range linear channel. One uncompensated ion chamber is connected to the safety channel. A second uncompensated ion chamber is used by the percent power and pulsing channels. Figure 7.1 shows the relative ranges of the channels and the detectors.

The detector current selector switch allows routing the current signals from the ion chambers to an external pico-ammeter. When either ion chamber is switched to the external meter, the rod withdrawal prohibit interlock is activated.

The fission chamber is connected to a pre-amplifier at the reactor top. The pre-amplifier monitors the high voltage to the fission chamber, provides an input point for test signals, and pre-amplifies the fission chamber signal for use in the wide range log and linear channels. If a loss of high voltage to the fission chamber is sensed, a bistable circuit will be tripped, resulting in a scram.

The wide range log channel provides a continuous indication from 10^{-8} to 110% of full power for the local meter and the console data recorder. The log power level signal is also used by the low source count bistable circuit, the 1 kW permissive bistable, the pulsing channel, and the period channel.

The period signal is obtained by differentiating the wide range log signal. Reactor period is displayed on a local meter. A bistable circuit provides a scram and an alarm when rate exceeds a predetermined limit. The period signal is also used by the servo system. The period circuit is disabled initially in Square-Wave mode and at all times in Pulse mode.

The wide range linear channel provides a signal based on 0 to 110% of the range selected by a 19-position range switch. The wide range linear signal is used by the console data recorder and the servo system.

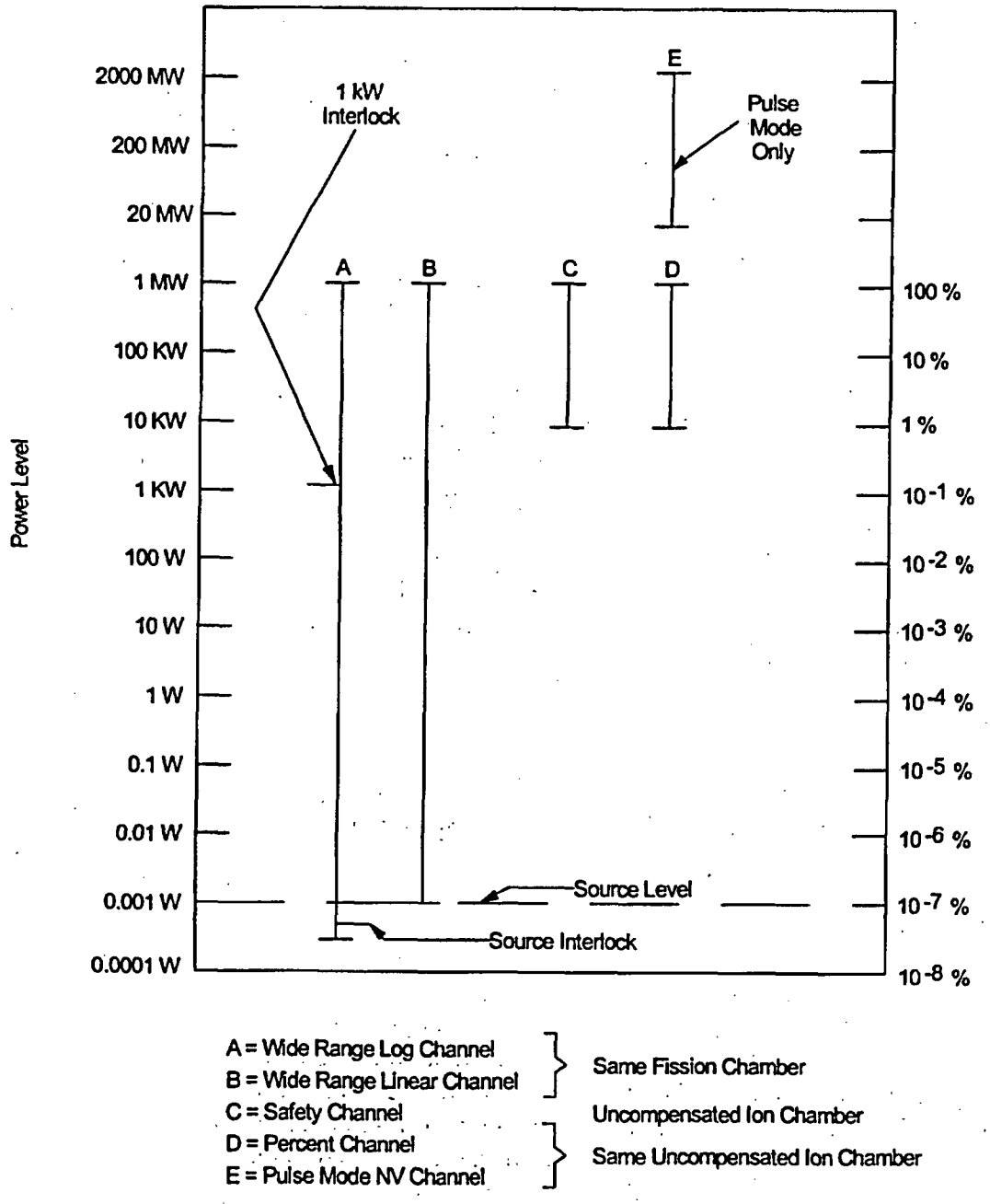

Figure 7.1 Relative Ranges of the OSTR Power Instrumentation

The safety channel provides a signal to a local meter scaled at 0 to 110% of full power. A bistable circuit provides scram and alarm functions if the high power setpoint is exceeded. The detector input to the safety channel is grounded in the Pulse mode of operation. A separate bistable circuit provides output to the reactor protection system upon a loss of detector high voltage.

The percent power channel is redundant in function to the safety channel. The percent power signal is also displayed on the scale of 0 to 110% of full power with high power scram and alarm outputs.

The pulsing channel displays peak power from a pulse on the scale of 0 to 100% of 1,000 MW in Pulse Low and 4,000 MW in Pulse High. A display of integrated energy is also provided on the scale of 0 to 100% of 20 MW-s for Pulse Low and 80 MW-s for Pulse High. A switch selects the energy to be displayed from either a two- or ten-second integration time. The pulsing channel is enabled when the mode switch is placed in either Pulse position. The energy integration period starts when the wide range log signal exceeds a reference level. This also enables the peak hold circuit and starts a one-minute timer. The peak power and energy displays are reset at the end of the one-minute period. The peak power is also recorded on the console data recorder.

The percent power channel and the pulsing channel are both part of the power range monitor. The power range monitor will produce a scram and alarm output in response to a non-operable condition. A non-operable condition results from one or more of the following: test switches activated, loss of operating voltage, or loss of detector high voltage.

7.2.3.2 Temperature Measurements

As illustrated in Figure 7.2, fuel temperature is measured by three thermocouples embedded in the instrumented fuel element. A multipoint selector on the console allows selection of one of the thermocouples or a test signal for display and comparison against the high and low setpoints. The displayed temperature is also recorded on the console data recorder. The high and low setpoint comparators both send alarms to the annunciator panel. In addition, the high comparator sends a scram signal to the reactor protection system. The multipoint selector also allows test inputs to be selected. When the multipoint selector is not in a position corresponding to an active thermocouple, the rod withdrawal prohibit interlock is activated.

Temperature of the bulk pool water is measured by two thermocouples located on either side of the primary tank. One thermocouple is connected to a dedicated thermometer on the console for display. A setpoint comparator sends a high temperature alarm to the annunciator panel when the measured temperature exceeds the setpoint. A selector switch

Figure 7.2 Instrumented Fuel Element

allows the second bulk water thermocouple as well as various points throughout the primary, secondary, and demineralized water systems to be selected for display on the console.

7.3 Reactor Control System

7.3.1 Control Rod Drives

The four control rods are positioned by control rod drives mounted on the reactor top center channel.

As illustrated in Figure 7.3, the safety, shim, and regulating control rod drives are rack-and-pinion linear actuators. An electromagnet is secured to the bottom of the draw tube to which the rack is mounted. The magnet is moved up or down in response to rotation of the pinion shaft. The control rod is attached to the armature by a long connecting rod. When the magnet is energized, the armature is magnetically coupled to the draw tube. De-energizing the magnet causes the rod to drop. A dash pot is incorporated into the armature section to decelerate the rod near the bottom following a scram. Limit switches sense when the magnet is fully withdrawn, the magnet is fully down, and the armature (and thereby the rod) is fully down. A ten-turn potentiometer is coupled to the pinion shaft to provide for rod position indication. The pinion shafts of the safety and shim control rod drives are shaft-coupled to AC gear reduction motors. The pinion shaft of the regulating control rod drive is chain-and-sprocket coupled to a DC stepper motor.

A connecting rod couples the transient rod to a piston rod assembly. As illustrated in Figure 7.4, the piston resides within an externally threaded cylinder. A ball screw nut acts on these external threads to raise or lower the cylinder. Rotation of the ball screw nut is accomplished by a worm gear coupled to an AC motor. A potentiometer is gear-driven by the worm gear shaft to provide rod position indication. A hydraulic shock absorber is incorporated into the top of the cylinder. Air from a compressor is connected to a normally-closed port of a three-way air solenoid valve. The common port is connected to the transient control rod drive cylinder below the piston. The normally-open port is vented. When the air solenoid valve is energized, air pressure is placed on the bottom of the piston causing the piston to be brought in contact with the shock absorber. The resulting reactivity insertion is dependant on the position of the cylinder prior to applying air. With air applied, energizing the motor in the up or down direction will cause the cylinder, piston, and control rod to move up or down as a unit. Scram of the transient rod is accomplished by de-energizing the air solenoid valve. This vents the air pressure under the piston and results in the control rod dropping. As illustrated in Figure 7.5, limit switches provide for sensing cylinder up, cylinder down, and rod down. A bracket extends over the top of the cylinder. A switch on the bracket opens a contact in the up circuitry when the shock absorber assembly contacts it. The bracket itself is substantial enough to stall the motor should the switch contact fail to open.

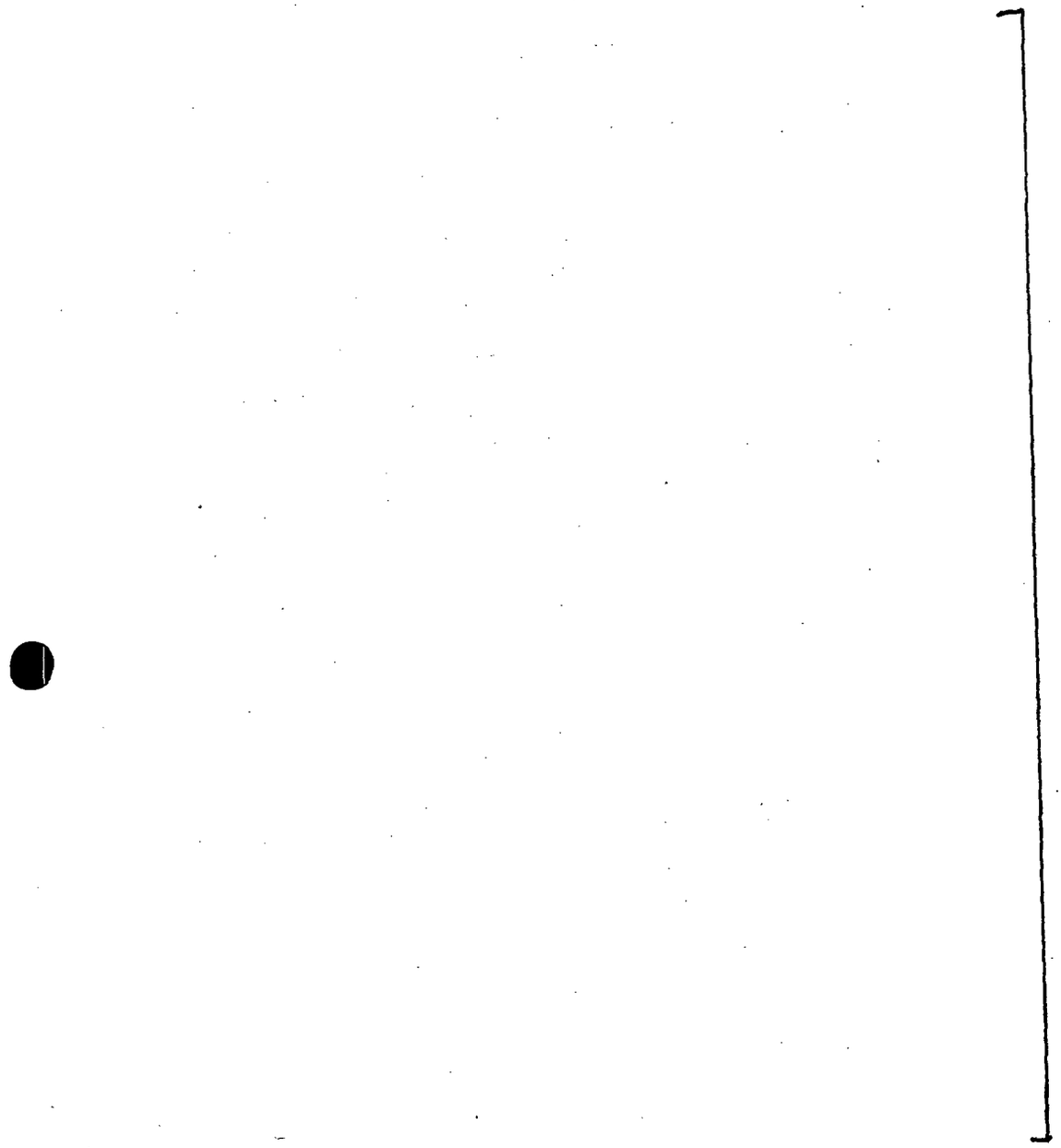

Figure 7.3 Standard Control Rod Drive and Limit Switches

Figure 7.4 Transient Rod Drive

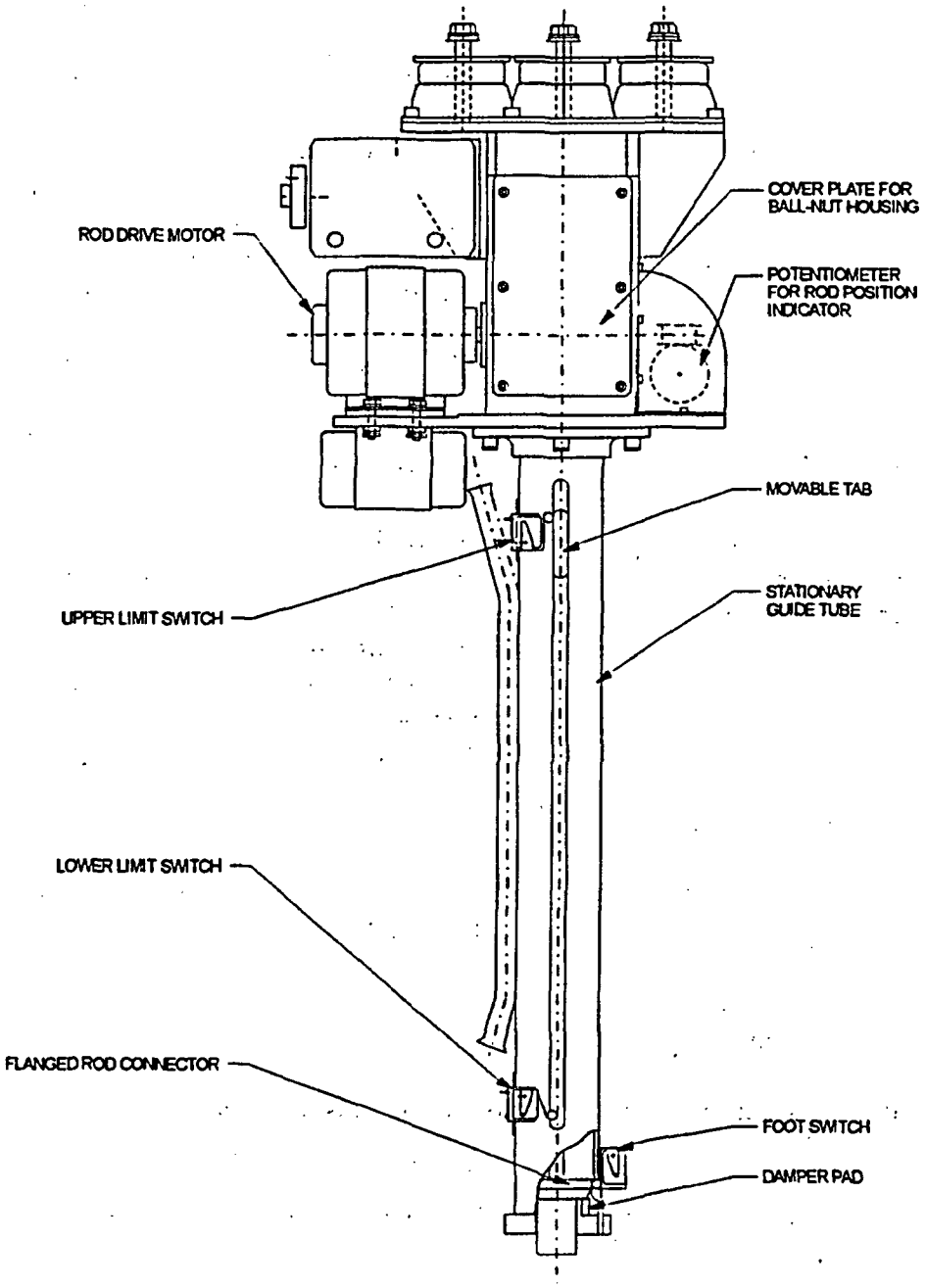

Figure 7.5 Transient Rod Drive Limit Switches

7.3.2 Servo System

In the Automatic and Square-Wave modes of operation, the regulating rod is controlled by the servo system to control reactor power based on input signals from the wide range linear channel, the reactor period channel, and the percent demand control.

In Automatic, wide range linear power is compared against the percent demand setting to obtain power error. The power error is limited at about 30 percent of full scale. The limited power error is compared against the inverted period signal to obtain total error. To reduce hunting, deadband comparators limit rod motion to total errors in excess of +/- 1%. The absolute of the total error is used for error proportional pulse width control. In response to a large error signal, the rod is driven almost continuously. As the magnitude of the total error gets smaller, the rod is driven for a smaller percentage of each 0.5-second interval. This reduces system overshoot during transients.

To perform a Square-Wave, the reactor must be configured in Steady-State mode. First, the reactor power is raised to some nominal low power (usually 15 W) with the air to the transient rod off. Second, the transient rod cylinder is raised to the position corresponding to the desired reactivity insertion. Third, the desired range is selected with the linear range switch. This causes wide-range linear power to indicate at the low end of scale. Finally, the mode switch is moved from Steady-State to Square Wave and the fire button pressed. Reactor power will increase to the desired power level and behave as if in Automatic mode.

7.3.3 Interlocks

The following are the interlocks utilized by the OSTR console:

- the transient rod, interlocked, both electrically and mechanically, to limit pulse reactivity insertions to less than $2.55;
- the 1-kW permissive interlock to prevent pulsing when wide range log power is above 1 kW;
- interlocks to prevent the safety, shim, and regulating rod drives from moving in pulse mode;
- interlock to ensure that only one control rod can be manually withdrawn at a time;
- the rod withdrawal prohibit interlock, activated by the low source count bistable circuit when wide-range log power is not greater than 2 cps and also activated by the period/log test switch, the detector current selector switch, and the fuel

temperature multipoint selector. An alarm on the annunciator panel is activated by the rod withdrawal prohibit interlock.

7.4 Reactor Protection System

7.4.1 Scram Circuits

The scram circuits function to shut down the reactor by dropping all four control rods to their fully inserted positions. Scram is accomplished by de-energizing the magnets for the safety, shim, regulating rods and by de-energizing the air solenoid valve for the transient rod.

A reactor scram will result under any of the following conditions:

- operator-initiated manual scram;
- fuel element temperature in excess of LSSS;
- safety or percent power channels measuring power in excess of the setpoint;
- period channel measuring rate of power increase in excess of the setpoint;
- loss of high voltage to the power measuring channels; or
- external scram.

7.5 Engineered Safety Features Actuation System

There are no engineered safety feature actuation systems.

7.6 Control Console and Display Instruments

7.6.1 Console Data Recorder

The console data recorder digitally records and displays wide-range log and linear power and fuel temperature. In Pulse mode, the log input is disconnected and the linear input is replaced with peak power.

7.6.2 Rod Position Indication

Four rod position indicators are mounted in the console, each above the respective rod control switches. Rod position is displayed as 0 to 100 % of withdrawal with 0.1% resolution.

7.6.3 Annunciator Panel

When an alarm is received at the annunciator panel, an audible signal will sound and a lighted annunciator will flash. When the operator presses the acknowledge button, the audible signal will be silenced and the lighted annunciator will be solidly illuminated. When the operator presses the reset button, if the alarm condition has not cleared, the annunciator will continue to be illuminated. If the alarm condition has cleared, the annunciator will be extinguished. Pressing the test button will cause all of the annunciators on the panel to be actuated. These annunciators can then be acknowledged and reset in the normal fashion.

7.7 Radiation Monitoring Systems

7.7.1 Area Radiation Monitors

Radiation levels are monitored at strategic locations throughout the reactor building. Each channel consists of a detector, a local meter with alert and alarm functions in the control room, and a remote indicator.

7.7.2 Airborne Radioactivity Monitors

Two dual channel airborne radioactivity monitors are in use at the OSTR. One unit samples the effluent from the reactor bay exhaust stack. The other unit is used as a continuous air monitor (CAM) on the reactor top.

In the stack monitor, air from the reactor bay exhaust stack is pulled through a paper particulate filter in close proximity to a detector connected to the particulate count rate meter. The sampled air then passes through a volume containing a detector connected to the gaseous count rate meter. The sampled air passes through the pump before being returned to the ducting on the suction side of the reactor bay exhaust fan. The pump is bypassed by a throttle valve to provide for flow adjustment.

The reactor top CAM samples and discharges air on the reactor top. In all other respects the operation of the CAM is similar to the stack monitor.

Alarms are provided on the annunciator panel for high and low counts on all four channels as well as low air flow.

A stack monitor high particulate or gaseous activity alarm will result in a ventilation shutdown signal to the reactor bay ventilation controller.

7.7.3 Primary Water Activity Monitor

A probe with a GM detector is located in a cavity in the monitor vessel in the demineralized water system. The detector is connected to a count rate meter in the right-hand-side cabinet. An alarm with adjustable setpoint is connected to the annunciator panel to alert the operator to a significant increase in primary water activity.

THIS PAGE INTENTIONALLY LEFT BLANK

CHAPTER 8

ELECTRICAL POWER SYSTEMS

Chapter 8 - Valid Pages
Rev. 0 7/01/2004

i	Rev. 0 7/01/2004
ii	Rev. 0 7/01/2004
1	Rev. 0 7/01/2004
2	Rev. 0 7/01/2004
3	Rev. 0 7/01/2004
4	Rev. 0 7/01/2004

TABLE OF CONTENTS

LIST OF FIGURES

THIS PAGE INTENTIONALLY LEFT BLANK

8 ELECTRICAL POWER SYSTEMS

8.1 Normal Electrical Power Systems

The design of the OSTR is such that the reactor can be shut down and safely maintained in a shutdown condition under a complete loss of electrical power.

A schematic representation of the electrical power system is provided in Figure 8.1.

Normal electrical power for the reactor and its associated equipment is supplied by two separate 4160-VAC, three-phase services from a substation located to the [redacted] of the Radiation Center. The service entrance conductors are contained in underground conduits from the substation. A 112.5-KVA transformer, located in the [redacted] provides power for the primary and secondary pumps, the cooling tower, and the air compressor.

The remainder of the reactor loads, as well as the majority of the Radiation Center complex, are supplied by a 500-KVA transformer located [redacted] A 400-amp breaker in the main switchgear supplies sub-distribution panel A located in [redacted] From there, power is distributed to panels and loads throughout the reactor building.

Power for reactor control and instrumentation equipment is [redacted]

8.2 Emergency Electrical Power Systems

The emergency power systems consist of a 6.5-kW propane-fueled generator, a 3.1-KVA UPS, and associated panels and switchgear.

The emergency power systems are designated as Systems A and B. As shown in Figure 8.2, System A loads are supplied by the [redacted] These loads include the reactor console and side cabinets, the reactor building public address amplifier, and the ventilation system controller. These loads normally receive conditioned power from the [redacted] and are unaffected by a loss of power to the building. The [redacted] is capable of carrying these loads on battery power for at least [redacted] A make-before-break bypass switch allows the [redacted] to be bypassed for maintenance without losing power to the System A loads.

System B loads include partial lighting for the control room and the adjacent hallway, CCTV monitors, the stack monitor pump, and the building fire alarm panel. These loads normally receive power from the building power distribution system. Upon a loss of power, these loads are interrupted. If the power loss lasts longer than about 20 seconds, the

Figure 8.1 Electrical Power System

Figure 8.2 Emergency Electrical Power System

generator will automatically start and supply power to these loads and the [redacted] Upon restoration of building power, the generator will continue to run for about one minute before automatically stopping. There is sufficient propane onsite to run the generator for [redacted] if necessary.

CHAPTER 9

AUXILIARY SYSTEMS

Chapter 9 - Valid Pages
Rev. 0 7/01/2004

i	Rev. 0 7/01/2004
ii	Rev. 0 7/01/2004
1	Rev. 0 7/01/2004
2	Rev. 0 7/01/2004
3	Rev. 0 7/01/2004
4	Rev. 0 7/01/2004
5	Rev. 0 7/01/2004
6	Rev. 0 7/01/2004
7	Rev. 0 7/01/2004
8	Rev. 0 7/01/2004

TABLE OF CONTENTS

LIST OF FIGURES

THIS PAGE INTENTIONALLY LEFT BLANK

9 Auxiliary Systems

9.1 Heating, Ventilation, and Air Conditioning Systems

The controlled ventilation system acts to reduce the consequences of fission products released from the fuel or other experimental facilities. The objective of the structure surrounding the OSTR is to ensure that provisions are made to reduce the amount of radioactivity released into the environment by maintaining a negative pressure within the reactor building during operation. Automatic shutdown of the ventilation system confines the free air volume of the reactor building during emergency conditions. Remote monitoring of the conditions within the reactor building can be conducted.

9.1.1 Reactor Building Confinement

The reactor bay floor is a 6-inch concrete slab placed on a 6-inch compacted granular base. The building superstructure consists of precast-prestressed exterior wall panels and poured-in-place pilasters. The building has a structural steel roof frame with a metal deck and insulating concrete fill, as well as a structural steel interior floor frame with metal formed concrete slabs. A bridge crane with a 5-ton capacity serves the reactor bay area.

The first floor contains: (1) the main floor area of the reactor bay, which accommodates the reactor and the fuel storage pits; (2) the heat exchanger room, which houses the reactor cooling system components; (3) the rabbit lab, which houses the pneumatic transfer system receiver-sender stations; (4) the reactor support lab; (5) the mechanical equipment room, which contains the reactor bay ventilation fan, pneumatic transfer system blower, and the reactor building pressure regulating systems; and (6) the hot cell, which is used as a radiation source storage area.

The second floor contains: (1) two offices, (2) a rest room, which incorporates a decontamination shower and dressing room; and (3) the health physics office and lab.

[redacted]

The third floor contains: (1) a conference room, which has windows that overlook the reactor bay; (2) the control room, which houses all the reactor controls and instrumentation; and (3) the reactor supervisor's office, which is adjacent to the control room.

[redacted]

The fourth floor contains: (1) an office; and (2) a mechanical equipment room, which houses the fume hood fans, main reactor bay exhaust fan, argon system fan, hot drain exhaust fan, and the stack monitor equipment.

9 Auxiliary Systems

9.1 Heating, Ventilation, and Air Conditioning Systems

The controlled ventilation system acts to reduce the consequences of fission products released from the fuel or other experimental facilities. The objective of the structure surrounding the OSTR is to ensure that provisions are made to reduce the amount of radioactivity released into the environment by maintaining a negative pressure within the reactor building during operation. Automatic shutdown of the ventilation system confines the free air volume of the reactor building during emergency conditions. Remote monitoring of the conditions within the reactor building can be conducted.

9.1.1 Reactor Building Confinement

The reactor bay floor is a 6-inch concrete slab placed on a 6-inch compacted granular base. The building superstructure consists of precast-prestressed exterior wall panels and poured-in-place pilasters. The building has a structural steel roof frame with a metal deck and insulating concrete fill, as well as a structural steel interior floor frame with metal formed concrete slabs. A bridge crane with a 5-ton capacity serves the reactor bay area.

The first floor contains: (1) the main floor area of the reactor bay, which accommodates the reactor and the fuel storage pits; (2) the heat exchanger room, which houses the reactor cooling system components; (3) the rabbit lab, which houses the pneumatic transfer system receiver-sender stations; (4) the reactor support lab; (5) the mechanical equipment room, which contains the reactor bay ventilation fan, pneumatic transfer system blower, and the reactor building pressure regulating systems; and (6) the hot cell, which is used as a radiation source storage area.

The second floor contains: (1) two offices, (2) a rest room, which incorporates a decontamination shower and dressing room; and (3) the health physics office and lab. A walkway is provided from the second floor hallway to the second level of the reactor structure. However, the door to the walkway is kept permanently locked for security reasons.

The third floor contains: (1) a conference room, which has windows that overlook the reactor bay; (2) the control room, which houses all the reactor controls and instrumentation; and (3) the reactor supervisor's office, which is adjacent to the control room. A walkway is provided from the third hallway to the third level (top) of the reactor structure.

The fourth floor contains: (1) an office; and (2) a mechanical equipment room, which houses the fume hood fans, main reactor bay exhaust fan, argon system fan, hot drain exhaust fan, and the stack monitor equipment.

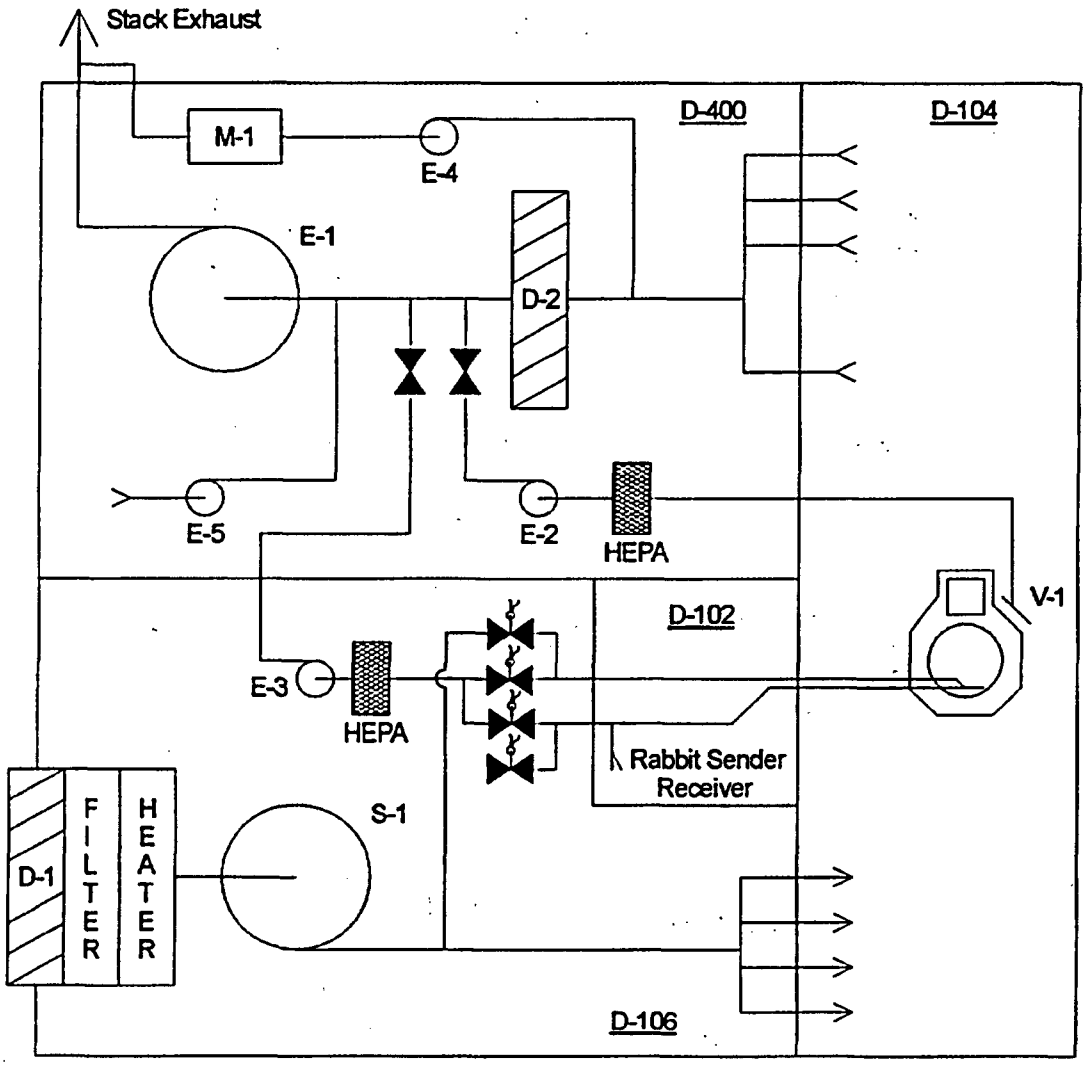

SYMBOL	Function
S-1	Rx Room Supply (12,000 CFM)
E-1	Rx Room Exhaust (12,000 CFM)
E-2	Argon Exhaust Fan (~5 CFM)
E-3	Rabbit Suction / Exhaust (135 CFM)
E-4	Stack Gas / Particulate Monitor Blower (~8 CFM)
E-5	Contaminated Water Drain Vent Fan
D-1	Supply Damper
D-2	Pressure Control Damper
M-1	Stack Gas Particulate Radiation Monitor
V-1	Argon Manifold

Figure 9.1 Reactor Bay Ventilation Schematic

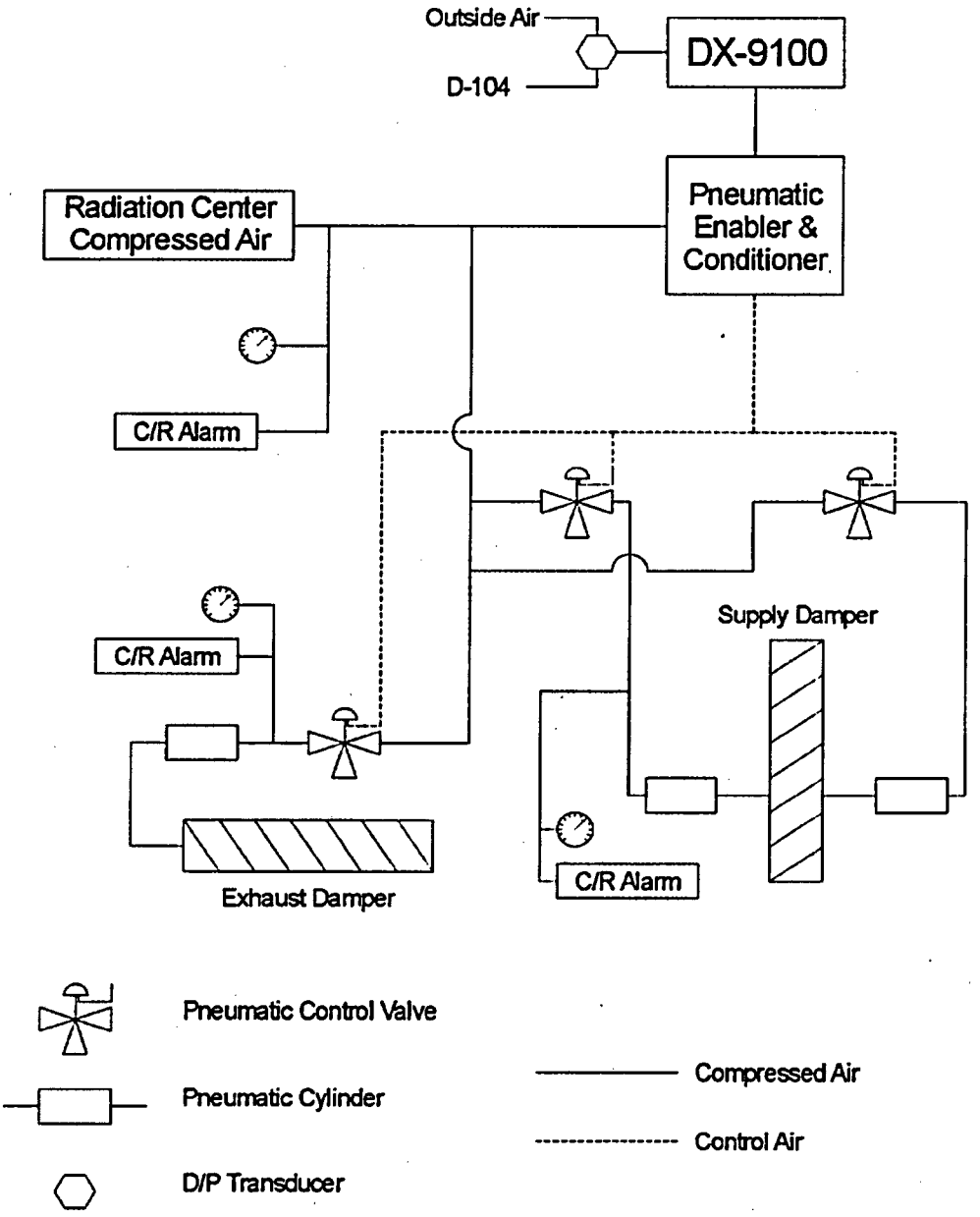

Figure 9.2 Reactor Bay Ventilation Control Schematic

fan discharges into the reactor bay main exhaust plenum. This discharge arrangement ensures the detection of radioactive gases from the drain line by the stack monitor.

All reactor building ventilation fans can be started and stopped manually from the [redacted] The reactor bay exhaust and supply fans are interlocked to start and stop with a single switch. In addition, the argon exhaust and the pneumatic transfer room hood fans are interlocked to turn off at the same time as the reactor bay fans.

9.1.3 Ventilation System Emergency Shutdown

The ventilation system is designed to provide for the automatic containment of airborne radioactive material. Stack gas and particulate detectors constantly monitor the outgoing reactor bay airflow using an isokinetic probe in the vertical exhaust stack to ensure accurate activity monitoring. Only two radioactive gases are normally produced: ^{16}N and ^{41}Ar. However, due to transport delays, the amount of ^{16}N (formed from $^{16}0$ in the pool water) reaching the detector is insignificant. Most of the ^{41}Ar produced during routine operation comes from the experimental facilities which have their own argon ventilation system exhausting directly to the stack. When the exhaust activity indicates that a substantial release of radioactivity is occurring, the ventilation system controller will open contacts for both the supply and exhaust fan motors. At the same time, the signal to the 3-way solenoid valves on the supply and exhaust dampers will be lost, causing them to vent and, thereby, closing the system supply and exhaust dampers. In addition, the argon and pneumatic transfer system hood fans will be shut down by opening contactors in-line with their power supply. The reason for ensuring that the hood fan in the pneumatic transfer station switches off when the reactor bay exhaust fan goes off is to maintain a negative pressure differential between the reactor bay and the adjoining rooms. The argon exhaust fan will not restart until the reactor supply and exhaust fans have been in operation for approximately one minute. A manual reset input by the operator is required to restart the system if the ventilation system is shut down for any reason.

9.2 Handling and Storage of Reactor Fuel

The fuel loading for the OSTR consists of approximately [redacted] elements, including [redacted] control rods, a transient rod, and instrumented element and graphite elements. [redacted]

Fuel handling consists of :

- receiving unirradiated fuel elements;
- transferring fresh unirradiated fuel into the reactor tank; and

- moving irradiated fuel elements within the core or to/from in-tank storage racks.

9.2.1 In-Tank Storage Racks

9.2.2 Fuel Handling Tool

9.2.3 Fuel Element Inspection Tool

The fuel element inspection tool is used to accurately inspect fuel elements for longitudinal growth and for bowing. The upper support plate of the inspection tool is secured to the top of the reactor tank. The inspection tool extends downward into the tank permitting the inspection of an irradiated fuel element while maintaining water shielding over the element. All parts of the tool that come in contact with the reactor water are either aluminum or stainless steel. The aluminum support tube is open at the bottom and top to allow water to fill the interior of the pipe.

Bowing of a fuel element is detected by a carefully machined cylinder (called a go/no-go gauge) attached to the bottom of the tool. If a fuel element will slide completely into the machined cylinder, its bow, if any, is less than the specified limit. When the element passes through the cylinder, it will come to rest on the plunger of a spring-loaded bellows assembly. The length of the fuel element is measured by pushing downward on the indexing rod until the indexing rod plug moves an incremental amount and touches the indexing plate. This action places the upper surface of the fuel element's triangular spacer at an indexed position common to all fuel elements measured. At the same time, the lower surface will displace a plunger. This displacement is measured with a dial indicator.

9.3 Fire Protection System

The purpose of the fire protection system is to provide detection and notification capability which will mitigate loss of property and life in the event of a fire. The reactor bay has thermal fixed/rate-of-rise fire detection as well as manual pull stations. The system is zoned, reports to an annunciator in room [redacted] of the Radiation Center, reports automatically to the [redacted], and activates an audible alarm system throughout the [redacted] A number of fire extinguishers are positioned in the reactor bay, adjacent rooms and laboratories. The fire extinguishers and detection system are regularly inspected by a contractor employed by OSU.

9.4 Communications

[redacted]

9.5 Possession and Use of Byproduct, Source and Special Nuclear Material

All activities using byproduct, source, and special nuclear material covered under the reactor license take place within the reactor building ([redacted]). Material covered under the reactor license may be located in various rooms within the Radiation Center for the purpose of analyzing samples with instrumentation otherwise unavailable in the reactor building (e. g., gamma spectroscopy, liquid scintillation counting, gross alpha/beta counting). Byproduct, source and special nuclear material use other than identified above is covered under State of Oregon Broad Scope License ORE-90005.

9.6 Cover Gas Control in Closed Primary Coolant Systems

This section is not applicable because no such system exists.

9.7 Other Auxiliary Systems

This section is not applicable because there are no other auxiliary systems.

9.8 References

9.1 Memorandum, Fabian C. Foushee to Distribution, "Storage of TRIGA® Fuel Elements," General Dynamics, General Atomic Division, March 1, 1966.

CHAPTER 10

EXPERIMENTAL FACILITIES AND UTILIZATION

Chapter 10 - Valid Pages
Rev. 0 7/01/2004

i	Rev. 0 7/01/2004
ii	Rev. 0 7/01/2004
1	Rev. 0 7/01/2004
2	Rev. 0 7/01/2004
3	Rev. 0 7/01/2004
4	Rev. 0 7/01/2004
5	Rev. 0 7/01/2004
6	Rev. 0 7/01/2004
7	Rev. 0 7/01/2004
8	Rev. 0 7/01/2004
9	Rev. 0 7/01/2004
10	Rev. 0 7/01/2004
11	Rev. 0 7/01/2004
12	Rev. 0 7/01/2004

TABLE OF CONTENTS

LIST OF FIGURES

THIS PAGE INTENTIONALLY LEFT BLANK

10 EXPERIMENTAL FACILITIES AND UTILIZATION

10.1 Summary Description

The Oregon State TRIGA® Reactor (OSTR) provides neutron and gamma irradiation facilities for use by Oregon State University instructors and researchers, and other public and institutional users. Locations for these facilities can be seen in the figures presented in Chapter 1. All systems are designed and operated to control the amount of radiation exposure received by the general public, as well as facility personnel. Incidental production of ^{41}Ar is also mitigated in order to minimize both the environmental release amounts and the exposure of personnel within the reactor facility. The following experimental facilities are provided at the OSTR:

- Three Radial Beamports and one Tangential Beamport;
- The Thermal Column;
- The Thermalizing Column;
- The Pneumatic Transfer system;
- The Central Thimble;
- Vertical Irradiation Tubes;
- The Rotating Rack; and
- The Argon Production Facility.

A list of currently approved experiments is maintained at the facility, and includes evolutions such as normal reactor operation and routine use of experimental facilities. Any evolution not included on the current list of approved experiments must be reviewed and approved in accordance with Section 10.3 prior to performance.

10.2 Experimental Facilities

10.2.1 Beamport Facilities

Four beamports penetrate the concrete shield and pass through the reactor tank water to the reflector region of the core. These ports provide beams of neutron and gamma radiation for a variety of experiments. They also provide irradiation facilities for large specimens (up to 6-inch diameter) in a region close to the core. Three of the beamports are oriented radially with respect to the center of the core, and the other port (B.P. #3) is tangential to the outer edge of the core. Two of the radial ports (B.P. #1 and B.P. #2) terminate at the outer edge of the reflector assembly; however, B.P. #1 is aligned with a cylindrical void in the reflector graphite. The last radial port (B.P. #4), which is called the piercing beamport, penetrates into the graphite reflector and terminates at the inner surface of the reflector assembly, just at the outer edge of the core. The tangential beamport (B.P. #3) terminates

at the outer surface of the reflector, but it is also aligned with a cylindrical void, which intersects the piercing port in the reflector graphite. This tangential port provides a neutron beam while reducing the amount of core gamma radiation. The purpose of the graphite void is to maximize the total radiation streaming down the port.

To shield the radiation streaming through the clearance between the beamports and the inner shielding plugs, the outer embedded portions of the beamports are stepped to allow larger diameter (8-inch) shielding plugs. These outer sections of the beamports are made of steel and are cadmium-plated on the inside for protection against corrosion. A small pipe to the argon vent system leads from each of these outer beamport sections and makes it possible to purge any accumulated radioactive gases.

The beamport inner sections are made of aluminum and are divided into two parts; one part with a nominal [redacted] inside diameter tube embedded in the concrete shield, and the other part a nominal [redacted] inside diameter tube welded to the aluminum tank. A gap, between the aluminum section embedded in the concrete and the aluminum section welded to the tank, has been provided to prevent stresses resulting from thermal expansion in the aluminum tank.

A steel shadow shield is placed around each beamport (in the concrete bioshield) to provide additional shielding for the area adjacent to the beamport. The shadow shield surrounds the [redacted] diameter aluminum portion of the beamport immediately adjacent to the [redacted] diameter steel section.

The piercing beamport that penetrates the reflector (B.P. #4) consists of a tube section embedded in the concrete shielding and a tube section flange-welded to the aluminum tank (these sections are discussed in the preceding paragraph). The innermost region is comprised of a tube section welded into the reflector assembly and a flexible bellows assembly that connects the inner two tube sections and compensates for construction tolerances.

Shielding is provided along the axis of the beamports to minimize the radiation levels outside the concrete structure when the beamports are not in use. The shielding consists of an inner concrete plug, an outer wooden plug, a lead-filled shutter and a lead-lined door.

The inner part of the beam-port shielding is a concrete-filled aluminum plug which is joined to an outer steel head. The shielding material in the inner plug consists of a thin liner of boral on the inner end followed by about 4 inches of lead, which is then followed by borated normal-density concrete and the outer steel head. The inner end of the shielding plug is cone-shaped to help guide the plug (during insertion) over the step in the beamport where the change in diameter occurs. The inner plug provides the major shielding in the beamport.

The outer section of the beamport shield is a wooden plug equipped with button-like protrusions to ensure centering and to reduce friction during insertion and removal. The outer plug is equipped with an electrical circuit consisting of a position switch mounted on the inner face of the plug and an electrical connector on the outer face of the plug. The switch can be actuated only by the inner plug when it is installed in the beamport. A beam plug annunciator circuit is provided in the control room which will indicate (by a light on the annunciator panel) when the inner and outer beam plugs are not both properly installed.

The outer end of the beamport is equipped with a lead-filled safety shutter and door to provide limited gamma shielding when the plugs are removed. It is mounted in a rectangular recessed box in the concrete shield. It is about 4 inches thick and is welded from steel plate and filled with lead. The shutter can be moved either by hand (if the beamport door is open) or by a push rod.

The recessed shutter box is covered with a steel door, which is lined with lead for additional shielding. The door is equipped with a rubber gasket and several screw-type clamps which permit the door to be closed tightly to prevent rapid loss of reactor tank water if a beamport should develop a serious leak. Whenever the beamport is not in use, the door is closed and locked to prevent accidental or unauthorized use.

10.2.2 The Thermal Column

The thermal column is a large, boral-lined, graphite-filled aluminum container situated on the south side of the reflector. Its outside dimensions are 4 feet by 4 feet in cross section by approximately 5 feet in length.

The thermal column liner is a seal-welded container fabricated in two sections from aluminum plate. The outer section is embedded in the concrete shield and the inner section is welded to, and is an integral part of, the aluminum tank. The surfaces of the outer section which are in contact with the concrete are wrapped with plastic tape for corrosion protection. The inner section (welded to the aluminum tank) extends to the graphite reflector and matches the contour of the reflector. The horizontal centerline coincides with that of the core centerline. In a vertical plane, the column extends approximately 12 inches above and below the reflector, with the centerlines of the column and the reflector coinciding.

The aluminum container is open toward the reactor room. Blocks of AGOT nuclear-grade graphite occupy the entire volume. The individual blocks are approximately 4 inches by 4 inches in cross section, the longest being 50 inches in length. All pieces are stamped with identification letters and numbers.

Five graphite blocks serve as removable stringers. These five stringers were machined slightly undersize for easy removal and insertion. The central stringer is aligned with an access plug in the thermal column door and it could, therefore, be removed and inserted without having to move the entire door. To gain access to the other four stringers, the thermal column door must be rolled back on its tracks.

Surrounding the graphite on the inside of the aluminum casing (on all four sides) are sheets of boral, which are incorporated in the design to reduce the production of capture gamma by reducing the neutron flux in the surrounding concrete shield.

The outer face of the thermal column is shielded by a track-mounted door. The door is recessed into the biological concrete shielding and is flush with the shield structure when closed. To reduce the radiation streaming, the door configuration is of a stepped design. The door is filled with heavy-aggregate concrete. Its total weight is about 19 tons. A four-wheeled carriage supports the door and rolls on two steel rails which are flush with the door. A boral sheet is attached to the movable door on the door surface facing the thermal column (inner side).

10.2.3 The Thermalizing Column

The thermalizing column is situated on the west side of the reflector, and is constructed into sections similar to the thermal column, but smaller. Its outer section extends from the bulk-shielding tank through the concrete shielding up to the aluminum reactor tank. The inner section of the column is welded to, and is an integral part of, the tank and extends inward to the reflector assembly and matches its contour. The construction of the thermalizing column in to two sections allows for thermal expansion of the aluminum reactor tank during reactor operation. The bulk-shielding experimental tank is 12 feet deep, 8 feet wide, and 9 feet long. The tank is lined with welded stainless steel.

The thermalizing column is fabricated from seal-welded aluminum. The horizontal centerline coincides with the centerline of the reactor core. The surface of the outer section, which is in contact with the concrete, is wrapped with plastic tape for corrosion protection. An aluminum (neutron window) cover plate separates and seals the bulk-shielding tank water from the thermalizing column. In the region adjacent to the concrete shield, the aluminum container is lined with boral sheets in the same manner as the thermal column.

At the inner end (the end nearest the reactor core), the column is filled with graphite blocks to an axial thickness of 8 inches. All the blocks are made from standard machined blocks of AGOT nuclear-grade graphite. This 8-inch wall of graphite is backed by a 2-inch thick lead slab.

10.2.4 The Pneumatic Transfer System

Very short-lived radioisotopes can be produced for analysis with the aid of the pneumatic transfer system which rapidly conveys specimens to and from the reactor core. The pneumatic transfer system, also known as the rabbit system, consists of a blower-and-filter assembly, a valve assembly, a terminus assembly, a receiver assembly, a control assembly, tubing and fittings.

The system is controlled from the sample preparation and receiving area [redacted] and may be operated either manually or automatically, i.e., with an electric timing device so the specimen capsule can be retrieved automatically from the core after a predetermined length of time. Four solenoid-operated valves control the air flow. The system operates on a pressure differential, drawing the specimen capsule into and out of the core by vacuum. Thus, the system is always under a negative pressure so that any leakage is always into the tubing system. All the air from the pneumatic system is passed through an absolute filter before it is discharged to the building exhaust system. A cutout switch in the [redacted] provides electric power to the blower motor, thus precluding unauthorized use of the rabbit system.

The specimen capsule, or rabbit is made of polyethylene. The capsule is designed to pass freely in a tube with a curved section no smaller than 2 feet. There are two styles of rabbit capsules used at the OSTR, a long version and a shorter version. A capsule is discarded when it shows a significant discoloration, as this indicates that is becoming embrittled by irradiation. A brittle capsule could shatter upon impact in the terminus, which would necessitate removal of the terminus from the core to retrieve the pieces of the capsule.

The blower-and-filter assembly is installed in room [redacted] on a wall-mounted steel angle support. The assembly consists of a blower, a manifold, plenum chambers, and a filter. The blower exhausts the system air into a vent pipe that discharges to the building exhaust stack. The blower is driven by a 220-VAC motor and is equipped with sealed ball bearings that have permanent lubrication and thus require no regular maintenance. The filter, which is sandwiched between the plenum chambers, has a medium of superfine glass and separators composed of Kraft paper. The minimum filter efficiency is 99.97 percent. This filter cannot be cleaned for reuse, but must be replaced when periodic visual inspection indicates a reduction in efficiency due to accumulation of impurities on the filter.

Adjacent to the blower assembly, four solenoid-operated valves are mounted on a common bracket. In the de-energized condition (for sample withdrawal from the core), valves 2 and 4 are open and valves 1 and 3 are closed. In the energized condition (for sample insertion), the valve lineup is opposite. Valves 1 and 4 open to the filtered air incoming from the building fresh air supply, and valves 2 and 3 are connected by flexible hoses through the plenum chambers and filter to the blower suction (See Fig. 10.2). Energized and de-

energized configurations ensure that pressure inside the rabbit system is always lower than ambient pressure whenever the blower is running.

The terminus assembly is located in the reactor tank. The bottom part which is a double tube, extends into the reactor core. The terminus support is shaped like the tip of a fuel-moderator element and will, therefore, fit into any fuel location in the core lattice. The prescribed location for the terminus assembly is in the "G" ring of the lattice and is presently located in G-2. The bottom part extends into the reactor core. The terminus support is shaped like the tip of a fuel-moderator and can, therefore, fit into any fuel location in the core lattice. The prescribed location for the terminus assembly is in the "G" ring of the lattice and is presently located in G-2. Approximately 6 inches above the top grid plate, the terminus end of the tube branches into two separate tubes, both of which extend to the top of the reactor tank. The tubes are made of aluminum. These tubes continue in to the pipe trench; one tube connecting the terminus assembly to the receiver, and the other connecting it to the blower assembly. To counteract buoyancy, the terminus assembly is weighted to keep it firmly in place in the core. The bottom of the internal tube is equipped with an aluminum spring shock absorber to absorb the impact of the specimen container when it is inserted into the terminus.

The specimen capsule is inserted in, and removed from, the pneumatic system through an aluminum cover in the receiver-sender assembly located in room [redacted]. The cover is hinged on the upper side and has a latch on the lower side, and it is designed to stop the ejected capsule in the receiver assembly. When inserted into the assembly, the capped end of the rabbit will rest on a removable shelf (with foam rubber on top) permitting proper closure of the cover. The foam rubber cushions the impact of the returning rabbit.

The control assembly consists of a mounted box that contains an electrical timer, two switches, and a red light. One of the switches on the control assembly is a 3-way selector that designates automatic or manual control. The other switch is the "in" or "out" control to be used when the selector is in manual. The electrical timer will retrieve the "rabbit" after a pre-set time provided the selector is in "automatic."

10.2.5 The Central Thimble

The central thimble, located in the center of the core, provides space for the irradiation of small samples at the top of the upper grid plate. It also makes possible the extraction of a highly collimated beam of neutron and gamma radiation.

The thimble is an aluminum tube and extends from the bridge straight down through the central hole of the removable hexagonal section in the top grid plate then through the lower grid plate, terminating at the safety plate. The central thimble is supported by the safety plate which is situated beneath the lower grid plate. An aluminum filler plug is used in the central thimble to preclude flux peaking in the core center.

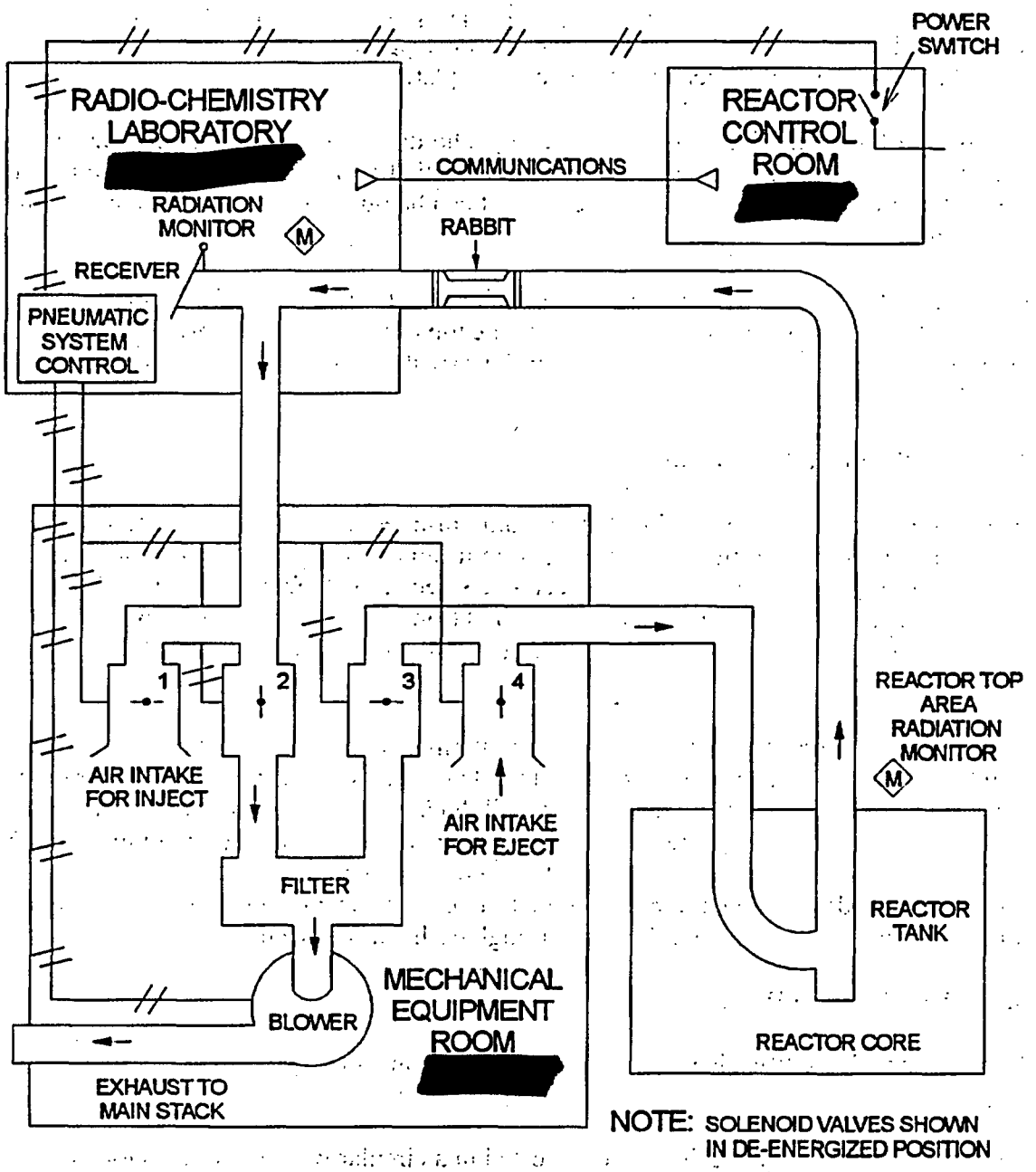

Figure 10.1 Pneumatic (Rabbit) System Schematic

Removable aluminum rings are located on the lower section of the central thimble tubing just above and below the removable hexagonal upper grid section. The rings, which are each fastened to the central thimble with set screws, support the hexagonal section and ensure its proper vertical placement in the top grid plate.

The top end of the central thimble is fastened by a holding fixture screwed into the center channel mounting plate. The holding fixture (a modified Weatherhead union) permits the tube to slide freely through it when loosened, but can be tightened to hold the tube securely in the fixture.

The water in the thimble can be removed (to make a neutron beam available for experimentation) by attaching a special cap to the top of the tube and applying air pressure to force the water down and through four small holes located near the bottom of the thimble.

10.2.6 Vertical Irradiation Tubes

The in-core irradiation tube (ICIT) and the cadmium-lined in-core irradiation tube (CLICIT) facilities are vertical tubes designed to irradiate samples in the reactor core. These facilities, when being used, are placed in a selected fuel element position in the core grid. This is usually the B-1 position. The CLICIT and ICIT consist of thin-walled aluminum tubing, a terminus assembly, cadmium lining (CLICIT only), a cap with a vent adapter and a vent hose.

Each tube is made up of two sizes of aluminum tubing. The longer inner tube is made of a 1¼-inch O.D. tube, 19 feet long, with a wall thickness of 0.058 inches. The shorter outer tube consists of a 1½-inch O.D. tube with a wall thickness of .065 inches turned down to 1.475-inch O.D. This outer tube is about 3 feet long and acts as the facility outer liner and terminus. It is shaped similar to a standard fuel element. Each has a 16-inch offset produced by bends of 10° positioned such that there is sufficient water above or below to reduce radiation streaming from the core through each vertical section.

10.2.7 The Rotating Rack

The rotating rack facility, also known as the Lazy Susan, consists primarily of four components:

- the rotary specimen rack, located in a circular well in the reflector assembly;
- the specimen-removal chute assembly;

- the tube-and-drive-shaft assembly; and
- the drive-and-indicator assembly.

The rotary specimen rack is an annular aluminum holder which surrounds the core and holds specimens during irradiation. This rack is located inside a ring-shaped, seal-welded aluminum housing, and is positioned by centering screws attached to the reflector assembly. The rack rotates on a stainless steel ball bearing assembly and consists of forty evenly-spaced tubular aluminum containers, open at the top and closed at the bottom, which serve as receptacles for specimen containers. Provisions have been made to remove condensation from the rack which could result from high humidity in the reactor area and low operating temperature.

The specimen-removal chute is an aluminum thin-walled pipe that begins in a funnel just below the top plate of the center-channel assembly. This funnel aids in insertion of the specimen container. Loading and unloading of the forty specimen containers in the rack takes place through the specimen-removal chute. The chute is offset by approximately 18 inches by means of large-radii tube bends to ensure adequate radiation shielding.

The rack is rotated from a drive system on top of the reactor; rotation is transmitted through a drive shaft inside a thin-walled pipe housing to a sprocket-and-chain drive in the rotary specimen rack housing. Motive force is provided by an electric motor or a hand crank. Since the thin-walled pipe enclosing the drive shaft is in a straight line from the reflector, radiation shielding is provided by several feet of polystyrene enclosed within the pipe.

The drive-and-indicator assembly is located on the center-channel cover at the top of the reactor tank. The assembly includes an indicator dial with 40 divisions (one for each rack position), a crank for rotating the specimen rack gear train, and a locking rod handle. The motorized drive permits continuous rotation at about one revolution per minute. The motorized drive consists of an electric motor, a worm gear and a slip clutch located inside the drive-and-indicator assembly box. Use of the motor assures a uniform average flux to all samples in the rack.

10.2.8 The Argon Production Facility

The Argon Production Facility is designed to irradiate highly purified argon gas in an irradiation chamber located next to the core at the inner end of Beamport #4 in order to produce a pre-determined amount of ^{41}Ar. The newly-created radioactive gas is then transferred to shipping casks for transport. The Argon Production Facility is a simple structure composed of ¼-inch gas transfer lines, an irradiation vessel, a movable liquid nitrogen condensing cup, a condenser bulb, a vacuum chamber, reach rod operated valves

and pressure indicators. Components are located inside the beamport, or enclosed within a concrete and lead blockhouse shield structure at the outer end of the beamport.

The production process begins by filling the irradiation chamber with ^{40}Ar gas. After the irradiation is complete, the condensation bulb is immersed in a small cup of liquid nitrogen. The $^{40}Ar/^{41}Ar$ mixture is then pulled from the irradiation chamber by differential pressure as it condenses within the condenser bulb volume. When the condensation process is complete, the liquid nitrogen cup is lowered and the liquified argon is allowed to expand into attached shipping casks. The valves on the casks are then shut and the entire system is purged to the vacuum chamber. Any radioactive argon remaining in the system is contained until eliminated by radioactive decay.

10.3 Experiment Review

Administrative requirements are in place at the OSTR to assure that all experiments are performed in a manner which will ensure the protection of the public. Experiment review meets the requirements of Regulatory Guide 2.2, and Standard ANSI N401-1974 (ANS-15.6) as modified by Regulatory Guide 2.4.

Experiments are classified according to potential impact on the facility, and potential radioisotope production as follows:

- Class A: these are experiments which involve small changes in reactivity, no external shielding changes, and/or limited amounts of radioisotope production;
- Class B: these experiments may involve larger changes in reactivity, external shielding changes, and/or larger amounts of radioisotope production; and
- Class C: these are special experiments involving unusual experiment setups, irradiation of special materials, such as [redacted] unusual fuel element arrangements, large in-core experimental facilities, etc.

Prior to performance, any new experiment must be reviewed and approved by the Reactor Operations Committee (ROC), a group of individuals generally knowledgeable in the fields of reactor engineering and nuclear safety. The composition and responsibilities of the ROC are specified in Chapter 12. Experiments are reviewed to ensure their performance in accordance with facility requirements. The ROC review and approval process also follows the provisions of 10 CFR 50.59 to ensure that the proposed experiment does not

constitute an unreviewed safety question and does not require a change in the Technical Specifications.

As part of the approval process, the experiment will be assigned a classification. Once an experiment has been approved, each performance of the experiment will be controlled and documented by an Irradiation Request (IR). The IR is also used to document that any isotopes produced are transferred only to appropriately-licensed users of radioactive material. For Class A experiments, the IR can be approved by the Reactor Supervisor. For Class B experiments, approval from the Reactor Supervisor and the Senior Health Physicist is required. Class C experiments are treated as new experiments each time they are performed, and must be resubmitted through the ROC for each performance.

In order to ensure the protection of the public, limitations are placed on experiments to minimize potential release of radioactive material due to 1) experimental failure [breach], 2) damage to reactor components, and 3) damage to reactor fuel. These limits are explicitly stated in Chapter 14. These limitations specify:

- maximum worth of any non-secured experiment, maximum worth of any single experiment and maximum total experiment worth. These limits determine maximum fuel element temperature;
- maximum amount of [redacted]aterial that may be placed in an experimental facility. This limit prevents damage to reactor components and fuel;
- maximum amount of ^{131}I - ^{135}I isotopes which may be present in a fueled experiment. This limit determines the maximum amount of these isotopes that could be released due to an experiment failure; and
- actions required in the event that hazardous material is introduced into the reactor tank. This limit ensures that the reactor shall not be operated with damaged fuel or components.

The radioisotopes produced at the OSTR may only be transferred to properly-licensed users. Individuals associated with Oregon State University may be approved to receive radioactive material under the authority of the OSU license by the Radiation Safety Committee. Other users must have a current Radioactive Material License. This information is verified during the approval of the IR, prior to performance of every experiment.

THIS PAGE INTENTIONALLY LEFT BLANK

CHAPTER 11

RADIATION PROTECTION PROGRAM AND WASTE MANAGEMENT

Chapter 11 - Valid Pages
Rev. 0 7/01/2004

i	Rev. 0 7/01/2004
ii	Rev. 0 7/01/2004
1	Rev. 0 7/01/2004
2	Rev. 0 7/01/2004
3	Rev. 0 7/01/2004
4	Rev. 0 7/01/2004
5	Rev. 0 7/01/2004
6	Rev. 0 7/01/2004
7	Rev. 0 7/01/2004
8	Rev. 0 7/01/2004
9	Rev. 0 7/01/2004
10	Rev. 0 7/01/2004
11	Rev. 0 7/01/2004
12	Rev. 0 7/01/2004
13	Rev. 0 7/01/2004
14	Rev. 0 7/01/2004
15	Rev. 0 7/01/2004
16	Rev. 0 7/01/2004
17	Rev. 0 7/01/2004
18	Rev. 0 7/01/2004
19	Rev. 0 7/01/2004
20	Rev. 0 7/01/2004
21	Rev. 0 7/01/2004
22	Rev. 0 7/01/2004
23	Rev. 0 7/01/2004
24	Rev. 0 7/01/2004
25	Rev. 0 7/01/2004
26	Rev. 0 7/01/2004

TABLE OF CONTENTS

LIST OF TABLES

11 RADIATION PROTECTION PROGRAM AND WASTE MANAGEMENT

This chapter deals with the radiation protection and waste management programs of the Oregon State TRIGA® Reactor (OSTR). The OSTR is housed within the OSU Radiation Center (RC) which is the University's institutional facility for the accommodation of teaching, research and service programs involving the use of ionizing radiation and radioactive material.

11.1 Radiation Protection

In order to ensure safety and productivity, the use of radiation-producing machines and radioactive materials must be conducted in strict accordance with established federal and state safety standards in order to minimize unnecessary radiation exposure to the users and to members of the general public. The objective of the OSTR Radiation Protection Program is to keep radiation exposures at the RC and to the general public "as low as reasonably achievable" (ALARA).

11.1.1 Radiation Sources

11.1.1.1 Airborne Radiation Sources

The radioisotopes ^{41}Ar and ^{16}N are the only airborne radioisotopes produced during normal reactor operations. In the reactor bay, ^{41}Ar is produced primarily from irradiation of dissolved air in the primary water which eventually evolves into the air of the reactor bay. This evolution results from the reduced solubility of argon gas in water as the water temperature increases. Additionally, ^{41}Ar can be generated from activated argon in air-filled irradiation facilities (e. g., rotating rack, thermal columns, beamports, and the pneumatic transfer system), but little or none of this ^{41}Ar gets into the reactor bay air. ^{16}N is predominately created by the reaction of fast neutrons with ^{16}O in water passing through the core. The amount of oxygen present in air, either in a beam path or entrained in the water near the reactor core, is insignificant compared to the amount of oxygen in water. Calculations and measurements have been performed to determine production and release rates of ^{41}Ar and ^{16}N due to normal reactor operations.

11.1.1.1.1 Estimated Annual Dose in the Unrestricted Area from ^{41}Ar Released During Routine Reactor Operations

The OSTR discharges ^{41}Ar through an exhaust stack that is 19.812 meters above ground level. Atmospheric dilution will reduce the ^{41}Ar concentration considerably before the exhaust plume returns to ground level.

When all irradiation facilities are configured such that the production of ^{41}Ar is maximized, the emission rate of ^{41}Ar in the stack effluent has been measured to be approximately 11μCi s^{-1}. Gamma spectroscopy of samples taken from the stack effluent on a quarterly basis have consistently found only ^{41}Ar present.

Based on this emission rate, the maximum ground level concentration of ^{41}Ar (χ_{max}) can be calculated from the Gaussian plume model as follows (Ref. 11.1):

$$\chi_{max} = \frac{Q}{\pi \sigma_y \sigma_z \mu} e^{\left[-\frac{1}{2}\left(\frac{y^2}{\sigma_y^2}+\frac{h_e^2}{\sigma_z^2}\right)\right]}$$

where:

Q = emission rate (11 μCi s^{-1});
σ_y = horizontal standard deviation of plume contaminant (m);
σ_z = vertical standard deviation of plume contaminant (m);
y = crosswind distance (0 m - centerline);
h_e = effective stack height (m); and
μ = mean wind speed (m s^{-1}).

The effective stack height (h_e) can be calculated from the following equation (Ref. 11.1):

$$h_e = h + d\left(\frac{v_s}{\mu}\right)^{1.4}$$

where:

h = physical stack height (19.812 m);
d = stack diameter (0.533 m);
v_s = stack effluent velocity (19.7 m s^{-1}); and
μ = mean wind speed (m s^{-1}).

The maximum ground level concentration occurs on the plume center line, for any atmospheric condition, at the downwind distance as follows (Ref 11.1):

$$\sigma_z = \frac{h_e}{\sqrt{2}}$$

The distance at which the maximum concentration occurs (d_{max}) can then be determined from charts illustrating σ_z vs. distance using the value of σ_z that corresponds to the maximum ground level concentration. Values for σ_y can likewise be determined from charts illustrating σ_y vs. distance at d_{max} (Ref. 11.1). Using the values given in Reference 11.2, the maximum TEDE, signified as D_{max}, received by a member of the general public may be estimated.

The results of calculating the annual TEDE to the general public from routine releases of ^{41}Ar into the unrestricted area are given in Table 11-1. It should be noted that in order to receive the doses shown in Table 11-1, an individual would be required to continuously occupy the specified location for a full year while the reactor operated continuously for a year in a configuration maximizing ^{41}Ar release and the atmospheric stability class remained constant. That being said, all calculated doses are well within all applicable limits in 10 CFR 20 for all scenarios.

Table 11-1 ^{41}Ar Concentrations and Annual Doses in the Unrestricted Area from ^{41}Ar Released During Routine Reactor Operations at Various Atmospheric Stability Classes

Atmospheric Stability Condition	μ ($m\ s^{-1}$)	h_e (m)	σ_y (m)	σ_z (m)	χ_{max} ($\mu Ci\ m^{-3}$)	d_{max} (m)	D_{max} (mrem)
A	1	54.5	54	39	6.25E-4	240	4
B	2	32.9	40	23	6.98E-4	240	5
C	4	24.8	30	18	6.18E-4	240	4
D	6	22.6	32	16	4.23E-4	400	3
E	2	32.9	55	23	5.07E-4	1000	3
F	2	32.9	75	23	3.72E-4	2200	3

As mentioned above, it is important to recognize that χ_{max} is based upon the release rate when all irradiation facilities are configured such that the production of ^{41}Ar is maximized. Normal operation involves running the reactor at full power with all beamport rod valves

closed and all argon manifold inputs from the beamports and thermal column valved-shut. This has the effect of trapping the air in the irradiation facilities. Additionally, a liquid nitrogen tank is allowed to evaporate into the rotating rack. This is called a nitrogen purge. As the nitrogen gas moves into the rotating rack, it displaces the air in the cavity. This, along with closing the argon manifold valves for the beamports and thermal column, significantly reduces the amount of ^{41}Ar produced and released.

The calculations performed in Table 11-1 assume that the nitrogen purge for the rotating rack is off and all the irradiation facility ventilation valves are open. This has the effect of introducing a maximum amount of air into various irradiation facilities, thereby maximizing the amount of ^{41}Ar generated. However, extensive experience and measurements show that when the nitrogen purge is used and the ventilation valves associated with the various irradiation facilities are closed (i.e., the configuration in which the OSTR is routinely operated), the effluent emission rate of ^{41}Ar, which almost entirely originates from the primary tank, is reduced by a factor of 10 down to approximately 1 $\mu Ci\ s^{-1}$. The values of χ_{max} and D_{max} are therefore also reduced by a factor of 10.

Determination of radiation dose to the general public from airborne effluents may also be carried out using several computer codes recognized by regulatory authorities. One such method involves the use of COMPLY (Ref. 11.3). Application of this code (V1.5D) to the projected ^{41}Ar releases from the OSTR using the data from Table 11-1 for atmospheric stability condition B predicts a maximum annual TEDE to the general public of 4.5 mrem.

11.1.1.1.2 Occupational Exposure to ^{41}Ar from Routine Reactor Operations

The only significant source of ^{41}Ar that contributes to occupational radiation exposure is that which is generated in, and released from, the reactor tank, regardless of the ventilation or irradiation facility valve configuration. As noted in the previous section, the stack effluent discharge rate for ^{41}Ar when the nitrogen purge is used and the ventilation valves associated with the various irradiation facilities are closed (i.e., the configuration in which the OSTR is routinely operated) is approximately 1 $\mu Ci\ s^{-1}$. With a stack effluent discharge rate of 1 $\mu Ci\ s^{-1}$, a volume flow rate of 4.4E6 $cm^3\ s^{-1}$, and assuming uniform mixing in the reactor bay, the concentration of ^{41}Ar in the reactor bay would be approximately 2.7E-7 $\mu Ci\ cm^{-3}$. This is well below the 10 CFR 20 listed Derived Air Concentration (DAC) for ^{41}Ar of 3.0E-6 $\mu Ci\ ml^{-1}$.

If one assumes that all the ^{41}Ar activity detected in the stack effluent while the OSTR is operating in a configuration which maximizes the ^{41}Ar production (a stack effluent discharge rate of 11 $\mu Ci\ s^{-1}$), to be present in the reactor bay air (a volume flow rate of 4.4E6 $cm^3\ s^{-1}$), and uniform mixing in the reactor bay air, the concentration of ^{41}Ar in the reactor bay would be approximately 2.5E-6 $\mu Ci\ cm^{-3}$. This is also below the DAC for ^{41}Ar. However, this is not a credible assumption based on the design of the ventilation system and the irradiation facilities.

While it is common practice to assume that uniform mixing occurs in the reactor bay air, measurements of ^{41}Ar in the reactor bay air suggest that it does not occur (Ref. 11.4). Air concentrations of ^{41}Ar varied measurably at different locations within the reactor bay. At the ground level of the reactor bay, concentrations reached an equilibrium of 5.0E-7 $\mu Ci\ ml^{-1}$ only after approximately four hours of continuous reactor operation at 1 MW. Air concentrations found on the surface of the reactor top averaged 2.4E-6 $\mu Ci\ ml^{-1}$. However, concentrations fell off dramatically as a function of height above the reactor top indicating that immersion dose calculations due to ^{41}Ar will greatly overestimate the dose. In fact, at a height of 1.0 meter above the reactor top, only one out of the five measurement locations yielded a result above the ^{41}Ar lower limit of detection (95%) of 1.8E-7 $\mu Ci\ ml^{-1}$.

All operational scenarios show that the concentration of ^{41}Ar will be significantly less than the DAC. Given the above considerations, any estimated occupational doses must be considered highly conservative upper limits for the TEDE due to ^{41}Ar evolving from the primary tank or irradiation facilities and certainly, in all cases, less than the limits specified in 10 CFR 20.

11.1.1.1.3 Occupational Exposure to ^{41}Ar Originating from the Beamports

Another source of ^{41}Ar from routine operations will be from beams exiting the bioshield into shielded beam halls. The largest possible beam would produce a 14 × 17-inch beam area at approximately 6 feet from the bioshield surface. If it is conservatively assumed that this cross-sectional area remains constant from the inner end of the beamport to 6 feet outside of the bioshield (17 feet), the entire volume of the beam would be 7.9E5 cm^3.

The total number of neutrons per second (I) passing at the end of the beam (exterior of the bioshield) can be calculated from:

$$I = JR,$$

where:

J = neutron beam intensity (4E6 n $cm^{-2}\ s^{-1}$); and
R = beam area (1,535 cm^2).

From this, the neutron intensity at the end of the beam (exterior to the bioshield) will be 6.1E9 n s^{-1}. The neutron intensity at the start of the beam (I_o) can be calculated using the equation:

$$I = I_o e^{-\Sigma t f}$$

where:

Σ = ^{40}Ar macroscopic thermal neutron absorption cross section (1.7E-5 cm^{-1});
t = beam length (518.16 cm); and
f = fraction of argon in air (9.4E-3).

The total interaction rate along the length of the beam (I- I_o) was calculated to be 5.1E5 s^{-1}. The production rate (P) of ^{41}Ar from the beam is calculated by:

$$P = \frac{(I_o - I)\lambda}{c}$$

where

c = 3.7E4 Bq per μCi.

The production of ^{41}Ar is calculated to be 1.5E-3 μCi s^{-1}. Assuming that the ^{41}Ar activity is evenly distributed over the entire room volume, the ^{41}Ar concentration can be calculated from:

$$[^{41}\mathrm{Ar}] = \frac{S}{\lambda V_r + q}$$

where:

[^{41}Ar] = ^{41}Ar concentration in the reactor bay (μCi ml^{-1});
S = source production rate of ^{41}Ar (1.5E-3 μCi s^{-1});
λ = decay constant for ^{41}Ar (1.06E-4 s^{-1});
V_r= room volume (3.877E9 cm^3); and
q = exhaust rate (4.4E6 cm^3 s^{-1}).

The concentration of ^{41}Ar in the reactor bay from the utilization of a beamport while the OSTR is operating at 1 MW was calculated to be 3.0E-10 μCi ml^{-1}. This is insignificant since this concentration is three orders of magnitude smaller than that produced by the primary tank.

11.1.1.1.4 Estimated Annual Dose in the Unrestricted Area from ^{16}N Released During Routine Reactor Operations

^{16}N is generated by the reaction of fast neutrons with oxygen. The oxygen present in air, either in a beam path or entrained in the water near the rector core, is insignificant compared to the oxygen in the water molecule in the liquid state. Production of ^{16}N resulting from the oxygen in air or air entrained in the cooling water can therefore be neglected.

The use of gamma spectroscopy to determine the concentration of ^{16}N in the air is difficult due to its very short half-life (7.2 s). Use of stack continuous air monitor data is not appropriate because the ^{16}N has decayed significantly by the time it reaches the stack. Exposure to the general public is negligible for this reason.

11.1.1.1.5 Occupational Exposure to ^{16}N from Routine Reactor Operations

The average exposure rate observed at the surface of the reactor tank is approximately 100 mR h^{-1} while the reactor is at 1 MW and with the diffuser in operation. In order to estimate the amount of ^{16}N being produced, it will be assumed that the only source term for the 100 mR h^{-1} exposure rate is ^{16}N. This is a conservative assumption because it neglects any contribution from ^{41}Ar or the core itself.

The exposure rate at the tank surface arising from ^{16}N near the surface is calculated by (Ref. 11.5):

$$\dot{X} = \frac{\lambda[^{16}N]_w}{2\mu K}\left(1 - E_2(\mu h)\right)$$

where:

$[^{16}N]_w$ = concentration of ^{16}N in the water (atoms cm^{-3});
λ = ^{16}N decay constant (9.71E-2 s^{-1});
μ = attenuation coefficient for 6 MeV-photons in water (0.0277 cm^{-1});
K = flux-to-exposure rate conversion (1.6E5 photons R^{-1} h cm^{-2} s^{-1});
h = thickness of ^{16}N bearing water; and
$E_2(\mu h)$ = exponential integral function (0).

For this calculation, the second order exponential integral function was conservatively assumed to be zero.

Aside from the dose rate at the reactor tank water surface, the contribution to exposure

rate from ^{16}N in the air is also important. In the reactor bay, the ^{16}N activity is affected by dilution, ventilation, and decay. The accumulation of ^{16}N in the reactor bay under equilibrium conditions ($[^{16}N]_a$) is determined by:

$$[^{16}N]_a = \frac{[^{16}N]_w v_e A}{\lambda V_r + q}$$

where:

$[^{16}N]_w$ = concentration of ^{16}N in the water (atoms cm^{-3});
v_e = escape velocity of ^{16}N from the water surface (0.009 cm s^{-1})[Ref. 11.6];
A = area of water surface (3.08E4 cm^2);
λ = decay constant for ^{16}N (9.71E-2 s^{-1});
V_r= room volume (3.877E9 cm^3); and
q = exhaust rate (4.4E6 cm^3 s^{-1}).

The gamma exposure rate due to immersion from an equilibrium concentration of ^{16}N in the air is calculated by:

$$\dot{X} = \frac{[^{16}N]_a B \lambda \left(1 - e^{-\mu_s R_0}\right)}{2 \mu_s g}$$

where:

B = dose buildup factor (assumed 1);
$[^{16}N]_a$ = ^{16}N concentration in the reactor bay air (atoms cm^{-3});
λ = decay constant for ^{16}N (9.71E-2 s^{-1});
μ_s = linear absorption coefficient (3.03E-5 cm^{-1} for air at 6 MeV);
R_o = radius of "reactor bay sphere" (975 cm); and
g = dose conversion factor (160 Bq cm^{-2} mR^{-1} h).

When the above three equations are solved simultaneously, the iteratively determined value for the concentration of ^{16}N in the primary water ($[^{16}N]_w$) was 9E6 atoms cm^{-3}. The resulting value for the concentration of ^{16}N in the reactor bay air ($[^{16}N]_a$) was 6.5 atoms cm^{-3}. These values will produce exposure rates at the water surface and immersion in air of 98.6 and 3.8 mR h^{-1}, respectively.

Shutting off the ventilation system (q=0) has very little effect upon the results. Similarly, experience has shown that shutting off the diffuser increases the exposure rate on the primary water surface by less than a factor of 2.

11.1.1.1.6 ^{41}Ar and ^{16}N from the Pneumatic Transfer System

Both ^{41}Ar and ^{16}N are produced in the section of the pneumatic transfer system that is located in the reactor core. During operation of the transfer system, air containing very small amounts of these two radioisotopes is exhausted from the system through a HEPA filter to the facility stack. However, even after numerous operations of this system, there have been no detectable increases in the release of these two radioisotopes. Therefore, the ^{41}Ar and ^{16}N from the pneumatic transfer system is not considered to be a measurable contributor to the radioisotopes released or exposure rates associated with OSTR operations.

11.1.1.2 Liquid Radioactive Sources

No liquid radioactive material is routinely produced or used in normal operations of the OSTR except for the neutron activation product impurities in the primary coolant. The majority of these impurities are removed by a mechanical filter and demineralizer resins. Non-routine liquid radioactive waste could be generated from decontamination or maintenance activities; however, based on past experience, the quantity and radioactivity concentrations would be small.

Radionuclides and their concentrations in the primary coolant vary depending on reactor power, reactor operating time and time since reactor shutdown, assuming that other variables remain constant. Routine liquid scintillation counting and gamma spectroscopy analysis of primary coolant water samples taken after several hours at 1 MW (equilibrium) reveal the presence of several radioisotopes. Typical concentration values for these radioisotopes are shown in Table 11-2. It is OSTR policy not to release liquid radioactivity as an effluent; therefore, the primary coolant does not represent a source of exposure to the general public during normal operations. Occupational exposure from liquid sources is also limited because there are few operations which require contact with the primary coolant and because of the short half-lives of most radionuclides present. In cases where contact is a potential, the primary water could be allowed to decay in order to significantly reduce radioactivity concentrations. Additionally, experience at the OSTR and other TRIGA® reactors has shown that ^{3}H is not a significant source of occupational exposure.

11.1.1.2.1 ^{16}N Radiation Dose Rates from the Primary Coolant System Components

The source term of ^{16}N has been addressed previously in Section 11.1.1.2, however, the potential for ^{16}N radiation dose rates from primary water piping and from the heat exchanger were not included in that discussion. Measurements of gamma dose rates at contact with these coolant system components after extended operation at 1 MW indicate that contact dose rates in the range of a 1-10 mrem h^{-1} are common. These radiation levels are not considered to represent a radiation protection problem as the entire system resides in the reactor bay which is designated a radiation area. There is no routine occupancy of locations close to these components. Consequently, occupational dose from this source is minimal.

Table 11-2 Predominant Radionuclides in the OSTR Primary Coolant

Radionuclide	Half-life	Typical Equilibrium Concentration ($\mu Ci\ ml^{-1}$)
^{24}Na	14.96 h	8.34E-5*
^{27}Mg	9.46 min	8.85E-5*
^{41}Ar	1.8 h	9.90E-4*
^{56}Mg	2.58 h	6.09E-5*
^{3}H	12 y	3.34E-4*
^{16}N	7.14 sec	2.36E+1‡

*Measured value
‡Calculated value

11.1.1.3 Solid Radioactive Sources

The major source of radiation and radioactivity from solid sources is the fission product generation in the reactor fuel. A typical OSTR fuel element will generate a radiation field of greater than 100 $R\ h^{-1}$ in air at three feet if removed from the reactor tank. As long as the fuel is contained within the water-filled tank, this source of radiation dose presents no personnel hazard. The tank is designed to preclude loss of its water and reactor operation would not take place if there were any difficulty in maintaining water level. The radiation field created by the complete loss of all water from the tank is addressed in Chapter 13.

Other possibilities for radiation exposure from solid radioactive material are from samples irradiated for research studies and reactor components which have spent a long time near the core. Dose rates from reactor fuel in cooling are several orders of magnitude lower than those in the operating core. This fuel is stored in fuel storage racks within the reactor tank. Sample handling equipment, procedures, and the use of aluminum for almost all structures near the core reduce exposure rates from samples and activated materials to levels which create no significant personnel hazard during operation or maintenance of the reactor. Radioactivity produced in research samples during irradiations is estimated before the irradiations are performed and equipment and procedures are in place to deal with the activity after the irradiation is completed. Another source of solid wastes are the resins used to remove both anion and cations from the primary water. The annual solid waste volume transferred to OSU Radiation Safety for land burial disposal typically runs 15-20 cubic feet and contains various radioisotopes such as ^{60}Co, ^{54}Mn, ^{46}Sc, and ^{47}Sc with a total activity in the high μCi range. A summary of the major sources of radioactive material at

the OSTR is shown in Table 11-3. Because the actual inventory of reactor fuel and other sources is subject to continuous change as part of the normal OSTR operation, the information in Table 11-3 is to be considered only representative.

Table 11-3 Representative Solid Radioactive Sources for the OSTR

11.1.2 Radiation Protection Program

The organization of the OSTR radiation safety program is discussed in Chapter 12. The Radiation Center's Radiation Protection Program is the responsibility of the RC Director and is under the supervision of the Senior Health Physicist. The Senior Health Physicist reports to the Radiation Center Director on all operational matters, but may report directly to the OSTR Reactor Operations Committee and/or OSU Radiation Safety Committee should such action be deemed necessary.

11.1.2.1 Organization of the Health Physics Staff

In addition to the Senior Health Physicist, the Health Physics Staff (radiation protection staff) includes a Health Physicist and Health Physics Monitors. The organizational structure, reporting pathways, and working relationships relating to the OSTR radiation protection program may be found in Chapter 12. Position qualifications will follow those outlined in ANSI/ANS 15.4, *Selection and Training of Personnel for Research Reactors.* The positions of authority and responsibility within the Health Physics Staff are as follows:

- Senior Health Physicist - the Senior Health Physicist reports directly to the Radiation Center Director. The Senior Health Physicist is responsible for directing the activities of the Health Physics Staff including the development and implementation of the OSTR Radiation Protection Program. The Senior Health Physicist has the authority and responsibility to halt perceived unsafe practices;

- Health Physicist - the Health Physicist reports to the Senior Health Physicist. The Health Physicist is responsible for implementing the OSTR Radiation Protection Program policies and procedures, and for providing day-to-day technical support and guidance to the Health Physics Monitors. The Health Physicist has the authority and responsibility to halt perceived unsafe practices; and

- Health Physics Monitors - Health Physics Monitors report to either the Senior Health Physicist or the Health Physicist. Health Physics Monitors are responsible for the required radiation surveys (daily, weekly, monthly, etc.) and other duties as assigned. The Health Physics Monitors have the authority and responsibility to halt perceived unsafe practices.

11.1.2.2 Working Interface Between Health Physics and Reactor Operations

The working relationship of the health physics program relative to reactor operations is described in Chapter 12. As shown in Figure 12.1, there is a clear separation of responsibilities for the two groups, each with a clear reporting line to the Radiation Center Director.

11.1.2.3 Health Physics Procedures and Document Control

Operation of the health physics program is carried out under the direction of the Senior Health Physicist using formal Radiation Center Health Physics Procedures. These procedures are reviewed and approved by the Senior Health Physicist. Procedures and other operational aspects of the Health Physics Staff are also audited an annual basis by the OSTR Reactor Operations Committee. Changes to the procedures, responsibilities, or other operational aspects of the Health Physics Staff are made at the discretion of the Senior Health Physicist. The original copy of the procedures is maintained by the Senior Health Physicist, who is also responsible for the distribution of the reproduced copies.

While not intended to be all inclusive, the following list provides an indication of typical radiation protection procedures used in the OSTR program:

- testing and calibration of area radiation monitors, facility air monitors, laboratory radiation detection systems, and portable radiation monitoring instrumentation;
- working in laboratories and other areas where radioactive materials are used;
- facility radiation monitoring program including routine and special surveys, personnel monitoring, monitoring and handling of radioactive waste, and sampling and analysis of gaseous effluents released from the facility;
- monitoring radioactivity in the environment surrounding the facility;
- administrative guidelines for the facility radiation protection program, including personnel orientation and training;
- receiving of radioactive materials at the facility and unrestricted releasing of materials and items from the facility;
- leak testing sealed sources containing radioactive materials;
- safe transporting of radioactive materials;
- general and personnel decontamination procedures;
- personnel exposure investigation procedures;

- personnel access procedures for the reactor bay;
- spill procedures;
- radiation work permit procedures; and
- ALARA procedures.

11.1.2.4 Radiation Protection Training

The radiation protection training is conducted by the Health Physics Staff. It is structured at different levels in order to meet the needs of different categories of facility staff and researchers using the reactor. All personnel and visitors entering the OSTR Reactor Building shall receive training in radiation protection sufficient for the work/visit, or shall be escorted by an individual who has received such training. Training shall cover the following areas in sufficient depth for the work being done. The general levels of training are as follows:

- Radiation/Radioactive Material User Orientation - All personnel permitted unescorted access to the OSTR Reactor Building shall receive training in radiation protection as required by 10 CFR 19.12. Initial training shall cover the following areas in sufficient depth for the work being done:
  - storage, transfer, and use of radiation and/or radioactive material in portions of the restricted area, including radioactive waste management and disposal;
  - health protection problems and health risks (including prenatal risks) associated with exposure to radiation and/or radioactive materials;
  - precautions and procedures to minimize radiation exposure (ALARA);
  - purposes and functions of protective devices;
  - applicable regulations and license requirements for the protection of personnel from exposure to radiation and/or radioactive materials;
  - responsibility of reporting potential regulatory and license violations or unnecessary exposure to radiation or radioactive materials;
  - appropriate response to warnings in the event of an unusual occurrence or malfunction that involves radiation or radioactive materials; and

- radiation exposure reports which workers will receive or may request.

An examination to demonstrate understanding of the material is required for each section of training. Refresher training is required on a three-year cycle thereafter, including an examination to demonstrate understanding of the material.

- Reactor Bay (Vital Area) Unescorted Access Orientation - All personnel permitted unescorted access to the OSTR vital area shall receive additional training to include the following:
  - reactor bay access control rules;
  - emergency evacuation procedures for the reactor bay;
  - dosimetry requirements for the reactor bay;
  - reactor control room entry procedures and control requirements;
  - key checkout and return;
  - reactor top security;
  - location and use of communication systems;
  - security door requirements;
  - general checkout procedures when exiting the reactor bay; and
  - emergency equipment location and use.

11.1.2.5 Audits

Specific auditing responsibilities and requirements are defined in Chapter 12. Briefly, auditing of the radiation protection program is performed by the Reactor Operations Committee (ROC). The ROC provides objective and independent reviews, evaluations, advice and recommendations on matters affecting nuclear safety at the OSTR. With respect to health physics activities, the ROC is responsible for auditing all procedures, personnel radiation doses, radioactive material shipments, radiation surveys, and radioactive effluents released to unrestricted areas.

11.1.2.6 Health Physics Records and Record Keeping

Radiation protection program records such as radiological survey data, personnel exposure reports, training records, inventories of radioactive materials, environmental monitoring results, waste disposal records, and many more, are maintained by the Health Physics Staff. The records will be retained for the life of the facility either in hard copy, or on photographic or electronic storage media. Records for the current and previous years are normally retained in the Health Physicist's office in binders or file cabinets. Other records are retained in long-term storage. Radiation protection records are required to be reviewed and signed by the Senior Health Physicist prior to filing.

11.1.3 ALARA Program

An ALARA program for the OSTR has been established in accordance with 10 CFR 20.1101. The bases for this program are the guidelines found in ANSI/ANS 15.11. The Radiation Center Director has the ultimate responsibility for the ALARA program, but has delegated this responsibility to the Senior Health Physicist.

The OSTR ALARA program is embedded in every aspect of health physics procedures and reactor operation to include, but not limited to:

- the Senior Health Physicist being required to review all proposed new uses of radiation or radioactive materials, including each time a sample is irradiated in the OSTR;
- exposure investigations being initiated when an individual receives greater than 50 mrem in one month or 500 mrem in a quarter. The investigation is focused on determining the cause of the exposure so that appropriate ALARA actions, if any, may be applied;
- personnel doses, shipping papers, radiation surveys, and radiation releases to the unrestricted area being audited quarterly while the procedures are reviewed annually; and
- the Senior Health Physicist being required to be involved during planning, design approval , and construction of new facilities; during planning implementation of new OSTR use; during maintenance activities; and during the management and disposal of radioactive waste.

11.1.4 Radiation Monitoring and Surveying

The main purpose of the radiation survey program is to assure radiological surveillance over selected OSTR work areas in order to provide current as well as characteristic data on the status of radiation conditions in such areas. Information of this type is used to confirm that safe radiation working conditions exist within the various operational areas under surveillance. The first objective is to assure that the monitoring program is organized such that routine radiation level and contamination level surveys of specific areas and activities within the facility are performed, and special radiation surveys necessary to support non-routine facility operations are also performed. A second objective of the program is to make frequent on-the-spot personal observations (along with recorded data) of radiation work areas. These observations may provide advance warning of needed corrections in order to ensure safe use and handling of radiation sources and other radioactive materials. A third objective is to use the information which has been gathered through completion of the first two objectives in order to ensure (and document) that all phases of the OSTR operational and radiation protection programs are in line with the goal of keeping radiation doses to personnel and releases of radioactivity to the environment ALARA.

11.1.4.1 Radiation Monitoring Equipment

Radiation monitoring equipment used in the OSTR is summarized in Table 11-4. Because equipment is updated and replaced as technology and performance changes, the equipment listed in Table 11-4 should be considered representative only.

11.1.4.2 Instrument Calibration

All radiation monitoring instrumentation is calibrated annually according to ANSI N323A-1997. If the instruments are not calibrated at the OSTR, they are sent to an appropriate calibration facility. Instrument calibrations are tracked by a computer-based system. Instrument calibration records are maintained by the Health Physics Staff. Calibration stickers showing pertinent calibration information (i. e., counting efficiency, the most recent calibration date, and the date the next calibration is due) are attached to all instruments.

Table 11-4 Radiation Monitoring Equipment Used in the OSTR Radiation Protection Program

Item	Location	Function
Continuous Air Monitor	Reactor Top	Airborne Particulate
Continuous Air Monitor	Effluent Stack	Airborne Particulate and Gas
Area Radiation Monitors	Various locations in reactor bay	Measure ambient gamma radiation fields
Portable Ion Chamber Survey Meters	Reactor Bay, D204, D102	Measure beta/gamma exposure rates
Portable Pancake-Probe GM Survey Meters	Reactor Bay, D204, D102	Measure beta/gamma surface contamination
μR Survey Meters	D204	Measure gamma exposure rates
Neutron Survey Meter	D104	Measure neutron dose rates
Alpha Survey Meters	D204	Measure alpha surface contamination
HPGe Gamma Spectroscopy System	B125	Gamma spectroscopy
Gas-Flow Proportional Counter	A138	Measure alpha/beta contamination on swipes
Hand-and-Foot Monitors	Reactor Building D-corridor 1st and 3rd Floors	Measure potential contamination on hands and feet prior to leaving radiation restricted areas
Direct Reading Pocket Dosimeters	Radiation Center Receptionist and reactor control room	Measure personnel gamma dose
TLDs	Various on-site and off-site locations	Measure environmental gamma radiation doses

11.1.4.3 Radiation Surveys

The radiation survey program is structured to make sure that adequate radiation measurements of both radiation fields and contamination are made commensurate with the amount and type of work being performed with radioactive material. The intent of such surveys is to prevent uncontrolled release of radioactive material and to minimize exposure. This program includes, but is not limited to:

- Daily Surveys - Daily Surveys are performed in areas where radioactive materials are frequently used. Such surveys involve direct radiation level measurements in areas known to contain constant or changing radiation fields and contamination surveys of the floors and other surfaces in the affected area are also done. Areas requiring daily surveys are determined at the discretion of the Senior Health Physicist;

- Weekly Surveys - Weekly Surveys are performed in areas where radioactive materials are less frequently used. These surveys involve direct radiation level measurements in areas known to possess constant or changing radiation fields and contamination surveys of the floors and other surfaces in the affected area are also done. Areas requiring weekly surveys are determined at the discretion of the Senior Health Physicist;

- Monthly Surveys - Monthly Surveys are performed in areas where radioactive materials are infrequently used. The monthly surveys involve direct radiation level measurements in areas known to possess constant or changing radiation fields and contamination surveys of the floors and other surfaces in the affected area are also done. Areas requiring monthly surveys are determined at the discretion of the Senior Health Physicist;

- Receipt Radiation Surveys - Receipt Radiation Surveys are required of all incoming packages of radioactive material;

- Special Surveys - Special Surveys are any non-routine radiation survey requested by any member of the OSTR staff when needed; and

- Release Surveys - A Release Survey is required of any object that is removed from a designated radiation/contamination area prior to it being released from that area.

11.1.5 Radiation Exposure Control and Dosimetry

11.1.5.1 Shielding

With regard to the basic shielding design of the OSTR:

- General Atomics has developed source terms to serve as a basis for reactor shielding design analysis;

- reactor shields for 1-MW TRIGA® reactors have been built and proven based on the preceding design analysis. Actual radiation measurements at the surface of the OSTR shield at 1 MW have shown that most radiation levels are about 1 to 2 mrem h^{-1} or less; and

- the OSTR shield is very similar in material type and thickness to other proven TRIGA® shields. Where basic shielding configurations have been changed (e. g., beamports), supplemental shielding was added, as needed, to maintain doses ALARA.

11.1.5.2 Ventilation

The OSTR ventilation system is specifically covered in Chapter 3. This section discusses only those ventilation design features that apply to radiation protection. The reactor bay ventilation system:

- maintains ^{41}Ar and ^{16}N levels at concentrations in the reactor bay consistent with keeping occupational doses below the limits in 10 CFR 20;

- is balanced such that the reactor bay is negative to both the laboratories and offices found in D-Corridor and to the outside atmosphere; and

- has HEPA filters on all ducts originating from irradiation or sample handling facilities.

11.1.5.3 Entry Control

In accordance with the regulations found in 10 CFR 20, the OSTR has many locations posted and controlled as radiation areas. Most other areas within the OSTR are restricted areas. The OSTR does not have any high or very high radiation areas. Should any be created, the entry controls and postings will follow that required in 10 CFR 20, Subpart G.

11.1.5.4 Protective Clothing and Equipment

Personnel protective clothing and equipment used in the OSTR include lab coats, gloves, safety glasses, face shields, coveralls, hoods and shoe covers. The OSTR has one decontamination shower and numerous pre-positioned decontamination kits and emergency equipment cabinets. The requirements for use of the various clothing and equipment are found in the health physics procedures.

Levels of airborne radioactive material do not warrant implementation of a respiratory protection program. Should the situation change in order to meet ALARA objectives, a program will be implemented in accordance with 10 CFR 20, Subpart H.

11.1.5.5 OSTR Occupational Radiation Levels

The OSTR typically operates for [redacted]. Additionally, an occupationally-exposed individual only spends a fraction of the time in areas where there is a potential for measurable radiation levels. Radiation surveys of the OSTR within the restricted area have been made numerous times during full-power operations. Typical values of radiation levels at various locations around the OSTR are given in Table 11-5. Taking into consideration the limited occupancy times, the relatively low dose rates observed, and typical personnel doses received by the OSTR staff (See Section 11.1.5.6), it is evident that all occupational doses can be maintained below the regulatory limits given in 10 CFR 20.

Table 11-5 Typical Radiation Levels at Various OSTR Locations at 1 MW

Facility/Location	Typical Dose Equivalent Rate at Contact (mrem h^{-1})	Typical Dose Equivalent Rate at 30 cm (mrem h^{-1})
Reactor Top	100	65
Reactor Bay Floor	1	1
Demineralizer Tank	25	1
Primary Water Pipes	10	2
Primary Water Filter	3	<1
Argon Manifold	3	1

11.1.5.6 Personnel Dosimetry

The Radiation Center provides personnel dosimeters to occupational workers to ensure compliance with the dose limits specified in 10 CFR 20. Personnel dosimetry devices used at the OSTR have been selected to provide monitoring of all radiation categories likely to be encountered. Table 11-6 summarizes the devices typically used.

Table 11-6 Typical Personnel Monitoring Devices Used at the OSTR

Type	Dose	Radiation Measured	Reading Frequency
Pocket Ion Chamber	Deep Dose Equivalent	Gamma	As Needed
TLD	Deep Dose Equivalent Eye Dose Equivalent Shallow Dose Equivalent	Beta, Gamma	Quarterly
Albedo TLD	Deep Dose Equivalent	Thermal Neutron	Quarterly
TLD Finger Ring	Extremity Dose Equivalent	Beta, Gamma	Monthly
CR-39 Track Etch	Deep Dose Equivalent	Fast Neutron	Quarterly

Before work with radioactive materials begins, the health physics staff will evaluate the likely or possible doses that an individual may receive. Personnel dosimeters are issued for any of the following conditions:

- before entry into high or very high radiations areas;
- when the deep dose equivalent could exceed 50 mrem in any one month;
- when the shallow dose equivalent could exceed 500 mrem in any one month; or
- when the total effective dose equivalent to minors or a declared-pregnant worker could exceed 50 mrem in a year.

Internal dosimetry evaluation is limited to two bioassay methods. The Radiation Center may analyze urine for the presence of ^{3}H using a liquid scintillation counter. Iodine uptake in the thyroid may be analyzed *in vivo* through a thyroid counting program established by OSU Radiation Safety. In emergency situations, arrangements would have to be made with Pacific Northwest National Laboratory in Richland, Washington for whole body *in vivo* counting using gamma spectroscopy. Bioassay is required under the following conditions:

- 2-24 hours after handling unsealed ^{3}H in any chemical form in quantities of 50 mCi or more in any week;

- 6-72 hours after handling unsealed radioactive iodine in any chemical form in quantities of 0.1 mCi or more; or

- as required by the Senior Health Physicist.

An abnormal dose reading investigation (ADRI) is performed by the health physics staff if a personnel dosimeter shows a reading that exceeds the stated ALARA investigation level or is unacceptable from an ALARA point of view. An ADRI involves documenting the abnormal reading, investigating the cause, and evaluating how it might be mitigated in the future. The ADRI is then filed with OSU Radiation Safety, the affected individual, and the OSTR. The ADRI is automatically performed when the dose in any reporting period exceeds 1% of the applicable regulatory limit for occupational workers in 10 CFR 20. Additionally, an ADRI is initiated for individuals designated as visitors when a measured dose exceeds 10 mrem.

Table 11-7 Average Annual Dose Equivalent Incurred by OSTR Staff in 2002

Type of Dose Incurred	Average Annual Dose Equivalent (mrem)	Highest Individual Annual Dose Equivalent (mrem)	Lowest Individual Annual Dose Equivalent (mrem)
Deep	44	77	10
Eye	54	84	20
Shallow	70	115	27
Extremity	102	441	0

11.1.5.7 Dosimetry Records

Records of personnel dosimetry, radiation surveys, effluent monitoring, environmental sample analysis, environmental dose rate measurements, area dosimetry, and environmental area dosimetry are kept for the life of the facility. The dosimetry results shown in Table 11-7 are only to be regarded as typical. As expected, annual doses vary due to changes in facilities, work, and procedures.

11.1.6 Contamination Control

Radioactive contamination is controlled at the OSTR by using written procedures for radioactive material handling, by using trained personnel, and by operating a monitoring

program designed to detect contamination in a timely manner. The program for routine monitoring to detect and identify fixed and loose contamination is described in Section 11.1.4. In addition to this monitoring program, the following items are also part of the program for contamination control at the OSTR:

- the reactor bay ([redacted] and the entire first floor of D-corridor are considered to be potentially contaminated with loose radioactive contamination. All personnel are required to survey before exiting these areas. All objects that leave these areas are also required to be surveyed before they are removed from these areas;

- at a minimum, all personnel are required to wear proper dosimetry, a lab coat, and gloves when working with unsealed radioactive material in the above areas;

- removal of samples from the reactor requires the presence of a Health Physics Monitor;

- procedures have been established for monitoring and handling contaminated equipment and components;

- staff and visitors are trained on the risks of contamination and on the techniques for avoiding, limiting, and controlling contamination;

- contamination events are documented in a Special Survey; and

- events which result in fixed contamination are normally documented as a report in the OSTR Decommissioning File.

11.1.7 Environmental Monitoring

Procedures have been developed to ensure the operation of a comprehensive monitoring program which incorporates an adequate number of sample types, collected at the appropriate frequencies, analyzed with sufficient sensitivity, and reported in a timely manner to provide an early indication of any environmental impacts.

On a quarterly basis, the Reactor Operations Committee audits the OSTR environmental monitoring program and the environmental data generated by the program. As a result of these audits, modifications have been made to improve the quality of the program.

With the exception of ^{41}Ar, there are virtually no pathways for radioactive materials from the OSTR to enter the unrestricted environment during normal facility operations.

The current environmental monitoring program consists of taking environmental samples at approximately 25 different locations and generally within 1,000 feet of the OSTR. Measurements taken include the following:

- direct gamma radiation measurements performed monthly (sensitivity ~5 $\mu R\ h^{-1}$);
- TLD measurements exchanged quarterly (sensitivity ~10 mR $quarter^{-1}$);
- soil samples obtained quarterly and analyzed for gross beta/gamma (sensitivity ~10 pCi g^{-1}), and gross alpha (sensitivity ~0.1 pCi g^{-1});
- vegetation samples obtained quarterly and analyzed for gross beta/gamma (sensitivity ~50 pCi g^{-1}), and gross alpha (sensitivity ~2 pCi g^{-1}); and
- water samples obtained quarterly and analyzed for gross alpha (sensitivity ~0.02 pCi ml^{-1}), gross beta (sensitivity ~0.06 pCi ml^{-1}), ^{3}H (sensitivity ~3 pCi ml^{-1}), and by gamma spectroscopy.

11.2 Radioactive Waste Management

The objective of the radioactive waste management program is to ensure that radioactive waste is minimized, and that it is properly handled, stored and disposed of. The Health Physics Staff is responsible for administering the radioactive waste management program which also includes any records associated with the program. All records are retained for the life of the facility.

11.2.1 Radioactive Waste Control

At the OSTR, radioactive waste is generally considered to be any item or substance which is no longer of use to the facility and which contains, or is suspected of containing, radioactivity above the natural background radioactivity. Equipment and components are categorized as waste by the OSTR staff. When possible, radioactive waste is initially segregated at the point of origin from items that will not be considered waste.

11.2.2 Solid Waste

As with most non-power reactors, solid waste is generated from reactor maintenance operations and irradiations of various experiments. The amount of solid waste is generally on the order of 20 cubic feet per year. No solid radioactive waste is intended to be retained or permanently stored on site. Appropriate radiation monitoring instrumentation will be used for identifying solid radioactive waste. Radioactive waste is packaged in metal drums

within the reactor bay of the OSTR. The waste is then transferred to OSU Radiation Safety for disposal.

11.2.3 Liquid Waste

It is the OSTR's policy not to routinely release radioactive liquid waste. Normal operations of the OSTR do not produce liquid radioactive waste, and if so, the liquid waste is contained locally and transferred to OSU Radiation Safety for disposal. The OSTR does have a 2,500-gallon hold-up tank, which is occasionally discharged to the local sewer system. Sampling, analysis, and release of the holdup tank contents are governed by a written procedure that assures that the release of any radioactivity that happens to be present is within the limits stated in 10 CFR 20, Appendix B, Table 3.

11.2.4 Gaseous Waste

Although ^{41}Ar is released from the OSTR stack as part of the facility ventilation exhaust, this release is not considered to be waste in the same sense as the solid and liquid waste which are collected and disposed of by the facility. The ^{41}Ar is usually classified as an effluent which is a routine part of the normal operation of the OSTR. In the OSTR facility, as in many non-power reactors, there are no special off-gas collection systems for the ^{41}Ar. Typically, this gas simply mixes with reactor room and other facility air and is discharged along with the normal ventilation exhaust.

11.3 References

11.1 Slade, D.H., Meteorology and Atomic Energy - 1968, TID-24190.

11.2 "External Dose-Rate Conversion Factors for Calculation of Dose to the Public," DOE/EH-0070, U.S. Department of Energy, Washington, D.C., 1988.

11.3 EPA 520/1-89-003, U.S. Environmental Protection Agency, Washington, D.C., (1.5D), 1989.

11.4 Anellis, L.G., Johnson, A.G., and Higginbotham, J.F., Argon-41 Production and Evolution at the Oregon State TRIGA® Reactor (OSTR). Eleventh Biennial U.S. TRIGA® User's Conference, Washington, D.C., 1988.

11.5 Schiager, K.J., Analysis of Radiation Exposures on or Near Uranium Tailings Piles, Radiation Data and Reports, pp. 411-425, July 1974.

11.6 Dorsey, N.E., "Properties of Ordinary Water-Substances," pp. 537-544, Reinhold Publ. Co., New York, New York.

CHAPTER 12

CONDUCT OF OPERATIONS

Chapter 12 - Valid Pages
Rev. 0 7/01/2004

i	Rev. 0 7/01/2004
ii	Rev. 0 7/01/2004
1	Rev. 0 7/01/2004
2	Rev. 0 7/01/2004
3	Rev. 0 7/01/2004
4	Rev. 0 7/01/2004
5	Rev. 0 7/01/2004
6	Rev. 0 7/01/2004
7	Rev. 0 7/01/2004
8	Rev. 0 7/01/2004
9	Rev. 0 7/01/2004
10	Rev. 0 7/01/2004
11	Rev. 0 7/01/2004
12	Rev. 0 7/01/2004
13	Rev. 0 7/01/2004
14	Rev. 0 7/01/2004

TABLE OF CONTENTS

LIST OF FIGURES

12 CONDUCT OF OPERATIONS

This chapter describes and discusses the Conduct of Operations at the Oregon State TRIGA® Reactor (OSTR). The Conduct of Operations involves the administrative aspects of facility operations, the facility emergency plan, the security plan, the reactor operator selection and requalification plan, and environmental reports.

12.1 Organization

The formal licensee of the OSTR is the President, Oregon State University. However, the Radiation Center Director is responsible for licensing and reporting information to the NRC. The President is informed of license issues via the normal university reporting channel, originating from the Radiation Center Director through the Vice Provost for Research to the President.

12.1.1 Structure

The management organization of the OSTR is structured to provide comprehensive and redundant internal oversight of reactor operations and radiation protection programs. It also meets the intent of ANSI/ANS 15.11, *Radiation Protection at Research Reactor Facilities*. As shown in Figure 12.1, the level 1(Director) and level 2 (Reactor Administrator and Senior Health Physicist) have formal reporting lines as well as documented secondary lines-of-communication if nuclear or radiation safety concerns cannot be resolved with the normal administrative reporting lines. Interaction between the health physicists, health physics monitors, Reactor Supervisor, and reactor operators is constant, although the reporting lines may be separate.

12.1.2 Responsibility

The following is a list of various offices/committees/personnel and their associated duties:

- President, Oregon State University - chief executive officer of the university;
- Executive Vice President and Provost - research and educational programs are administered through the Office of the Executive Vice President and Provost. Separate officers assist with the administration of research activities and academic affairs with functions delegated to the Vice Provost for Research and the Vice President for Finance and Administration;

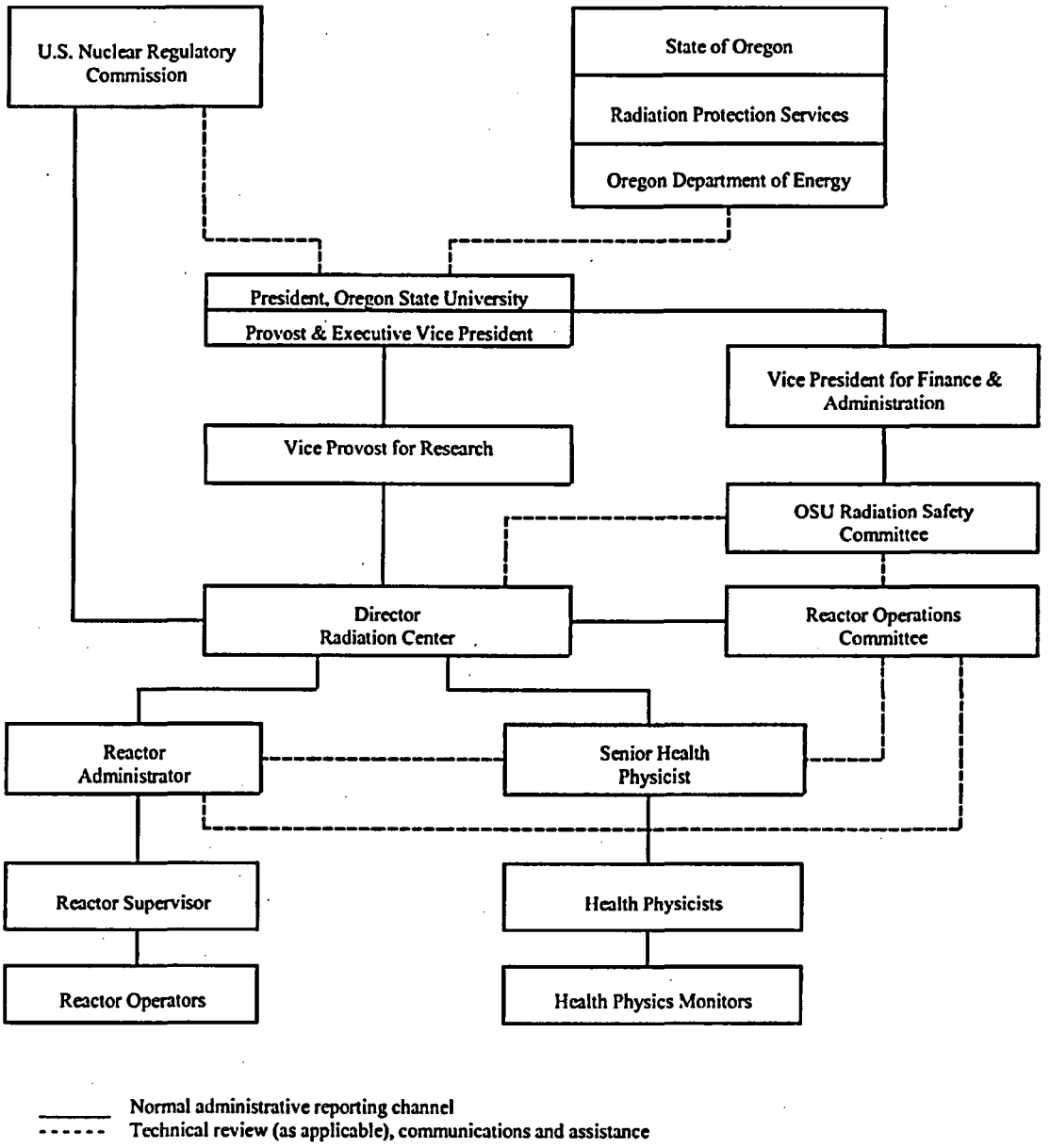

Figure 12.1 OSTR Administrative Organizational and Reporting Line Chart

- Vice Provost for Research - research programs associated with the university are administered through the Research Office. The Radiation Center is administered through the Research Office;

- Vice President for Finance and Administration - university business activities are administered through the Office of Finance and Administration. One responsibility of the office is the administration and operation of safety programs for the university;

- Radiation Safety Committee - this standing university committee has jurisdiction over matters dealing with radiation uses and radiological safety necessary to protect the health and welfare of the staff and students of Oregon State University;

- Reactor Operations Committee - this standing university committee independently reviews, evaluates, and approves safety standards associated with the operation and use of the Oregon State TRIGA® Reactor and its experimental facilities;

- Radiation Center Director - the Director is accountable for ensuring all licensing requirements, including implementation and enforcement, in accordance with the NRC codes and guides. This is a level 1 position;

- Reactor Administrator - the Reactor Administrator is responsible to the Radiation Center Director for guidance, oversight, and technical support of reactor operations. The Reactor Administrator shall be certified as a Senior Reactor Operator. This is a level 2 position;

- Senior Health Physicist - the Senior Health Physicist is responsible to the Radiation Center Director for directing the activities of Health Physics personnel including the development and implementation of the Radiation Safety Program. This is a level 2 position;

- Reactor Supervisor - the Reactor Supervisor is responsible to the Reactor Administrator for directing the activities of Reactor Operators and for the day-to-day operation and maintenance of the reactor. The Reactor Supervisor shall be certified as a Senior Reactor Operator. This is a level 3 position;

- Reactor Operator - the Reactor Operator reports to the Reactor Supervisor and is primarily involved in the manipulation of reactor controls, monitoring

of instrumentation, and operations and maintenance of reactor related equipment. A Reactor Operator shall be certified as either a Senior Reactor Operator or a Reactor Operator. This is a level 4 position;

- Health Physicist - the Health Physicist is responsible to the Senior Health Physicist for the implementation of the Radiation Safety Program; and

- Health Physics Monitor - the Health Physics Monitor is responsible to the Health Physicist for radiological monitoring of all aspects of reactor operations.

12.1.3 Staffing

All reactivity changes shall be made by, or in the presence and under the direction of, the licensed operator of record at the time the reactivity changes are made.

At least two of the following people, the licensed operator of record included, shall be present in the Radiation Center Complex while the reactor is operating:

- Radiation Center Director;

- Reactor Administrator;

- Reactor Supervisor;

- Senior Reactor Operator or Reactor Operator;

- Senior Health Physicist; or

- Health Physicist.

The Reactor Supervisor shall be required to be present at the facility only during the initial startup each day or at the initial startup of a new experiment. At all other times while the reactor is, or may be, operating, the Reactor Supervisor may be away from the facility provided:

- he/she carries a portable radio receiver or cell phone which is operable;

- he/she verifies with the operator on duty at least daily that the receiver is operable;

- he/she remains at all times within the range of the radio receiver and at no time further than 10 miles from the facility;
- he/she contacts the facility (via telephone or radio receiver) within 10 minutes after receiving any message from the operator on duty; and
- he/she is able to go to the facility expeditiously, if necessary.

For any maintenance affecting the components inside the reactor tank or affecting other installed experimental facilities such as the beamports, at least two persons shall be present at the maintenance site, one of whom must be, at a minimum, a licensed reactor operator.

12.1.4 Selection and Training of Personnel

The OSTR shall select individuals with the requisite experience and qualifications recommended in ANSI/ANS 15.4, *Selection and Training of Personnel for Research Reactors*. All personnel shall have a combination of academic training, experience, health, and skills commensurate with their level of responsibility. General orientation and training for all personnel who work in the Radiation Center meets the requirements of 10 CFR 19 and ANSI/ANS 15.4. Topics covered as part of this training include:

- Organization;
- Security and Access Control;
- Radiation and Occupational Safety; and
- Emergency Procedures.

12.1.4.1 General Training for Radiation Center Personnel

Training for all personnel within the Radiation Center who work with radioactive materials is specifically discussed in Chapter 11.

12.1.4.2 Initial Reactor Operator Training

For initial training for either a reactor operator or a senior reactor operator, the following documents shall be studied and knowledge demonstrated:

- Training Volume 1: General Description of Reactor and Facilities;
- Training Volume 2: Reactor Instrumentation and Control;

- Training Volume 3: Reactor Physics, Kinetics, and TRIGA® Characteristics;
- Training Volume 4: Reactor Operating Procedures;
- Training Volume 5: Radiation Protection;
- Emergency Response Plan;
- Emergency Response Implementation Plan;
- License, Technical Specifications, and Experiments; and
- Physical Security Plan.

12.1.5 Radiation Safety

This is covered in Chapter 11.

12.2 Review and Audit Activities

The general scope of responsibility of the Reactor Operations Committee (ROC) shall be to independently review, evaluate, and approve safety standards associated with the operation and use of the OSTR and its experimental facilities.

12.2.1 Composition and Qualifications

Appointed by the Radiation Center Director, the ROC membership shall be composed of at least five members, including the chairman. The ROC membership should include, but is not limited to, the following individuals:

- Radiation Center Director;
- Reactor Administrator;
- Reactor Supervisor;
- Senior Health Physicist;
- individual with expertise in nuclear engineering;
- individual with expertise in another branch of engineering; and

- individual with expertise in radiation chemistry, nuclear chemistry, health physics, or radiation biology.

12.2.2 Charter and Rules

The ROC shall conduct its review and audit functions in accordance with a written charter. This charter shall include provisions for:

- meeting frequency;
- voting rules;
- quorums;
- method of submission and content of presentations to the committee;
- use of subcommittees; and
- review, approval and dissemination of meeting minutes.

12.2.3 Review Function

The responsibilities of the ROC, or a designated subcommittee thereof, shall include, but are not limited to, the following:

- review and approval of experiments utilizing the reactor facilities;
- review and approval of all changes to the safety analysis report or technical specifications;
- review and approval of all new procedures and substantive changes to existing procedures;
- review all changes to the facility or safety evaluations under 10 CFR 50.59;
- review of the operation and operational records of the facility;
- review of abnormal performance of plant equipment and operating anomalies; and

- review of all events which are required by regulations or Technical Specifications to be reported to the NRC within 24 hours.

12.2.4 Audit Function

The ROC, or a designated subcommittee thereof, shall audit the reactor operations and health physics programs annually. The audit shall include, but not be limited to, the following:

- inspection of reactor operating records;
- inspection of the reactor operating area; and
- reportable occurrences.

12.3 Procedures

Written procedures shall be prepared and approved prior to initiating any of the activities listed in this section. The procedures shall be approved by the Reactor Administrator. The procedures are reviewed by the ROC annually to ensure that they are appropriate. The procedures shall be adequate to assure the safe operation of the reactor, but will not preclude the use of independent judgement and action should the situation require. The following two sections list areas that will typically require written procedures.

12.3.1 Reactor Operations

The following activities will typically require written procedures:

- startup, operation, and shutdown of the reactor;
- fuel loading, unloading, and movement;
- routine maintenance of the control rod drives and reactor safety and interlock systems or other routine maintenance that could have an effect on reactor safety;
- testing and calibration of reactor instrumentation and controls, control rods and control rod drives;
- administrative controls for operations, maintenance, and conduct of irradiations and experiments that could affect reactor safety or core reactivity;

- implementation of the Emergency Response Plan; and
- actions to be taken to correct specific and foreseen potential malfunctions of any systems, including responses to alarms and abnormal reactivity changes.

12.3.2 Health Physics

The following activities will typically require written procedures:

- testing and calibration of area radiation monitors, facility air monitors, laboratory radiation detection systems, and portable radiation monitoring instrumentation;
- working with radioactive materials;
- facility radiation monitoring program including routine and special surveys, personnel monitoring, monitoring and handling of radioactive waste, and sampling and analysis of solid and liquid waste and gaseous effluents released from the facility;
- monitoring radioactivity in the environment surrounding the facility;
- personnel orientation and training;
- receipt of radioactive materials at the facility, and unrestricted release of materials and items from the facility; and
- transportation of radioactive materials.

12.4 Required Actions

This is covered in the OSTR Technical Specifications.

12.5 Reports

This is covered in the OSTR Technical Specifications.

12.6 Records

This is covered in the OSTR Technical Specifications.

12.7 Emergency Planning

The OSTR Emergency Response Plan contains detailed information concerning the OSTR response to emergency situations. The OSTR Emergency Response Plan is written to be in accordance with ANSI/ANS 15.16, *Emergency Planning for Research Reactors.*

The Emergency Response Plan is designed to provide response capabilities to emergency situations involving the OSTR. Detailed implementing procedures are referenced in this plan. This approach provides the OSTR emergency staff the flexibility to cope with a wide range of emergency situations without requiring frequent revisions to the plan.

Primary responsibility for the plan and response to and recovery from emergencies rests with the Emergency Director who is normally the Radiation Center Director. Implementation of the plan on a day-to-day basis is the responsibility of the Reactor Administrator who serves as the Emergency Coordinator in an emergency. Provisions for reviewing, modifying, and approving the emergency implementation procedures are defined in the plan to assure that adequate measures to protect the staff and general public are in effect at all times.

12.8 Security Planning

The OSTR Physical Security Plan contains detailed information concerning the OSTR security measures. The plan provides the OSTR with criteria and actions for protecting the facility from such acts as intrusion, theft, civil disorder and bomb threats.

Primary responsibility for the plan and facility security rests with the Principal Security Officer who is normally the Radiation Center Director. Implementation of the plan on a day-to-day basis during hours of operations is also the responsibility of the Principal Security Officer.

12.9 Quality Assurance

Quality assurance can be found throughout the operating and health physics procedures. It is not called out as a separate document.

12.10 Operator Training and Requalification

This reactor operator training and requalification program is designed to satisfy the requirements of the NRC's rules contained in 10 CFR 55. It also generally complies with the requalification program in ANSI/ANS 15.4, *Selection and Training of Personnel for Research Reactors.*

12.10.1 Responsibility

The responsibility for this program rests with the Reactor Supervisor. This responsibility shall cover the following items:

- selecting knowledgeable individuals to give classroom lectures and to supervise retraining operations;
- certifying to the Reactor Administrator that each individual has successfully completed the requalification program; and
- granting of exemptions to the requalification program as provided for in this plan.

12.10.2 Schedule

The requalification program shall be conducted on a cycle not to exceed two years. Upon conclusion, it will be promptly repeated.

12.10.3 Content

The requalification program shall consist of preplanned lectures, written examinations, an annual operating examination, and routine reactor operations.

12.10.4 Annual Lectures

Lectures shall be given annually (not to exceed 15 months) which cover the following:

- Emergency Response Plan; and
- Physical Security Plan.

12.10.5 Biennial Lectures

Lectures shall be given biennially (not to exceed 30 months) which cover the following:

- facility design, characteristics, instrument control and safety systems;
- reactor principles;
- operating procedures, Technical Specifications, and administrative procedures; and

- radiation protection.

12.10.6 Written Examinations

Written examinations shall be given covering the lecture material. The individual giving the lecture on a particular subject shall formulate, administer, and grade the written examination on that subject. Any licensed individual preparing and grading an examination is exempt from taking that examination. All written examinations will be proctored by the individual administering the exam, or by their appointed representative, but shall not be an individual taking the exam.

A grade equal to or greater than 75% will constitute a passing grade. Failure to achieve a passing grade will result in an accelerated retraining program in the subject area failed. This accelerated retraining program will be left to the discretion of the Reactor Supervisor.

The Reactor Supervisor may require an operator to participate in an accelerated requalification program when it is deemed needed by virtue of examinations or operating test results.

12.10.7 Quarterly Operating Requirements

To maintain a current license, each calendar quarter, a reactor operator shall operate the reactor for a minimum of four (4) hours and perform a supervised reactor startup, including a core excess measurement and increase to power.

To maintain a current license, each calendar quarter, a senior reactor operator shall operate the reactor for a minimum of four (4) hours and perform a supervised reactor startup, including a core excess measurement and increase to power. For senior reactor operators, direct supervision of these operations may be considered equivalent to actual performance.

If a licensed reactor operator or senior reactor operator has not met the quarterly operating requirements, then before resumption of licensed duties, the operator or senior operator shall:

- satisfactorily perform the annual operating exam; and
- operate the reactor for a minimum of six (6) hours under the direction of a Senior Reactor Operator.

12.10.8 Annual Operating Exam

To maintain a current license, each calender year, each reactor operator or senior reactor operator shall successfully complete an annual operating exam to be administered by the Reactor Supervisor. Successful completion is left to the discretion of the Reactor Supervisor. The annual operating exam for the Reactor Supervisor shall be administered by a senior reactor operator.

The annual operating exam shall include the following:

- reactor startup;
- core excess measurement;
- increase power to 1 MW;
- change in power level ≥10% in manual;
- record a set of console logs;
- respond to any annunciators;
- shut down the reactor;
- state responses, or respond to, all of the following situations:
    a) loss of coolant;
    b) loss of electrical power;
    c) loss or malfunction of a nuclear instrumentation;
    d) rod drop;
    e) inability to drive rods;
    f) fuel cladding failure; and
    g) reactor top or stack CAM alarm.

12.10.9 Medical Certification

All reactor operators and senior reactor operators shall undergo a medical examination by a physician biennially, not to exceed two-and-a-half (2.5) years. The physician should be conversant with the medical requirements of this program. Following completion of the medical examination, an NRC Form 396 shall be signed by the Radiation Center Director.

12.10.10 Records

Required documents and records pertaining to the requalification program for a reactor operator or senior reactor operator shall be maintained until the respective operator's license is renewed or surrendered.

12.11 Startup Plan

This is not applicable.

12.12 Environmental Reports

This shall be submitted as a separate document.

CHAPTER 13

ACCIDENT ANALYSES

Chapter 13 - Valid Pages
Rev. 0 7/01/2004

i	Rev. 0 7/01/2004	39	Rev. 0 7/01/2004
ii	Rev. 0 7/01/2004	40	Rev. 0 7/01/2004
iii	Rev. 0 7/01/2004	41	Rev. 0 7/01/2004
iv	Rev. 0 7/01/2004	42	Rev. 0 7/01/2004
1	Rev. 0 7/01/2004		
2	Rev. 0 7/01/2004		
3	Rev. 0 7/01/2004		
4	Rev. 0 7/01/2004		
5	Rev. 0 7/01/2004		
6	Rev. 0 7/01/2004		
7	Rev. 0 7/01/2004		
8	Rev. 0 7/01/2004		
9	Rev. 0 7/01/2004		
10	Rev. 0 7/01/2004		
11	Rev. 0 7/01/2004		
12	Rev. 0 7/01/2004		
13	Rev. 0 7/01/2004		
14	Rev. 0 7/01/2004		
15	Rev. 0 7/01/2004		
16	Rev. 0 7/01/2004		
17	Rev. 0 7/01/2004		
18	Rev. 0 7/01/2004		
19	Rev. 0 7/01/2004		
20	Rev. 0 7/01/2004		
21	Rev. 0 7/01/2004		
22	Rev. 0 7/01/2004		
23	Rev. 0 7/01/2004		
24	Rev. 0 7/01/2004		
25	Rev. 0 7/01/2004		
26	Rev. 0 7/01/2004		
27	Rev. 0 7/01/2004		
28	Rev. 0 7/01/2004		
29	Rev. 0 7/01/2004		
30	Rev. 0 7/01/2004		
31	Rev. 0 7/01/2004		
32	Rev. 0 7/01/2004		
33	Rev. 0 7/01/2004		
34	Rev. 0 7/01/2004		
35	Rev. 0 7/01/2004		
36	Rev. 0 7/01/2004		
37	Rev. 0 7/01/2004		
38	Rev. 0 7/01/2004		

TABLE OF CONTENTS

LIST OF TABLES

LIST OF TABLES (Continued)

THIS PAGE INTENTIONALLY BLANK

13.0 ACCIDENT ANALYSIS

13.1 Introduction

In about 1980, the U.S. Nuclear Regulatory Commission requested an independent and fresh overview analysis of credible accidents for TRIGA® and TRIGA®-fueled reactors. Such an analysis was considered desirable since safety and licensing concepts had changed over the years. The study resulted in NUREG/CR-2387, Credible Accident Analysis for TRIGA® and TRIGA®-fueled Reactors (Ref. 13.1). The information developed by the TRIGA® experience base, plus appropriate information from NUREG/CR-2387, serve as a basis for some of the information presented in this chapter.

The reactor physics and thermal-hydraulic conditions in the OSTR at a power level of 1 MW are established in Chapter 4. In this chapter, it was assumed that two different TRIGA® fuel types might be used in the OSTR: [redacted]wt% fuel with [redacted]% enrichment and [redacted] fuel at [redacted]wt% with [redacted]% enrichment.

The fuel temperature is a limit on operation in both steady-state and pulse modes. This limit stems from the out-gassing of hydrogen from U-ZrH fuel and the subsequent stress produced in the fuel element cladding material. The strength of the stainless steel cladding as a function of temperature sets the upper limit on the fuel temperature. Fuel temperature limits of 1,100 °C (with clad < 500 °C) and 930 °C (with clad > 500 °C) for U-ZrH with a H/Zr ratio less than 1.70 have been set to preclude the loss of clad integrity.

Nine credible accidents for research reactors were identified in NUREG-1537 (Ref. 13.2) as follows:

- the maximum hypothetical accident (MHA);
- insertion of excess reactivity;
- loss of coolant accident (LOCA);
- loss of coolant flow;
- mishandling or malfunction of fuel;
- experiment malfunction;
- loss of normal electrical power;
- external events; and
- mishandling or malfunction of equipment.

This chapter contains analyses of postulated accidents that have been categorized into one of the above nine groups. Some categories contain accidents that do not appear applicable or credible for the OSTR, but this is acknowledged in a brief discussion of the category. Some categories contain an analysis of more than one accident even though one is usually

limiting in terms of impact. Any accident having significant radiological consequences was included.

For those events that do not result in the release of radioactive materials from the fuel, only a qualitative evaluation of the event is presented. Events leading to the release of radioactive material from a fuel element were analyzed to the point where it was possible to reach the conclusion that a particular event was, or was not, the limiting event in that accident category. The MHA for TRIGA® reactors is the cladding failure of a single irradiated fuel element in air with no radioactive decay of the contained fission products taking place prior to the release.

13.2 Accident Initiating Events and Scenarios, Accident Analysis, and Determination of Consequences

13.2.1 Maximum Hypothetical Accident (MHA)

13.2.1.1 Accident Initiating Events and Scenarios

A single fuel element could fail at any time during normal reactor operation or while the reactor is in a shutdown condition, due to a manufacturing defect, corrosion, or handling damage. This type of accident is very infrequent, based on many years of operating experience with TRIGA® fuel, and such a failure would not normally incorporate all of the necessary operating assumptions required to obtain a worst-case fuel-failure scenario.

For the OSTR, the MHA has been defined as the cladding rupture of one highly irradiated fuel element with no radioactive decay followed by the instantaneous release of the noble gas and halogen fission products into the air. For the OSTR, with two different possible fuel types, a [redacted] fuel element was chosen as the irradiated element since a [redacted] element contains the most ^{235}U and, hence, the highest inventory of fission products. The failed fuel element was assumed to have been operated at the highest core power density for a continuous period of one year at 1 MW. This results in all of the halogens and noble gases (except Kr-85) reaching their saturated activities.

This is the most severe accident for a TRIGA® reactor and is analyzed to determine the limiting or bounding potential radiation doses to the reactor staff and to the general public in the unrestricted area. A less severe, but more credible accident, involving this same single element having a cladding failure in water will also be analyzed. This latter accident more correctly falls into the Mishandling or Malfunction of Fuel accident category and will be addressed there.

During the lifetime of the OSTR, used fuel within the core may be moved to new positions or removed from the reactor. Fuel elements are moved only during periods when the reactor is in a shutdown condition. Also, the OSTR is never operated continuously at 1 MW for a period longer than 8-10 hours, let alone a period of one year.

Nevertheless, this MHA has been analyzed for the OSTR.

Three different scenarios have been chosen for analysis:

- Scenario A:

  In this scenario, the entire north wall of the reactor room instantly vanishes. No credible cause for this occurrence can be imagined. The noble gas and halogen fission products that have been released to the reactor room air are assumed to mix instantly and uniformly with the room air. This reactor room air then moves out through the missing wall at the mean wind speed (1 m sec^{-1}). This is assumed to be a ground level release. It takes 8.52 seconds for the entire volume of the reactor room air to be evacuated. Thus, individuals outside the reactor room will be exposed to a radioactive cloud for a period of 8.52 seconds;

- Scenario B:

  This scenario again assumes that the noble gas and halogen fission products instantly and uniformly mix with the reactor room air. The fission products that have been released to the reactor room air are then exhausted at the stack ventilation rate (4.39×10^6 cm^3sec^{-1}). The path for this release is not specified. It could possibly be through the small door on the NE corner of the building, or it could be through the stack if the vent fans didn't shut down and the dampers did not close. The air is assumed to be discharged at ground level, and no credit is taken for an elevated release. The time to evacuate the entire volume of the reactor room is 14.7 minutes, and this is, therefore, the exposure time for individuals outside the reactor room; and

- Scenario C:

  This scenario also assumes that the noble gas and halogen fission products instantly and uniformly mix with the reactor room air. The reactor room air then leaks from the room at the leak rate of 1.69×10^4 cm^3sec^{-1} as specified in the original OSTR SAR (Ref. 13.3). In this case, it would take 63.7 hours for the entire volume of the reactor room air to be evacuated, and this is the exposure time for individuals outside the reactor room. This is also assumed to be a ground level release.

13.2.1.2 Accident Analysis and Determination of Consequences

As stated earlier, it is assumed that the OSTR is fueled with [redacted] fuel elements and that the reactor has operated continuously at 1 MW for a period of one year. Thus, all halogens and all noble gases (except Kr-85) are at their saturation activity. The highest-power-density [redacted] element fails and releases the noble gases and halogens to the cladding gap. This highest-power-density element has a power density of 15.9 kW per element, and a maximum-to-average power factor of 1.42 (Ref. 13.4). The fission product inventory of halogen and noble gases are given in Table 13-1 for this element. The inventory assumes a saturated activity is present and is based upon the fission yield for each isotope.

Considerable effort has been expended to measure and define the fission product release fractions for TRIGA® fuels. Data on this aspect of fuel performance are reported in Refs. 13.5 - 13.11. Using this data, GA developed a conservative correlation for fission product release to be

$$e = 1.5\times 10^{-5} + 3.6\times 10^{3} \exp\left\{\frac{-1.34\times 10^{4}}{(T+273)}\right\}.$$

At an average fuel temperature of 500 °C, this release fraction is 1.22×10^{-4}. This fuel temperature (500 °C) is much higher than the actual expected average fuel temperature of 322 °C, and results in a release fraction about 7.8 times higher.

Once the fission products are released to the gap, this activity is released when the cladding fails. If the release is in air (MHA), then this activity is released directly into the reactor room air. If the release occurs in the pool water, then the fission products must migrate through the water before being released to the reactor room air. Once released into the reactor room air, a further reduction of the halogen activity is expected to occur due to plateout in the building.

Thus, the fraction (w) of the fission product inventory released from a single fuel element which reaches the reactor room air and, subsequently, the atmosphere in the unrestricted environment is:

$$w = e\, f\, g\, h;$$

where:

e = the fraction released from the fuel to the fuel-cladding gap;
f = the fraction released from the fuel-cladding gap to the reactor room air (if no water is present), or to the pool water (if water is present);
g = the fraction released from the pool water to the reactor room air; and
h = the fraction released from the reactor room air to the outside unrestricted environment, due to plateout in the reactor room.

Table 13-1 Saturated Activities for Highest Power Density [redacted] Fuel Element

For the accident where the cladding failure occurs in air, it is very conservatively assumed that 25% of the halogens released to the cladding gap are eventually available for release from the reactor room to the outside environment. This value is based on historical usage and recommendations (Refs. 13.5 - 13.13), where Reference 13.5 recommends a 50% release of the halogens from the gap to the air. References 13.6 and 13.7 apply a natural reduction factor of 50% due to plateout in the reactor building. Combining the 50% release from the gap with the 50% plateout results in the 25% total release. However, this value appears to be quite conservative, since References 13.10 and 13.11 quote a 1.7% release from the gap rather than 50%.

For the accident in air, 100% of the noble gases are assumed to be available for release to the unrestricted environment.

For the accident in water, it is conservatively assumed that most of the halogens released from the cladding gap remain in the water and are removed by the demineralizer. A small fraction, 5%, of the halogens is assumed to escape from the water to the reactor room air. Combining this with the 50% release from the gap to the water, the result is that 2.5% of the halogens in the gap are released to the reactor room. Again, 50% of these plateout in the reactor room before release to the outside environment. For the noble gases in water, 100% are assumed to be available for release to the unrestricted environment.

The experience at TMI-2, along with recent experiments, indicate that the 50% halogen release fraction is much too large. Possibly as little at 0.06% of the iodine reaching the cladding gap may be released into the reactor room due in part to a large amount of the elemental iodine reacting with cesium to form CsI, a compound much less volatile and more water soluble that elemental iodine (Ref. 13.11).

The values for these various release fractions are given in Tables 13-2 and 13-3. For the OSTR, the prevailing wind is from the south, blowing to the north. The minimum distance to the unrestricted environment (10 m), the minimum distance to the nearest occupied office building (100 m), and the minimum distance to the nearest permanent residence (267 m) are also to the north. For this accident, therefore, it was assumed that the wind is blowing from south to north.

For any atmospheric stability (Pasquill) class, a ground-level release always gives a higher concentration at any given distance than an elevated release. Thus, it was assumed that there were only ground level releases, which do not take credit for any release heights nor building wake effects. Furthermore, the more stable the atmospheric class, the higher the concentration. Therefore, it was assumed that the most stable atmospheric class

(Pasquill F) prevailed for all scenarios. Also, the lower the wind speed, the higher the concentration. Thus, it was assumed that a low wind speed of 1 m sec^{-1} existed for all scenarios.

Table 13-2 Release Fraction Components

Fission product	f No pool water	f With pool water	g No pool water	g With pool water	h
Noble gas	1.0	1.0	N/A	1.0	1.0
Halogens	0.5	0.5	N/A	0.05	0.5

Table 13-3 Total Release Fraction

Fission product	w No pool water	w With pool water
Noble gas	1.22 E-4	1.22 E-4
Halogens	3.05 E-5	1.53 E-6

The methodology of NRC Regulatory Guide 1.145 (Ref. 13.14) was used. For distances greater than 100 m, the values for horizontal and vertical dispersion coefficients were also taken from this guide. For distances from 10 m to 100 m, which are not treated in Regulatory Guide 1.145, data were obtained locally from the OSTR (Ref. 13.15). The values for the dispersion coefficients and χ/Q are given in Table 13-4.

Furthermore, it was assumed that all of the fission products were released to the unrestricted area by a single reactor room air change, which would maximize the dose rate to persons exposed to the plume during the accident.

Table 13-4 Atmospheric Dispersion Coefficients and χ/Q Values for Pasquill F and Mean Wind Speed of 1 m sec^{-1}

Distance (m)	σ_y (m)	σ_z (m)	χ/Q (sec m^{-3})
10	1.29	1.04	5.93 E-2
50	2.45	1.20	2.71 E-2
100	3.90	2.20	9.27 E-3
150	6.18	3.22	4.00 E-3
200	8.21	4.13	2.35 E-3
250	10.21	4.98	1.57 E-3
267	10.88	5.25	1.39 E-3

Additional parameters used in this accident were:

- reactor room ventilation exhaust rate: 4.39 E+6 cm^{3}sec^{-1};
- reactor room leak rate: 1.69 E+4 cm^{3}sec^{-1};
- reactor room volume: 3.88 E+9 cm^3;
- area of north face of reactor building: 2.31E+2 m^2;
- receptor breathing rate: 3.3 E-4 m^{3}sec^{-1}: (NRC "light work" rate); and
- dose conversion factors:
  internal: based on DOE/EH-0071 (Ref. 13.16);
  external: based on DOE/EH-0070 (Ref. 13.17).

The committed dose equivalent (CDE) to the thyroid and the committed effective dose equivalent (CEDE) for members of the general public at a given distance downwind from the facility for all isotopes of concern may each be calculated by:

$$\left(\text{CDE or CEDE}\right)_D = \sum_i \left[\frac{\left(\frac{\chi}{Q}\right)_D \text{BR DCF}_{int,i} A_i \lambda_v \left[e^{-\lambda_i t_1} - e^{-\lambda_i t_2}\right]}{\lambda_i} \right],$$

where:

$(\chi/Q)_D$ = atmospheric dispersion factor at a given distance D (s m^{-3});
BR = breathing rate (m^3 s^{-1});
$DCF_{int,i}$ = internal dose conversion factor for isotope i (mrem μCi^{-1}) [Ref. 13.16];
A_i = initial activity of isotope i released into the reactor room (μCi);
R_v = ventilation or leakrate of air from the reactor bay (m^3 s^{-1});
V = reactor room volume (m^3);
λ_v = ventilation constant = R_v/V (s^{-1});
λ_i = decay constant for isotope i (s^{-1});
t_1 = time when plume first arrives at the receptor point (s); and
t_2 = time when plume has passed the receptor point (s).

The deep dose equivalent (DDE) to members of the general public at a given distance downwind from the facility for both the thyroid and the whole body may each be calculated by:

$$\left(DDE_{Thyroid} \text{ or } DDE_{WB}\right)_D = \sum_i \left[\frac{\left(\frac{\chi}{Q}\right)_D DCF_{ext,i}\, A_i\, \lambda_v \left[e^{-\lambda_i t_1} - e^{-\lambda_i t_2}\right]}{\lambda_i} \right],$$

where:

$DCF_{ext,i}$ = external dose rate conversion factor for isotope i (mrem m^3 μCi^{-1} s^{-1}) [Ref. 13.17].

The CDE and CEDE for personnel in the reactor room for a given stay-time may each be calculated by:

$$\left(CDE \text{ or } CEDE\right)_{ST} = \sum_i \left[\frac{DCF_{int,i}\, A_i\, BR \left[1 - e^{-\lambda_{eff} t_{ST}}\right]}{\lambda_{eff}\, V} \right],$$

where:

$\lambda_{eff} = \lambda_i + \lambda_v$; and
t_{ST} = stay-time of personnel (s).

The DDE to personnel in the reactor room for a given stay-time for both the thyroid and the whole body may be calculated by:

$$\left(DDE_{Thyroid} \text{ or } DDE_{WB}\right)_{ST} = \sum_i \left[\frac{DCF_{ext,i}\, A_i \left[1 - e^{-\lambda_{eff} t_{ST}}\right]}{\lambda_{eff}\, V} \right].$$

The results of these calculations for all three scenarios are shown in Tables 13-5 through 13-10. As seen from the tables, Scenario A gives the highest doses to the general public at any distance, as might be expected since the activity was released in a very short time leaving little time for radioactive decay. Scenario C gives the lowest doses at any given distance since the release occurs over a long time and radioactive decay becomes significant. Also, as expected, the doses were highest at the shortest distance (i.e., the site boundary). In all cases, doses for the general public and occupational workers were all well below the annual dose limits specified by 10 CFR 20.

Table 13-5 Occupational Radiation Doses in the Reactor Room Following a Single Element Failure in Air - Scenario A

Reactor Room Occupancy (minutes)	$CDE_{Thyroid} + DDE_{Thyroid}$ (mrem)	TEDE (mrem)
2	28	1
5	28	1

Table 13-6 Radiation Doses to Members of the General Public Following a Single Element Failure in Air - Scenario A

Distance (m)	$CDE_{Thyroid} + DDE_{Thyroid}$ (mrem)	TEDE (mrem)
10	389	19
50	178	8
100	61	3
150	26	1
200	15	1
250	10	<1
267	9	<1

Table 13-7 Occupational Radiation Doses in the Reactor Room Following a Single Element Failure in Air - Scenario B

Reactor Room Occupancy (minutes)	$CDE_{Thyroid} + DDE_{Thyroid}$ (mrem)	TEDE (mrem)
2	190	9
5	429	20

Table 13-8 Radiation Doses to Members of the General Public Following a Single Element Failure in Air - Scenario B

Distance (m)	$CDE_{Thyroid} + DDE_{Thyroid}$ (mrem)	TEDE (mrem)
10	386	17
50	176	8
100	60	3
150	26	1
200	15	1
250	10	<1
267	9	<1

Table 13-9 Occupational Radiation Doses in the Reactor Room Following a Single Element Failure in Air - Scenario C

Reactor Room Occupancy (minutes)	$CDE_{Thyroid} + DDE_{Thyroid}$ (mrem)	TEDE (mrem)
2	203	10
5	505	23

Table 13-10 Radiation Doses to Members of the General Public Following a Single Element Failure in Air - Scenario C

Distance (m)	$CDE_{Thyroid} + DDE_{Thyroid}$ (mrem)	TEDE (mrem)
10	278	9
50	127	4
100	43	1
150	19	1
200	11	<1
250	7	<1
267	7	<1

13.2.2 Insertion of Excess Reactivity

13.2.2.1 Accident Initiating Events and Scenarios

The most credible generic accident is the inadvertent rapid insertion of positive reactivity that could, if large enough, produce a transient resulting in fuel overheating and a possible breach of cladding integrity. Operator error or failure of the automatic power level control system could cause such an event due to the uncontrolled withdrawal of a single control rod, or possibly even the withdrawal of more than one control rod. Flooding or removal of

beamport inserts could also have a positive effect on reactivity, but not as severe as the removal of a control rod. In a separate scenario, a large reactivity insertion was postulated to create fuel cladding temperatures that might cause a metal-water reaction, but for many reasons this accident is not considered to be a safety risk in TRIGA® reactors.

13.2.2.2 Accident Analysis and Determination of Consequences

13.2.2.2.1 Maximum Reactivity Insertion

Raising the temperature of TRIGA® fuel has a strong, prompt negative reactivity effect, which can overcome a rapid reactivity insertion such as that produced by the rapid removal of the transient rod. The quantity that causes this effect is the prompt negative temperature coefficient of the fuel, discussed in Chapter 4. There is a limit to the protection provided by this feedback, since the peak fuel temperature attained before the feedback terminates the transient increases with the magnitude of the inserted reactivity. The Nordheim-Fuchs model (Refs. 13.18 and 13.19) was used to compute the maximum reactivity pulse that can occur without exceeding the safety limit on fuel temperature established in Chapter 4.

In the Nordheim-Fuchs model, it is assumed the transient is so rapid that 1) the temperature rise is adiabatic, and 2) delayed neutrons can be neglected. Thus, the model is given by the following set of coupled differential equations:

$$\frac{dP}{dt} = [\rho - \beta]\frac{P}{\ell},$$

$$\frac{dT}{dt} = \frac{P}{C(T)}, \text{ and}$$

$$\rho(T) = \rho_0 - [\alpha(T)][T - T_0],$$

where P is the reactor power, ρ is the time-dependent reactivity, ℓ is the neutron lifetime, β is the effective delayed neutron fraction, T is the core-average temperature, T_0 is the initial temperature, ρ_0 is the reactivity insertion, α is the temperature-dependent prompt reactivity feedback coefficient, and C is the temperature-dependent whole-core heat capacity.

The quantity of interest is ΔT, the difference between the maximum and initial values of the core-average fuel temperature. From the definition of ΔT, the peak fuel temperature can be found to be

$$T_{peak} = T_0 + PF[\Delta T] = T_0 + PF[T - T_0],$$

where T_o is the initial temperature and PF is the total peaking factor.

In the above equations, the desire is to find the value of ρ_o that yields a $T_{peak} = 1{,}100$ °C. In the Nordheim-Fuchs model, at the end of the reactivity burst, one gets the maximum fuel temperature (T_{peak}), and the total inserted reactivity is

$$\rho = 2[\beta - \rho_0].$$

Thus, one gets the equation:

$$\alpha[T - T_0] + 2[\beta - \rho_0] = 0.$$

Knowing the total peaking factor (PF) and the peak temperature, one can find the core-average temperature, T. With given values for β and initial fuel temperature (T_o), and the expression for α, one can calculate ρ_o.

The following input values were used for all calculations here:

$\beta = 0.007$;
$\ell = 32$ msec;
$T_o = 20$ °C;
PF = 3.41 (fuel); and
PF = 3.25 (fuel).

Using these values for T_o and PF, the values of core-average temperature that correspond to a peak fuel temperature of 1,100 °C are 337 °C for fuel and 352 °C for fuel.

The case where the peak fuel temperature was 1,150 °C for fuel and 1,000 °C for fuel was also calculated. For this case, the core-average temperatures were 351 °C for fuel and 322 °C for fuel.

The maximum fuel temperature was not found to change with reasonable variations in ℓ. The value of β is well known. The value of T_o is the nominal zero-power fuel temperature. The value of PF is the largest total peaking factor expected for each fuel type in the core.

The reactivity insertion limit (ρ_o) is shown for three cases in Table 13-11. Each case has a different combination of fuel type and core-average burnup. The expressions for heat capacity, C, as a function of temperature correspond to a core size of fuel elements and fuel elements ( ). The values for α are taken from the literature by fitting the negative temperature coefficient curves for the various fuel types to polynomials.

The different values for α are directly responsible for the differences in the reactivity insertion limit among the three cases.

The lowest value of ρ_o is used in this section as it gives the worst-case result. This is \$2.59 for [redacted] fuel at end-of-life. This value of reactivity insertion gives the maximum fuel temperature of 1,100 °C for [redacted] fuel at end-of-life. This same reactivity insertion for other types of fuel at beginning- or end-of-life would yield peak fuel temperatures below 1,000 °C. There are at least two reasons why this is a conservative bound. One is that this is at the end-of-life for the [redacted] fuel, and the [redacted] core would most likely not be at that stage, hence the prompt feedback would be higher. Another reason is that the peaking factor used in the calculation is significantly higher than would be the actual case for [redacted] fuel at end-of-life. Also, maximum fuel temperatures for [redacted] up to 1,150 °C are allowable and this peak temperature (1,100 °C) is below that.

Table 13-11 Maximum Reactivity Insertion and Related Quantities for Various Fuels and Burnups

Fuel type	Burnup (% MWD/rod)	Heat Capacity for total core (watt-sec °C^{-1})	Prompt Negative Temperature Coefficient ($\Delta k/k$ °C)	Reactivity (\$) T_{peak} = 1,100 °C for all fuel	Reactivity (\$) T_{peak} = 1,150 °C for [redacted] fuel, T_{peak} = 1,000 °C for [redacted] fuel
[redacted]	independent	$7.00 \times 10^4 + 145\ T$	$7.16 \times 10^{-5} + 2.33 \times 10^{-7}\ T - 4.35 \times 10^{-10}\ T^2 + 2.09 \times 10^{-13}\ T^3$	\$3.58	\$3.51
[redacted]	BOL	$6.91 \times 10^4 + 142\ T$	$2.9 \times 10^{-5} + 2.03 \times 10^{-7}\ T$	\$3.21	\$3.37
[redacted]	EOL	$6.91 \times 10^4 + 142\ T$	$2.9 \times 10^{-5} + 1.22 \times 10^{-7}\ T$	\$2.59	\$2.70

13.2.2.2.2 Uncontrolled Withdrawal of a Control Rod

The OSTR routinely operates with three different core configurations: normal, CLICIT, AND ICIT. The ICIT core contains an In-Core Irradiation Tube (ICIT) and the CLICIT core contains a Cadmium-Lined In-Core Irradiation Tube (CLICIT). The worths of the four control rods vary somewhat depending upon the core configuration. The

configuration that gives the highest worths of the rods is the normal core, and this is the core used in this analysis.

Good experimental data exist for the control rod worths and rod withdrawal times for this normal configuration of [redacted] fuel. Each rod has an active length of [redacted]. Data for this configuration are given in Table 13-12.

Table 13-12 Control Rod Data for Normal Configuration [redacted] Core

Control Rod	Total Worth ($)	Rod position at $T = T_0$ (% withdrawn)	Rod position at P = 1 MW (% withdrawn)	Total rod withdrawal time (sec)	Reactivity insertion rate ($ sec^{-1})
Transient	[redacted]	38	49	33.81	[redacted]
Safety	[redacted]	38	49	48.09	[redacted]
Shim	[redacted]	38	49	48.20	[redacted]
Regulating	[redacted]	54	47	36.18	[redacted]

Operator error or failure of the automatic power level control system could cause one of the control rods to be driven out, starting either at low power or high power levels. The most reactive rod is the transient rod and this rod also has the fastest withdrawal time. This rod was considered in this accident.

To analyze this accident, the one-delay group model was used with the prompt jump approximation. For a linear increase in reactivity (a ramp input), this model gives (Ref. 13.19):

$$\frac{P}{P_o} = \exp(-\lambda t)\left\{\frac{\beta}{[\beta - \gamma t]}\right\}^a,$$

where:

P = final power level;
P_o = initial power level;
β = total delayed neutron fraction = .007;
λ = one group decay constant (sec^{-1}) = .405 sec^{-1};
t = time (sec);
γ = linear insertion rate of reactivity ($\Delta k/k$ sec); and
$a = 1 + \lambda\beta/\gamma$.

For the case with an initial power level of 100 watts, and the trip setpoint at 1.06 MW, the reactor power was calculated to reach the trip setpoint in about 5.06 seconds. Assuming it takes 0.5 seconds for the signal to cause actual release of the rods, the peak reactivity inserted would be $1.06. This is considerably less than the limiting reactivity insertion of $2.59, given in Section 13.2.2.2.1, and, thus, should produce no adverse safety effects.

For the case with the initial power at 1 MW, and the trip setpoint again at 1.06 MW, the reactor power was calculated to reach the trip setpoint in 0.28 seconds. Again, allowing for 0.5 seconds for the rods to be released, the peak reactivity inserted would be $0.15. This is well below the limiting reactivity insertion of $2.59.

13.2.2.2.3 Uncontrolled Withdrawal of All Control Rods

For this accident, all four control rods were assumed to be withdrawn simultaneously. For this accident to happen, there must be multiple failures in the control system.

The initial power level was assumed again to be 100 watts, and the trip setpoint was 1.06 MW. The total reactivity insertion rate was equal to the sum of the four rod insertion rates: $0.47 sec^{-1}. The trip setpoint was reached in about 2.12 seconds, and again assuming 0.5 seconds elapsed before the rods were released, the total reactivity inserted was $1.23. This is still well below the limiting reactivity insertion of $2.59.

13.2.2.2.4 Beamport Flooding

The only credible accident in the class is the possible flooding of one or more of the beamports. In this case air or inert gas would be replaced with water, and this would constitute a positive reactivity insertion. It has been estimated that the worth of one flooded beamport tube would be about $0.25 (Ref. 13.26). If all four beamports were flooded, the total effect would be $1.00 of positive reactivity added. Even if this estimate of beamport reactivity worth doubled, the net effect would still be less than the limiting reactivity insertion of $2.59. This, therefore, does not represent a significant safety event.

13.2.2.2.5 Metal-Water Reactions

Although metal-water reactions have occurred in some reactor accidents or destructive tests, the evidence from these events and laboratory experiments shows that a dispersed liquid metal is required for a violent chemical reaction to occur (Refs. 13.1 and 13.18). The conditions for a solid metal-water reaction are not readily achievable in a reactor system such as the OSTR.

Water quench tests on TRIGA® fuel have been conducted to fuel temperatures as high as 1,200 °C without significant effect. Since the operating temperatures at 1 MW do not

approach this temperature, this effect does not represent a safety risk. [redacted] The limits set on excess reactivity preclude this.

13.2.3 Loss of Coolant Accident (LOCA)

13.2.3.1 Accident Initiating Events and Scenarios

Loss of coolant from the OSTR could occur primarily through one of two scenarios: pumping water from the reactor tank, or reactor tank failure. These scenarios are analyzed as part of this section.

13.2.3.2 Accident Analysis and Determination of Consequences

13.2.3.2.1 Pumping Water from the Reactor Tank

The outlet for the primary water is located about 4 feet below the normal tank water level. This line and the primary water inlet line each have a syphon break about 22 inches below the normal tank water level. The intake for the water purification system is at the normal water level surface, and if the water level drops about 3 inches or more, this begins to suck air. Thus the normal water systems could only pump water down about 22 inches below the normal tank water level, and could not accidentally pump the tank dry.

13.2.3.2.2 Reactor Tank Failure

[redacted]

Leaks caused by corrosion would be small leaks, which would be detected in the routine daily inspection, and makeup water could be supplied before the tank water level had lowered significantly. If the leak persisted or was larger, the reactor fuel could be unloaded and the leak repaired.

[redacted] such an event occurred while the reactor was operating at peak power, the reactor would shut down because of the voiding of the water from the core, even if there were no scram.

In this unlikely event, almost all of the water pouring on the reactor floor would run [redacted] The volume of the waste holdup tank is about 2,950 gallons. The water in this tank is checked for release concentrations, then the water is dumped when the tank level reaches about 1,800 gallons. Thus there is always at least about 1,100 spare gallons in the tank, and often more. The trench can hold about 3,000 gallons. Therefore, about 4,100 gallons or more of the total 4,600 gallons of reactor tank water could be held in the pipe trench and holdup tank.

There are two immediate considerations of such a catastrophic loss of water: cooling of the reactor core, and dose rates around the uncovered core. The consequences of each of these will be discussed in the following sections.

13.2.3.2.2.1 Cooling of Reactor Core

If all coolant is suddenly lost when the reactor has been operating at full power for a considerable period, the primary concern is the maximum fuel temperature that might be reached and whether or not the fuel cladding will remain intact. This accident has been analyzed in numerous reports previously (Refs. 13.3, 13.4, 13.21 - 13.23) , and addressed in Chapter 4 of this report. All of these reports reach the same conclusion: natural convective air cooling of the fuel will keep the maximum fuel temperature well below the temperature for cladding failure if the reactor operates at a maximum power level of 1.5 MW or below. In NUREG/CR-2387, this accident was also examined and the conclusion was that, for a reactor such as the OSTR, a loss of coolant accident was not credible (Ref. 13.1).

13.2.3.2.2.2 Radiation Levels from the Uncovered Core

If the reactor core suddenly becomes uncovered after sustained operation at full power, high radiation doses might be expected from the uncovered core. Radiation doses at three locations are calculated here: at the grating over the top of the reactor, at a point in the reactor room, and at the nearest fence boundary to the unrestricted area. These latter two doses would be scattered doses from the reactor room roof.

The basic assumption is that the reactor has been operating at a maximum power level of 1 MW for one continuous year, and then the water is instantly lost. This is a very conservative assumption, since there is no conceivable way the OSTR could be operated continuously, 24 hours per day, at 1 MW for one year. The OSTR only operates on an 8-hour-per-day shift for 5 days per week.

The total fission product activity as a function of time after shutdown was determined using the standard equation (Ref. 13.24):

$$A(t) = 1.4 \times 10^6 \, P\left[t^{-0.2} - (t+T)^{-0.2}\right](Ci)$$

where:

P = reactor thermal power (MW);
t = time after shutdown (days); and
T = operating time (days).

For this calculation: P = 1 MW and T = 365 days.

The total fission product activity will be calculated at 5 different times after shutdown: 10 seconds, 1 hour, 1 day, 1 week, and 1 month.

The reactor core was modeled as a cylinder of radius 22.2 cm and a height of 38.1 cm. This assumes that the fuel is filling all grid positions out through the F ring of the core, which is essentially the case for [redacted]uel in a normal core configuration. Therefore, the source term for this analysis (S_v) was determined by dividing the total activity by the volume of this cylinder:

$$S_v = \frac{\left(3.7 \times 10^{10}\right) A}{\pi R^2 h} \left(\gamma\, cm^{-3}\, \sec^{-1}\right),$$

where:

R = core radius (cm) = 22.2 cm;
h = core height (cm) = 38.1 cm; and
3.7×10^{10} converts curies to gamma rays, assuming one gamma ray of energy 1 MeV per disintegration.

The total activity and the source strength are shown in Table 13-13.

13.2.3.2.2.3 Dose Rate Directly Above Core

The reactor core, shutdown and drained of water, was treated as a uniform bare cylindrical source of 1-MeV photons. Its dimensions were taken to be equal to those of the active core lattice. No accounting was made of sources other than fission product decay gammas, and no credit was taken for attenuation through the fuel element end pieces and the upper grid plate. The first of these assumptions is optimistic, the second conservative, and the net effect is conservative. The conservative assumption of a uniformly distributed source of 1-MeV gammas was balanced by not assuming any buildup in the core.

Table 13-13 Total Fission Product Activity and Source Strength After Shutdown

Time After Shutdown	Fission Product Activity (Ci)	Source Strength S_v (γ cm^{-3} sec^{-1})
10 seconds	[redacted]	5.11 x 10[redacted]
1 hour	[redacted]	7.78 x 10[redacted]
1 day	[redacted]	6.08 x 10[redacted]
1 week	[redacted]	3.26 x 10[redacted]
1 month	[redacted]	1.79 x 10[redacted]

The dose rate was calculated at a point on the axis of the core cylinder at a distance of 610 cm (20 feet) from the top of the core. This is the distance from the top of the core to a point about 3 feet above the tank cover grating.

The dose rate was determined from the equation:

$$\varphi = \left[\frac{S_v R^2}{4\mu_c a^2}\right]\left[1 - \exp(-\mu_c h)\right](\gamma\ \mathrm{cm}^{-2}\ \mathrm{sec}^{-1}),$$

where:

R = core radius (22.2 cm);
H = core height (38.1 cm);
μ_c = core attenuation coefficient (0.28 cm^{-1});
a = distance from top of core to dose point (610 cm); and
S_v = source strength.

The dose conversion factor, K, for effective dose equivalent per unit photon fluence was obtained from ICRP 51, Table 2 (Ref. 13.25). This has been calculated for photons incident on an anthropomorphic phantom from various geometries. The worst case (highest dose factor) was for the anterior to posterior geometry, and this was used for this case. For 1-MeV photons, this value of K was 4.60×10^{-12} Sv cm^2 γ^{-1}.

The results are given in Table 13-14 and are in agreement with the MNRC and Torrey Pines TRIGA® reactors (Refs. 13.22 and 13.26), when corrections are made for the operating power levels.

Table 13-14 Dose Rates on OSTR Reactor Top After a Loss of Pool Water Accident Following 1-MW Operation

Time After Shutdown	Effective Dose Equivalent Rate (rem h^{-1})
10 seconds	1.00×10^{4}
1 hour	1.52×10^{3}
1 day	1.19×10^{3}
1 week	6.39×10^{2}
1 month	3.51×10^{2}

13.2.3.2.2.4 Dose Rate From Scattered Radiation in Reactor Room

The purpose of this section is to calculate the dose rate to a person in the reactor room not in the direct beam from the exposed core, but subject to scattered radiation from the reactor room ceiling. The dose point was chosen to be 3 feet above the reactor room floor at a point in the SE corner of the room. This is the area where radioactive material is packaged for shipping and is frequently occupied. It is also the farthest distance one can get from the edge of the reactor and remain in the reactor room. The ceiling is about 20.6 feet above the reactor top. The ceiling is assumed to be a concrete slab. The concrete slab assumption gives the worst case scattering, but it should be noted that the roof over the reactor is only corrugated metal and not a thick concrete slab. Therefore, in reality the scattering will not be as great as calculated because the radiation from the unshielded core will undergo minimal interaction with the roof.

The following equation was used to find the flux at the dose point from scattered radiation (Ref. 13.27):

$$\varphi = \frac{(6.03\times 10^{23})\rho Z I_0 C \frac{\delta\sigma}{\delta\Omega}}{A x^2 \left\{\mu_0 + \mu_1 \left[\frac{\cos\theta_0}{\cos\theta_1}\right]\right\}} \left(\gamma\ \mathrm{cm}^{-1}\ \mathrm{sec}^{-1}\right),$$

where:

ρ = density of the scattering material (concrete) = 2.3 g cm^{-3};
Z/A = ratio of the average atomic number to the atomic mass;
I_0C = incident beam times the cross section of the beam (γ sec^{-1});
x = distance from scattering point to dose point = 1.78 x 10^3 cm;
μ_0 = attenuation coefficient in scattering material for incident photons = 0.146 cm^{-1};
μ_1 = attenuation coefficient in scattering material for scattered photons = 0.292;
θ_0 = incident angle, measured from normal to the scatterer = 0°;
θ_1 = scattered angle, measured from normal to the scatterer = 49°; and
$\delta\sigma/\delta\Omega$ = differential Klein-Nishina scattering cross section (cm^2).

It was assumed that the source photons which reached the top of the reactor tank were incident normally to the concrete roof ($\theta_0 = 0$) at a point directly over the core. Thus:

$$I_0 C = S_0 \omega = \frac{\pi R^2 S_v \omega}{\mu_c},$$

where S_0 is the strength of a point source equal to the total radioactivity and placed at a point which is one mean free path from the top of the reactor (μ_c^{-1}).

The expression ω is the fractional solid angle subtended by the equivalent point source to the top of the reactor tank. Thus:

$$\omega = \frac{1}{2}\left\{1 - \frac{z}{\left[z^2 + r^2\right]^{\frac{1}{2}}}\right\},$$

where:

r = radius of reactor tank = 99.1 cm; and
z = distance from equivalent point source to top of tank = [redacted]

The energy of the scattered photons is given by:

$$E = \frac{E_0}{1 + \frac{E_0\left[1 - \cos\beta\right]}{0.51}},$$

where E_o is the incident photon energy (1 MeV) and β is the scattering angle = π- (θ_0+ θ_i). In this case, θ_o = 0°. For this case, β = 131° and E = 0.234 MeV.

The differential scattering cross section is given by:

$$\frac{\delta\sigma}{\delta\Omega} = \frac{r_e^2}{2\left\{\frac{E}{E_0} - \frac{\left[E\sin\beta\right]^2}{E_0^2} + \left[\frac{E}{E_0}\right]^3\right\}} \left(cm^2\right),$$

where r_e is the classical electron radius = 2.818×10^{-13} cm.

For this case,

$$\frac{\delta\sigma}{\delta\Omega} = \left(8.56 \times 10^{-27}\right) cm^2.$$

As before, the ICRP 51, Table 2 dose factors were used. Again, the anterior to posterior geometry was used as it gave the largest dose factor for 0.234-MeV scattered photons. This dose factor was 1.15×10^{-12} Sv cm^{-2} γ^{-1}.

The results of the calculations for the scattered radiation into the reactor room are given in Table 13-15.

Table 13-15 Scattered Radiation Dose Rates in the OSTR Reactor Room After a Loss of Pool Water Accident Following 1-MW Operation

Time after shutdown	Effective Dose Equivalent Rate (mrem h^{-1})
10 seconds	327
1 hour	49.7
1 day	38.9
1 week	20.8
1 month	11.4

13.2.3.2.2.5 Dose Rate from Scattered Radiation at Facility Fence

The purpose of this section is to calculate the dose rate to a person at the north facility fence not in the direct beam from the exposed core, but subject to scattered radiation from the reactor room ceiling. The dose point was chosen to be 3 feet above the ground at the north facility fence. This is the closest point a member of the public would be able to occupy. The slant distance to this point from the center of the reactor room ceiling above the reactor tank (the scattering point) is about 125.9 feet, or 3.836×10^3 cm.

The calculational methodology is exactly the same as that used in Section 13.2.3.2.2.2. Values used were the same except as indicated below:

$\mu_1 = 0.292$ cm^{-1};
$\theta_1 = 72.3°$;
$E = 0.281$ MeV;
$\beta = 107.7°$;
$x = 3.836 \times 10^3$ cm;
$\delta\sigma/\delta\Omega = 9.19 \times 10^{-27}$; and
$K = 1.45 \times 10^{-12}$ Sv cm^2 sec^{-1}.

If credit is taken for attenuation in the scattered beam as it passes through the reactor room north wall, then the scattered flux is multiplied by an additional factor of exp $[-\mu_w b]$, where

μ = attenuation coefficient for concrete for 0.28-MeV photons (0.254 cm^{-1}) and b is the slant distance through the wall (16.6 cm).

The results of this calculation are given in Table 13-16.

Table 13-16 Scattered Radiation Dose Rates at the OSTR Facility Fence After a Loss of Pool Water Accident Following 1-MW Operation

Time After Shutdown	Effective Dose Equivalent Rate (mrem h^{-1}) No attenuation in reactor wall	Effective Dose Equivalent Rate (mrem h^{-1}) Including attenuation in reactor wall
10 seconds	50.6	1.49×10^{-2}
1 hour	7.7	2.27×10^{-3}
1 day	6.0	1.78×10^{-3}
1 week	3.2	9.5×10^{-4}
1 month	1.8	5.22×10^{-4}

13.2.4 Loss of Coolant Flow

13.2.4.1 Accident Initiating Events and Scenarios

Loss of coolant flow could occur due to failure of a key component in the reactor primary or secondary cooling system (e.g., a pump), loss of electrical power, or blockage of a coolant flow channel. Operator error could also cause loss of coolant flow.

The OSTR tank holds [redacted] gallons of water, or about [redacted] kg of water. At a steady-state power level of 1 MW, the bulk water temperature would increase adiabatically at a rate of about 0.82 °C min^{-1}. Under these conditions, the operator has ample time to reduce the power and place the heat-removal system back into operation before any abnormal temperature is reached in the reactor bulk water. The OSTR has annunciators indicating that the primary water pump is off, the secondary water pump is off, and cooling tower fans are off. These will alert the operator to an abnormal condition and should allow time for corrective action prior to reaching the bulk water temperature alarm setpoint of 42 °C.

13.2.4.2 Accident Analysis and Determination of Consequences

13.2.4.2.1 Loss of Coolant Flow Without Immediate Operator Action

If the OSTR were operated without coolant flow for an extended period of time, and there was no heat removal by the reactor coolant systems, voiding of the water in the core could occur and the water level in the reactor tank would decrease because of evaporation. The sequence of events postulated for this very unlikely scenario is as follows:

- the reactor would continue to operate at a power level of 1 MW (provided the rods were adjusted to maintain power) and would heat the tank water at a rate of about [redacted] until the tank water reached the bulk water high temperature alarm setpoint. This setpoint is at 42 °C. The normal bulk water temperature, when operating at 1 MW, ranges from 35 to 40 °C, depending on the outside air temperature. Thus, it would take from [redacted] minutes to [redacted] minutes to reach the alarm setpoint. Assuming the operator did not notice this alarm and did not take any corrective action, the bulk water would continue to rise above 42 °C. It would then take an additional [redacted] minutes for the water in the tank to reach the saturation temperature. At this time, voids in the core would cause power oscillations and the negative void coefficient would cause a reduction in power if control rods were not adjusted to maintain power; and

- if it is assumed that the operator or automatic control system maintained power at 1 MW, and still assuming that the system is adiabatic except for the evaporation process, about 1,596 kg h^{-1} would be vaporized. The reactor tank water level would decrease, and it would take about [redacted] hours for the water level to reach the top of the core, and an additional [redacted] hours to vaporize all of the water remaining in the tank. The reactor, however, would shut down as the water level dropped past the top of the fuel.

It is considered inconceivable that such an operating condition would go undetected. Water level, water flow, and water temperature alarms would certainly alert the operator. Also, as the water level decreases, the reactor room radiation monitors would alarm. Because of all of these factors, water would be added to the tank and/or the reactor would be shut down to mitigate the problem.

13.2.5 Mishandling or Malfunction of Fuel

13.2.5.1 Accident Initiating Events and Scenarios

Events which could cause accidents at the OSTR in this category include (1) fuel handling accidents where an element is dropped underwater and damaged severely enough to breach the cladding, (2) simple failure of the fuel cladding due to a manufacturing defect or corrosion, and (3) overheating of the fuel with subsequent cladding failure during steady-state or pulsing operations.

13.2.5.2 Accident Analysis and Determination of Consequences

All three scenarios mentioned in Section 13.2.5.1 result in a single fuel element failure in water. In the unlikely event that this failure occurred in air, this is the MHA analyzed in Section 13.2.1.2.

At various points in the lifetime of the OSTR, fuel elements are moved to new positions or removed from the core. Fuel elements are moved only during periods when the reactor is shutdown.

Assumptions for this accident are almost exactly the same as those used for the MHA, except for one thing: the presence of the pool water contains most of the halogens and, thereby, reduces the halogen dose contribution.

The assumptions for this accident and the method of analysis of this accident were described in Section 13.2.1.2. The same three scenarios (A, B, and C) used in the MHA are used to analyze this accident, although Scenario C is the most credible for this accident.

The results for this accident for the three scenarios are given in Tables 13.17 to 13.22.

The results of this accident show that for all three scenarios the radiation doses to the general public are well below the annual limits in 10 CFR 20, with the maximum dose being 6 mrem TEDE at 10 meters (the site boundary) for any of the scenarios. The occupational radiation doses to workers in the reactor room are also well below the occupational annual limits in 10 CFR 20, with the maximum dose being 23 mrem TEDE for a 5-minute exposure. Five minutes is very ample time for workers to evacuate the room if such an accident were to occur.

Table 13-17 Occupational Radiation Doses in the Reactor Room Following a Single Element Failure in Water - Scenario A

Reactor Room Occupancy (minutes)	$CDE_{Thyroid} + DDE_{Thyroid}$ (mrem)	TEDE (mrem)
2	2	<1
5	2	<1

Table 13-18 Radiation Doses to Members of the General Public Following a Single Element Failure in Water - Scenario A

Distance (m)	$CDE_{Thyroid} + DDE_{Thyroid}$ (mrem)	TEDE (mrem)
10	25	6
50	11	2
100	4	1
150	2	<1
200	1	<1
250	1	<1
267	1	<1

Table 13-19 Occupational Radiation Doses in the Reactor Room Following a Single Element Failure in Water - Scenario B

Reactor Room Occupancy (minutes)	$CDE_{Thyroid} + DDE_{Thyroid}$ (mrem)	TEDE (mrem)
2	12	3
5	26	6

Table 13-20 Radiation Doses to Members of the General Public Following a Single Element Failure in Water - Scenario B

Distance (m)	$CDE_{Thyroid} + DDE_{Thyroid}$ (mrem)	TEDE (mrem)
10	23	4
50	10	2
100	4	1
150	2	<1
200	1	<1
250	1	<1
267	1	<1

Table 13-21 Occupational Radiation Doses in the Reactor Room Following a Single Element Failure in Water - Scenario C

Reactor Room Occupancy (minutes)	$CDE_{Thyroid} + DDE_{Thyroid}$ (mrem)	TEDE (mrem)
2	13	3
5	31	6

Table 13-22 Radiation Doses to Members of the General Public Following a Single Element Failure in Water - Scenario C

Distance (m)	$CDE_{Thyroid} + DDE_{Thyroid}$ (mrem)	TEDE (mrem)
10	14	1
50	6	<1
100	2	<1
150	1	<1
200	1	<1
250	<1	<1
267	<1	<1

Since most of the halogens released from the fuel element will be retained in the primary water, the majority of this activity will end up in the demineralizer tank. The exposure rate from the demineralizer tank can be estimated by:

$$\dot{X} = 6CEN\left(R\,h^{-1}\text{ at }1\,\text{foot}\right),$$

where:

C = number of halogen curies retained in the demineralizer tank (Ci);
E = energy of gamma rays (MeV) = 1; and
N = number of gamma rays per disintegration = 1.

From Section 13.2.1.2, the total saturated activity of the halogens is [redacted] curies. Of this, 1.22×10^{-4} is released to the gap, 0.5 of the gap activity is released to the water, and 0.95 of this remains in the water. Thus, the number of curies retained in the demineralizer tank is [redacted] Ci. The assumption that the average energy of the gamma rays from the halogens is 1 MeV is rather conservative.

Thus,

$$\dot{X} = 2.0\,R\,h^{-1}\ @1\,foot.$$

Surrounding the sides of the OSTR demineralizer tank is 6 inches of high-density concrete (no shielding on top). With μ_c for this concrete equal to about 0.20 cm^{-1} for 1-MeV gammas, the overall attenuation factor for the concrete shield is about 4.75×10^{-2}. This reduces the exposure rate to about 96 mR h^{-1} at one foot.

A fuel loading error is another potential way that a fuel element might overheat and result in a cladding failure. In the OSTR, the normal fuel loading would consist of a core comprised of all of the same type of fuel elements (e.g., [redacted] It is possible, however, for the OSTR to operate with a mixed core (e.g., [redacted] and [redacted] The OSTR Technical Specifications require that if a mixed core is used, it must consist of no less than [redacted] elements located in a [redacted]

To reach a configuration where a high power density in an element might exist which might push the limits on cladding integrity, a gross error in fuel loading must have existed. For example, [redacted] elements were loaded into the B and C rings, with [redacted] in the D rings and beyond. Then, if an [redacted] element in the B ring was replaced with a [redacted] element, this [redacted] element might experience a higher than normal power density. It is still unlikely that the [redacted] element would experience a power density of 32 kW, since the power density

for a [redacted] element in a full-[redacted] core in the B ring is about 16 kW. It has been shown that a power density of 32 kW would still not produce cladding failure.

13.2.6 Experiment Malfunction

13.2.6.1 Accident Initiating Events and Scenarios

Improperly controlled experiments involving the OSTR could potentially result in damage to the reactor, unnecessary radiation exposure to facility staff and members of the general public, and unnecessary releases of radioactivity into the unrestricted area. Mechanisms for these occurrences include the production of excess amounts of radionuclides with unexpected radiation levels, and the creation of unplanned pressures in irradiated materials. These materials could subsequently vent into the irradiation facilities or into the reactor room causing damage from the pressure release or an uncontrolled release of radioactivity. Other mechanisms for damage, such as large reactivity changes, are also possible.

13.2.6.2 Accident Analysis and Determination of Consequences

There are two main sets of procedural and regulatory requirements that relate to experiment review and approval. These are the Oregon State TRIGA® Operating Procedures (OSTROP) and the OSTR Technical Specifications. These requirements are focused on ensuring that experiments will not fail, and they also incorporate requirements to assure that there is no reactor damage and no radioactivity releases or radiation doses which exceed the limits of 10 CFR 20, should failure occur. For example, the OSTROP contain detailed procedures for the safety review and approval of all reactor experiments.

Safety related reviews of proposed experiments require the performance of specific safety analyses of proposed activities to assess such things as generation of radionuclides and fission products (e.g., radioiodines), and to ensure evaluation of reactivity worth, chemical and physical characteristics of materials under irradiation, corrosive and explosive characteristics of materials, and the need for encapsulation. This process is an important step in ensuring the safety of reactor experiments and has been successfully used for many years at research reactors to help assure the safety of experiments placed in these reactors. Therefore, this process is expected to be an effective measure in assuring experiment safety at the OSTR.

In the OSTR Technical Specifications, a limit of $1.00 has been placed on the reactivity worth of non-secured experiments. This is well below the maximum reactivity limit of $2.59 established in Section 13.2.2 and would result in fuel temperatures well below the safety limit.

A limit of $2.55 has also been placed on the reactivity worth of any single experiment. This is below the maximum reactivity limit of $2.59 established in Section 13.2.2 and would result in fuel temperatures below the safety limit.

A further limit on the reactivity worth of all experiments has been set at $3.00. The OSTROP require that the reactor be shut down before any experiments are moved. The Technical Specifications require that the OSTR shutdown margin be at least $0.57 with the most reactive rod withdrawn. The transient rod is the most reactive rod, with a worth of [redacted]. Therefore with all the rods inserted, the reactor is shutdown by at least $4.62. If all experiments were removed, the reactor would still be shutdown by at least $1.62.

Limiting the generation of certain fission products in fueled experiments also helps to assure that occupational radiation doses as well as doses to the general public, due to experiment failure with subsequent fission product release, will be within the limits prescribed in 10 CFR 20. A limit of 1.5 curies of $^{131\text{-}135}I$ is specified in the OSTR Technical Specifications. This amount of iodine isotopes is very small compared to the approximately [redacted] curies which are present in the single fuel element failure analyzed in Section 13.2.1 (failure in air) and Section 13.2.5 (failure in water). In both cases, the occupational doses and the doses to the general public in the unrestricted area due to radioiodine are within 10 CFR 20 limits. Therefore, limiting experiments to 1.5 curies of radioiodine will result in projected doses well within the 10 CFR 20 limits.

Projected damage to the reactor from experiments involving explosives varies significantly depending on the quantity of explosives being irradiated and where the explosives are placed relative to critical reactor components and safety systems. If in the reactor tank, the OSTR Technical Specification limit the amount of explosive materials, such as gunpowder, TNT, nitroglycerin, or PETN, to quantities less than 25 milligrams. Also, the Technical Specifications state that the pressure produced upon detonation of the explosive must have been calculated and/or experimentally demonstrated to be less than the design pressure of the container. The following discussion shows that the irradiation of explosives up to 25 milligrams could be safely performed if the containment is properly chosen.

A 25-milligram quantity of explosives, upon detonation, releases approximately [redacted] calories ([redacted] joules) of energy, with the creation of [redacted] cm^3 of gas. For the explosive TNT, the density is 1.654 gm cm^{-3}, so that 25 mg represents a volume of [redacted] cm^3. If the assumption is made that the energy release occurs as an instantaneous change in pressure, the total force on the encapsulation material is the sum of the two pressures. For a 1-cm^3 volume, the energy release of [redacted] joules represents a pressure of [redacted] atmospheres. The instantaneous change in pressure due to gas production in the same volume adds another [redacted] atmospheres. The total pressure within a 1-cm^3 capsule is then [redacted] atmospheres for the complete reaction of 25 mg of explosives.

Typical construction materials of capsules are stainless steel, aluminum, and polyethylene. Table 13-23 lists the mechanical properties of these encapsulation materials.

Table 13-23 Material Strengths

Material	Yield Strength ($\times 10^3$ psi)	Ultimate Strength ($\times 10^3$ psi)	Density (g cm^{-3})
Stainless Steel (type 304)	35	85	7.98
Aluminum (alloy 6061)	40	45	2.739
Polyethylene	1.7	1.4	0.923

Analysis of the encapsulation materials determines the material stress limits that must exist to confine the reactive equivalent of 25 mg of explosives. The stress limit in a cylindrical container with thin walls is one-half the pressure times the ratio of the capsule diameter-to-wall thickness. This is the hoop stress. The hoop stress is 2 times the longitudinal stress, and hence hoop stress is limiting. Thus:

$$\sigma_{max} = \frac{p\,d}{2\,t},$$

where:

σ_{max} = maximum hoop stress in container wall;
p = total pressure within the container;
d = diameter of the container; and
t = wall thickness of the container.

When evaluating an encapsulation material's ability to confine the reactive equivalent of 25 mg of explosives, the maximum stress in the container wall is required to be less than or equal to the yield strength of the material:

$$\frac{p\,d}{2\,t} \le \sigma_{yield},$$

where σ_{yield} is the yield strength. Solving this equation for d/t provides an easy method of evaluating an encapsulation material:

$$\frac{d}{t} \leq \frac{2\sigma_{yield}}{p}.$$

Assuming an internal pressure of [redacted] atmospheres ([redacted] psi), maximum values of d/t for the encapsulation materials are displayed in Table 13-24. The results indicate that a polyethylene vial is not a practical container since its wall thickness must be at least 4.5 times the diameter. However, both the aluminum and the stainless steel make satisfactory containers.

Table 13-24 Container Diameter-to-Thickness Ratio

Material	d/t
Stainless Steel (type 304)	4.5
Aluminum (alloy 6061)	5.1
Polyethylene (low density)	0.22

As a result of the preceding analysis, a limit of 25 mg of TNT-equivalent explosives is deemed to be a safe limitation on explosives which may be irradiated in facilities located inside the reactor tank, provided that the proper container material with appropriate diameter and wall thickness is used.

13.2.7 Loss of Normal Electrical Power

13.2.7.1 Accident Initiating Events and Scenarios

Loss of electrical power to the OSTR could occur due to many events and scenarios that routinely affect commercial power.

13.2.7.2 Accident Analysis and Determination of Consequences

Since the OSTR does not require emergency backup systems to safely maintain core cooling, there are no credible reactor accidents associated with the loss of electrical power. A backup power system is present at the OSTR that mainly provides [redacted] This backup system consists of a [redacted] The system will provide emergency power immediately after the loss of regular electrical

power. It will continue to supply power for a period of a [redacted] This system is maintained and checked on a daily basis to ensure that it is capable of operating properly. Battery-powered emergency lights are also located throughout the facility to allow for inspection of the reactor and for an orderly evacuation of the facility.

Loss of normal electrical power during reactor operations is addressed in the reactor operating procedures, which require that, upon loss of normal power, an orderly shut down is to be initiated by the operator on duty. The backup power supply will allow monitoring of the orderly shut down and verification of the reactor's shutdown condition.

13.2.8 External Events

13.2.8.1 Accident Initiating Events and Scenarios

Hurricanes, tornadoes, and floods are virtually nonexistent in the area around the OSTR. Therefore, these events are not considered to be viable causes of accidents for the reactor facility. In addition, seismic activity in the Corvallis area is relatively low compared to other areas in the Pacific Northwest.

13.2.8.2 Accident Analysis and Determination of Consequences

There are no accidents in this category that would have more on-site or off-site consequences than the MHA analyzed in Section 13.2.1, and, therefore, no additional specific accidents are analyzed in this section.

13.2.9 Mishandling or Malfunction of Equipment

13.2.9.1 Accident Initiating Events and Scenarios

No credible accident initiating events were identified for this accident class. Situations involving an operator error at the reactor controls, a malfunction or loss of safety-related instruments or controls, and an electrical fault in the control rod system were anticipated at the reactor design stage. As a result, many safety features, such as control system interlocks and automatic reactor shutdown circuits, were designed into the overall TRIGA® Control System (Chapter 7). TRIGA® fuel also incorporates a number of safety features (Chapter 4) which, together with the features designed into the control system, assure safe reactor response, including in some cases reactor shutdown.

Malfunction of confinement or containment systems would have the greatest impact during the MHA, if used to lessen the impact of such an accident. However, as shown in

Section 13.2.1, no credit is taken for confinement or containment systems in the analysis of the MHA for the OSTR. Furthermore, no safety considerations at the OSTR depend on confinement or containment systems.

Rapid leaks of liquids have previously been addressed in Section 13.2.3. Although no damage to the reactor occurs as a result of these leaks, the details of the previous analyses provide a more comprehensive explanation.

13.2.9.2 Accident Analysis and Determination of Consequences

Since there were no credible initiating events identified, no accident analysis was performed for this section and no consequences were identified.

13.3 References

13.1 Credible Accident Analyses for TRIGA and TRIGA-fueled Reactors, NUREG/CR-2387, PNL-4028, April 1982.

13.2 Guidelines for Preparing and Reviewing Applications for the Licensing of Non-Power Reactors, Format and Content, NUREG-1537, Part 1, February 1996.

13.3 Safety Analysis Report for the Oregon State University TRIGA Research Reactor, Oregon State University, Corvallis, OR, August 1968.

13.4 Amendment No. 4 to the Safety Analysis Report for the Oregon State University TRIGA Reactor, Oregon State University, Corvallis, OR, Sept. 11, 1975.

13.5 "The Calculations of Distance Factors for Power and Test Reactor Sites," J.J.DiMunno et al, TID-14844, U.S. Atomic Energy Commission, March 1962.

13.6 Regulatory Guide 3.33, "Assumptions Used for Evaluating the Potential Radiological Consequences of Accidental Nuclear Criticality in a Fuel Reprocessing Plant," U.S. Nuclear Regulatory Commission, April 1977.

13.7 Regulatory Guide 3.34, "Assumptions Used for Evaluating the Potential Radiological Consequences of Accidental Nuclear Criticality in a Uranium Fuel Fabrication Plant," U.S. Nuclear Regulatory Commission, July 1979.

13.8 Regulatory Guide 1.5, "Assumptions Used for Evaluating the Potential Radiological Consequences of a Loss of Coolant Accident for Pressurized Water Reactors," U.S. Nuclear Regulatory Commission, June 1974 (Also see Regulatory Guide 1.3 on BWRs).

13.9 "A Guide to Radiological Accident Considerations for Siting and Design of DOE Nonreactor Nuclear Facilities," J.C. Elder et at, LA-10294-MS, Los Alamos National Laboratory, January 1986.

13.10 Nuclear Power Reactor Safety, E.E. Lewis, John Wiley and Sons, 1977, p. 521.

13.11 Nuclear Engineering, Theory and Technology of Commercial Nuclear Power, R.A. Knief, Hemisphere Publishing, 1992, pp. 353, 431.

13.12 "Fuel Elements for Pulsed TRIGA Research Reactors," M.T. Simnad et al, Nuc. Tech. Vol. 28, January 1976

13.13 "The U-ZrH_x Alloy: Its Properties and Use in TRIGA Fuel," M.T. Simnad, General Atomic Report E-117-833, February 1980.

13.14 Regulatory Guide 1.145, "Atmospheric Dispersion Models for Potential Accident Consequence Assessments at Nuclear Power Plants," U.S. Nuclear Regulatory Commission, August 1979.

13.15 "Calculated Atmospheric Radioactivity from the OSU TRIGA Research Reactor Using the Gaussian Plume Diffusion Model," Bright M.K. Wong, Oregon State University Department of Nuclear Engineering Report 7903, August 1979.

13.16 "Internal Dose Conversion Factors for Calculation of Dose to the Public," DOE/EH-0071, U.S. Department of Energy, Washington, D.C., 1988

13.17 "External Dose Rate Conversion Factors for Calculation of Dose to the Public," DOE/EH-0070, U.S. Department of Energy, Washington, D.C., 1988

13.18 "Kinetic Behavior of TRIGA Reactors," G.B. West et al, GA-7882, General Atomics, March 31, 1967.

13.19 Dynamics of Nuclear Reactors, David Hetrick, U. of Chicago Press, 1971.

13.20 "Low Enriched TRIGA Fuel-Water Quench Safety Test," GA-A15413, General Atomics, June 1979.

13.21 Stationary Neutron Radiography System, Final Safety Analysis Report, McClellan Air Force Base, Sacramento, CA, August 1990.

13.22 Safety Analysis Report for the Torrey Pines TRIGA Mark III Reactor, GA-9064, General Atomics, January 5, 1970.

13.23 Safety Analysis Report for the TRIGA Reactor Facility, University of Texas at Austin, May 1991.

13.24 Introduction to Nuclear Engineering, 2nd Edition, John R. Lamarsh, Addison-Wesley, 1983, p. 72.

13.25 "Data for Use in Protection Against External Radiation," International Commission on Radiation Protection, ICRP Report No. 51, Pergamon Press, March 1987.

13.26 Safety Analysis Report, Revision 2, McClellan Nuclear Radiation Center, McClellan Air Force Base, Sacramento, CA, April 1998.

13.27 Introduction to Nuclear Engineering, 2nd Edition, Richard Stephenson, McGraw-Hill, 1958, pp. 209-213.

THIS PAGE INTENTIONALLY BLANK

CHAPTER 14

TECHNICAL SPECIFICATIONS

(The Technical Specifications are contained in USNRC Operating License R-106, Appendix A)

THIS PAGE INTENTIONALLY LEFT BLANK

CHAPTER 15

FINANCIAL QUALIFICATIONS

Chapter 15 - Valid Pages
Rev. 0 7/01/2004

i	Rev. 0 7/01/2004
ii	Rev. 0 7/01/2004
1	Rev. 0 7/01/2004
2	Rev. 0 7/01/2004

TABLE OF CONTENTS

LIST OF TABLES

THIS PAGE INTENTIONALLY LEFT BLANK

15 Financial Qualifications

15.1 Financial Ability to Construct a Non-Power Reactor

This is not applicable for a renewal application.

15.2 Financial Ability to Operate a Non-Power Reactor

In fiscal year 2003, the appropriation from the State of Oregon for the entire Radiation Center totaled $613,932. As shown in Table 15-1, the total expenses for that year were $716,770. Expenses and outside income specific to the OSTR are given in Table 15-2. Expenses increased by 3% in FY04 and are projected to increase by 5% for each of the remaining years. The difference between appropriations and expenses accounted for is from returned overhead, grants, and service charges.

	FY 03	FY 04	FY 05	FY 06	FY 07	FY 08
Administrative	$210,966	$221,514	$232,590	$244,219	$256,430	$269,252
Teaching & Instruction	$ 69,706	$ 73,191	$ 76,851	$ 80,693	$ 84,728	$ 88,964
Reactor	$381,295	$385,758	$405,046	$425,298	$446,563	$468,891
Building Maintenance	$ 54,803	$ 57,543	$ 60,421	$ 63,442	$ 66,614	$ 69,944
	$716,770	$738,007	$774,907	$813,652	$854,335	$897,052

Table 15-1 Current and Projected Expenses for the Radiation Center

	FY 03	FY 04	FY 05	FY 06	FY 07	FY 08
Unclassified Salary	$182,407	$191,527	$201,103	$211,158	$221,716	$232,802
Classified Salary	$115,218	$120,979	$127,028	$133,379	$140,048	$147,050
Student Wages	$ 4,960	$ 5,207	$ 5,468	$ 5,741	$ 6,028	$ 6,330
Payroll Expenses	$119,108	$125,063	$131,316	$137,882	$144,776	$152,015
Services & Supplies	$ 55,491	$ 58,265	$ 61,179	$ 64,238	$ 67,449	$ 70,822
Travel	$ 217	$ 227	$ 239	$ 251	$ 263	$ 277
Equipment	$ 9,000	$ 9,450	$ 9,923	$ 10,419	$ 10,940	$ 11,487
Campus Income	$ (58,116)	$(61,021)	$(64,072)	$(67,276)	$(70,640)	$ (74,172)
Non-campus Income	$ (60,895)	$(63,940)	$(67,137)	$(70,493)	$(74,018)	$ (77,719)
Cost Share Expense	$ 13,906					
Total	$381,295	$385,758	$405,046	$425,298	$446,563	$468,891

Table 15-2 Breakdown of Expenses and Outside Income for the OSTR

The salary numbers given include direct salaries and benefits. These numbers do not include the infrastructure provided by the university such as electrical power, heating, and most building maintenance.

The institutional funding is appropriated by the State of Oregon. The administration of the university has been very supportive. The fact that this application for renewal has been signed by the administration indicates this support.

While the OSTR does perform some commercial irradiation services, this represents only a very small percentage of either expense or income. Commercial activities at this time are limited to isotope production. Assuming that cost is proportional to operating time, then commercial work comprises less than 1% of the cost of owning and operating the facility. In accordance with 10 CFR 50.21, the OSTR should therefore be licensed as a Class 104 facility.

15.3 Financial Ability to Decommission the Facility

Oregon State University is a state institution. Therefore, in accordance with the provisions of 10 CFR 50.75(e)(2)(iv) the funds needed for decommissioning will be requested through appropriate state channels and will be obtained sufficiently in advance of decommissioning to prevent delay of required activities.

By the letter dated July 11, 1990, the University estimated the cost of decommissioning at $3 million [Ref. 15.1]. In 1993, the cost of decommissioning was estimated to be $6 million based upon studies of the decommissioning of existing facilities (at that time) that seemed to indicate that the cost of decommissioning was increasing significantly greater that allowed from the consumer price index or the formula given in 10 CFR 50.75(c)(2). The 1993 estimate has been updated annual as required by 10 CFR 50.75(g)(3) using data and methodology supplied in NUREG-1307 [Ref. 15.3]. The current estimated cost of decommissioning the OSTR is estimated between $7.9 and $14.3 million.

15.4 References

15.1 Letter to USNRC Document Control Desk from L. Edwin Coate dated July 11, 1990.

15.2 U.S. Nuclear Regulatory Commission, "Report on Waste Burial Charges: Changes in Decommisioning Waste Disposal Costs at Low-Level Waste Burial Facilities," NUREG-1307, Rev. 10.